# Mathematical Analysis of Minnaert Resonances for Acoustic Metamaterials

Diss. ETH No. 25214

# Mathematical Analysis of Minnaert Resonances for Acoustic Metamaterials

A thesis submitted to attain the degree of
DOCTOR OF SCIENCES of ETH ZÜRICH
(Dr. sc. ETH Zürich)

presented by

BRIAN FITZPATRICK

BSc. Computer Science and Information Technology, National University of Ireland Galway

MSc. Mathematical Modelling, University of Limerick

born on 16.04.1980

citizen of Ireland

accepted on the recommendation of
Prof. Dr. Habib Ammari, ETH Zürich, examiner
Prof. Dr. Richard Craster, Imperial College London, co-examiner
Prof. Dr. Gilles Lebeau, Université de Nice Sophia-Antipolis, co-examiner

2018

# Abstract

The propagation of acoustic waves in bubbly media has long been of interest in the mathematics, physics, and engineering communities. In recent years, the interest in this subject has heightened with the advent of acoustic metamaterials that exhibit spectacular properties such as absorption of practically all incoming acoustic energy (super-absorption), and the ability to focus acoustic waves beyond the diffraction limit (super-focusing). The key mechanism underlying these and other extraordinary properties involving acoustic wave propagation through a liquid containing bubbles is the phenomenon of sub-wavelength resonance. Sub-wavelength resonance occurs when an object resonantly couples with an incident wave whose wavelength is much larger than the characteristic size of the object.

In this thesis, it is first shown that a single arbitrary shaped bubble in an infinite liquid possesses a sub-wavelength resonance called the Minnaert resonance. This resonance is due to the high contrast in mass densities between the bubble and the surrounding medium and it makes the air bubble an ideal sub-wavelength resonator (the bubble can be more than two orders of magnitude smaller than the wavelength at the resonant frequency). Then, slighlty below the Minnaert resonant frequency, with an appropriate bubble volume fraction, a high contrast effective medium is obtained, making the sub-wavelength focusing of waves achievable.

Using bubble dimers, it is proved that the effective mass density and bulk modulus of the bubbly fluid can both be negative over a non-empty range of frequencies. A bubble dimer is a system that consists of two identical separated spherical bubbles. It features two slightly different sub-wavelength resonances, called the hybridized Minnaert resonances.

The opening of a sub-wavelength phononic bandgap is demonstrated by considering a periodic arrangement of bubbles and exploiting their Minnaert resonance. It is shown that there exists a sub-wavelength bandgap in this bubbly crystal. The sub-wavelength bandgap is mainly due to the cell resonance of the bubbles in the quasi-static regime and is quite different from the usual bandgaps in photonic and phononic crystals, where the bandgap opens at a wavelength which is comparable to the period of the structure. Finally, this sub-wavelength bandgap is used to demonstrate cavities, very similar to those obtained in standard photonic and phononic crystals, albeit of deeply sub-wavelength dimensions. The key idea used to obtain a cavity of this nature is to increase the size of a single bubble inside the crystal, thus creating a defect.

# Résumé

La propagation d'ondes acoustiques dans les milieux à bulles a récemment fait l'objet de très nombreuses études expérimentales. En effet, les propriétés acoustiques des milieux à bulles sont fascinantes. Il a notamment été mis en évidence que le couplage entre les bulles pouvait conduire à des effets de super-focalisation, de bandes interdites sub-longueur d'onde mais aussi que ces milieux à bulles pouvaient jouer le rôle d'absorbeurs acoustiques ou encore d'émetteurs cohérents d'ondes acoustiques. Toutes ces propriétés extraordinaires trouvent leur origine dans la notion de résonance sub-longueur d'onde.

Dans cette thèse, nous décrivons tout d'abord la pulsation à basses fréquences d'une bulle d'air de forme quelconque dans un liquide. Nous introduisons la notion de résonance sub-longueur d'onde et nous obtenons une formule asymptotique de cette résonance basse fréquence en fonction du contraste entre les densités de l'air et du liquide. Nous démontrons ensuite les propriétés de super-focalisation d'un nuage de bulles illuminé à une fréquence légérement supérieure à cette fréquence de résonance. Nous démontrons également qu'une couche de bulles peut se comporter à certaines fréquences résonantes sub-longueur d'onde comme un absorbeur parfait pour des ultrasons. En utilisant des dimères de bulles, qui peuvent être approchés par la somme d'un monopole et d'un dipole résonants, nous obtenons, grâce à un effet d'hybridation des résonances, des matériaux acoustiques à indices négatifs pour une certaine bande de fréquence.

D'autre part, nous démontrons l'existence d'une gamme de fréquences pour laquelle la propagation dans un cristal de bulles n'est pas autorisée au-dessus d'une certaine fréquence de résonance critique. Contrairement aux matériaux structurés à l'échelle de la longueur d'onde qui mettent en jeu des effets de périodicité pour créer une bande interdite, ici celle-ci est uniquement due à la réponse en opposition de phase des résonateurs sub-longueur d'onde. Enfin, nous démontrons la possibilité de piéger une onde acoustique dans une cavité sub-longueur d'onde.

# Contents

# Introduction

The purpose of this thesis is to understand acoustic wave propagation through a liquid containing bubbles. Bubbly media have fascinating acoustic properties. For example, a very small volume fraction of air bubbles in water is enough to modify the effective velocity of sound in the medium [25, 37, 56, 65]. One of our motivations is the use of bubbles in super-resolution medical ultrasonic imaging [43]. At particular low frequencies known as *Minnaert resonances* [86], bubbles behave as strong sound scatterers. The enhancement of their acoustic signature allows for the use of ultrasonic techniques to detect, localize, and characterize them inside a visco-elastic opaque medium [65]. Bubbles are present in many other important applications. The extraordinary acoustic properties of bubbly media are being used to design new acoustic materials. The Minnaert resonance of the bubbles persists when they are no longer embedded in a liquid, but in a soft elastic medium [33, 72].

A remarkable property of spherical bubbles is that they oscillate harmonically, pulsating with a breathing mode characterized by their Minnaert frequencies, provided that the contrast in densities between the gas inside the bubbles and the surrounding liquid is high [51]. Many interesting physical works have been devoted to the acoustic bubble problem, some examples being the super-absorption of acoustic waves [72], sub-wavelength focusing using ultrasound time-reversal mirrors [65], and the characterization of bandgaps in structured bubbly media [70]. Nevertheless, the characterization of Minnaert resonances for arbitrary shaped bubbles and the analysis of the propagation of acoustic waves inside bubbly media at the Minnaert frequencies have been longstanding problems.

## Sub-wavelength resonance

In general, if an acoustic wave impinges upon an object that is small in comparison with its wavelength, the effect of the object on wave scattering is negligible; the object is essentially invisible. However, at sub-wavelength resonant frequencies, the scattering of waves from the object is greatly enhanced and can have a noticeable effect on wave propagation. It transpires that gas bubbles in water are very strong sub-wavelength resonators. The low frequency resonance of bubbles arises due to the high contrast in mass densities between the air in a bubble and the surrounding liquid. This resonance is called the Minnaert resonance in honor of the Belgian physicist Marcel Minnaert who first derived the resonant frequency of an air bubble in water [86]. The Minnaert resonance frequency can also be obtained by linearizing the Rayleigh-Plasset equation

which governs the radial displacements of a spherical bubble in an infinite liquid driven by an incident pressure wave [40].

Recently experimental physicists have exploited the sub-wavelength resonance properties of bubbly media to experimentally demonstrate the possibility of deeply sub-wavelength control of acoustic waves [65, 72, 70, 71]. They have shown that it is indeed possible to achieve effects such as super-absorption and super-focusing of acoustic energy in real-world situations.

It is necessary to gain a precise understanding of how these effects arise in order to build upon them and advance the field of acoustic metamaterials. The aim of this work is to develop this knowledge by performing a rigorous mathematical modeling and analysis of the sub-wavelength resonance properties of bubbly media.

## Contributions

To obtain precise control over the properties of acoustic metamaterials, and thus control acoustic wave propagation, we need to remove limitations on what parameters we are able to work with. Hence, in many sections of this work we do not limit ourselves to spherical air bubbles. Instead we work with arbitrary shaped acoustic sub-wavelength resonators, of which spherical objects are a special case. The frequency response of a resonator is dependent on its shape so by deriving formulas for arbitrary shaped resonators we pave the way to gaining precise control over the frequency ranges at which sub-wavelength resonance effects can occur. We derive the Minnaert resonance of an arbitrary shaped resonator in an infinite liquid in Chapter 2 and show that it reduces to the standard Minnaert resonance formula if the shape is chosen to be a sphere. In addition, we obtain a rigorous monopole approximation of the field scattered by the bubble in terms of a scattering coefficient that blows up near the Minnaert resonance frequency.

In order to explain the super-absorption phenomenon, in Chapter 3, we consider a bubble meta-screen which is a periodic array of bubbles above a reflective surface. We derive an approximation for the scattered field in terms of an effective reflection coefficient that characterizes the response of the meta-screen to incident acoustic waves. We derive a quasi-periodic Minnaert resonance formula and show that as we approach this resonance the reflection coefficient goes to zero, thus explaining the incredible absorption properties of bubble meta-screens.

Phononic crystals constructed using bubbly media have been experimentally shown to have sub-wavelength bandgaps which are frequency ranges in which wave propagation is prohibited. These frequency ranges corresponds to the case when the characteristic size of the bubbles in the crystal is much smaller than the wavelength. In Chapter 4 we prove that such a bandgap exists and that it occurs when the contrast in mass densities between the bubbles and the surrounding liquid is sufficiently high. Furthermore, we show that this bandgap opens slightly above a critical resonance.

In Chapter 5 we consider the time-reversal of acoustic waves. In general, it is not possible to focus time-reversed acoustic waves in a liquid into regions smaller than half the operating wavelength due to the Rayleigh diffraction limit. However, if the liquid contains a large number of air bubbles and the excitation frequency is near the Minnaert resonance frequency it becomes possible to overcome this limitation and achieve super-focusing of acoustic waves. We derive a point scatterer approximation for the propagation of waves in a bubbly fluid and use this to numerically show that sub-wavelength focusing of acoustic waves is indeed achievable.

Another method of achieving super-focusing of acoustic waves is through the use of double-negative metamaterials. These are materials in which the effective material parameters both become negative simultaneously, thus giving rise to a negative effective refractive index which can be used to construct an acoustic super-lens. In Chapter 6 we introduce the notion of a bubble dimer, which consists of two identical bubbles that are close together, but not too close, in comparison to their size. While a single bubble has a Minnaert resonance, a bubble dimer has hybridized Minnaert resonances. We prove that using a bubbly media consisting of these bubble dimers, when the excitation frequency is near the hybridized Minnaert resonances, it is possible for both the effective mass density and the effective bulk modulus to become negative simultaneously.

In Chapter 7 we extend our work on bubbly phononic crystals in Chapter 4 by considering the case when the crystal features a defect. To create a defect we slightly enlarge one of the bubbles in the periodic array. The presence of this defect gives rise to a localized mode which decays exponentially away from the defect. We prove the existence of a defect mode in a bubbly crystal constructed from spherical bubbles.

In summary, the work in this thesis rigorously explains several recent discoveries in experimental physical acoustics and sheds new light on the phenomenon of acoustic sub-wavelength resonance in acoustic metamaterials.

The results of this thesis are published in [8, 6, 11, 7, 10, 9].

# 1. Preliminaries

In this thesis we consider problems involving the scattering of acoustic waves by one or more bubbles embedded inside some homogeneous liquid. Here we introduce various physical parameters and mathematical objects that will be used frequently throughout this work.

## 1.1. System parameters

We denote by $\rho_b, \kappa_b, v_b, k_b$ the mass density, bulk modulus, wave speed, and wavenumber of gas inside a bubble. The corresponding parameters for the background medium are $\rho, \kappa, v, k$. The following relations hold:

$$v = \sqrt{\frac{\kappa}{\rho}}, \quad v_b = \sqrt{\frac{\kappa_b}{\rho_b}}, \quad k = \frac{\omega}{v}, \quad k_b = \frac{\omega}{v_b}. \tag{1.1}$$

We also introduce two dimensionless contrast parameters:

$$\delta = \frac{\rho_b}{\rho}, \quad \tau = \frac{k_b}{k} = \frac{v}{v_b} = \sqrt{\frac{\rho_b \kappa}{\rho \kappa_b}}. \tag{1.2}$$

## 1.2. Regime

We assume that the wave speeds outside and inside the bubble are both of order one, *i.e.*, the contrast between the wave speeds is not significant. We also assume that there is a large contrast in the mass densities. In summary, we assume that

$$\delta \ll 1, \quad \tau = O(1).$$

Note that for air and water in standard conditions we have that $\delta \approx 1.2 \times 10^{-3}$.

## 1.3. Layer potentials

Let $G^0(x,y)$ be the fundamental solution of the Laplace equation:

$$G^0(x,y) = \begin{cases} \dfrac{1}{2\pi}\ln|x-y|, & d=2, \\ -\dfrac{1}{4\pi|x-y|}, & d=3. \end{cases} \tag{1.3}$$

Let $G^k(x,y)$ for $k \neq 0$ be the fundamental solution of the Helmholtz equation:

$$G^k(x,y) = \begin{cases} -\dfrac{i}{4}H_0^{(1)}(k|x-y|), & d=2, \\ -\dfrac{e^{ik|x-y|}}{4\pi|x-y|}, & d=3. \end{cases} \tag{1.4}$$

We denote by $H^1$ the standard Sobolev space. For a given bounded domain $D$ in $\mathbb{R}^d$ where $d \in \{2,3\}$ with Lipschitz boundary $\partial D$, the single layer potential $\mathcal{S}_D^k : L^2(\partial D) \to H^1(\partial D), H^1_{\mathrm{loc}}(\mathbb{R}^d)$ associated with wavenumber $k$ is defined by

$$\mathcal{S}_D^k[\psi](x) := \int_{\partial D} G^k(x,y)\psi(y)d\sigma(y), \quad x \in \mathbb{R}^d. \tag{1.5}$$

We define the Neumann-Poincaré operator $\mathcal{K}_D^{k,*} : L^2(\partial D) \to L^2(\partial D)$ by

$$\mathcal{K}_D^{k,*}[\psi](x) := \text{p.v.} \int_{\partial D} \frac{\partial G^k(x,y)}{\partial \nu(x)}\psi(y)d\sigma(y), \quad x \in \partial D, \tag{1.6}$$

where p.v. stands for the Cauchy principal value. In the case when $k = 0$ we omit the superscripts and write $\mathcal{S}_D$ and $\mathcal{K}_D^*$, respectively. Note that in three dimensions $\mathcal{S}_D : L^2(\partial D) \to H^1(\partial D)$ is invertible [17].

We denote by $\partial/\partial\nu$ the outward normal derivative and by $|_\pm$ the limits from outside and inside $D$. The following jump relations hold:

$$\frac{\partial}{\partial\nu}\Big|_\pm \mathcal{S}_D^k[\psi](x) = \left(\pm\frac{1}{2}I + \mathcal{K}_D^{k,*}\right)[\psi](x), \quad x \in \partial D. \tag{1.7}$$

## 1.4. Quasi-periodic layer potentials

Let $Y$ be the unit cell $[0,1]^d$ in $\mathbb{R}^d$. For $\alpha \in [0,2\pi)^d$, the function $G^{\alpha,k}$ is defined to satisfy

$$(\triangle_x + k^2)G^{\alpha,k}(x,y) = \sum_{n\in\mathbb{Z}^d} \delta(x-y-n)e^{in\cdot\alpha},$$

where $\delta$ is the Dirac delta function and $G^{\alpha,k}$ is $\alpha$-quasi-periodic, i.e., $e^{-\mathrm{i}\alpha\cdot x}G^{\alpha,k}(x,y)$ is periodic in $x$ with respect to $Y$. It is known that $G^{\alpha,k}$ can be written as

$$G^{\alpha,k}(x,y)=\sum_{n\in\mathbb{Z}^d}\frac{e^{\mathrm{i}(2\pi n+\alpha)\cdot(x-y)}}{k^2-|2\pi n+\alpha|^2},$$

if $k\neq|2\pi n+\alpha|$ for any $n\in\mathbb{Z}^d$ [17].

Let $D$ be a bounded domain in $\mathbb{R}^d$ with a connected Lipschitz boundary satisfying $\overline{D}\subset Y$. We define a quasi-periodic single layer potential $\mathcal{S}_D^{\alpha,k}:L^2(\partial D)\to H^1(\partial D),H^1_{\mathrm{loc}}(\mathbb{R}^d)$ by

$$\mathcal{S}_D^{\alpha,k}[\psi](x)=\int_{\partial D}G^{\alpha,k}(x,y)\psi(y)d\sigma(y),\quad x\in\mathbb{R}^3.$$

Then $\mathcal{S}^{\alpha,k}[\psi]$ is an $\alpha$-quasi-periodic function satisfying the Helmholtz equation $(\triangle+k^2)u=0$. It satisfies a jump formula:

$$\frac{\partial}{\partial\nu}\Big|_{\pm}\mathcal{S}_D^{\alpha,k}[\psi](x)=\left(\pm\frac{1}{2}I+(\mathcal{K}_D^{-\alpha,k})^*\right)[\psi](x),\quad \text{a.e. } x\in\partial D,$$

where $(\mathcal{K}_D^{-\alpha,k})^*:L^2(\partial D)\to L^2(\partial D)$ is the operator given by

$$(\mathcal{K}_D^{-\alpha,k})^*[\psi](x)=\text{p.v.}\int_{\partial D}\frac{\partial}{\partial\nu(x)}G^{\alpha,k}(x,y)\psi(y)d\sigma(y).$$

We remark that it is known that $\mathcal{S}_D^{\alpha,0}:L^2(\partial D)\to H^1(\partial D)$ is invertible for $\alpha\neq 0$ [17].

## 1.5. Floquet transform

A function $f(x)$ is said to be $\alpha$-quasi-periodic in the variable $x\in\mathbb{R}^d$ if $e^{-i\alpha\cdot x}f(x)$ is periodic. Given a function $f\in L^2(\mathbb{R}^d)$, the Floquet transform is defined as

$$\mathbb{F}[f](x,\alpha)=\sum_{m\in\mathbb{Z}^d}f(x-m)e^{i\alpha\cdot m},\tag{1.8}$$

which is $\alpha$-quasi-periodic in $x$ and periodic in $\alpha$. Let $Y=[0,1)^d$ be the unit cell and $BZ:=\mathbb{R}^d/2\pi\mathbb{Z}^d\simeq[0,2\pi)^d$ be the so-called first Brillouin zone. The Floquet transform is an invertible map $\mathbb{F}:L^2(\mathbb{R}^d)\to L^2(Y\times BZ)$, with inverse (see, for instance, [64, 17])

$$\mathbb{F}^{-1}[g](x)=\frac{1}{(2\pi)^d}\int_{BZ}g(x,\alpha)\,\mathrm{d}\alpha.$$

## 1.6. Incident and scattered fields

Define $u^{in}$ to be an incident field which we assume to be a plane wave for simplicity:

$$u^{in}(x) = e^{ik\theta\cdot x},$$

where $\theta$ is a unit vector in $\mathbb{R}^d$. For a total field $u$, we denote by $u^s := u - u^{in}$ the scattered field which is subject to the Sommerfeld radiation condition:

$$\left|\frac{\partial u^s}{\partial \nu} - iku^s\right| = O(|x|^{-(d+1)/2}), \quad \text{as } x \to \infty \text{ uniformly in } \frac{x}{|x|}.$$

We abbreviate the Sommerfeld radiation condition throughout this thesis by SRC.

## 1.7. Notation

Denote by $\mathcal{L}(X, Y)$ the space of bounded linear operators between normed vector spaces $X$ and $Y$. Denote by $\langle\cdot,\cdot\rangle$ the $L^2$ scalar product, and by $\|\cdot\|$ the associated norm.

We denote the volume of a domain $D$ by $|D|$.

Denote by $\mathbb{1}_{\partial D} \in H^1(\partial D)$ the constant function on $\partial D$ with value 1. Let $\psi_0 \in \text{Ł}^2(\partial D)$ be such that [12]

$$\left(-\frac{1}{2}I + \mathcal{K}_D^*\right)[\psi_0] = 0, \quad \int_{\partial D} \psi_0 = 1.$$

The capacity of $\partial D$ is defined as

$$\text{Cap}_D := -\langle\psi_0, \mathbb{1}_{\partial D}\rangle = -\langle(\mathcal{S}_D)^{-1}[\mathbb{1}_{\partial D}], \mathbb{1}_{\partial D}\rangle \tag{1.9}$$

The $\alpha$-quasi-periodic capacity of $\partial D$ is defined as

$$\text{Cap}_{D,\alpha} := -\langle(\mathcal{S}_D^{\alpha,0})^{-1}[\mathbb{1}_{\partial D}], \mathbb{1}_{\partial D}\rangle. \tag{1.10}$$

# 2. Minnaert Resonance of an Arbitrary Shaped Sub-wavelength Resonator

In this chapter, through the application of layer potential techniques and Gohberg-Sigal theory we derive an original formula for the Minnaert resonance frequencies of arbitrarily shaped bubbles. We also provide a mathematical justification for the monopole approximation of the scattering of acoustic waves by bubbles at their Minnaert resonant frequency. Our results are complemented by a numerical simulation which serves to validate our formula in two dimensions.

## 2.1. Introduction

In this chapter we derive original formulas for the Minnaert resonances of bubbles of arbitrary shapes in both two and three dimensions using layer potential techniques and Gohberg-Sigal theory [17, 52]. Our formulas can be generalized to multiple interacting bubbles. They are expressed in terms of the capacity and the volume of the bubble. We also provide a mathematical justification for the monopole approximation and demonstrate the enhancement of the scattering in the far field at the Minnaert resonances. We show that there is a correspondence between bubbles in water and plasmonic nanoparticles in that both raise similar fundamental questions [19, 22, 27]. However, the mathematical formulation of Minnaert resonances is much more involved than the formulation of plasmonic resonances, which are characterized in terms of the spectrum of the Neumann-Poincaré integral operator [5, 26, 53, 58].

The Minnaert resonance is a low frequency resonance in which the wavelength is much larger than the size of the bubble [40]. Our aim in this chapter is to provide for the first time a mathematical framework for investigating bubbles as sub-wavelength acoustic resonators and rationalizing their extraordinary acoustic properties. Our results have important applications. They can be used to show that at the Minnaert resonance it is possible to achieve super-focusing of acoustic waves or imaging of passive sources with a resolution beyond the Rayleigh diffraction limit [23, 24]. Foldy's approximation applies and yields to the conclusion that the medium surrounding the source behaves like a high contrast dispersive medium [50]. As the dispersion is small, it has little effect on the super-focusing and super-resolution phenomena. Effective equations for wave propagation in bubbly liquids have been derived in the low frequency regime where the frequency is much smaller than the Minneart resonance frequency [31, 32, 59]. In this

chapter, however, we are more concerned with acoustic wave propagation in the resonant regime and in the behavior of bubbles as sub-wavelength resonators.

The chapter is organized as follows. In Section 2.2 we consider the scattering of acoustic waves in three dimensions by a single bubble and derive its Minnaert resonances in terms of its capacity, volume, and material parameters. In Section 2.3 we derive the point scatterer approximation of the bubble in the far-field. A derivation of the two-dimensional Minnaert resonance is given in Section 2.4. In Section 2.5 we perform a numerical simulation in two dimensions to illustrate the main findings of this chapter. The chapter ends with some concluding remarks.

## 2.2. The Minnaert resonance

We consider the scattering of acoustic waves by a single bubble embedded in a homogeneous liquid, subject to the regime specified in Section 1.2. Assume that the bubble is of size order one and occupies a bounded and simply connected domain $D$ with $\partial D \in C^{1,s}$ for $0 < s < 1$.

Let $u^{in}$ be the incident wave defined in Section 1.6. The scattering problem can be modeled by the following system of equations:

$$\begin{cases} (\Delta + k^2)u = 0 & \text{in } \mathbb{R}^3\backslash\overline{D}, \\ (\Delta + k_b^2)u = 0 & \text{in } D, \\ u|_- = u|_+ & \text{on } \partial D, \\ \dfrac{1}{\rho_b}\dfrac{\partial u}{\partial \nu}\Big|_- = \dfrac{1}{\rho}\dfrac{\partial u}{\partial \nu}\Big|_+ & \text{on } \partial D, \\ u^s := u - u^{in} & \text{satisfies the SRC.} \end{cases} \tag{2.1}$$

The solution $u$ of (2.1) can be written as

$$u = \begin{cases} u^{in} + \mathcal{S}_D^k[\psi] & \text{in } \mathbb{R}^3\backslash\overline{D}, \\ \mathcal{S}_D^{k_b}[\psi_b] & \text{in } D, \end{cases} \tag{2.2}$$

for some surface potentials $\psi, \psi_b \in L^2(\partial D)$ [14].

Throughout this chapter, we denote by $\mathcal{H} = L^2(\partial D) \times L^2(\partial D)$ and by $\mathcal{H}_1 = H^1(\partial D) \times L^2(\partial D)$.

Using the jump relations for the single layer potential (1.7), it is straightforward to derive that $\psi$ and $\psi_b$ satisfy the following system of boundary integral equations:

$$\mathcal{A}(\omega, \delta)[\Psi] = F, \tag{2.3}$$

where $\mathcal{A}(\omega,\delta) \in \mathcal{L}(\mathcal{H},\mathcal{H}_1)$ is given by

$$\mathcal{A}(\omega,\delta) = \begin{pmatrix} \mathcal{S}_D^{k_b} & -\mathcal{S}_D^{k} \\ -\frac{1}{2}I + \mathcal{K}_D^{k_b,*} & -\delta(\frac{1}{2}I + \mathcal{K}_D^{k,*}) \end{pmatrix},$$

and

$$\Psi = \begin{pmatrix} \psi_b \\ \psi \end{pmatrix}, \quad F = \begin{pmatrix} u^{in} \\ \delta \frac{\partial u^{in}}{\partial \nu} \end{pmatrix}.$$

One can show that the scattering problem (2.1) is equivalent to the boundary integral equations (2.3).

The resonance of the bubble in the scattering problem (2.3) can be defined as all the complex numbers $\omega$ with negative imaginary part such that there exists a nontrivial solution to the following equation:

$$\mathcal{A}(\omega,\delta)[\Psi] = 0. \tag{2.4}$$

These can be viewed as the characteristic values of the operator-valued analytic function (with respect to $\omega$) $\mathcal{A}(\omega,\delta)$. We are interested in the quasi-static resonance of the bubble, which is the resonance frequency at which the size of the bubble is much smaller than the wavelength of the incident wave outside the bubble. In the literature, this resonance is called the Minnaert resonance [40]. Due to our assumptions on the bubble being of size order one, and the wave speed outside of the bubble also being of order one, this resonance should lie in a small neighborhood of the origin in the complex plane. In what follows, we apply the Gohberg-Sigal theory to find this resonance.

We first look at the limiting case when $\delta = \omega = 0$. It is clear that

$$\mathcal{A}_0 := \mathcal{A}(0,0) = \begin{pmatrix} \mathcal{S}_D & -\mathcal{S}_D \\ -\frac{1}{2}I + \mathcal{K}_D^{*} & 0 \end{pmatrix}. \tag{2.5}$$

Let $\mathcal{A}_0^*$ be the adjoint of $\mathcal{A}$.

**Lemma 2.2.1.** *We have*

*(i)* $Ker(\mathcal{A}_0) = span\{\Psi_0\}$ *where*

$$\Psi_0 = \alpha_0 \begin{pmatrix} \psi_0 \\ \psi_0 \end{pmatrix},$$

*with* $\psi_0 = \mathcal{S}_D^{-1}[\mathbb{1}_{\partial D}]$ *and the constant* $\alpha_0$ *being chosen such that* $\|\Psi_0\| = 1$*;*

*(ii)* $Ker(\mathcal{A}_0^*) = span\{\Phi_0\}$ *where*

$$\Phi_0 = \beta_0 \begin{pmatrix} 0 \\ \mathbb{1}_{\partial D} \end{pmatrix}$$

*with the constant* $\beta_0$ *being chosen such that* $\|\Phi_0\| = 1$.

The above lemma shows that $\omega = 0$ is a characteristic value for the operator-valued analytic function $\mathcal{A}(\omega, \delta)$. By Gohberg-Sigal theory, we can conclude the following result about the existence of the quasi-static resonance.

**Lemma 2.2.2.** *For any $\delta$, sufficiently small, there exists a characteristic value $\omega_0 = \omega_0(\delta)$ to the operator-valued analytic function $\mathcal{A}(\omega, \delta)$ such that $\omega_0(0) = 0$ and $\omega_0$ depends on $\delta$ continuously. This characteristic value is also the quasi-static resonance (or Minnaert resonance).*

We next perform asymptotic analysis on the operator $\mathcal{A}(\omega, \delta)$. Using the expansions in Appendix A.1.1, we can derive the following result.

**Lemma 2.2.3.** *In the space $\mathcal{L}(\mathcal{H}, \mathcal{H}_1)$, we have*

$$\mathcal{A}(\omega,\delta) := \mathcal{A}_0+\mathcal{B}(\omega,\delta) = \mathcal{A}_0+\omega\mathcal{A}_{1,0}+\omega^2\mathcal{A}_{2,0}+\omega^3\mathcal{A}_{3,0}+\delta\mathcal{A}_{0,1}+\delta\omega^2\mathcal{A}_{2,1}+O(\omega^4)+O(\delta\omega^3),$$

*where*

$$\begin{aligned}
\mathcal{A}_{1,0} &= \begin{pmatrix} v_b^{-1}\mathcal{S}_{D,1} & -v^{-1}\mathcal{S}_{D,1} \\ 0 & 0 \end{pmatrix}, \quad \mathcal{A}_{2,0} = \begin{pmatrix} v_b^{-2}\mathcal{S}_{D,2} & -v^{-2}\mathcal{S}_{D,2} \\ v_b^{-2}\mathcal{K}_{D,2}^* & 0 \end{pmatrix}, \\
\mathcal{A}_{3,0} &= \begin{pmatrix} v_b^{-3}\mathcal{S}_{D,3} & -v^{-3}\mathcal{S}_{D,3} \\ v_b^{-3}\mathcal{K}_{D,3}^* & 0 \end{pmatrix}, \quad \mathcal{A}_{0,1} = \begin{pmatrix} 0 & 0 \\ 0 & -(\frac{1}{2}I + \mathcal{K}_D^*) \end{pmatrix}, \\
\mathcal{A}_{2,1} &= \begin{pmatrix} 0 & 0 \\ 0 & -v^{-2}\mathcal{K}_{D,2}^* \end{pmatrix}.
\end{aligned} \tag{2.6}$$

We define a projection $\mathcal{P}_0$ from $\mathcal{H}$ to $\mathcal{H}_1$ by

$$\mathcal{P}_0[\Psi] := \langle \Psi, \Psi_0 \rangle \Phi_0,$$

and denote by

$$\tilde{\mathcal{A}}_0 = \mathcal{A}_0 + \mathcal{P}_0.$$

The following results hold.

**Lemma 2.2.4.** *We have*

*(i) The operator $\tilde{\mathcal{A}}_0$ is a bijective operator in $\mathcal{L}(\mathcal{H}, \mathcal{H}_1)$. Moreover, $\tilde{\mathcal{A}}_0[\Psi_0] = \Phi_0$.*

*(ii) The adjoint of $\tilde{\mathcal{A}}_0$, $\tilde{\mathcal{A}}_0{}^*$, is a bijective operator in $\mathcal{L}(\mathcal{H}_1, \mathcal{H})$. Moreover, $\tilde{\mathcal{A}}_0{}^*[\Phi_0] = \Psi_0$.*

*Proof.* By construction, and the fact that $\mathcal{S}_D$ is bijective from $L^2(\partial D)$ to $H^1(\partial D)$ [15], we can show that $\tilde{\mathcal{A}}_0$ is a bijective. So too is $\tilde{\mathcal{A}}_0{}^*$. We only need to show that $\tilde{\mathcal{A}}_0{}^*[\Phi_0] = \Psi_0$. Indeed, we can check that $\mathcal{P}_0^*[\theta] = \langle \theta, \Phi_0 \rangle \Psi_0$. Thus, it follows that

$$\tilde{\mathcal{A}}_0{}^*[\Phi_0] = \mathcal{P}_0^*[\Phi_0] = \langle \Phi_0, \Phi_0 \rangle \Psi_0 = \Psi_0,$$

which completes the proof. □

Our main result in this section is stated in the following theorem. It characterizes the Minnaert frequencies in terms of the shape of the bubbles.

**Theorem 2.2.5.** *In the quasi-static regime, there exists two resonances for a single bubble:*

$$\begin{aligned}\omega_{0,0}(\delta) &= \sqrt{\frac{\mathrm{Cap}_D}{|D|}}v_b\delta^{\frac{1}{2}} - i\frac{\mathrm{Cap}_D^2 v_b^2}{8\pi v|D|}\delta + O(\delta^{\frac{3}{2}}),\\ \omega_{0,1}(\delta) &= -\sqrt{\frac{\mathrm{Cap}_D}{|D|}}v_b\delta^{\frac{1}{2}} - i\frac{\mathrm{Cap}_D^2 v_b^2}{8\pi v|D|}\delta + O(\delta^{\frac{3}{2}}),\end{aligned}$$

*The first resonance $\omega_{0,0}$ is called the Minnaert resonance.*

*Proof.*
**Step 1.** We find the resonance by solving the following equation

$$\mathcal{A}(\omega,\delta)[\Psi_\delta] = 0. \tag{2.7}$$

Since $\mathcal{A}(0,0)[\Psi_0] = 0$, we may view $\Psi_\delta$ as a perturbation of $\Psi_0$ and write it as $\Psi_\delta = \Psi_0 + \Psi_1$. In order to uniquely determine $\Psi_1$, we assume that

$$\langle \Psi_1, \Psi_0\rangle = 0. \tag{2.8}$$

Note that we let the coefficient of $\Psi_0$ to be one for the purpose of normalization. Since $\Psi_\delta$ is defined up to multiplicative constant, (2.8) holds without loss of generality by changing $\Psi_0 + \Psi_1$ to $\Psi_0 + \big(\Psi_1 - \langle\Psi_0,\Psi_1\rangle\Psi_0\big)/(1+\langle\Psi_0,\Psi_1\rangle)$.

**Step 2.** Since $\tilde{\mathcal{A}}_0 = \mathcal{A}_0 + \mathcal{P}_0$, (2.7) is equivalent to the following

$$(\tilde{\mathcal{A}}_0 - \mathcal{P}_0 + \mathcal{B})[\Psi_0 + \Psi_1] = 0.$$

Observe that as the operator $\tilde{\mathcal{A}}_0 + \mathcal{B}$ is invertible for sufficiently small $\delta$ and $\omega$, we can apply $(\tilde{\mathcal{A}}_0 + \mathcal{B})^{-1}$ to both sides of the above equation to deduce that

$$\Psi_1 = (\tilde{\mathcal{A}}_0 + \mathcal{B})^{-1}\mathcal{P}_0[\Psi_0] - \Psi_0 = (\tilde{\mathcal{A}}_0 + \mathcal{B})^{-1}[\Phi_0] - \Psi_0. \tag{2.9}$$

**Step 3.** Using the orthogonality condition (2.8), we arrive at the following equation:

$$A(\omega,\delta) := \Big\langle (\tilde{\mathcal{A}}_0 + \mathcal{B})^{-1}[\Phi_0], \Psi_0 \Big\rangle - 1 = 0 \tag{2.10}$$

**Step 4.** We calculate $A(\omega,\delta)$. Using the identity

$$(\tilde{\mathcal{A}}_0 + \mathcal{B})^{-1} = \Big(I + \tilde{\mathcal{A}}_0{}^{-1}\mathcal{B}\Big)^{-1}\tilde{\mathcal{A}}_0{}^{-1} = \Big(I - \tilde{\mathcal{A}}_0{}^{-1}\mathcal{B} + \tilde{\mathcal{A}}_0{}^{-1}\mathcal{B}\tilde{\mathcal{A}}_0{}^{-1}\mathcal{B} + ...\Big)\tilde{\mathcal{A}}_0{}^{-1},$$

and the fact that

$$\tilde{\mathcal{A}}_0{}^{-1}[\Phi_0] = \Psi_0,$$

we obtain

$$\begin{aligned}
A(\omega,\delta) &= -\omega\left\langle \mathcal{A}_{1,0}[\Psi_0],\Phi_0\right\rangle - \omega^2\left\langle \mathcal{A}_{2,0}[\Psi_0],\Phi_0\right\rangle - \omega^3\left\langle \mathcal{A}_{3,0}[\Psi_0],\Phi_0\right\rangle \\
&\quad -\delta\left\langle \mathcal{A}_{0,1}[\Psi_0],\Phi_0\right\rangle + \omega^2\left\langle \mathcal{A}_{1,0}\tilde{\mathcal{A}_0}^{-1}\mathcal{A}_{1,0}[\Psi_0],\Phi_0\right\rangle \\
&\quad +\omega^3\left\langle \mathcal{A}_{1,0}\tilde{\mathcal{A}_0}^{-1}\mathcal{A}_{2,0}[\Psi_0],\Phi_0\right\rangle + \omega^3\left\langle \mathcal{A}_{2,0}\tilde{\mathcal{A}_0}^{-1}\mathcal{A}_{1,0}[\Psi_0],\Phi_0\right\rangle \\
&\quad +\omega\delta\left\langle \mathcal{A}_{1,0}\tilde{\mathcal{A}_0}^{-1}\mathcal{A}_{0,1}[\Psi_0],\Phi_0\right\rangle + \omega\delta\left\langle \mathcal{A}_{0,1}\tilde{\mathcal{A}_0}^{-1}\mathcal{A}_{1,0}[\Psi_0],\Phi_0\right\rangle \\
&\quad +\omega^3\left\langle \mathcal{A}_{1,0}\tilde{\mathcal{A}_0}^{-1}\mathcal{A}_{1,0}\tilde{\mathcal{A}_0}^{-1}\mathcal{A}_{1,0}[\Psi_0],\Phi_0\right\rangle + O(\omega^4) + O(\delta^2).
\end{aligned}$$

It is clear that $\mathcal{A}_{1,0}^*[\Phi_0]=0$. Consequently, we get

$$\begin{aligned}
A(\omega,\delta) &= -\omega^2\left\langle \mathcal{A}_{2,0}[\Psi_0],\Phi_0\right\rangle - \omega^3\left(\mathcal{A}_{3,0}[\Psi_0],\Phi_0\right) - \delta\left\langle \mathcal{A}_{0,1}[\Psi_0],\Phi_0\right\rangle \\
&\quad +\omega^3\left\langle \mathcal{A}_{2,0}\tilde{\mathcal{A}_0}^{-1}\mathcal{A}_{1,0}[\Psi_0],\Phi_0\right\rangle + \omega\delta\left\langle \mathcal{A}_{0,1}\tilde{\mathcal{A}_0}^{-1}\mathcal{A}_{1,0}[\Psi_0],\Phi_0\right\rangle \\
&\quad +O(\omega^4) + O(\delta^2).
\end{aligned}$$

In the next four steps, we calculate the terms $\langle \mathcal{A}_{2,0}[\Psi_0],\Phi_0\rangle$, $\langle \mathcal{A}_{3,0}[\Psi_0],\Phi_0\rangle$, $\langle \mathcal{A}_{0,1}[\Psi_0],\Phi_0\rangle$, $\left\langle \mathcal{A}_{2,0}\tilde{\mathcal{A}_0}^{-1}\mathcal{A}_{1,0}[\Psi_0],\Phi_0\right\rangle$ and $\left\langle \mathcal{A}_{0,1}\tilde{\mathcal{A}_0}^{-1}\mathcal{A}_{1,0}[\Psi_0],\Phi_0\right\rangle$.

**Step 5.** We have

$$\begin{aligned}
\left\langle \mathcal{A}_{2,0}[\Psi_0],\Phi_0\right\rangle &= \alpha_0\beta_0 v_b^{-2}\left\langle \mathcal{K}_{D,2}^*[\psi_0],\mathbb{1}_{\partial D}\right\rangle = \alpha_0\beta_0 v_b^{-2}\left\langle \psi_0,\mathcal{K}_{D,2}[\mathbb{1}_{\partial D}]\right\rangle \\
&= -\alpha_0\beta_0 v_b^{-2}\int_{\partial D} d\sigma(x)\mathcal{S}_D^{-1}[\mathbb{1}_{\partial D}](x)\int_D dy G^0(x,y) \\
&= -\alpha_0\beta_0 v_b^{-2}\int_D dy\int_{\partial D} d\sigma(x)G^0(x,y)\mathcal{S}_D^{-1}[\mathbb{1}_{\partial D}](x) \\
&= -\alpha_0\beta_0 v_b^{-2}\int_D dy \\
&= -\alpha_0\beta_0 v_b^{-2}|D|.
\end{aligned}$$

**Step 6.** On the other hand, we have

$$\begin{aligned}
\left\langle \mathcal{A}_{3,0}[\Psi_0],\Phi_0\right\rangle &= \alpha_0\beta_0 v_b^{-3}\left\langle \psi_0,\mathcal{K}_{D,3}[\mathbb{1}_{\partial D}]\right\rangle = \alpha_0\beta_0 v_b^{-3}\left\langle \psi_0,\frac{i}{4\pi}|D|\right\rangle \\
&= \alpha_0\beta_0 v_b^{-3}|D|\frac{i}{4\pi}\left\langle \mathcal{S}_D^{-1}[\mathbb{1}_{\partial D}],\mathbb{1}_{\partial D}\right\rangle = -\alpha_0\beta_0 v_b^{-3}|D|\frac{i}{4\pi}\mathrm{Cap}_D.
\end{aligned}$$

**Step 7.** It is easy to see that

$$\left\langle \mathcal{A}_{0,1}[\Psi_0],\Phi_0\right\rangle = -\left\langle \psi_0,\mathbb{1}_{\partial D}\right\rangle = -\alpha_0\beta_0\left\langle \mathcal{S}_D^{-1}[\mathbb{1}_{\partial D}],\mathbb{1}_{\partial D}\right\rangle = \alpha_0\beta_0\mathrm{Cap}_D.$$

**Step 8.** We now calculate the term $\left\langle \mathcal{A}_{0,1}\tilde{\mathcal{A}}_0{}^{-1}\mathcal{A}_{1,0}[\Psi_0], \Phi_0 \right\rangle$. We have

$$\begin{aligned}
\mathcal{A}_{1,0}[\Psi_0] &= \begin{pmatrix} (\tau^{-1}-1)v^{-1}\mathcal{S}_{D,1}[\psi_0] \\ 0 \end{pmatrix} = \begin{pmatrix} (\tau^{-1}-1)v^{-1}\frac{i}{4\pi}\mathrm{Cap}_D \\ 0 \end{pmatrix}, \\
\mathcal{A}^*_{0,1}[\Phi_0] &= \begin{pmatrix} 0 \\ -\left(\frac{1}{2}I + \mathcal{K}_D\right)[\mathbb{1}_{\partial D}] \end{pmatrix} = \begin{pmatrix} 0 \\ -\mathbb{1}_{\partial D} \end{pmatrix}.
\end{aligned}$$

We need to calculate

$$\tilde{\mathcal{A}}_0^{-1}\begin{pmatrix} \mathbb{1}_{\partial D} \\ 0 \end{pmatrix}.$$

Assume that

$$(\mathcal{A}_0 + \mathcal{P}_0)\begin{pmatrix} y_b \\ y \end{pmatrix} = \begin{pmatrix} \mathcal{S}_D[y_b - y] \\ (-\frac{1}{2}I + \mathcal{K}_D^*)[y_b] \end{pmatrix} + (\langle y_b, \psi_0\rangle + \langle y, \psi_0\rangle)\begin{pmatrix} 0 \\ \mathbb{1}_{\partial D} \end{pmatrix} = \begin{pmatrix} \mathbb{1}_{\partial D} \\ 0 \end{pmatrix}$$

By solving the above equations directly, we obtain that $y_b = \frac{1}{2}\psi_0, y = -\frac{1}{2}\psi_0$. Therefore,

$$\tilde{\mathcal{A}}_0^{-1}\begin{pmatrix} \mathbb{1}_{\partial D} \\ 0 \end{pmatrix} = \begin{pmatrix} \frac{1}{2}\psi_0 \\ -\frac{1}{2}\psi_0 \end{pmatrix}.$$

It follows that

$$\left\langle \mathcal{A}_{0,1}\tilde{\mathcal{A}}_0{}^{-1}\mathcal{A}_{1,0}[\Psi_0], \Phi_0 \right\rangle = (\tau^{-1}-1)v^{-1}\frac{i}{8\pi}\mathrm{Cap}_D\langle\psi_0, \mathbb{1}_{\partial D}\rangle = (1-\tau^{-1})v^{-1}\frac{i}{8\pi}\mathrm{Cap}_D^2\alpha_0\beta_0.$$

**Step 9.** We calculate the term $\left\langle \mathcal{A}_{2,0}\tilde{\mathcal{A}}_0{}^{-1}\mathcal{A}_{1,0}[\Psi_0], \Phi_0 \right\rangle$. Using the results in Step 8., we obtain

$$\begin{aligned}
\left\langle \mathcal{A}_{2,0}\tilde{\mathcal{A}}_0{}^{-1}\mathcal{A}_{1,0}[\Psi_0], \Phi_0 \right\rangle &= \left\langle \tilde{\mathcal{A}}_0{}^{-1}\mathcal{A}_{1,0}[\Psi_0], \mathcal{A}^*_{2,0}[\Phi_0] \right\rangle \\
&= \frac{i(\tau^{-1}-1)\tau v_b^{-3}}{8\pi}\mathrm{Cap}_D\alpha_0\beta_0\left\langle \psi_0, \mathcal{K}_{D,2}[\mathbb{1}_{\partial D}] \right\rangle \\
&= \frac{i(1-\tau^{-1})\tau v_b^{-3}}{8\pi}\mathrm{Cap}_D|D|\alpha_0\beta_0.
\end{aligned}$$

**Step 10.** Considering the above results, we can derive

$$\begin{aligned}
A(\omega,\delta) &= \alpha_0\beta_0\Bigg(v_b^{-2}|D|\omega^2 + \frac{i\tau(\tau^{-1}+1)v_b^{-3}|D|\mathrm{Cap}_D}{8\pi}\omega^3 - \mathrm{Cap}_D\delta \\
&\quad -\frac{i(\tau^{-1}-1)v^{-1}\mathrm{Cap}_D^2}{8\pi}\omega\delta\Bigg) \\
&\quad +O(\omega^4) + O(\delta^2).
\end{aligned}$$

We now solve $A(\omega,\delta) = 0$. It is clear that $\delta = O(\omega^2)$, and thus $\omega_0(\delta) = O(\sqrt{\delta})$. Write

$$\omega_0(\delta) = a_1\delta^{\frac{1}{2}} + a_2\delta + O(\delta^{\frac{3}{2}}).$$

We get

$$v_b^{-2}|D|\left(a_1\delta^{\frac{1}{2}}+a_2\delta+O(\delta^{\frac{3}{2}})\right)^2+\frac{i\tau(\tau^{-1}+1)v_b^{-3}|D|\mathrm{Cap}_D}{8\pi}\left(a_1\delta^{\frac{1}{2}}+a_2\delta+O(\delta^{\frac{3}{2}})\right)^3$$
$$-\mathrm{Cap}_D\delta-\frac{i(\tau^{-1}-1)v^{-1}\mathrm{Cap}_D^2}{8\pi}\left(a_1\delta^{\frac{1}{2}}+a_2\delta+O(\delta^{\frac{3}{2}})\right)\delta+O(\delta^2)=0.$$

From the coefficients of the $\delta$ and $\delta^{\frac{3}{2}}$ terms, we obtain

$$v_b^{-2}|D|a_1^2-\mathrm{Cap}_D=0,$$
$$2v_b^{-2}|D|a_1a_2+\frac{i\tau(\tau^{-1}+1)v_b^{-3}|D|\mathrm{Cap}_D}{8\pi}a_1^3-\frac{i(\tau^{-1}-1)v^{-1}\mathrm{Cap}_D^2}{8\pi}a_1=0,$$

which yields

$$\begin{aligned}
a_1 &= \pm\sqrt{\frac{\mathrm{Cap}_D}{|D|}}v_b,\\
a_2 &= -\frac{i(\tau^{-1}+1)v^{-1}\mathrm{Cap}_D}{16\pi}a_1^2+\frac{i(\tau^{-1}-1)\mathrm{Cap}_D^2v_b^2}{16\pi v|D|}\\
&= -\frac{i(\tau^{-1}+1)\mathrm{Cap}_D^2v_b^2}{16\pi v|D|}+\frac{i(\tau^{-1}-1)\mathrm{Cap}_D^2v_b^2}{16\pi v|D|}\\
&= \frac{-i\mathrm{Cap}_D^2v_b^2}{8\pi v|D|}.
\end{aligned}$$

This completes the proof of the theorem. □

A few remarks are in order.

**Remark 2.2.6.** *Using the method developed above, we can also obtain the full asymptotic expansion for the resonance with respect to the small parameter $\delta$.*

**Remark 2.2.7.** *In the case of a collection of $N$ identical bubbles, with separation distance much larger than their characteristic sizes, the Minnaert resonance for a single bubble will be split into $N$ resonances. The splitting will be related to the eigenvalues of a $N$-by-$N$ matrix which encodes information on the configuration of the $N$ bubbles. This can be proved by a similar argument as in [23].*

**Remark 2.2.8.** *Taking into consideration the above theorem, we can deduce that if the bubble is represented by $D = tB$ for some small positive number $t$ and a normalized domain $B$ with size of order one, then the Minnaert resonance for $D$ is given by the following formula*

$$\omega_{0,0}(\delta)=\frac{1}{t}\left[\sqrt{\frac{\mathrm{Cap}_B}{|B|}}v_b\delta^{\frac{1}{2}}-i\frac{\mathrm{Cap}_B^2v_b^2}{8\pi v|B|}\delta+O(\delta^{\frac{3}{2}})\right].$$

**Remark 2.2.9.** *In the special case when $D$ is the unit sphere, we have* $\mathrm{Cap}_D = 4\pi$, $|D| = \frac{4\pi}{3}$. *Consequently,*

$$\begin{aligned}\sqrt{\frac{\mathrm{Cap}_D}{|D|}}v_b &= \sqrt{3}v_b,\\ \frac{\mathrm{Cap}_D^2 v_b^2}{8\pi v|D|} &= \frac{3v_b^2}{2v}.\end{aligned}$$

*Therefore, the Minnaert resonance is given by*

$$\begin{aligned}\omega_{0,0}(\delta) &= \sqrt{3}v_b\delta^{\frac{1}{2}} - i\frac{3v_b^2}{2v}\delta + O(\delta^{\frac{3}{2}}),\\ &= \sqrt{\frac{3\kappa_b}{\rho}} - i\frac{3}{2}\kappa_b\sqrt{\frac{1}{\rho\kappa}} + O((\frac{\rho_b}{\rho})^{\frac{3}{2}}).\end{aligned}$$

## 2.3. The point scatterer approximation

We now solve the scattering problem (2.1) with the incident field $u^{in}$ defined in 1.6. This models the case when the bubble is excited by sources in the far field (throughout the chapter, a point $x$ is said to be in the far field of the bubble $D$ if the distance between $x$ and $D$ is much larger than the size of $D$).

We need the following lemma.

**Lemma 2.3.1.** *The following estimates hold in $\mathcal{H}$:*

$$(\tilde{\mathcal{A}}_0 + \mathcal{B})^{-1}[F] = u^{in}(y_0)\begin{pmatrix}\frac{1}{2}\psi_0\\ -\frac{1}{2}\psi_0\end{pmatrix} + O(\omega) + O(\delta).$$

*Proof.* Let $F = F_1 + F_2$, where

$$F_1 = \begin{pmatrix}u^{in}(y_0)\\ 0\end{pmatrix}, \quad F_2 = F - F_1 = \begin{pmatrix}O(\omega)\\ \delta\frac{\partial u^{in}}{\partial\nu}\end{pmatrix}.$$

It is clear that $F_2 = O(\omega)$ in $\mathcal{H}_1$. Using the fact that

$$(\tilde{\mathcal{A}}_0 + \mathcal{B})^{-1} = {\tilde{\mathcal{A}}_0}^{-1} + O(\omega) + O(\delta),$$

we obtain

$$\begin{aligned}(\tilde{\mathcal{A}}_0 + \mathcal{B})^{-1}[F] &= (\tilde{\mathcal{A}}_0 + \mathcal{B})^{-1}[F_1] + (\tilde{\mathcal{A}}_0 + \mathcal{B})^{-1}[F_2],\\ &= {\tilde{\mathcal{A}}_0}^{-1}[F_1] + O(\omega) + O(\delta),\\ &= u^{in}(y_0)\begin{pmatrix}\frac{1}{2}\psi_0\\ -\frac{1}{2}\psi_0\end{pmatrix} + O(\omega) + O(\delta),\end{aligned}$$

which is the desired result. □

The following monopole approximation holds.

**Theorem 2.3.2.** *In the far field, the solution to the scattering problem (2.1) has the following point-wise behavior*

$$u^s(x) = g(\omega, \delta, D)\,(1 + O(\omega) + O(\delta) + o(1))\,u^{in}(y_0)G^k(x, y_0),$$

*where $y_0$ is the center of the bubble and the scattering coefficient $g$ is given below:*

*(i) Regime I: $\omega \ll \sqrt{\delta}$,*

$$g(\omega, \delta, D) = O(\frac{\omega^2}{\delta}) + O(\omega); \tag{2.11}$$

*(ii) Regime II: $\frac{\omega}{\sqrt{\delta}} = O(1)$,*

$$g(\omega, \delta, D) = \frac{\mathrm{Cap}_D}{1 - (\frac{\omega_M}{\omega})^2 + i\gamma}, \tag{2.12}$$

*where*

$$\omega_M = \sqrt{\frac{\mathrm{Cap}_D}{|D|}} v_b^2 \delta^{\frac{1}{2}}, \quad \gamma = \frac{(\tau^{-1}+1)v^{-1}\mathrm{Cap}_D\omega}{8\pi} - \frac{(\tau^{-1}-1)\mathrm{Cap}_D^2 v_b^2}{8\pi v|D|\omega}\delta$$

*are the real part of the Minnaert resonance frequency and the damping constant respectively. In particular, the Minnaert resonance occurs in this regime.*

*(iii) Regime III: $\sqrt{\delta} \ll \omega \ll 1$,*

$$g(\omega, \delta, D) = \mathrm{Cap}_D + O\left(\frac{\delta}{\omega}\right). \tag{2.13}$$

*Proof.*
**Step 1.** We write $\Psi = \alpha u^{in}(y_0)\Psi_0 + \Psi_1$ with $\langle \Psi_1, \Psi_0 \rangle = 0$. Then,

$$(\tilde{\mathcal{A}}_0 - \mathcal{P}_0 + \mathcal{B})[\alpha u^{in}(y_0)\Psi_0 + \Psi_1] = F$$

implies that

$$\left(I - (\tilde{\mathcal{A}}_0 + \mathcal{B})^{-1}\mathcal{P}_0\right)[\alpha u^{in}(y_0)\Psi_0 + \Psi_1] = (\tilde{\mathcal{A}}_0 + \mathcal{B})^{-1}[F],$$

which yields

$$\alpha u^{in}(y_0)\Psi_0 + \Psi_1 - \alpha u^{in}(y_0)(\tilde{\mathcal{A}}_0 + \mathcal{B})^{-1}\Phi_0 = (\tilde{\mathcal{A}}_0 + \mathcal{B})^{-1}[F].$$

As a result, we get

$$\alpha u^{in}(y_0) \;=\; \frac{\langle (\tilde{\mathcal{A}}_0 + \mathcal{B})^{-1}[F], \Psi_0 \rangle}{1 - \left\langle (\tilde{\mathcal{A}}_0 + \mathcal{B})^{-1}[\Phi_0], \Psi_0 \right\rangle} = -\frac{\langle (\tilde{\mathcal{A}}_0 + \mathcal{B})^{-1}[F], \Psi_0 \rangle}{A(\omega, \delta)},$$

$$\Psi_1 \;=\; (\tilde{\mathcal{A}}_0+\mathcal{B})^{-1}[F]+\alpha u^{in}(y_0)(\tilde{\mathcal{A}}_0+\mathcal{B})^{-1}[\Phi_0]-\alpha u^{in}(y_0)\Psi_0.$$

By Lemma 2.3.1, we have

$$\Psi_1 = u^{in}(y_0)\begin{pmatrix}\frac{1}{2}\psi_0\\ -\frac{1}{2}\psi_0\end{pmatrix}+O(\omega)+O(\delta).$$

**Step 2.** We calculate the scattered far field. Note that

$$\begin{aligned}\mathcal{S}_D^k[\psi_0](x) &= \int_{\partial D} G^k(x,y)\psi_0(y)d\sigma(y)=\int_{\partial D} G^k(x,y_0)(1+O(\omega)+o(1))\psi_0(y)d\sigma(y)\\ &= G^k(x,y_0)\langle \mathcal{S}_D^{-1}[\mathbb{1}_{\partial D}],\mathbb{1}_{\partial D}\rangle(1+O(\omega)+o(1))\\ &= -\mathrm{Cap}_D G^k(x,y_0)(1+O(\omega)+o(1)).\end{aligned}$$

Therefore,

$$\begin{aligned}u^s(x) &= (\alpha_0\alpha u^{in}(y_0)-\frac{1}{2}u^{in}(y_0)+O(\omega)+O(\delta))\mathcal{S}_D^k[\psi_0](x)\\ &= -(\alpha_0\alpha u^{in}(y_0)-\frac{1}{2}u^{in}(y_0)+O(\omega)+O(\delta))\mathrm{Cap}_D G^k(x,y_0)(1+O(\omega)+o(1)),\\ &= g(\omega,\delta,D)u^{in}(y_0)G^k(x,y_0)(1+O(\omega)+O(\delta)+o(1)),\end{aligned}$$

where we have introduced

$$g(\omega,\delta,D)=-(\alpha_0\alpha-\frac{1}{2})\mathrm{Cap}_D. \tag{2.14}$$

$g$ is called the scattering coefficient of the bubble.

**Step 3.** We prove that

$$\alpha=\frac{\left(\omega^2 v_b^{-2}|D|+\delta\mathrm{Cap}_D\right)\beta_0+O(\delta\omega)+O(\omega^3)}{-2A(\omega,\delta)}. \tag{2.15}$$

Let $F=F_1+F_2$, where

$$F_1=\begin{pmatrix}u^{in}\\ 0\end{pmatrix},\quad F_2=F-F_1=\begin{pmatrix}0\\ \delta\frac{\partial u^{in}}{\partial\nu}\end{pmatrix}.$$

Then

$$\alpha u^{in}(y_0)=-\frac{\left\langle(\tilde{\mathcal{A}}_0+\mathcal{B})^{-1}[F_1],\Psi_0\right\rangle+\left\langle(\tilde{\mathcal{A}}_0+\mathcal{B})^{-1}[F_2],\Psi_0\right\rangle}{A(\omega,\delta)}:=-\frac{I_1+I_2}{A(\omega,\delta)}.$$

It is clear that $F_2=O(\delta\omega)$ in $\mathcal{H}_1$, and thus

$$I_2=\langle(\tilde{\mathcal{A}}_0+\mathcal{B})^{-1}[F_2],\Psi_0\rangle=O(\delta\omega).$$

We now investigate $I_1 = \langle(\tilde{\mathcal{A}}_0 + \mathcal{B})^{-1}[F_1], \Psi_0\rangle$. We have

$$\begin{aligned} I_1 &= \left\langle I - \tilde{\mathcal{A}_0}^{-1}\mathcal{B} + \tilde{\mathcal{A}_0}^{-1}\mathcal{B}\tilde{\mathcal{A}_0}^{-1}\mathcal{B} + ...)\tilde{\mathcal{A}_0}^{-1}[F_1], \Psi_0 \right\rangle \\ &= \langle \tilde{\mathcal{A}_0}^{-1}[F_1], \Psi_0\rangle - \langle \mathcal{B}\tilde{\mathcal{A}_0}^{-1}[F_1], \Phi_0\rangle + \langle \mathcal{B}\tilde{\mathcal{A}_0}^{-1}\mathcal{B}\tilde{\mathcal{A}_0}^{-1}[F_1], \Phi_0\rangle + ... \\ &= \langle F_1, \Phi_0\rangle - \langle \tilde{\mathcal{A}_0}^{-1}[F_1], \mathcal{B}^*\Phi_0\rangle + \langle \tilde{\mathcal{A}_0}^{-1}\mathcal{B}\tilde{\mathcal{A}_0}^{-1}[F_1], \mathcal{B}^*[\Phi_0]\rangle + ... \\ &= -\langle \tilde{\mathcal{A}_0}^{-1}[F_1], \mathcal{B}^*[\Phi_0]\rangle + \langle \tilde{\mathcal{A}_0}^{-1}\mathcal{B}\tilde{\mathcal{A}_0}^{-1}[F_1], \mathcal{B}^*[\Phi_0]\rangle + ..., \end{aligned}$$

where we have used the fact that $\langle F_1, \Phi_0\rangle = 0$ and $(\tilde{\mathcal{A}_0}^{-1})^*[\Psi_0] = \Phi_0$.

Note that

$$\mathcal{B}^*[\Phi_0] = \omega\mathcal{A}^*_{1,0}[\Phi_0] + \omega^2\mathcal{A}^*_{2,0}[\Phi_0] + \omega^3\mathcal{A}^*_{3,0}[\Phi_0] + \delta\mathcal{A}^*_{0,1}[\Phi_0] + O(\omega^4) + O(\delta\omega^2).$$

Using the facts that

$$\tilde{\mathcal{A}_0}^{-1}[F_1] = u^{in}(y_0)\begin{pmatrix} \frac{1}{2}\psi_0 \\ -\frac{1}{2}\psi_0 \end{pmatrix} + O(\omega),$$

and

$$\begin{aligned} \mathcal{A}^*_{1,0}[\Phi_0] &= 0, \quad \mathcal{A}^*_{2,0}[\Phi_0] = \beta_0\begin{pmatrix} v_b^{-2}\mathcal{K}^*_{D,2}[\mathbb{1}_{\partial D}] \\ 0 \end{pmatrix}, \\ \mathcal{A}^*_{3,0}[\Phi_0] &= \beta_0\begin{pmatrix} v_b^{-3}\mathcal{K}^*_{D,3}[\mathbb{1}_{\partial D}] \\ 0 \end{pmatrix}, \quad \mathcal{A}^*_{0,1}[\Phi_0] = -\beta_0\begin{pmatrix} 0 \\ \mathbb{1}_{\partial D} \end{pmatrix}, \end{aligned}$$

we can conclude that

$$\begin{aligned} I_1 &= -\left\langle \tilde{\mathcal{A}_0}^{-1}[F_1], \omega^2\mathcal{A}^*_{2,0}[\Phi_0] + \delta\mathcal{A}^*_{0,1}[\Phi_0] + O(\delta\omega) + O(\omega^3)\right\rangle, \\ &= -\frac{1}{2}u^{in}(y_0)\beta_0\left(\omega^2\langle\psi_0, v_b^{-2}\mathcal{K}_{D,2}[\mathbb{1}_{\partial D}]\rangle + \delta\langle\psi_0, \mathbb{1}_{\partial D}\rangle\right) + O(\delta\omega) + O(\omega^3), \\ &= \frac{1}{2}\left(\omega^2 v_b^{-2}|D| + \delta\mathrm{Cap}_D\right)\beta_0 u^{in}(y_0) + O(\delta\omega) + O(\omega^3), \end{aligned}$$

which completes the proof of (2.15).

**Step 4.** Recall the formula for $A(\omega, \delta)$ in the previous section and (2.15), we have

$$-\frac{2g(\omega, \delta, D)}{\mathrm{Cap}_D} = \frac{-\omega^2 v_b^{-2}|D| - \delta\mathrm{Cap}_D + O(\delta\omega) + O(\omega^3)}{\sigma} - 1,$$

where

$$\begin{aligned} \sigma &= v_b^{-2}|D|\omega^2 + \frac{i(\tau^{-1}+1)\tau v_b^{-3}|D|\mathrm{Cap}_D}{8\pi}\omega^3 \\ &\quad -\mathrm{Cap}_D\delta - \frac{i(\tau^{-1}-1)v^{-1}\mathrm{Cap}_D^2}{8\pi}\omega\delta \\ &\quad +O(\omega^4) + O(\delta^2). \end{aligned}$$

The asymptotic behavior of $g$ in different regimes follows immediately from the above formula. This completes the proof of the theorem. □

**Remark 2.3.3.** *Using the method developed above together with the results of Section 2.4, we can derive a similar monopole approximation in the far field for a single bubble in two dimensions.*

## 2.4. The Minnaert resonance in two dimensions

In this section, we derive the Minnaert resonance for a single bubble in two dimensions using the same method we developed for the three-dimensional case. The main differences between the two-dimensional case and the three-dimensional case are as follows: (1) the single layer potential $\mathcal{S}_D$ may not be invertible from $L^2(\partial D)$ to $H^1(\partial D)$ in two dimensions, while this property always holds in three dimensions. We refer to [17, 97] for more detail on this issue; (2) there is a logarithmic singularity in the asymptotic expansion of the single layer potential $\mathcal{S}_D^k$ for small $k$. These create some difficulties which we address here.

Recall that

$$\mathcal{A}(\omega,\delta)=\begin{pmatrix}\mathcal{S}_D^{k_b} & -\mathcal{S}_D^{k}\\ -\frac{1}{2}I+\mathcal{K}_D^{k_b,*} & -\delta(\frac{1}{2}I+\mathcal{K}_D^{k,*})\end{pmatrix},$$

where the boundary integral operators $\mathcal{S}_D^k$ and $\mathcal{K}_D^{k,*}$ are defined Section 1.3 and their asymptotic expansions are given in Appendix A.1.2.

We denote by

$$\mathcal{A}_0:=\begin{pmatrix}\hat{\mathcal{S}}_D^{k_b} & -\hat{\mathcal{S}}_D^{k}\\ -\frac{1}{2}I+\mathcal{K}_D^{*} & 0\end{pmatrix}, \tag{2.16}$$

where $\hat{\mathcal{S}}_D^k$ (resp. $\hat{\mathcal{S}}_D^{k_b}$) is defined by (A.9) (resp. with $k$ replaced by $k_b$).

Note that the kernel space of the operator $-\frac{1}{2}I+\mathcal{K}_D^*$ has dimension one. We choose $\psi_0$ to be the real-valued function in this kernel space which has unit norm in $L^2(\partial D)$. We have $\mathcal{K}_D^*[\psi_0]=\frac{1}{2}\psi_0$. One can show that

$$\mathcal{S}_D[\psi_0]=\gamma_0 \quad \text{on } \partial D \tag{2.17}$$

for some constant $\gamma_0$ (see [17, 97]). There are two cases:

(i) Case I: $\gamma_0=0$.

(ii) Case II: $\gamma_0\neq 0$.

In Case I, it is clear that $\mathcal{S}_D$ is not invertible from $L^2(\partial D)$ to $H^1(\partial D)$. In case II, we can show that $\mathcal{S}_D$ is invertible from $L^2(\partial D)$ to $H^1(\partial D)$.

In Case II, we remark that $\langle \mathbb{1}_{\partial D},\psi_0\rangle \neq 0$. Indeed, assume on the contrary that $\langle \mathbb{1}_{\partial D},\psi_0\rangle=0$. Then

$$\langle \mathcal{S}_D[\psi_0],\psi_0\rangle=\gamma_0\langle \mathbb{1}_{\partial D},\psi_0\rangle=0,$$

which further implies that $\psi_0=0$. This contradiction proves our assertion.

**Lemma 2.4.1.** *In both cases, the operator $\hat{\mathcal{S}}_D^k$ is invertible in $\mathcal{L}(L^2(\partial D), H^1(\partial D))$.*

*Proof.* We first show that $\hat{\mathcal{S}}_D^k$ is injective. Assume that

$$\hat{\mathcal{S}}_D^k[y] = \mathcal{S}_D[y] + \eta_k \langle y, \mathbb{1}_{\partial D}\rangle = 0 \quad \text{for some } y \in L^2(\partial D).$$

In Case I, we have $\mathcal{S}_D[y] \perp \psi_0$ in $L^2(\partial D)$, therefore, $\eta_k \langle y, \mathbb{1}_{\partial D}\rangle \langle \mathbb{1}_{\partial D}, \psi_0\rangle = 0$. Since $\langle \mathbb{1}_{\partial D}, \psi_0\rangle \neq 0$, we obtain $\langle y, \mathbb{1}_{\partial D}\rangle = 0$. It follows that $\mathcal{S}_D[y] = 0$. But this implies that $y = c\psi_0$ for some constant $c$. Using the condition $\langle y, \mathbb{1}_{\partial D}\rangle = 0$ again, we derive $c = 0$, which shows that $y = 0$.

In Case II, we have $\mathcal{S}_D[\psi_0] \neq 0$. Since $\mathcal{S}_D[y] = -\eta_k \langle y, \mathbb{1}_{\partial D}\rangle$, we see that $y = c\psi_0$ for some constant $c$. Therefore,

$$\gamma_0 c + \eta_k c \langle \psi_0, 1\rangle = c(\gamma_0 + \eta_k \langle \psi_0, \mathbb{1}_{\partial D}\rangle) = 0.$$

Note that $\gamma_0 + \eta_k \langle \psi_0, \mathbb{1}_{\partial D}\rangle \neq 0$, which follows from the fact that both $\gamma_0$ and $\langle \psi_0, \mathbb{1}_{\partial D}\rangle$ are real numbers while $\eta_k$ is a complex number with nonzero imaginary part. Thus we have $c = 0$, and $y = 0$ follows immediately.

The surjectivity of $\hat{\mathcal{S}}_D^k$ follows from the fact that $\hat{\mathcal{S}}_D^k$ is Fredholm with index zero. This completes the proof of the lemma. □

We have the following properties for the operator $\mathcal{A}_0$.

**Lemma 2.4.2.** *We have*

*(i)* $Ker(\mathcal{A}_0) = span\{\Psi_0\}$ *where*

$$\Psi_0 = \alpha_0 \begin{pmatrix} \psi_0 \\ a\psi_0 \end{pmatrix}$$

*with*

$$a = \begin{cases} \dfrac{\eta_{k_b}}{\eta_k}, & \text{in Case I,} \\ \dfrac{\gamma_0 + \langle \psi_0, \mathbb{1}_{\partial D}\rangle \eta_{k_b}}{\gamma_0 + \langle \psi_0, \mathbb{1}_{\partial D}\rangle \eta_k}, & \text{in Case II,} \end{cases}$$

*and the constant $\alpha_0$ being chosen such that $\|\Psi_0\| = 1$;*

*(ii)* $Ker(\mathcal{A}_0^*) = span\{\Phi_0\}$ *where*

$$\Phi_0 = \beta_0 \begin{pmatrix} 0 \\ \mathbb{1}_{\partial D} \end{pmatrix}$$

*with the constant $\beta_0$ being chosen such that $\|\Phi_0\| = 1$.*

*Proof.* We first find the kernel space of $\mathcal{A}_0$. Assume that

$$\mathcal{A}_0 \begin{pmatrix} y_b \\ y \end{pmatrix} = \begin{pmatrix} \hat{\mathcal{S}}_D^{k_b}[y_b] - \hat{\mathcal{S}}_D^{k}[y] \\ (-\frac{1}{2}I + \mathcal{K}_D^*)[y_b] \end{pmatrix} = 0 \quad \text{for some } y, y_b \in L^2(\partial D).$$

We have

$$\begin{aligned} \mathcal{S}_D[y_b - y] + \eta_{k_b}\langle y_b, \mathbb{1}_{\partial D}\rangle - \eta_k \langle y, \mathbb{1}_{\partial D}\rangle &= 0 \quad \text{on } \partial D, \qquad (2.18) \\ (-\frac{1}{2}I + \mathcal{K}_D^*)[y_b] &= 0 \quad \text{on } \partial D. \qquad (2.19) \end{aligned}$$

From (2.19), we see that $y_b$ is a multiple of $\psi_0$. We let $y_b = \psi_0$. We now find the function $y$.

In Case I, we have $\mathcal{S}_D[y_b - y] \perp \psi_0$. Similarly to the proof in Lemma 2.4.1, we can derive that $y = c\psi_0$ for some constant $c$ which satisfies

$$\eta_{k_b}\langle \psi_0, \mathbb{1}_{\partial D}\rangle - \eta_k c \langle \psi_0, \mathbb{1}_{\partial D}\rangle = 0.$$

Thus, it follows that $c = \eta_{k_b}/\eta_k$.

In Case II, $\mathcal{S}_D$ is invertible. From (2.18), we can derive that $\psi_0 - y$ is a multiple of $\psi_0$, which further implies that $y = c\psi_0$ for some constant $c$. Plugging this back to (2.18), we obtain

$$(1-c)\gamma_0 + \eta_{k_b}\langle \psi_0, \mathbb{1}_{\partial D}\rangle - \eta_k c \langle \psi_0, \mathbb{1}_{\partial D}\rangle = 0.$$

Therefore,

$$c = \frac{\gamma_0 + \langle \psi_0, \mathbb{1}_{\partial D}\rangle \eta_{k_b}}{\gamma_0 + \langle \psi_0, \mathbb{1}_{\partial D}\rangle \eta_k}.$$

Note that $\gamma_0 + \langle \psi_0, \mathbb{1}_{\partial D}\rangle \eta_k \neq 0$ because the $\eta_k$ has nonzero imaginary part. This completes the proof of the first part of the Lemma.

The second part of the Lemma follows easily from the fact that the operator $\hat{\mathcal{S}}_D^k$ is injective. This completes the proof of the Lemma. □

We next perform an asymptotic analysis in terms of $\delta$ and $\omega$ on the operator $\mathcal{A}(\omega, \delta)$.

**Lemma 2.4.3.** *In the space $\mathcal{L}(\mathcal{H}, \mathcal{H}_1)$, we have*

$$\mathcal{A}(\omega,\delta) := \mathcal{A}_0 + \mathcal{B}(\omega,\delta) = \mathcal{A}_0 + \omega^2 \ln\omega \mathcal{A}_{1,1,0} + \omega^2 \mathcal{A}_{1,2,0} + \delta \mathcal{A}_{0,1} + O(\delta\omega^2 \ln\omega) + O(\omega^4 \ln\omega),$$

*where*

$$\begin{aligned} \mathcal{A}_{1,1,0} &= \begin{pmatrix} v_b^{-2}\mathcal{S}_{D,1}^{(1)} & -v^{-2}\mathcal{S}_{D,1}^{(1)} \\ v_b^{-2}\mathcal{K}_{D,1}^{(1),*} & 0 \end{pmatrix}, \\ \mathcal{A}_{1,2,0} &= \begin{pmatrix} v_b^{-2}\left(\ln v_b^{-1}\mathcal{S}_{D,1}^{(1)} + \mathcal{S}_{D,1}^{(2)}\right) & -v^{-2}\left(\ln v^{-1}\mathcal{S}_{D,1}^{(1)} + \mathcal{S}_{D,1}^{(2)}\right) \\ v_b^{-2}\left(\ln v_b^{-1}\mathcal{K}_{D,1}^{(1),*} + \mathcal{K}_{D,1}^{(2),*}\right) & 0 \end{pmatrix}, \qquad (2.20) \\ \mathcal{A}_{0,1} &= \begin{pmatrix} 0 & 0 \\ 0 & -(\frac{1}{2}I + \mathcal{K}_D^*) \end{pmatrix}. \end{aligned}$$

We define a projection $\mathcal{P}_0$ by

$$\mathcal{P}_0[\Psi] := \langle \Psi, \Psi_0 \rangle \Phi_0,$$

and denote by

$$\tilde{\mathcal{A}}_0 = \mathcal{A}_0 + \mathcal{P}_0.$$

With the help of Lemma 2.4.1, we can establish the following results.

**Lemma 2.4.4.** *We have*

*(i) The operator $\tilde{\mathcal{A}}_0$ is a bijective operator in $\mathcal{L}(\mathcal{H}, \mathcal{H}_1)$. Moreover, $\tilde{\mathcal{A}}_0[\Psi_0] = \Phi_0$;*

*(ii) ${\tilde{\mathcal{A}}_0}^*$ is a bijective operator in $\mathcal{L}(\mathcal{H}_1, \mathcal{H})$. Moreover, ${\tilde{\mathcal{A}}_0}^*[\Phi_0] = \Psi_0$.*

Our main results in two dimensions are summarized in the following theorem.

**Theorem 2.4.5.** *In the quasi-static regime, there exist resonances (or the Minnaert resonance) for a single bubble. Their leading order terms are given by the roots of the following equation:*

$$\omega^2 \ln \omega + \left( \ln v_b^{-1} + 1 + \frac{c_1}{b_1} - \frac{\gamma_0}{(\psi_0, 1)} \right) \omega^2 - \frac{1}{4|D|} \frac{a\delta}{b_1} = 0, \tag{2.21}$$

*where the constants $b_1, c_1$ are defined in Section A.1.2, $\gamma_0$ in (2.17) and $a$ in Lemma 2.4.2.*

*Proof.* As in Theorem 2.2.5, we can show that the resonances are the roots of the following equation

$$A(\omega, \delta) := \left\langle (\tilde{\mathcal{A}}_0 + \mathcal{B})^{-1}[\Phi_0], \Psi_0 \right\rangle - 1 = 0.$$

By a direct calculation, we further have

$$\begin{aligned} A(\omega, \delta) &= -\omega^2 \ln \omega \, \langle \mathcal{A}_{1,1,0}[\Psi_0], \Phi_0 \rangle - \omega^2 \, \langle \mathcal{A}_{1,2,0}[\Psi_0], \Phi_0 \rangle \\ &\quad -\delta \, \langle \mathcal{A}_{0,1}[\Psi_0], \Phi_0 \rangle + O(\omega^4 \ln \omega) + O(\delta \omega^2 \ln \omega). \end{aligned}$$

It is clear that

$$\begin{aligned} (\mathcal{A}_{1,1,0})^*[\Phi_0] &= \begin{pmatrix} \beta_0 v_b^{-2} \mathcal{K}_{D,1}^{(1)}[\mathbb{1}_{\partial D}] \\ 0 \end{pmatrix}, \\ (\mathcal{A}_{1,2,0})^*[\Phi_0] &= \begin{pmatrix} \beta_0 v_b^{-2} (\ln v_b^{-1} \mathcal{K}_{D,1}^{(1)}[\mathbb{1}_{\partial D}] + \mathcal{K}_{D,1}^{(2)}[\mathbb{1}_{\partial D}]) \\ 0 \end{pmatrix}, \\ \mathcal{A}_{0,1}[\Psi_0] &= \begin{pmatrix} 0 \\ -\alpha_0 v_b^{-2} (\frac{1}{2} I + \mathcal{K}_D^*)[a\psi_0] \end{pmatrix} = \begin{pmatrix} 0 \\ -\alpha_0 a v_b^{-2} \psi_0 \end{pmatrix}. \end{aligned}$$

It follows that

$$\begin{aligned}
\langle \mathcal{A}_{1,1,0}[\Psi_0], \Phi_0\rangle &= \alpha_0\beta_0\langle \psi_0, v_b^{-2}\mathcal{K}_{D,1}^{(1)}[\mathbb{1}_{\partial D}]\rangle = \alpha_0\beta_0\langle \psi_0, v_b^{-2}4\bar{b}_1|D|\rangle \\
&= 4\alpha_0\beta_0 v_b^{-2} b_1|D|\langle \psi_0, \mathbb{1}_{\partial D}\rangle; \\
\langle \mathcal{A}_{1,2,0}[\Psi_0], \Phi_0\rangle &= \alpha_0\beta_0\left\langle \psi_0, v_b^{-2}[\ln v_b^{-1}\mathcal{K}_{D,1}^{(1)}[\mathbb{1}_{\partial D}] + \mathcal{K}_{D,1}^{(2)}[\mathbb{1}_{\partial D}]\right\rangle \\
&= 4\alpha_0\beta_0 v_b^{-2}\ln v_b^{-1} b_1|D|\langle \psi_0, \mathbb{1}_{\partial D}\rangle + \\
&\quad \alpha_0\beta_0 v_b^{-2}\left\langle \psi_0, (2\bar{b}_1 + 4\bar{c}_1)|D| + 4\bar{b}_1\int_D \ln|x-y|dy\right\rangle \\
&= \alpha_0\beta_0 v_b^{-2}|D|(4b_1\ln v_b^{-1} + 4b_1 + 4c_1)\langle \psi_0, \mathbb{1}_{\partial D}\rangle + 4b_1\alpha_0\beta_0 v_b^{-2}\langle \psi_0, \int_D \ln|x-y|dy\rangle \\
&= 4\alpha_0\beta_0 v_b^{-2}|D|(b_1\ln v_b^{-1} b_1 + b_1 + c_1)\langle \psi_0, \mathbb{1}_{\partial D}\rangle - 4b_1\alpha_0\beta_0 v_b^{-2}\gamma_0|D|; \\
(\mathcal{A}_{0,1}[\Psi_0], \Phi_0) &= -\alpha_0\beta_0 a v_b^{-2}\langle \psi_0, \mathbb{1}_{\partial D}\rangle,
\end{aligned}$$

where we have used the fact

$$\begin{aligned}
\langle \psi_0, \int_D \ln|x-y|dy\rangle &= \int_{\partial D}\psi_0(x)d\sigma(x)\int_{\partial D}\ln|x-y|dy = \int_D dy\int_{\partial D}\ln|x-y|\psi_0(x)d\sigma(x) \\
&= \int_D -\gamma_0 dy = -\gamma_0|D|
\end{aligned}$$

in the second equality above. Therefore, we derive that

$$\begin{aligned}
4b_1|D|\langle \psi_0, \mathbb{1}_{\partial D}\rangle\omega^2\ln\omega + 4\bigg(|D|(b_1\ln v_b^{-1} + b_1 + c_1)\langle \psi_0, \mathbb{1}_{\partial D}\rangle - b_1\gamma_0|D|\bigg)\omega^2 \\
-a\delta\langle \psi_0, \mathbb{1}_{\partial D}\rangle + O(\omega^4\ln\omega) + O(\delta\omega^2\ln\omega) = 0.
\end{aligned}$$

This completes the proof of the lemma. □

**Remark 2.4.6.** *In the special case when $D$ is the unit disk, we have $|D| = \pi$ and $\gamma_0 = 0$. Therefore, the Minnaert resonance in two dimensions is given by the roots of the following equation:*

$$\omega^2\ln\omega + (\ln v_b^{-1} + 1 + \frac{c_1}{b_1})\omega^2 - \frac{1}{4\pi}\frac{a\delta}{b_1} = 0. \tag{2.22}$$

**Remark 2.4.7.** *We can use the same method as in Section 2.3 to derive the point scatterer approximation for the scattering by a single bubble in two dimensions.*

## 2.5. Numerical illustrations

In this section we perform a numerical simulation to validate the formula for the Minnaert resonant frequency in two dimensions which we derived in Theorem 2.4.5.

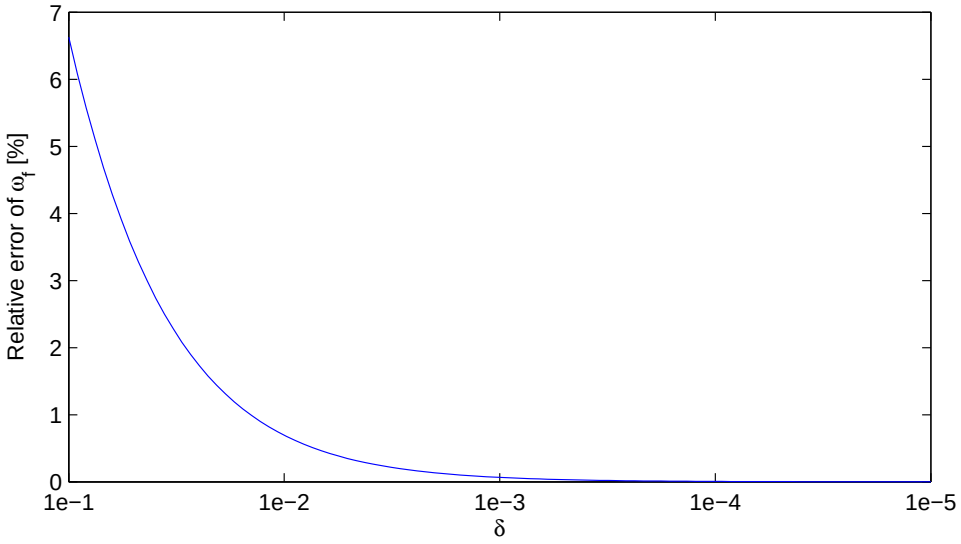


Figure 2.1.: The relative error of the Minnaert resonance $\omega_c$ obtained by the two dimensional formula (2.22) becomes negligible when we are in the appropriate high contrast regime.

We first determine the characteristic value $\omega_c$ of $\mathcal{A}(\omega, \delta)$ in (2.4) numerically. We then calculate the complex root $\omega_f$ of (2.22) that has a positive real part. Comparing $\omega_c$ and $\omega_r$ over a range of appropriate values of $\delta$ allows us to judge the accuracy of the formula.

In order to perform the analysis in the appropriate regime, which was described in Section 2.2, we take $\rho = \kappa = 1000$ and $\rho_b = \kappa_b = c$, where $c$ is chosen such that the wave speed in both air and water is of order 1 and $\delta \in \{10^{-i}\}$, $i \in \{1, \ldots, 5\}$. We use $2^9$ points to discretize the unit circle used in the calculation of the layer potentials that form $\mathcal{A}$. Calculating $\omega_c$ is equivalent to determining the smallest $\omega$ such that $\mathcal{A}(\omega, \delta)$ has a zero eigenvalue. We have

$$\omega_c = \min_{\omega \in \mathbf{C}} \{\omega |\ \lambda(\omega) = 0\} \quad \lambda \in \sigma(\mathcal{A}(\omega, \delta)),$$

and we approach $\lambda(\omega) = 0$ as a complex root finding problem which can be calculated using Muller's method [17, 36]. Muller's method is applied again in order to find the root $\omega_f$ satisfying (2.22). The resonant frequencies $\omega_c$ and $\omega_f$, along with the relative errors, for specific values of $\delta$ are given in Table 2.1. In Figure 2.1 it can be seen that the relative error becomes very small when $\delta \ll 1$, confirming the excellent accuracy of the formula. In particular, we note that when $\delta = 10^{-3}$, which is close to the usual contrast between water and air, the difference between $\omega_c$ and $\omega_f$ is negligible with a relative error of only 0.0652%.

| $\delta$ | $\omega_c$ | $\omega_f$ | Relative error |
|---|---|---|---|
| $10^{-1}$ | $0.261145 - 0.150949i$ | $0.250455 - 0.134061i$ | 5.8203% |
| $10^{-2}$ | $0.075146 - 0.023976i$ | $0.074681 - 0.023687i$ | 0.6727% |
| $10^{-3}$ | $0.021001 - 0.004513i$ | $0.020987 - 0.004508i$ | 0.0652% |
| $10^{-4}$ | $0.005950 - 0.000959i$ | $0.005949 - 0.000959i$ | 0.0062% |
| $10^{-5}$ | $0.001714 - 0.000221i$ | $0.001714 - 0.000221i$ | 0.0030% |

Table 2.1.: A comparison between the characteristic value $\omega_c$ of $\mathcal{A}(\omega, \delta)$ and the root of the two dimensional resonance formula (2.22) with positive real part $\omega_f$, over several values of $\delta$.

## 2.6. Concluding remarks

In this chapter we have investigated the acoustic wave propagation problem in bubbly media and for the first time rigorously derived the low frequency Minnaert resonances. Furthermore, we have provided a mathematical justification for the monopole approximation. Our results are validated by several numerical experiments in two dimensions. The techniques developed in this chapter can be used in characterizing bubbly media from spectroscopic measurements of the velocity and attenuation of ultrasound waves. They can be easily extended to viscous liquids [60]. They definitively open a door for a mathematical and numerical framework for investigating acoustic wave propagation in bubbly media. Based on the framework introduced in this chapter, it will be shown in Chapter 3 that the super-absorption effect can be achieved using bubble meta-screens. In Chapter 5, we will mathematically justify Foldy's approximation and quantify time-reversal and the super-focusing effect in bubbly media probed near and below their Minnaert resonant frequencies [25].

# 3. Perfect Absorption using Sub-wavelength Acoustic Resonators

The aim of this chapter is to provide a mathematical and numerical framework for the analysis and design of bubble meta-screens. An acoustic meta-screen is a thin sheet with patterned sub-wavelength structures, which nevertheless has a macroscopic effect on acoustic wave propagation. In this chapter, periodic sub-wavelength bubbles mounted on a reflective surface (with Dirichlet boundary conditions) are considered. It is shown that the structure behaves as an equivalent surface with Neumann boundary conditions at the Minnaert resonant frequency which corresponds to a wavelength much greater than the size of the bubbles. An analytical formula for this resonance is derived. Numerical simulations confirm its accuracy and show how it depends on the ratio between the periodicity of the lattice, the size of the bubble, and the distance of the meta-screen from the reflective surface. The results of this chapter formally explain the super-absorption behavior observed in [V. Leroy et al., Phys. Rev. B, 2015].

## 3.1. Introduction

In this chapter we study the reflection properties of a meta-screen from a mathematical point of view. Broadly speaking, a meta-screen is a thin sheet with patterned sub-wavelength structures which has a macroscopic effect on the reflection and transmission of waves.

One way to design meta-screens is to place microscopic gas inclusions along a periodic lattice. The properties of such screens have been studied in recent years, with spectacular results. In [70, 71], it was experimentally shown how the reflection and transmission coefficients vary with respect to the wavelength of the incoming acoustic wave. It was later shown how super-absorption may be achieved with these meta-screens [72], *i.e.*, vanishing reflection and transmission coefficients.

These phenomena can be explained by the use of sub-wavelength resonators in the design of the meta-screens. In [21] for instance, a mathematical justification was given for a meta-screen made of sub-wavelength plasmonic particles, in which resonance is due to a negative dielectric coefficient [19]. Helmholtz resonators can also be used in such designs [23, 95]. Here, we focus on Minnaert bubbles, which act like plasmonic nanoparticules. We refer the reader to [19, 22, 26, 27, 53] for the mathematical analysis of resonances for plasmonic nanoparticles.

In the present chapter, we use similar techniques as in [21] to study the reflection properties of a meta-screen when both the typical size of the periodic cell, and the size of the bubbles are sub-wavelength, and the contrast $\delta^{-1}$ is large. We also investigate the limiting case when the typical size of the periodic cell goes to 0 and $\delta$ goes to 0, proportional to the square of the typical size of the periodic cell. Note that in the case where $\delta$ is a fixed parameter, the usual homogenization techniques can be applied, and a large literature already exists on describing boundary layer effects [1, 2, 4]. In our case, because of the excitation of resonance, one must resort to other methods. The idea of using an unbounded parameter as the size of the cells goes to zero is not new, and is sometimes referred to as high-contrast homogenization [30, 34, 45]. This technique has already been successful in explaining some spectacular physical phenomena [29].

Our main result is the following. We consider periodic sub-wavelength bubbles above a reflective surface (with Dirichlet boundary conditions). Then, under the appropriate scaling $\delta = \mu(\varepsilon a)^2$, the Minnaert resonance can be excited at a fixed frequency of order one, and the surface behaves as an equivalent surface with Neumann boundary condition at this frequency at the limit $\varepsilon a \to 0$. The theorem is valid for all shapes of Minnaert resonators. When taking into account some extra physical damping effects that do not appear in our mathematical model [60], this eventually explains the super-absorption behavior witnessed in [72] (see Remark 3.2.4). The Dirichlet boundary condition is used only for simplicity of the presentation. Similar effective boundary conditions can be obtained by using exactly the same approach presented here for a penetrable half-space.

The chapter is structured as follows. In Section 3.2, we fix the notations of the experiment under consideration, and state our main result, the proof of which is detailed in Section 3.3. The proof uses layer potential techniques and asymptotic expansions. Finally, numerical results are presented in Section 3.4.

## 3.2. Statement of the problem

We consider a reflective surface, on top of which small scatterers are arranged along some periodic lattice. A typical example of such a situation is air bubbles arranged in water, as described in [72, 71].

Let us fix some notation. We will state our results in dimension $d \in \{2, 3\}$, and write $\mathbb{R}^d \ni x = (\bar{x}, x_d)$, with $\bar{x} \in \mathbb{R}^{d-1}$ and $x_d \in \mathbb{R}$.

The geometry of the meta-screen problem is shown in Figure 3.1. We let $\partial\mathbb{R}^d_+ := \{x \in \mathbb{R}^d,\ x_d = 0\}$ represent the reflective plane, and $\mathbb{R}^d_\pm := \{x \in \mathbb{R}^d,\ \pm x_d > 0)$ be the upper and lower half space.

The shape of the bubbles is described by a simply connected domain $D \subset \mathbb{R}^d_+$ with smooth boundary $\partial D$. The bubbles are arranged periodically along a lattice $\mathcal{R}$ of $\mathbb{R}^{d-1}$.

For instance, if $d = 2$, then $\mathcal{R} = a\mathbb{Z}$ for some $a > 0$. The background medium is $\mathbb{R}^d_+ \setminus \overline{\Omega^\varepsilon}$.

For $\varepsilon > 0$, we denote by $\Omega^\varepsilon$ the volume occupied by the bubbles. More specifically, we set

$$\Omega^\varepsilon := \bigcup_{R \in \mathcal{R}} \varepsilon \left(D + R\right).$$

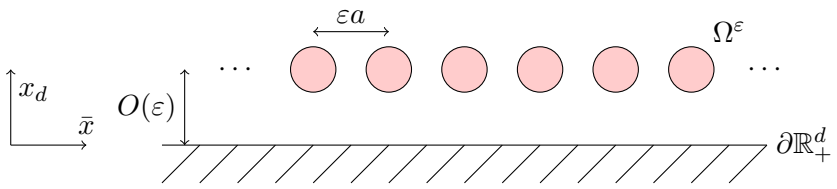


Figure 3.1.: The geometry of the bubble meta-screen.

We consider the scattering of acoustic waves by this meta-screen.

We assume that $\delta \ll 1$. With appropriate physical units, we also assume that $k = O(1)$, $k_b = O(1)$, and the size of $D$ is also of order one.

Let $U^{\text{in}}$ be the incoming plane wave impinging on the plane $\partial\mathbb{R}^d_+$ from the upper half-space. More specifically,

$$U^{\text{in}} = U^{\text{in}}_{\mathbf{k}}(X) = u_0 \mathrm{e}^{-\mathrm{i}\mathbf{k}\cdot X} = u_0 \mathrm{e}^{-\mathrm{i}\bar{k}\cdot\bar{X}} \mathrm{e}^{-\mathrm{i}k_d X_d},$$

where $u_0$ is the amplitude of the incident plane wave and $\mathbf{k} = (\bar{k}, k_d) \in \mathbb{R}^{d-1} \times \mathbb{R}$, with $k_d > 0$ and $|\mathbf{k}| = k$, is the wave vector. The acoustic scattering problem can be modeled by the following system of equations (we use capital letters for macroscopic fields)

$$\begin{cases} (\Delta + k^2)U^\varepsilon = 0 & \text{in } \mathbb{R}^d_+ \setminus \overline{\Omega^\varepsilon}, \\ (\Delta + k_b^2)U^\varepsilon = 0 & \text{in } \Omega^\varepsilon, \\ U^\varepsilon|_- = U^\varepsilon|_+ & \text{on } \partial\Omega^\varepsilon, \\ \dfrac{1}{\rho_b}\dfrac{\partial U^\varepsilon}{\partial \nu}\Big|_- = \dfrac{1}{\rho}\dfrac{\partial U^\varepsilon}{\partial \nu}\Big|_+ & \text{on } \partial\Omega^\varepsilon, \\ U^\varepsilon = 0 & \text{on } \partial\mathbb{R}^d_+. \end{cases} \tag{3.1}$$

Similar to diffraction problems for gratings, the above system of equations is complemented by certain outgoing radiation condition imposed on the scattered field $U^s := U^\varepsilon - U^{\text{in}}$. More precisely, we are interested in the quasi-periodic solutions such that

$$U^\varepsilon(\bar{X} + \varepsilon R, X_d) = e^{-i\mathbf{k}\cdot\varepsilon R} U^\varepsilon(X)$$

for all $\bar{X} \in \mathbb{R}^{d-1}, R \in \mathcal{R}$. Therefore in the domain above the layer of bubbles, we have the usual Rayleigh-Bloch expansion for the scattered field. Then the outgoing radiation condition can be imposed by assuming that all the modes in the Rayleigh-Bloch expansion are either decaying exponentially or propagating along the $X_d$-direction. Since in our case we assume that the period of the bubble structure is of order $\varepsilon$ which is much smaller than $k = O(1)$, the outgoing radiation condition takes the following specific form

$$U^s(X) \sim a\mathrm{e}^{-\mathrm{i}\bar{k}\cdot\bar{X}}\mathrm{e}^{\mathrm{i}k_d X_d} \quad \text{as} \quad X_d \to \infty. \tag{3.2}$$

for some constant $a$. In the general case where $U^{\text{in}}$ is a superposition of plane waves, we can decompose $U^{\text{in}}$ using Bloch-Floquet theory [93, 17]. We obtain a family of problems to solve, each one with its own outgoing radiation condition. The final solution is then the superposition of all these solutions. The solution $U^\varepsilon$ to (3.1)-(3.2) is to be found in the set $\mathcal{H} := \{u \in H^1_{\text{loc}}(\mathbb{R}^d_+) : u = 0 \text{ on } \partial\mathbb{R}^d_+\}$.

Such problems have been extensively studied using homogenization theory in recent decades. For instance, the scattered field is well-understood as $\varepsilon \to 0$, and is of order $\varepsilon$ [2, 4, 5]. In the present chapter, we study the special case where the contrast $\delta$ is also scaled with $\varepsilon \to 0$. As we will see, such a regime, which is accessible physically, presents some interesting features.

More specifically, according to [8], there is a resonance phenomenon in the regime $\sqrt{\delta} \sim \varepsilon$ (Minnaert resonance). In the sequel, we fix $\mu > 0$, and study (3.1), with

$$\delta := \delta_\varepsilon = \mu\varepsilon^2.$$

In this case, standard homogenization techniques are no longer applicable and new techniques are needed.

In the absence of bubbles (*i.e.*, $D = \emptyset$), the solution of (3.1) is simply

$$U_0(X) := U^{\text{in}}_{\mathbf{k}}(\bar{X}, X_d) - U^{\text{in}}_{\mathbf{k}}(\bar{X}, -X_d) = -2\mathrm{i}u_0\mathrm{e}^{-\mathrm{i}\bar{k}\cdot\bar{X}}\sin(k_d X_d). \tag{3.3}$$

Note that $U_0(X) - U^{\text{in}}_{\mathbf{k}}(\bar{X}, X_d)$ satisfies the outgoing radiation condition (3.2).

In the presence of bubbles, we expect this solution to be perturbed. Our goal is to describe the main contribution of this perturbation. In order to state our results, we introduce some extra-notation. First, we introduce a constant $\mu_M$ defined by

$$\mu_M := \frac{k_b^2|D|}{C^+_{D,\mathcal{R}}}, \tag{3.4}$$

where $|D|$ is the volume of $D$, and $C^+_{D,\mathcal{R}}$ is the periodic capacity defined in Definition 3.3.5. Then we introduce the scattering function

$$g_s(\mu,\varepsilon) := \frac{\varepsilon M_1}{1 - \frac{\mu_M}{\mu} - \varepsilon\mathrm{i}\frac{M_1^2 k_d C^+_{D,\mathcal{R}}}{|\Gamma|}}, \tag{3.5}$$

where the constant $M_1$ is defined in (3.26) below and $|\Gamma|$ is the volume of the fundamental cell of $\mathcal{R}$. We also introduce the functions $\alpha_0$ and $\alpha_1$: $\alpha_0$ is the (unique) solution to the problem

$$\begin{cases} \Delta\alpha_0 = 0 & \text{in } \mathbb{R}^d_+ \setminus \overline{\Omega^1}, \\ \alpha_0|_+ = 1 & \text{on } \partial\Omega^1, \\ \alpha_0 - \alpha_{0,\infty} & \text{is exponentially decaying as } x_d \to \infty, \\ \alpha_0 = 0 & \text{on } \partial\mathbb{R}^d_+. \end{cases} \tag{3.6}$$

and $\alpha_1$ is the (unique) solution to the problem

$$\begin{cases} \Delta\alpha_1 = 0 & \text{in } \mathbb{R}^d_+ \setminus \overline{\Omega^1}, \\ \alpha_1|_+ = x_d|_+ & \text{on } \partial\Omega^1, \\ \alpha_1 - \alpha_{1,\infty} & \text{is exponentially decaying as } x_d \to \infty, \\ \alpha_1 = 0 & \text{on } \partial\mathbb{R}^d_+. \end{cases} \tag{3.7}$$

The exact values of $\alpha_{0,\infty}$ and $\alpha_{1,\infty}$ are given in Lemma 3.3.10 below. The function $\alpha_0$ is related to the monopole moment of bubbles, while $\alpha_1$ is related to their dipole moment.

Finally, we introduce a functional space. Let $L \in \mathbb{R}^+$ be large enough so that for all $y \in D$, it holds that $y_d \leq L$ (hence $0 \leq y_d \leq L$). For $a \in \mathbb{R}^+$, we denote by $S_a := \mathbb{R}^{d-1} \times (a, \infty)$, and we denote by $W^{1,\infty}(S_a)$ the usual Sobolev space with norm

$$\|f\|_{W^{1,\infty}(S_a)} := \|f\|_{L^\infty(S_a)} + \|\nabla f\|_{L^\infty(S_a)}.$$

Our main result is the following.

**Theorem 3.2.1.** *There exists $C \in \mathbb{R}^+$ such that, for all $\varepsilon > 0$ and all $\mu > 0$, it holds that*

$$\left\| U^\varepsilon(X) - U_0(X) - \left( U_1^\varepsilon(X) + U_{\mathrm{BL}}^\varepsilon\left(X, \frac{X}{\varepsilon}\right)\right)\right\|_{W^{1,\infty}(S_{\varepsilon L})} \leq C\varepsilon \left| g_s(\mu,\varepsilon)\right|,$$

*where $U_0$ was defined in* (3.3)*,*

$$\begin{aligned} U_1^\varepsilon(X) &:= (2\mathrm{i}u_0k_d)\mathrm{e}^{\mathrm{i}(k_dX_d - \bar{k}\cdot\bar{X})}\left(\varepsilon\alpha_{1,\infty} - g_s(\mu,\varepsilon)\alpha_{0,\infty}\right), \\ U_{\mathrm{BL}}^\varepsilon(X,x) &:= (2\mathrm{i}u_0k_d)\mathrm{e}^{-\mathrm{i}\bar{k}\cdot\bar{X}}\left[\varepsilon\left(\alpha_1(x) - \alpha_{1,\infty}\right) - g_s(\mu,\varepsilon)\left(\alpha_0(x) - \alpha_{0,\infty}\right)\right], \end{aligned}$$

*and $g_s(\mu,\varepsilon)$ is defined by (3.5). Moreover, $U_{\mathrm{BL}}^\varepsilon$ is exponentially decaying as $x_d \to \infty$.*

The proof of the above theorem will be given in Section 3.3. The function $U^{\varepsilon}_{\mathrm{BL}}$ describes the behavior of the field near the bubbles (at distances of order $O(\varepsilon)$), while the function $U^{\varepsilon}_{1}$ describes the far field. Both functions have an $O(\varepsilon)$ part due to the dipole moment, and a resonant part $g_s(\mu,\varepsilon)$ due to the monopole moment.

In particular, from the behavior of $U^{\varepsilon}$ in the far-field, namely

$$U^{\varepsilon}(X) \approx u_0 \mathrm{e}^{-\mathrm{i}(k_d X_d + \bar{k}\cdot\bar{X})} + u_0\left(-1 + 2\mathrm{i}k_d\left(\varepsilon\alpha_{1,\infty} - g_s(\mu,\varepsilon)\alpha_{0,\infty}\right)\right)\mathrm{e}^{\mathrm{i}(k_d X_d - \bar{k}\cdot\bar{X})},$$

we can write,

$$U^{s}(X) \approx R_{\varepsilon} U^{\mathrm{in}}_{\mathbf{k}}(\bar{X}, -X_d),$$

where

$$R_{\varepsilon} = -1 + 2\mathrm{i}k_d\left(\varepsilon\alpha_{1,\infty} - g_s(\mu,\varepsilon)\alpha_{0,\infty}\right)$$

is called the reflection coefficient. As a consequence and in view of the fact that the solution to the following system of equations

$$\begin{cases} \left(\Delta + k^2\right) V_0 = 0 \quad \text{on} \quad \mathbb{R}^d_+, \\ V - U^{\mathrm{in}} \quad \text{satisfies the outgoing radiation condition (3.2)}, \\ \dfrac{\partial V_0}{\partial x_d} = 0 \quad \text{on} \quad \partial\mathbb{R}^d_+, \end{cases}$$

is simply

$$V_0(X) := U^{\mathrm{in}}_{\mathbf{k}}(\bar{X}, X_d) + U^{\mathrm{in}}_{\mathbf{k}}(\bar{X}, -X_d),$$

we obtain

**Theorem 3.2.2.** *In the case when $\mu = \mu_M$, in the limit as $\varepsilon \to 0$, we get*

$$\lim_{\varepsilon\to 0} R_{\varepsilon} = -1 + 2 = 1.$$

*Therefore the equivalent screen has Neumann boundary condition for the wave equation.*

**Remark 3.2.3.** *If $\mu$ is very close or equal to $\mu_M$, then we may neglect the effect of $\alpha_{1,\infty}$ for simplicity. Hence, we obtain*

$$R_{\varepsilon} \approx -1 - 2\left(\frac{\varepsilon\mathrm{i}k_d M_1^2 C^{+}_{D,\mathcal{R}}|\Gamma|^{-1}}{1 - \frac{\mu_M}{\mu} - \mathrm{i}\varepsilon\frac{k_d M_1^2 C^{+}_{D,\mathcal{R}}}{|\Gamma|}}\right).$$

*Let*

$$\omega^{+}_{M} := \sqrt{\frac{\delta C^{+}_{D,\mathcal{R}}}{|D|}}\, v_b \tag{3.8}$$

*be the (quasi-periodic) Minnaert resonant frequency. Using the frequency variable $\omega$ instead of $\mu$, we see that if $\omega$ is very close or equal to $\omega^{+}_{M}$, then*

$$R(\omega) \approx -1 - 2\left(\frac{\mathrm{i}\frac{\omega M_1^2 C^{+}_{D,\mathcal{R}}}{v_d|\Gamma|}}{1 - \left(\frac{\omega}{\omega^{+}_{M}}\right)^2 - \mathrm{i}\frac{\omega M_1^2 C^{+}_{D,\mathcal{R}}}{v_d|\Gamma|}}\right). \tag{3.9}$$

*Note that $\omega_M^+$ has a similar expression to the usual Minnaert resonance $\omega_M$ found in [8, 86].*

**Remark 3.2.4.** *The term $\eta_{\rm rad} := \frac{\omega M_1^2 C_{D,\mathcal{R}}^+}{v_d|\Gamma|}$ in the denominator of (3.9) is called the radiative damping. It is possible to include more realistic damping effects [60]. In this case, one should replace $\eta_{\rm rad}$ by $\eta := \eta_{\rm rad} + \eta_{\rm other}$, where $\eta_{\rm other}$ includes all the remaining sources of damping. Note that in the particular case where $\eta_{\rm other} = \eta_{\rm rad}$ so that $\eta = 2\eta_{\rm rad}$, then at the resonant frequency $\omega = \omega_M$ we obtain that $R(\omega) \approx 0$. This eventually explains the super-absorption phenomenon experimented in [72]: all the incoming energy is dissipated with damping effects.*

The proof of Theorem 3.2.1 is given in the next section. It relies on the theory of quasi-periodic layer potentials.

## 3.3. Proof of Theorem 3.2.1.

### 3.3.1. Quasi-periodic Green's functions

We recall in this section the definition and properties of quasi-periodic layer potentials [17, Part 3]. Recall that $\mathcal{R}$ is a lattice of the plane $\mathbb{R}^{d-1}$. We let $\mathcal{R}^*$ be its reciprocal lattice, and denote by $\Gamma$ the unit cell of $\mathcal{R}$. For instance, if $d = 2$ with $\mathcal{R} = a\mathbb{Z}$, then $\mathcal{R}^* = (2\pi/a)\mathbb{Z}$ and $\Gamma = (-a/2, a/2)$.

**Quasi-periodic Green's function without Dirichlet boundary condition.** We first introduce, for $\mathbf{k} \in \mathbb{R}^d$, the quasi-periodic Green's function $G_\sharp^{\mathbf{k}}$ which is defined by

$$G_\sharp^{\mathbf{k}}(x) = \sum_{R\in\mathcal{R}} G^{\mathbf{k}}(x)\mathrm{e}^{-\mathrm{i}\bar{k}\cdot R}$$

where $G^{\mathbf{k}}$ is the Green's function to the free space Helmholtz equation

$$\left(\Delta + k^2\right) G^{\mathbf{k}}(x) = \delta_{\mathbf{0}}(x)$$

with the Sommerfeld radiation condition. It is clear that $G_\sharp^{\mathbf{k}}$ is the solution to the following equation

$$\left(\Delta + k^2\right) G_\sharp^{\mathbf{k}}(x) := \Big(\sum_{R\in\mathcal{R}} \mathrm{e}^{-\mathrm{i}\bar{k}\cdot\bar{x}}\delta_R(\bar{x})\Big)\,\delta_0(x_d) = \Big(\sum_{R\in\mathcal{R}} \mathrm{e}^{-\mathrm{i}\bar{k}\cdot R}\delta_R(\bar{x})\Big)\,\delta_0(x_d), \qquad (3.10)$$

with the outgoing radiation condition. Here and after, $\delta_R(\bar{x})\delta_0(x_d)$ denotes the Dirac mass at the point $(R, 0)$. It holds that $G_\sharp^{\mathbf{k}}(x, y) := G_\sharp^{\mathbf{k}}(x - y)$.

We now derive some basic properties for the quasi-periodic Green's function $G_\sharp^{\mathbf{k}}$. The following lemma is needed.

**Lemma 3.3.1.** *The solutions to* $(\partial_{xx}^2 + \alpha) f_\alpha = \delta_0$ *are*

$$f_\alpha(x) = \begin{cases} \dfrac{1}{2}|x| & \alpha = 0, \\ \dfrac{1}{2\mathrm{i}\sqrt{\alpha}} \mathrm{e}^{\mathrm{i}\sqrt{\alpha}|x|} & \alpha > 0, \\ \dfrac{1}{2\sqrt{-\alpha}} \mathrm{e}^{\sqrt{-\alpha}|x|} & \alpha < 0. \end{cases}$$

*Proof.* It is enough to check that $f_\alpha$ is the solution to $(\partial_{xx}^2 + \alpha) f_\alpha = \delta_0$. Recall that in the sense of distributions, $|x|' = 2\Theta(x) - 1$, where $\Theta$ is the Heaviside function $\Theta(x) := \mathbb{1}(x > 0)$, and that $|x|'' = 2\Theta'(x) = 2\delta_0$. Note also that $(|x|')^2 = 1$. The proof follows by standard calculations. □

We deduce from Lemma 3.3.1 the following result.

**Lemma 3.3.2.** *If* $\mathbf{k} = \mathbf{0}$*, then*

$$G_\sharp^{\mathbf{0}}((\bar{x}, x_d)) = \frac{|x_d|}{2|\Gamma|} - \sum_{\ell \in \mathcal{R}^* \setminus \{\mathbf{0}\}} \frac{1}{2|\Gamma|\,|\ell|} \mathrm{e}^{-|\ell|\,|x_d|} \mathrm{e}^{\mathrm{i}(\ell \cdot \bar{x})}. \tag{3.11}$$

*If* $\mathbf{k} \in \mathbb{R}^d$ *satisfies* $k^2 < \inf\{|\ell - \bar{k}|,\ \ell \in \mathcal{R}^* \setminus \{\mathbf{0}\}\}$*, then*

$$G_\sharp^{\mathbf{k}}((\bar{x}, x_d)) = \frac{\mathrm{e}^{-\mathrm{i}\bar{k}\cdot\bar{x}} \mathrm{e}^{\mathrm{i}k_d\,|x_d|}}{2\mathrm{i}k_d|\Gamma|} - \sum_{\ell \in \mathcal{R}^* \setminus \{0\}} \frac{\mathrm{e}^{-\mathrm{i}\bar{k}\cdot\bar{x}}}{2|\Gamma|\sqrt{|\ell - \bar{k}|^2 - k^2}} \mathrm{e}^{-\sqrt{|\ell-\bar{k}|^2-k^2}|x_d|} \mathrm{e}^{\mathrm{i}(\ell\cdot\bar{x})}. \tag{3.12}$$

*Proof.* In order to compute $G_\sharp^{\mathbf{k}}(x)$, we introduce $\widetilde{G_\sharp^{\mathbf{k}}}(x) = \mathrm{e}^{\mathrm{i}\bar{k}\cdot\bar{x}} G_\sharp^{\mathbf{k}}(x)$, so that $G_\sharp^{\mathbf{k}}(x) = \mathrm{e}^{-\mathrm{i}\bar{k}\cdot\bar{x}} \widetilde{G_\sharp^{\mathbf{k}}}(x)$. In particular, $\widetilde{G_\sharp^{\mathbf{k}}}$ is the $\mathcal{R}$-periodic solution to $\left(\Delta - 2\mathrm{i}\bar{k}\cdot\nabla_{\bar{x}} + k_d^2\right) \widetilde{G_\sharp^{\mathbf{k}}}(x) := \sum_{R\in\mathcal{R}} \delta_R(\bar{x})\delta_0(x_d)$. We consider its Fourier expansion, and write

$$\widetilde{G_\sharp^{\mathbf{k}}}(\bar{x}, x_d) = \sum_{\ell \in \mathcal{R}^*} c_\ell(x_d) \mathrm{e}^{\mathrm{i}\ell\cdot\bar{x}}.$$

Thanks to the Poisson summation formula

$$\sum_{R\in\mathcal{R}} \delta(x + R) = \frac{1}{|\Gamma|} \sum_{\ell\in\mathcal{R}^*} \mathrm{e}^{\mathrm{i}\ell\cdot\bar{x}},$$

we obtain that $c_\ell$ must be the solution to

$$\forall \ell \in \mathcal{R}^*, \quad \left(\partial_{x_d x_d}^2 + k^2 - |\ell - \bar{k}|^2\right) c_\ell = \frac{1}{|\Gamma|}\delta_0.$$

The proof then follows from Lemma 3.3.1. □

From (3.12), we see that $G_\sharp^{\varepsilon\mathbf{k}}$ has an asymptotic expansion of the form

$$G_\sharp^{\varepsilon\mathbf{k}}(x) = \frac{1}{2\mathrm{i}\varepsilon k_d|\Gamma|} + G_{0,\sharp}^{\mathbf{k}}(x) + \sum_{n=1}^{\infty} \varepsilon^n G_{n,\sharp}^{\mathbf{k}}(x), \tag{3.13}$$

where the kernels $G_{n,\sharp}^{\mathbf{k}}$ for $n \geq 1$ can be computed explicitly and shown to be smoother than $G_{0,\sharp}^{\mathbf{k}}$ [17]. Especially, together with (3.11), we have

$$G_{0,\sharp}^{\mathbf{k}}(x) = \frac{k_d|x_d| - \bar{k}\cdot\bar{x}}{2k_d|\Gamma|} - \sum_{\ell\in\mathcal{R}^*\setminus\{\mathbf{0}\}} \frac{\mathrm{e}^{-|\ell|\,|x_d|}\mathrm{e}^{\mathrm{i}(\ell\cdot\bar{x})}}{2|\Gamma|\,|\ell|} = G_\sharp^{\mathbf{0}}(x) - \frac{\bar{k}\cdot\bar{x}}{2k_d|\Gamma|}. \tag{3.14}$$

We will also need the exact formula for $G_{1,\sharp}^{\mathbf{k}}$. After some straightforward calculations we find that

$$G_{1,\sharp}^{\mathbf{k}}(x) = \frac{\mathrm{i}\left(k_d|x_d| - \bar{k}\cdot\bar{x}\right)^2}{4k_d|\Gamma|} - \bar{k}\cdot g_{1,\sharp}(x), \tag{3.15}$$

where $g_{1,\sharp}$ is a function independent of $\mathbf{k}$. Explicitly,

$$g_{1,\sharp}(x) := \sum_{\ell\in\mathcal{R}^*\setminus\{\mathbf{0}\}} \frac{\mathrm{e}^{-|\ell|\,|x_d|}\mathrm{e}^{\mathrm{i}(\ell\cdot\bar{x})}}{2|\Gamma|\,|\ell|}\left(\frac{\ell}{|\ell|^2} + \frac{\ell}{|\ell|}|x_d| - \mathrm{i}\bar{x}\right).$$

By change of variable $\ell \to -\ell$, we obtain that

$$g_{1,\sharp}(x) = \frac{\mathrm{i}}{2}\sum_{\ell\in\mathcal{R}^*\setminus\{\mathbf{0}\}} \frac{\mathrm{e}^{-|\ell|\,|x_d|}}{|\Gamma|\,|\ell|}\left(\left(\frac{\ell}{|\ell|^2} + \frac{\ell}{|\ell|}|x_d|\right)\sin(\ell\cdot\bar{x}) - \bar{x}\cos(\ell\cdot\bar{x})\right). \tag{3.16}$$

In particular, we see that $g_{1,\sharp}$ satisfies the symmetry relations

$$g_{1,\sharp}(\bar{x}, x_d) = g_{1,\sharp}(\bar{x}, -x_d) = -g_{1,\sharp}(-\bar{x}, x_d). \tag{3.17}$$

Note that there is a singularity in (3.13) as $\varepsilon$ goes to 0. Finally, expanding (3.10) in powers of $\varepsilon$ leads to the equations

$$\begin{cases} \Delta G_{0,\sharp}^{\mathbf{k}} = \displaystyle\sum_{R\in\mathcal{R}} \delta_R\delta_0, \\ \Delta G_{1,\sharp}^{\mathbf{k}} = \displaystyle\sum_{R\in\mathcal{R}} -\mathrm{i}R\delta_R\delta_0, \\ \Delta G_{n+2,\sharp}^{\mathbf{k}} + k^2 G_{n,\sharp}^{\mathbf{k}} = \displaystyle\sum_{R\in\mathcal{R}} \frac{(-\mathrm{i}\bar{k}\cdot R)^{n+2}}{(n+2)!}\delta_R\delta_0, \quad \forall n \geq 2. \end{cases} \tag{3.18}$$

The quasi-periodic Green's function would be an adequate tool to study the problem *without* the Dirichlet boundary condition $U^\varepsilon = 0$ on $\partial\mathbb{R}^d_+$. In this chapter however, we study the problem *with* the Dirichlet boundary condition to explain the phenomenon seen in [72] for instance.

**Quasi-periodic Green's function with Dirichlet boundary condition** We introduce the quasi-periodic-Dirichlet Green's function defined by

$$G_+^{\mathbf{k}}(x,y) := G_\sharp^{\mathbf{k}}((\bar{x}-\bar{y}, x_d - y_d)) - G_\sharp^{\mathbf{k}}((\bar{x}-\bar{y}, x_d + y_d)). \tag{3.19}$$

This Green's function is no longer translational invariant (in the sense $G_+^{\mathbf{k}}(x,y) \neq G_+^{\mathbf{k}}(x-y,\mathbf{0})$), but satisfies the Dirichlet boundary condition $G_+^{\mathbf{k}}(x,y) = 0$ for $y \in \mathbb{R}^d_+$ and $x \in \partial\mathbb{R}^d_+$. From (3.12), we deduce that $G_+^{\varepsilon\mathbf{k}}$ admits an asymptotic expansion of the form

$$G_+^{\varepsilon\mathbf{k}}(x,y) = \sum_{n=0}^{\infty} \varepsilon^n G_{n,+}^{\mathbf{k}}(x,y), \tag{3.20}$$

where

$$G_{n,+}^{\mathbf{k}}(x,y) := G_{n,\sharp}^{\mathbf{k}}((\bar{x}-\bar{y}, x_d - y_d)) - G_{n,\sharp}^{\mathbf{k}}((\bar{x}-\bar{y}, x_d + y_d)).$$

Note that $G_+^{\varepsilon\mathbf{k}}$ is no longer singular as $\varepsilon$ goes to 0. This makes the problem with Dirichlet boundary condition easier to study analytically. Moreover, from (3.14) we can check that

$$G_{\mathbf{0},+}^{\mathbf{k}}(x,y) = G_+^{\mathbf{k}=\mathbf{0}}(x,y).$$

Note that this equality does not hold for the quasi-periodic Green function without Dirichlet boundary condition (see (3.14)). We also need the expression of $G_{1,+}^{\mathbf{k}}$. We get

$$G_{1,+}^{\mathbf{k}}(x,y) = \frac{-\mathrm{i}}{2|\Gamma|}\left(2k_d x_d y_d + \bar{k}\cdot(\bar{x}-\bar{y})\left(|x_d - y_d| - |x_d + y_d|\right)\right) - \bar{k}\cdot g_{1,+}(x,y), \tag{3.21}$$

with

$$g_{1,+} := g_{1,\sharp}(\bar{x}-\bar{y}, x_d - y_d) - g_{1,\sharp}(\bar{x}-\bar{y}, x_d + y_d).$$

From (3.17), we see that $g_{1,+}$ satisfies the symmetry relation

$$g_{1,+}(x,y) = -g_{1,+}(y,x). \tag{3.22}$$

Finally, from (3.18), we deduce that

$$\Delta_y G_{1,+}^{\mathbf{k}}(x,y) = \sum_{R\in\mathcal{R}} (-\mathrm{i}\bar{k}\cdot R)\delta_R(\bar{x}-\bar{y})\left(\delta_0(x_d - y_d) - \delta_0(x_d + y_d)\right),$$

and that, for $n \in \mathbb{N}$,

$$\Delta_y G_{n+2,+}^{\mathbf{k}}(x,y) + k^2 G_{n,+}^{\mathbf{k}}(x,y) = \sum_{R\in\mathcal{R}} \frac{(-\mathrm{i}\bar{k}\cdot R)^{n+2}}{(n+2)!}\delta_R(\bar{x}-\bar{y})\left(\delta_0(x_d - y_d) - \delta_0(x_d + y_d)\right).$$

In particular, if $x, y \in \bar{D}$, then, since $\delta_R(\bar{x}-\bar{y}) = 0$ except for $R = \mathbf{0}$ (and $\bar{x} = \bar{y}$), we have

$$\Delta_x G_{1,+}^{\mathbf{k}} = \Delta_y G_{1,+}^{\mathbf{k}} = 0 \quad \text{and} \quad \forall n \in \mathbb{N}, \quad \Delta_y G_{n+2,+}^{\mathbf{k}}(x,y) = -k^2 G_{n,+}^{\mathbf{k}}(x,y). \tag{3.23}$$

### 3.3.2. Quasi-periodic-Dirichlet layer potentials

We now introduce the quasi-periodic-Dirichlet layer potential operators. We denote by $H^{-1/2} := H^{-1/2}(\partial D)$ and by $H^{1/2} := H^{1/2}(\partial D)$ the usual fractional Sobolev spaces on surfaces [77]. In the sequel, we use $\langle \cdot, \cdot \rangle$ for the $H^{1/2}, H^{-1/2}$ duality pairing. We denote by $\mathbb{1}_{\partial D} \in H^{1/2}$ the constant function with value 1 on $\partial D$, and we also introduce $H_0^{-1/2} := \left\{ f \in H^{-1/2},\ \langle \mathbb{1}_{\partial D}, f \rangle = 0 \right\}$.

The quasi-periodic-Dirichlet single-layer potential $\mathcal{S}_+^{\mathbf{k}} : H^{-1/2} \to H^{1/2}$ and the quasi-periodic Neumann-Poincaré operator $\mathcal{K}_+^{\mathbf{k},*} : H^{-1/2} \to H^{-1/2}$ are respectively defined, for smooth functions $\psi \in C^\infty(\partial D)$ for all $x \in \partial D$ by

$$\mathcal{S}_+^{\mathbf{k}}[\psi](x) := \int_{\partial D} G_+^{\mathbf{k}}(x,y)\psi(y)\mathrm{d}\sigma(y),$$
$$\mathcal{K}_+^{\mathbf{k},*}[\psi](x) := \int_{\partial D} \frac{\partial G_+^{\mathbf{k}}}{\partial \nu(x)}(x,y)\psi(y)\mathrm{d}\sigma(y).$$

For simplicity, we write $\mathcal{K}_+^* := \mathcal{K}_+^{\mathbf{0},*}$ and $\mathcal{S}_+ := \mathcal{S}_+^{\mathbf{0}}$. We also introduce the operator $\widetilde{\mathcal{S}_+^{\mathbf{k}}} : H^{-1/2} \to H^1_{\mathrm{loc}}(\mathbb{R}^d_+)$ for all $x \in \mathbb{R}^d_+$ defined by

$$\widetilde{\mathcal{S}_+^{\mathbf{k}}}[\psi](x) := \int_{\partial D} G_+^{\mathbf{k}}(x,y)\psi(y)\mathrm{d}\sigma(y). \tag{3.24}$$

**Lemma 3.3.3.**

*(i) For all $\mathbf{k} \in \mathbb{R}^d$, the operator $\mathcal{S}_+^{\mathbf{k}} : H^{-1/2} \to H^{1/2}$ is bounded and invertible with bounded inverse. Moreover, for $\mathbf{k} = \mathbf{0}$, it holds that $\mathcal{S}_+^* = \mathcal{S}_+$.*

*(ii) For all $\mathbf{k} \in \mathbb{R}^d$, the operator $\mathcal{K}_+^{\mathbf{k},*}$ is compact on $H^{-1/2}$, and the operator $\mathcal{K}_+^{\mathbf{k}}$ is compact on $H^{1/2}$.*

*(iii) (Jump formulae) It holds that*

$$\widetilde{\mathcal{S}_+^{\mathbf{k}}}\Big|_+ = \widetilde{\mathcal{S}_+^{\mathbf{k}}}\Big|_- = \mathcal{S}_+^{\mathbf{k}} \quad \text{and} \quad \left(\frac{\partial}{\partial \nu}\widetilde{\mathcal{S}_+^{\mathbf{k}}}\right)\Big|_\pm = \pm\frac{1}{2}I + \mathcal{K}_+^{\mathbf{k},*}.$$

*(iv) For $\mathbf{k} = \mathbf{0}$, it holds that $\sigma(\mathcal{K}_+^*) = \sigma(\mathcal{K}_+) \subset (-1/2, 1/2]$ and that*

$$\mathrm{Ker}\left(\mathcal{K}_+ - \frac{1}{2}I\right) = \mathrm{Span}\{\mathbb{1}_{\partial D}\}, \quad \text{and} \quad \mathrm{Ker}\left(\mathcal{K}_+^* - \frac{1}{2}I\right) = \mathrm{Span}\{\psi_0^+\},$$

*where $\psi_0^+ \in H^{-1/2}$ is the (unique) function in $\mathrm{Ker}\left(\mathcal{K}_+^* - \frac{1}{2}I\right)$ such that $\langle \mathbb{1}_{\partial D}, \psi_0^+ \rangle = 1$.*

*(v) The operator $(-\frac{1}{2}I + \mathcal{K}_+^*)$ acting on $H_0^{-1/2}$ is invertible with bounded inverse.*

Finally, we define

$$C^+_{D,\mathcal{R}} = -\left\langle \mathcal{S}_+^{-1}\mathbb{1}_{\partial D}, \mathbb{1}_{\partial D}\right\rangle, \tag{3.25}$$

$$M_1 = \left\langle \psi_0^+, x_d|_{\partial D}\right\rangle. \tag{3.26}$$

We have the following result.

**Lemma 3.3.4.**

*(i) For all $x \in D$, $\widetilde{\mathcal{S}_+}[\psi_0^+](x) = -1/C^+_{D,\mathcal{R}}$, so that $\mathcal{S}_+[\psi_0^+] = -(1/C^+_{D,\mathcal{R}})\mathbb{1}_{\partial D}$.*

*(ii) Let $\psi_1^+ := \left(-\frac{1}{2}I + \mathcal{K}_+^*\right)^{-1}[\nu_d] \in H_0^{-1/2}$, where $\nu_d$ is the d-component of the outward normal $\nu$ to $\partial D$. Then it holds that*

$$\widetilde{\mathcal{S}_+}[\psi_1^+](x) = x_d - M_1, \quad \forall x \in D,$$

*so that*

$$\mathcal{S}_+[\psi_1^+](x) = x_d|_{\partial D} - M_1, \quad \forall x \in \partial D.$$

*n particular,*

$$\mathcal{S}_+^{-1}[x_d|_{\partial D}] = \psi_1^+ - C^+_{D,\mathcal{R}} M_1 \psi_0^+.$$

*Proof.* The proof of *(i)* is straightforward. Let us prove *(ii)*. For all $M \in \mathbb{R}$, the function $f(x) := x_d - M$ satisfies $\Delta f = 0$ and $\frac{\partial}{\partial \nu} f|_- = \nu_d$. Together with the jump formulae, we deduce that

$$\forall x \in D, \quad \widetilde{\mathcal{S}_+}[\psi_1^+](x) = x_d - M,$$

where $M$ is chosen so that $\langle \mathbb{1}_{\partial D}, \psi_1^+\rangle = 0$. To calculate $M$, we notice that

$$0 = \langle \mathbb{1}_{\partial D}, \psi_1^+\rangle = \langle \mathbb{1}_{\partial D}, \mathcal{S}_+^{-1}[x_d - M\mathbb{1}_{\partial D}]\rangle = \langle \mathcal{S}_+^{-1}[\mathbb{1}], x_d - M\mathbb{1}_{\partial D}\rangle = -C^+_{D,\mathcal{R}}\langle \psi_0^+, x_d - M\mathbb{1}_{\partial D}\rangle.$$

The result follows. □

**Definition 3.3.5.** *We call the constant $C^+_{D,\mathcal{R}}$ the periodic capacity of $D$ with respect to the lattice $\mathcal{R}$.*

**Remark 3.3.6.** *The periodic capacity $C^+_{D,\mathcal{R}}$ is positive. Both $C^+_{D,\mathcal{R}}$ and $M_1$ depend on the lattice $\mathcal{R}$.*

### 3.3.3. Equivalent formulation

We now rescale the problem (3.1)-(3.2). Recall that $\delta = \delta_\varepsilon = \mu\varepsilon^2$. In the sequel, we denote by $X$ the macroscopic variable and by $x := \frac{X}{\varepsilon}$ the microscopic one. We denote

by $u(x) := U(\varepsilon x)$. With this change of variables, (3.1)-(3.2) are equivalent to

$$\begin{cases} \left(\Delta + \varepsilon^2 k^2\right) u^\varepsilon = 0 & \text{in } \mathbb{R}^d_+ \setminus \overline{\Omega^1}, \\ \left(\Delta + \varepsilon^2 k_b^2\right) u^\varepsilon = 0 & \text{in } \Omega^1, \\ u^\varepsilon|_+ = u^\varepsilon|_- & \text{on } \partial\Omega^1, \\ \left.\dfrac{\partial u^\varepsilon}{\partial \nu}\right|_- = \mu\varepsilon^2 \left.\dfrac{\partial u^\varepsilon}{\partial \nu}\right|_+ & \text{on } \partial\Omega^1, \\ u^\varepsilon - U^{\text{in}}_{\varepsilon\mathbf{k}} & \text{satisfies an outgoing radiation condition,} \\ u^\varepsilon = 0 & \text{on } \partial\mathbb{R}^d_+, \end{cases} \tag{3.27}$$

where the outgoing radiation condition is similar to (3.2). We use layer potentials to solve (3.27) in $\mathcal{H}$. We consider the case when the incidence angle is such that $\bar{k}^2 \leq k_b^2$. The case $\bar{k}^2 \geq k_b^2$ can be treated in a similar manner. We set $k_{b,d} = \sqrt{k_b^2 - \bar{k}^2}$, and denote by $\mathbf{k}_b = (\bar{k}, k_{b,d}) \in \mathbb{R}^d$ the vector such that $|\mathbf{k}_b| = k_b$. The solution to (3.27) can be represented by

$$u^\varepsilon(x) = \begin{cases} U^{\text{in}}_{\varepsilon\mathbf{k}}(\bar{x}, x_d) - U^{\text{in}}_{\varepsilon\mathbf{k}}(\bar{x}, -x_d) + \widetilde{\mathcal{S}^{\varepsilon\mathbf{k}}_+}[\psi](x) & \text{for } x \in \mathbb{R}^d \setminus \overline{\Omega^1}, \\ \widetilde{\mathcal{S}^{\varepsilon\mathbf{k}_b}_+}[\psi_b](x) & \text{for } x \in \Omega^1, \end{cases} \tag{3.28}$$

where $\psi_b, \psi \in H^{-1/2}$ are some surface potentials to find [14]. In the sequel, we denote by $\mathcal{H}^{--} := H^{-1/2} \times H^{-1/2}$ and by $\mathcal{H}^{+-} := H^{1/2} \times H^{-1/2}$. After some straightforward calculations and using Lemma 3.3.3, we see that (3.27) is equivalent to finding $\Psi(\varepsilon) = (\psi_b, \psi)^t \in \mathcal{H}^{--}$ such that

$$\mathcal{A}(\varepsilon)\Psi(\varepsilon) = F(\varepsilon), \tag{3.29}$$

where

$$\mathcal{A}(\varepsilon) := \begin{pmatrix} \mathcal{S}^{\varepsilon\mathbf{k}_b}_+ & -\mathcal{S}^{\varepsilon\mathbf{k}}_+ \\ -\frac{1}{2}I + \mathcal{K}^{\varepsilon\mathbf{k}_b,*}_+ & -\mu\varepsilon^2\left(\frac{1}{2}I + \mathcal{K}^{\varepsilon\mathbf{k},*}_+\right) \end{pmatrix} \tag{3.30}$$

and

$$\begin{aligned} F(\varepsilon) &:= \begin{pmatrix} U^{\text{in}}_{\varepsilon\mathbf{k}}(\bar{x}, x_d)|_+ - U^{\text{in}}_{\varepsilon\mathbf{k}}(\bar{x}, -x_d)|_+ \\ \delta_\varepsilon \frac{\partial}{\partial\nu}\left(U^{\text{in}}_{\varepsilon\mathbf{k}}(\bar{x}, x_d) - U^{\text{in}}_{\varepsilon\mathbf{k}}(\bar{x}, -x_d)\right)|_+ \end{pmatrix} \\ &= -2\mathrm{i}u_0 \begin{pmatrix} \sin(\varepsilon k_d x_d) \\ \varepsilon^3\mu\left(k_d\nu_d\cos(\varepsilon k_d x_d) - \mathrm{i}\bar{k}\cdot\bar{\nu}\sin(\varepsilon k_d\nu_d)\right) \end{pmatrix} \mathrm{e}^{-\mathrm{i}\varepsilon\bar{k}\cdot\bar{x}}. \end{aligned} \tag{3.31}$$

By Lemma 3.3.3, $\mathcal{A}(\varepsilon)$ is a bounded operator from $\mathcal{H}^{--}$ to $\mathcal{H}^{+-}$. We study (3.29) by using Taylor expansion. Following the decomposition (3.20), we write

$$\mathcal{S}^{\varepsilon\mathbf{k}}_+ = \mathcal{S}_+ + \sum_{n=1}^{\infty} \varepsilon^n \mathcal{S}^{\mathbf{k}}_{n,+} \quad \text{and} \quad \mathcal{K}^{\varepsilon\mathbf{k},*}_+ = \mathcal{K}^*_+ + \sum_{n=1}^{\infty} \varepsilon^n \mathcal{K}^{\mathbf{k},*}_{n,+}, \tag{3.32}$$

where the convergence holds in $\mathcal{L}(H^{-1/2}, H^{1/2})$ and $\mathcal{L}(H^{-1/2})$ respectively, and where, for $n \in \mathbb{N}^*$, $\psi \in H^{-1/2}$ and $x \in \partial D$,

$$\mathcal{S}^{\mathbf{k}}_{n,+}[\psi](x) := \int_{\partial D} G^{\mathbf{k}}_{n,+}(x,y)\psi(y)\mathrm{d}\sigma(y) \quad \text{and} \quad \mathcal{K}^*_{n,+}[\psi](x) := \int_{\partial D} \frac{\partial G^{\mathbf{k}}_{n,+}}{\partial \nu(x)}(x,y)\psi(y)\mathrm{d}\sigma(y).$$

Then we write

$$\mathcal{A}(\varepsilon) = \mathcal{A}_0 + \mathcal{B}(\varepsilon) \quad \text{with} \quad \mathcal{B}(\varepsilon) := \sum_{n=1}^{\infty} \varepsilon^n \mathcal{A}_n,$$

where

$$\mathcal{A}_0 := \begin{pmatrix} \mathcal{S}_+ & -\mathcal{S}_+ \\ -\frac{1}{2}I + \mathcal{K}^*_+ & 0 \end{pmatrix}, \quad \mathcal{A}_1 := \begin{pmatrix} \mathcal{S}^{\mathbf{k}_b}_{1,+} & -\mathcal{S}^{\mathbf{k}}_{1,+} \\ \mathcal{K}^{\mathbf{k}_b,*}_{1,+} & 0 \end{pmatrix}, \quad \mathcal{A}_2 := \begin{pmatrix} \mathcal{S}^{\mathbf{k}_b}_{2,+} & -\mathcal{S}^{\mathbf{k}}_{2,+} \\ \mathcal{K}^{\mathbf{k}_b,*}_{2,+} & -\mu\left(\frac{1}{2}I + \mathcal{K}^*_+\right) \end{pmatrix},$$

and, for $n \geq 3$,

$$\mathcal{A}_n := \begin{pmatrix} \mathcal{S}^{\mathbf{k}_b}_{n,+} & -\mathcal{S}^{\mathbf{k}}_{n,+} \\ \mathcal{K}^{\mathbf{k}_b,*}_{n,+} & -\mu\mathcal{K}^{\mathbf{k},*}_{n-2,+} \end{pmatrix}.$$

It is standard to check that the convergence holds in $\mathcal{L}(\mathcal{H}^{--}, \mathcal{H}^{+-})$. We would like to approximate $\mathcal{A}(\varepsilon)^{-1}$ by $\mathcal{A}_0^{-1}$. Unfortunately, this is not possible, since the operator $\mathcal{A}_0$ is not invertible. Indeed it is easy to check that $\mathrm{Ker}(\mathcal{A}_0) = \mathrm{Span}\left\{\begin{pmatrix} \psi_0^+ \\ \psi_0^+ \end{pmatrix}\right\}$. In order to handle this difficulty, we perturb the operator $\mathcal{A}_0$ (see also the method used in [8]). We introduce a rank-1 projection operator $\Pi \in \mathcal{L}(H^{-1/2})$ defined by

$$\forall \psi \in H^{-1/2}, \quad \Pi[\psi] = \langle \mathbb{1}_{\partial D}, \psi \rangle \, \psi_0^+,$$

and we set

$$\widetilde{\mathcal{A}_0} := \mathcal{A}_0 + \mathcal{P} \quad \text{and} \quad \widetilde{\mathcal{A}}(\varepsilon) := \mathcal{A}(\varepsilon) + \mathcal{P}, \quad \text{with} \quad \mathcal{P} := \begin{pmatrix} 0 & 0 \\ \Pi & 0 \end{pmatrix}.$$

**Lemma 3.3.7.** *The operator $\widetilde{\mathcal{A}_0}$ is bounded and is invertible with inverse*

$$\widetilde{\mathcal{A}_0}^{-1} = \begin{pmatrix} 0 & (-\frac{1}{2}I + \mathcal{K}^*_+ + \Pi)^{-1} \\ -\mathcal{S}_+^{-1} & (-\frac{1}{2}I + \mathcal{K}^*_+ + \Pi)^{-1} \end{pmatrix}.$$

Recall that we want to calculate $\Psi$, the solution to (3.29). We introduce

$$Q := \begin{pmatrix} \Pi & 0 \\ 0 & 0 \end{pmatrix}, \quad \Psi_- := (1-Q)\Psi \quad \text{and} \quad \Psi_+ := Q\Psi \quad \text{so that} \quad \Psi = \Psi_- + \Psi_+.$$

For the sake of clarity, we introduce the vectors $\Phi_1, \Phi_2 \in \mathcal{H}^{--}$ and $\Phi_3, \Phi_4 \in \mathcal{H}^{+-}$ defined by

$$\Phi_1 := \begin{pmatrix} \psi_0^+ \\ 0 \end{pmatrix}, \quad \Phi_2 := \begin{pmatrix} 0 \\ \psi_0^+ \end{pmatrix}, \quad \Phi_3 := \begin{pmatrix} \mathbb{1}_{\partial D} \\ 0 \end{pmatrix}, \quad \text{and} \quad \Phi_4 := \begin{pmatrix} 0 \\ \mathbb{1}_{\partial D} \end{pmatrix}.$$

Note that $\Psi_+ = \alpha\Phi_1$ for some $\alpha \in \mathbf{C}$. The equation (3.29) is therefore equivalent to

$$\left(\widetilde{\mathcal{A}_0} + \mathcal{B}(\varepsilon) - \mathcal{P}\right)(\alpha\Phi_1 + \Psi_-) = F(\varepsilon). \tag{3.33}$$

From Lemma 3.3.7, we deduce that for $\varepsilon$ small enough, the operator $\widetilde{\mathcal{A}_0} + \mathcal{B}(\varepsilon)$ is invertible, and that its inverse is given by the Neumann series

$$\widetilde{\mathcal{A}}(\varepsilon)^{-1} = \left(\widetilde{\mathcal{A}_0} + \mathcal{B}(\varepsilon)\right)^{-1} = \widetilde{\mathcal{A}_0}^{-1} + \sum_{n=1}^{\infty}(-1)^n \left(\widetilde{\mathcal{A}_0}^{-1}\mathcal{B}(\varepsilon)\right)^n \widetilde{\mathcal{A}_0}^{-1}, \tag{3.34}$$

where the convergence holds in $\mathcal{L}(\mathcal{H}^{+-}, \mathcal{H}^{--})$. Applying $\left(\widetilde{\mathcal{A}_0} + \mathcal{B}(\varepsilon)\right)^{-1}$ to both sides of (3.33), and using the fact that $\mathcal{P}\Phi_1 = \Phi_2$ and that $\mathcal{P}\Psi_- = 0$, we obtain

$$\alpha\Phi_1 + \Psi_- - \alpha\left(\widetilde{\mathcal{A}_0} + \mathcal{B}(\varepsilon)\right)^{-1}\Phi_2 = \left(\widetilde{\mathcal{A}_0} + \mathcal{B}(\varepsilon)\right)^{-1} F(\varepsilon).$$

Finally, we notice that $\langle \Phi_3, \Psi_- \rangle = 0$. By taking the duality product with $\Phi_3$, we see that (3.29) is equivalent to the following

$$\begin{cases} \alpha = \dfrac{\left\langle \Phi_3, \left(\widetilde{\mathcal{A}_0} + \mathcal{B}(\varepsilon)\right)^{-1} F(\varepsilon) \right\rangle}{1 - \left\langle \Phi_3, \left(\widetilde{\mathcal{A}_0} + \mathcal{B}(\varepsilon)\right)^{-1}\Phi_2 \right\rangle}, \\ \Psi_- = \left(\widetilde{\mathcal{A}_0} + \mathcal{B}(\varepsilon)\right)^{-1} F(\varepsilon) - \alpha\Phi_1 + \alpha\left(\widetilde{\mathcal{A}_0} + \mathcal{B}(\varepsilon)\right)^{-1}\Phi_2. \end{cases} \tag{3.35}$$

### 3.3.4. Asymptotic expansions

We now solve (3.35) using asymptotic expansions in $\varepsilon$. We first present some identities which are needed in the sequel.

**Lemma 3.3.8.** *The following identities hold.*

$$\begin{aligned} &(i)\ \mathcal{K}^{\mathbf{k}}_{1,+}[\mathbb{1}_{\partial D}] = 0, \\ &(ii)\ \mathcal{K}^{\mathbf{k}}_{2,+}[\mathbb{1}_{\partial D}](x) = -k^2 \int_D G^{\mathbf{0}}_+(x,y)\mathrm{d}y, \\ &(iii)\ \mathcal{K}^{\mathbf{k}}_{3,+}[\mathbb{1}_{\partial D}](x) = -k^2 \int_D G^{\mathbf{k}}_{1,+}(x,y)\mathrm{d}y. \end{aligned}$$

*Proof.* First, we recall that $G^{\mathbf{k}}_{1,+}(x,y)$ satisfies (3.23). In particular,

$$(i) \quad \mathcal{K}^{\mathbf{k}}_{1,+}[\mathbb{1}_{\partial D}](x) = \int_{\partial D} \partial_{\nu(y)} G^{\mathbf{k}}_{1,+}(x,y)\mathrm{d}\sigma(y) = \int_D \Delta_x G^{\mathbf{k}}_{1,+}(x,y)\mathrm{d}x = 0.$$

Also, using (3.23), we obtain

$$(ii)\quad \mathcal{K}^{\mathbf{k}}_{2,+}[\mathbb{1}_{\partial D}](x)=\int_{\partial D}\partial_{\nu_y}G^{\mathbf{k}}_{2,+}(x,y)\mathrm{d}\sigma(y)=\int_D\Delta_y G^{\mathbf{k}}_{2,+}(x,y)\mathrm{d}y=-k^2\int_D G^{\mathbf{0}}_{+}(x,y)\mathrm{d}y,$$

and similarly,

$$(iii)\quad \mathcal{K}^{\mathbf{k}}_{3,+}[\mathbb{1}_{\partial D}](x)=\int_{\partial D}\partial_{\nu_y}G^{\mathbf{k}}_{3,+}(x,y)\mathrm{d}\sigma(y)=-k^2\int_D G^{\mathbf{k}}_{1,+}(x,y)\mathrm{d}y.$$

□

We start with the calculation of $\alpha$.

**Evaluation of** $\left\langle \Phi_3, \left(\widetilde{\mathcal{A}_0}+\mathcal{B}(\varepsilon)\right)^{-1}\Phi_2\right\rangle$**.** From (3.34), we have in $\mathcal{L}(\mathcal{H}^{+-},\mathcal{H}^{--})$

$$\begin{aligned}\left(\widetilde{\mathcal{A}_0}+\mathcal{B}(\varepsilon)\right)^{-1}=&\widetilde{\mathcal{A}_0}^{-1}-\varepsilon\left(\widetilde{\mathcal{A}_0}^{-1}\mathcal{A}_1\widetilde{\mathcal{A}_0}^{-1}\right)+\varepsilon^2\left(\left[\widetilde{\mathcal{A}_0}^{-1}\mathcal{A}_1\right]^2\widetilde{\mathcal{A}_0}^{-1}-\widetilde{\mathcal{A}_0}^{-1}\mathcal{A}_2\widetilde{\mathcal{A}_0}^{-1}\right)\\&-\varepsilon^3\left(\left[\widetilde{\mathcal{A}_0}^{-1}\mathcal{A}_1\right]^3\widetilde{\mathcal{A}_0}^{-1}+\widetilde{\mathcal{A}_0}^{-1}\mathcal{A}_3\widetilde{\mathcal{A}_0}^{-1}\right)\\&+\varepsilon^3\left(\widetilde{\mathcal{A}_0}^{-1}\mathcal{A}_1\widetilde{\mathcal{A}_0}^{-1}\mathcal{A}_2\widetilde{\mathcal{A}_0}^{-1}+\widetilde{\mathcal{A}_0}^{-1}\mathcal{A}_2\widetilde{\mathcal{A}_0}^{-1}\mathcal{A}_1\widetilde{\mathcal{A}_0}^{-1}\right)+O(\varepsilon^4).\end{aligned}\tag{3.36}$$

Here the remainder term $O(\varepsilon^4)$ is an operator whose norm in $\mathcal{L}(\mathcal{H}^{+-},\mathcal{H}^{--})$ is dominated by $C\varepsilon^4$ for some positive constant $C$. It holds that $\widetilde{\mathcal{A}_0}^{-1}\Phi_2=\Phi_1+\Phi_2$ and $\left(\widetilde{\mathcal{A}_0}^{-1}\right)^*\Phi_3=\Phi_4$. Moreover, using Lemma 3.3.8 we have

$$\left(\widetilde{\mathcal{A}_0}^{-1}\mathcal{A}_1\right)^*\Phi_3=\mathcal{A}_1^*\Phi_4=\begin{pmatrix}\mathcal{K}^{\mathbf{k}_b}_{1,+}[\mathbb{1}_{\partial D}]\\0\end{pmatrix}=0.$$

As a consequence, (3.36) simplifies into

$$\begin{aligned}\left\langle \Phi_3, \left(\widetilde{\mathcal{A}_0}+\mathcal{B}(\varepsilon)\right)^{-1}\Phi_2\right\rangle=&1-\varepsilon^2\left\langle\Phi_4,\mathcal{A}_2(\Phi_1+\Phi_2)\right\rangle-\varepsilon^3\left\langle\Phi_4,\mathcal{A}_3(\Phi_1+\Phi_2)\right\rangle\\&+\varepsilon^3\left\langle\Phi_4,\mathcal{A}_2\widetilde{\mathcal{A}_0}^{-1}\mathcal{A}_1(\Phi_1+\Phi_2)\right\rangle+O(\varepsilon^4),\end{aligned}\tag{3.37}$$

where the remainder term $O(\varepsilon^4)$ is a number dominated by $C\varepsilon^4$ for some positive constant $C$. Let us evaluate each of the terms on the right hand side of (3.37). First, it holds that

$$\left\langle\Phi_4,\mathcal{A}_2(\Phi_1+\Phi_2)\right\rangle=\left\langle\mathbb{1}_{\partial D},\mathcal{K}^{\mathbf{k}_b,*}_{2,+}[\psi_0^+]\right\rangle-\mu\left\langle\mathbb{1}_{\partial D},\left(\frac{1}{2}I+\mathcal{K}^*_+\right)\psi_0^+\right\rangle.$$

Recall that $\mathcal{K}^*_+[\psi_0^+]=\frac{1}{2}I\psi_0^+$. By Lemma 3.3.8, we have

$$\left\langle\mathcal{K}^{\mathbf{k}_b}_{2,+}[\mathbb{1}_{\partial D}],\psi_0^+\right\rangle=-k_b^2\int_{\partial D}\int_D G^{\mathbf{0}}_+(x,y)\psi_0^+(x)\mathrm{d}y\mathrm{d}\sigma(x)=-k_b^2\int_D\widetilde{S_+}[\psi_0^+](y)\mathrm{d}y=\frac{k_b^2|D|}{C^+_{D,\mathcal{R}}}.$$

Hence,

$$\langle \Phi_4, \mathcal{A}_2(\Phi_1+\Phi_2)\rangle = \frac{k_b^2|D|}{C^+_{D,\mathcal{R}}} - \mu = \mu_M - \mu,$$

where $\mu_M$ was defined in (3.4). Similarly, using Lemma 3.3.8, one gets

$$\langle \Phi_4, \mathcal{A}_3(\Phi_1+\Phi_2)\rangle = \left\langle \mathbb{1}_{\partial D}, \mathcal{K}^{\mathbf{k}_b,*}_{3,+}[\psi_0^+]\right\rangle = -k_b^2 C_1,$$

where

$$C_1 := \int_D \int_{\partial D} G^{\mathbf{k}_b}_{1,+}(x,y)\psi_0^+(x)\mathrm{d}\sigma(x)\mathrm{d}y. \tag{3.38}$$

Finally, it remains to evaluate $\left\langle \Phi_4, \mathcal{A}_2\widetilde{\mathcal{A}_0}^{-1}\mathcal{A}_1(\Phi_1+\Phi_2)\right\rangle$. First, we have that

$$\mathcal{A}_1[\Phi_1+\Phi_2] = \begin{pmatrix} \left(\mathcal{S}^{\mathbf{k}_b}_{1,+} - \mathcal{S}^{\mathbf{k}}_{1,+}\right)[\psi_0^+] \\ \mathcal{K}^{\mathbf{k}_b,*}_{1,+}[\psi_0^+] \end{pmatrix}.$$

By noticing that $\bar{k_b} = \bar{k}$, together with the expression (3.21), we see that the contribution of $\bar{k}$ in $\mathcal{S}^{\mathbf{k}_b}_{1,+} - \mathcal{S}^{\mathbf{k}}_{1,+}$ cancels. Hence,

$$\left(\mathcal{S}^{\mathbf{k}_b}_{1,+} - \mathcal{S}^{\mathbf{k}}_{1,+}\right)[\psi_0^+] = (k_{b,d}-k_d)\int_{\partial D} \frac{-\mathrm{i}x_d y_d}{|\Gamma|}\psi_0^+(y)\mathrm{d}\sigma(y) = \frac{-\mathrm{i}M_1}{|\Gamma|}(k_{b,d}-k_d)\,x_d.$$

In particular,

$$\widetilde{\mathcal{A}_0}^{-1}\mathcal{A}_1[\Phi_1+\Phi_2] = \begin{pmatrix} (-\frac{1}{2}I + \mathcal{K}_+^* + \Pi)^{-1}\mathcal{K}^{\mathbf{k}_b,*}_{1,+}[\psi_0^+] \\ (-\frac{1}{2}I + \mathcal{K}_+^* + \Pi)^{-1}\mathcal{K}^{\mathbf{k}_b,*}_{1,+}[\psi_0^+] - \dfrac{-\mathrm{i}M_1}{|\Gamma|}(k_{b,d}-k_d)\left(\psi_1^+ - M_1 C^+_{D,\mathcal{R}}\psi_0^+\right) \end{pmatrix}.$$

On the other hand, we have (using the fact that $\mathcal{K}_+[\mathbb{1}_{\partial D}] = \mathbb{1}_{\partial D}$)

$$\mathcal{A}_2^*\Phi_4 = \begin{pmatrix} \mathcal{K}^{\mathbf{k}_b}_{2,+}[\mathbb{1}_{\partial D}] \\ -\mu\left(\frac{1}{2}I + \mathcal{K}_+\right)\mathbb{1}_{\partial D}\end{pmatrix} = \begin{pmatrix} -k_b^2\int_D G^{\mathbf{0}}_+(x,y)\mathrm{d}y \\ -\mu\mathbb{1}_{\partial D}\end{pmatrix}. \tag{3.39}$$

Altogether, we obtain that

$$\begin{aligned}\left\langle \Phi_4, \mathcal{A}_2\widetilde{\mathcal{A}_0}^{-1}\mathcal{A}_1(\Phi_1+\Phi_2)\right\rangle = \; & -k_b^2\left\langle \textstyle\int_D G^{\mathbf{0}}_+(x,y)\mathrm{d}y, \left(-\frac{1}{2}I + \mathcal{K}_+^* + \Pi\right)^{-1}\mathcal{K}^{\mathbf{k}_b,*}_{1,+}[\psi_0^+]\right\rangle \\ & + \frac{\mathrm{i}\mu M_1^2 C^+_{D,\mathcal{R}}}{|\Gamma|}(k_{b,d}-k_d).\end{aligned}$$

We now compute the first term on the right hand side of the above equation. Let $H : \bar{D} \to \mathbf{C}$ be defined by

$$H(x) := \int_{\partial D} G^{\mathbf{k}_b}_{1,+}(x,y)\psi_0^+(y)\mathrm{d}\sigma(y), \quad \forall x \in \bar{D},$$

and set $T = \mathcal{S}_+^{-1}[H|_-]$ and $I = \int_{\partial D} T \mathrm{d}\sigma$. Thanks to (3.23), we see that $\Delta H = 0$ on $D$. Together with the jump relation formulae (see Lemma 3.3.3), we deduce that

$$\left(-\frac{1}{2}I + \mathcal{K}_+^*\right)[T] = \frac{\partial}{\partial \nu} H\big|_- = \mathcal{K}_{1,+}^{\mathbf{k}_b,*}[\psi_0^+].$$

Therefore

$$\left(-\frac{1}{2}I + \mathcal{K}_+^* + \Pi\right)^{-1} \mathcal{K}_{1,+}^{\mathbf{k}_b,*}[\psi_0^+] = T - I\psi_0^+.$$

It follows that

$$\begin{aligned}
&\left\langle \textstyle\int_D G_+^{\mathbf{0}}(x,y)\mathrm{d}y, \left(-\frac{1}{2}I + \mathcal{K}_+^* + \Pi\right)^{-1} \mathcal{K}_{1,+}^{\mathbf{k}_b,*}[\psi_0^+] \right\rangle \\
&= \int_D \left( \int_{\partial D} G_+^{\mathbf{0}}(x,y) \left(T - I\psi_0^+\right)(y) \mathrm{d}\sigma(y) \right) \mathrm{d}x \\
&= \int_D \widetilde{\mathcal{S}_+} \left[T - I\psi_0^+\right](x)\mathrm{d}x = \int_D H(x)\mathrm{d}x + I\frac{|D|}{C_{D,\mathcal{R}}^+} = C_1 + I\frac{|D|}{C_{D,\mathcal{R}}^+},
\end{aligned}$$

where $C_1$ was defined in (3.38). It remains to compute the constant $I$. We have

$$\begin{aligned}
I &= \langle \mathbb{1}_{\partial D}, T\rangle = \langle \mathbb{1}_{\partial D}, \mathcal{S}_+^{-1}[H]\rangle = \langle \mathcal{S}_+^{-1}[\mathbb{1}_{\partial D}], H\rangle = -C_{D,\mathcal{R}}^+ \langle \psi_0^+, H\rangle \\
&= -C_{D,\mathcal{R}}^+ \int_{\partial D}\int_{\partial D} G_{1,+}^{\mathbf{k}_b}(x,y)\psi_0^+(x)\psi_0^+(y)\mathrm{d}\sigma(x)\mathrm{d}\sigma(y) \\
&= \frac{-C_{D,\mathcal{R}}^+}{2} \int_{\partial D}\int_{\partial D} \psi_0^+(x)\psi_0^+(y)\left(G_{1,+}^{\mathbf{k}_b}(x,y) + G_{1,+}^{\mathbf{k}_b}(y,x)\right)\mathrm{d}\sigma(x)\mathrm{d}\sigma(y),
\end{aligned}$$

where we performed the change of variable $(x,y) \to (y,x)$ to obtain the last equality. From the expression of $G_{1,+}^{\mathbf{k}_b}$ in (3.21) and the symmetry relation (3.22), we get

$$I = \frac{\mathrm{i}C_{D,\mathcal{R}}^+}{|\Gamma|} k_{b,d} \int_{\partial D} x_d \psi_0(x)\mathrm{d}\sigma(x) \int_{\partial D} y_d \psi_0(y)\mathrm{d}\sigma(y) = \frac{\mathrm{i}M_1^2 C_{D,\mathcal{R}}^+}{|\Gamma|} k_{b,d}.$$

Altogether, the above calculations yield

$$\begin{aligned}
&1 - \left\langle \Phi_3, \left(\widetilde{\mathcal{A}_0} + \mathcal{B}(\varepsilon)\right)^{-1} \Phi_2 \right\rangle_{\mathcal{H}^{--}} \\
&= \varepsilon^2(\mu_M - \mu) + \varepsilon^3\left(-k_b^2 C_1\right) - \varepsilon^3\left(-k_b^2\left[C_1 + \frac{\mathrm{i}M_1^2|D|}{|\Gamma|}k_{b,d}\right] + \frac{\mathrm{i}\mu M_1^2 C_{D,\mathcal{R}}^+}{|\Gamma|}(k_{b,d} - k_d)\right) + O(\varepsilon^4) \\
&= \varepsilon^2(\mu_M - \mu) + \varepsilon^3 \mathrm{i}\frac{M_1^2}{|\Gamma|}\left(k_b^2 k_{b,d}|D| - \mu(k_{b,d} - k_d)C_{D,\mathcal{R}}^+\right) + O(\varepsilon^4) \\
&= \varepsilon^2(\mu_M - \mu)\left(1 + \varepsilon\mathrm{i}\frac{M_1^2 k_{b,d} C_{D,\mathcal{R}}^+}{|\Gamma|}\right) + \varepsilon^3 \mathrm{i}\mu\frac{M_1^2 k_d C_{D,\mathcal{R}}^+}{|\Gamma|} + O(\varepsilon^4).
\end{aligned}$$

**Evaluation of** $\left\langle \Phi_3, \left(\widetilde{\mathcal{A}_0} + \mathcal{B}(\varepsilon)\right)^{-1} F(\varepsilon) \right\rangle$**.** From (3.31), we obtain that

$$F = \varepsilon F_1 + \varepsilon^2 F_2 + \varepsilon^3 F_3 + O(\varepsilon^4),$$

with

$$F_1 := -2\mathrm{i}u_0 \begin{pmatrix} k_d x_d \\ 0 \end{pmatrix}, \quad F_2 := -2\mathrm{i}u_0 \begin{pmatrix} -\mathrm{i}(\bar{k}\cdot\bar{x})k_d x_d \\ 0 \end{pmatrix},$$
$$F_3 := -2\mathrm{i}u_0 \begin{pmatrix} \frac{1}{6}(k_d x_d)^3 - \frac{1}{2}(\bar{k}\cdot\bar{x})^2 k_d x_d \\ \mu k_d \nu_d \end{pmatrix}.$$

Using the decomposition (3.36) and similar estimates as before, we get

$$\left\langle \Phi_3, \left(\widetilde{\mathcal{A}_0} + \mathcal{B}(\varepsilon)\right)^{-1} F(\varepsilon) \right\rangle = \varepsilon \left\langle \Phi_3, \widetilde{\mathcal{A}_0}^{-1} F_1 \right\rangle + \varepsilon^2 \left\langle \Phi_3, \widetilde{\mathcal{A}_0}^{-1} F_2 \right\rangle$$
$$- \varepsilon^3 \left\langle \Phi_3, \widetilde{\mathcal{A}_0}^{-1} \mathcal{A}_2 \widetilde{\mathcal{A}_0}^{-1} F_1 \right\rangle + \varepsilon^3 \left\langle \Phi_3, \widetilde{\mathcal{A}_0}^{-1} F_3 \right\rangle + O(\varepsilon^4).$$

Note that $\left\langle \Phi_3, \widetilde{\mathcal{A}_0}^{-1} F_1 \right\rangle = \left\langle \Phi_3, \widetilde{\mathcal{A}_0}^{-1} F_2 \right\rangle = \left\langle \Phi_3, \widetilde{\mathcal{A}_0}^{-1} F_3 \right\rangle = 0$. Also, using (3.39), we have

$$\left\langle \Phi_3, \widetilde{\mathcal{A}_0}^{-1} \mathcal{A}_2 \widetilde{\mathcal{A}_0}^{-1} F_1 \right\rangle = \left\langle \Phi_4, \mathcal{A}_2 \widetilde{\mathcal{A}_0}^{-1} F_1 \right\rangle = -2\mathrm{i}u_0 k_d \mu \left\langle \mathbb{1}_{\partial D}, \psi_1^+ - M_1 C^+_{D,\mathcal{R}} \psi_0^+ \right\rangle$$
$$= 2\mathrm{i}u_0 k_d \mu M_1 C^+_{D,\mathcal{R}}.$$

Therefore, we can conclude that

$$\left\langle \Phi_3, \left(\widetilde{\mathcal{A}_0} + \mathcal{B}(\varepsilon)\right)^{-1} F(\varepsilon) \right\rangle = -\varepsilon^3 2\mathrm{i}u_0 k_d \mu M_1 C^+_{D,\mathcal{R}} + O(\varepsilon^4).$$

**Evaluation of** $\alpha$**.** From the above calculations, we deduce that

$$\alpha = -\frac{\varepsilon 2\mathrm{i}u_0 \mu k_d M_1 C^+_{D,\mathcal{R}} + O(\varepsilon^2)}{(\mu_M - \mu)\left(1 + \varepsilon \mathrm{i}\frac{M_1^2 k_{b,d} C^+_{D,\mathcal{R}}}{|\Gamma|}\right) + \varepsilon \mathrm{i}\mu \frac{M_1^2 k_d C^+_{D,\mathcal{R}}}{|\Gamma|} + O(\varepsilon^2)}.$$

In order to simplify this expression, we recall the scattering function $g_s(\mu, \varepsilon)$ defined in (3.5). We can check that

$$\alpha = \left(2\mathrm{i}u_0 k_d C^+_{D,\mathcal{R}} + O(\varepsilon)\right) \cdot g_s(\mu, \varepsilon),$$

in the sense that there exists $C \in \mathbb{R}^+,\ \forall \varepsilon \geq 0,\ \forall \mu > 0$ such that

$$\left|\alpha - (2\mathrm{i}u_0 k_d) C^+_{D,\mathcal{R}} g_s(\mu, \varepsilon)\right| \leq C\varepsilon |g_s(\mu, \varepsilon)|.$$

**Evaluation of $\Psi_-$.** We finally calculate $\Psi_-$ defined in the second equation of (3.35). Using similar calculations as before, we get

$$\begin{aligned}\Psi_- &= \varepsilon\widetilde{\mathcal{A}_0}^{-1}F_1 - \alpha\Phi_1 + \alpha\widetilde{\mathcal{A}_0}^{-1}\Phi_2 + O(\varepsilon^2 + |\varepsilon\alpha|)\\ &= (2\mathrm{i}u_0k_d)\left(\varepsilon\begin{pmatrix}0\\ \psi_1^+ - M_1C^+_{D,\mathcal{R}}\psi_0^+\end{pmatrix} + g_s(\mu,\varepsilon)C^+_{D,\mathcal{R}}\begin{pmatrix}0\\ \psi_0^+\end{pmatrix}\right) + O(\varepsilon|g_s(\mu,\varepsilon)|).\end{aligned} \tag{3.40}$$

The remainder term $O(\varepsilon|g_s(\mu,\varepsilon)|)$ is an element in the space $\mathcal{H}^{--}$ whose norm is bounded by $C\varepsilon|g_s(\mu,\varepsilon)|$ for some positive constant $C$.

### 3.3.5. Microscopic scattered field

Recall (3.28), we have

$$u^\varepsilon(x) = -2\mathrm{i}u_0\sin(\varepsilon k_d x_d)\mathrm{e}^{-\mathrm{i}\varepsilon\bar{k}\cdot\bar{x}} + u_s^\varepsilon(x),$$

where $u_s^\varepsilon := \widetilde{\mathcal{S}_+^{\varepsilon k}}[\psi_\varepsilon]$ is the scattered field. Note that $\Psi_+$ does not contribute to the field outside the bubbles. Using (3.40), we obtain that

$$\begin{aligned}u_s^\varepsilon(x) &= (2\mathrm{i}u_0k_d)\int_D G_+^{\varepsilon\mathbf{k}}(x,y)\left(\varepsilon\left[\psi_1^+ - M_1C^+_{D,\mathcal{R}}\psi_0^+\right] + g_s(\mu,\varepsilon)C^+_{D,\mathcal{R}}\psi_0^+\right)(y)\mathrm{d}\sigma(y)\\ &\quad + O(\varepsilon|g_s(\mu,\varepsilon)|).\end{aligned} \tag{3.41}$$

We now simplify the above integral by exploiting the decomposition of $G_+^{\varepsilon\mathbf{k}}$. Recall that $L>0$ is chosen such that, for all $y\in D$, it holds that $0\le y_d\le L$. Together with (3.19), we obtain that, for $x_d\ge L$, we have $G_+^{\mathbf{k}} = G_{+,p}^{\mathbf{k}} + G_{+,e}^{\mathbf{k}}$, where

$$\begin{aligned}G_{+,p}^{\mathbf{k}}(x,y) &= \left(\frac{\mathrm{e}^{\mathrm{i}k_d(x_d-y_d)}}{2\mathrm{i}k_d|\Gamma|} - \frac{\mathrm{e}^{\mathrm{i}k_d(x_d+y_d)}}{2\mathrm{i}k_d|\Gamma|}\right)\mathrm{e}^{-\mathrm{i}\bar{k}\cdot\bar{x}} = -\frac{\sin(k_dy_d)}{k_d|\Gamma|}\mathrm{e}^{\mathrm{i}(k_dx_d-\bar{k}\cdot\bar{x})},\\ G_{+,e}^{\mathbf{k}}(x,y) &= -\sum_{\ell\in\mathcal{R}^*\setminus\{\mathbf{0}\}}\left(\frac{\mathrm{e}^{\mathrm{i}(\ell-\bar{k})\cdot(\bar{x}-\bar{y})}}{|\Gamma|\sqrt{|\ell-\bar{k}|^2-k^2}}\sinh\left(\sqrt{|\ell-\bar{k}|^2-k^2}y_d\right)\right)\mathrm{e}^{-\sqrt{|\ell-\bar{k}|^2-k^2}x_d}.\end{aligned}$$

It is clear that $G_{+,p}^{\mathbf{k}}$ consists of a single propagating mode, while $G_{+,e}^{\mathbf{k}}$ consists of the evanescent modes which are exponentially decaying away from the plane.

Accordingly, we write $\widetilde{\mathcal{S}_+^{\mathbf{k}}} = \widetilde{\mathcal{S}_{+,p}^{\mathbf{k}}} + \widetilde{\mathcal{S}_{+,e}^{\mathbf{k}}}$, with

$$\begin{aligned}\widetilde{\mathcal{S}_{+,p}^{\mathbf{k}}}[\psi](x) &= \int_{\partial D} G_{+,p}^{\mathbf{k}}(x,y)\psi(y)\mathrm{d}\sigma(y),\\ \widetilde{\mathcal{S}_{+,e}^{\mathbf{k}}}[\psi](x) &= \int_{\partial D} G_{+,e}^{\mathbf{k}}(x,y)\psi(y)\mathrm{d}\sigma(y).\end{aligned}$$

In particular, in the case when $\mathbf{k}=0$, we can deduce using (3.11) that

$$\widetilde{S^{\mathbf{k}=\mathbf{0}}_{+,p}}[\psi](x) = -\frac{1}{|\Gamma|}\int_{\partial D} y_d\psi(y)\mathrm{d}\sigma(y), \tag{3.42}$$

$$\widetilde{S^{\mathbf{k}=\mathbf{0}}_{+,e}}[\psi](x) = \widetilde{S_+}[\psi](x)+\frac{1}{|\Gamma|}\int_{\partial D} y_d\psi(y)\mathrm{d}\sigma(y), \tag{3.43}$$

for $\psi\in H^{-1/2}$ and $x_d\geq L$.

Following (3.14) and (3.19), we set

$$\widetilde{S^{\mathbf{k}}_{+,p,0}}[\psi](x) := -\mathrm{e}^{\mathrm{i}(k_d x_d-\bar{k}\cdot\bar{x})}\frac{1}{|\Gamma|}\int_{\partial D} y_d\psi(y)\mathrm{d}\sigma(y).$$

and

$$\widetilde{S^{\mathbf{k}}_{+,e,0}}[\psi](x) := \mathrm{e}^{-\mathrm{i}\bar{k}\cdot\bar{x}}\left(\widetilde{S_+}[\psi](x)+\frac{1}{|\Gamma|}\int_{\partial D} y_d\psi(y)\mathrm{d}\sigma(y)\right).$$

The operators $\widetilde{S^{\varepsilon\mathbf{k}}_{+,p,0}}$ and $\widetilde{S^{\varepsilon\mathbf{k}}_{+,e,0}}$ are good approximations for $\widetilde{S^{\varepsilon\mathbf{k}}_{+,p}}$ and $\widetilde{S^{\varepsilon\mathbf{k}}_{+,e}}$ respectively. Actually, from the expression of $G^{\mathbf{k}}_{+,p}$ and $G^{\mathbf{k}}_{+,e}$, we have the following results.

**Lemma 3.3.9.** *There exists $C\in\mathbb{R}^+$ such that, for all $\varepsilon\geq 0$, all $x_d\geq L$ and all $\psi\in H^{-1/2}$, it holds that*

$$\left|\left(\widetilde{S^{\varepsilon\mathbf{k}}_{+,p}}-\widetilde{S^{\varepsilon\mathbf{k}}_{+,p,0}}\right)[\psi]\right|(x)+\frac{1}{\varepsilon}\left|\nabla\left(\widetilde{S^{\varepsilon\mathbf{k}}_{+,p}}-\widetilde{S^{\varepsilon\mathbf{k}}_{+,p,0}}\right)[\psi]\right|(x)\leq C\left\|\psi\right\|_{H^{-1/2}}\varepsilon^2,$$

*and that*

$$\left|\left(\widetilde{S^{\varepsilon\mathbf{k}}_{+,e}}-\widetilde{S^{\varepsilon\mathbf{k}}_{+,e,0}}\right)[\psi]\right|(x)+\frac{1}{\varepsilon}\left|\nabla\left(\widetilde{S^{\varepsilon\mathbf{k}}_{+,e}}-\widetilde{S^{\varepsilon\mathbf{k}}_{+,e,0}}\right)[\psi]\right|(x)\leq C\left\|\psi\right\|_{H^{-1/2}}\varepsilon.$$

Now, we determine the functions $\alpha_1$ and $\alpha_2$ defined in (3.6)-(3.7).

**Lemma 3.3.10.** *The function $-C^+_{D,\mathcal{R}}\widetilde{S_+}[\psi^+_0]$ is the solution to (3.6), while the function $\widetilde{S_+}[\psi^+_1-M_1C^+_{D,\mathcal{R}}\psi^+_0]$ is the solution to (3.7), i.e.,*

$$-C^+_{D,\mathcal{R}}\widetilde{\mathcal{S}_+}[\psi^+_0]=\alpha_0 \quad \textit{and} \quad \widetilde{S_+}[\psi^+_1-M_1C^+_{D,\mathcal{R}}\psi^+_0]=\alpha_1.$$

*In particular, from (3.43) and the fact that $G^{\mathbf{k}=\mathbf{0}}_{+,e}$ is exponentially decaying, it holds that*

$$\alpha_{0,\infty}=-\frac{1}{|\Gamma|}\int_{\partial D} y_d\left(-C^+_{D,\mathcal{R}}\psi^+_0\right)=\frac{M_1C^+_{D,\mathcal{R}}}{|\Gamma|} \tag{3.44}$$

*and*

$$\alpha_{1,\infty}=-\frac{1}{|\Gamma|}\int_{\partial D} y_d\left(\psi^+_1-M_1C^+_{D,\mathcal{R}}\psi^+_0\right)=\frac{-\langle y_d,\psi^+_1\rangle}{|\Gamma|}+\frac{M_1^2C^+_{D,\mathcal{R}}}{|\Gamma|}. \tag{3.45}$$

Finally, we are ready to prove our main result Theorem 3.2.1.

**Proof of Theorem 3.2.1**

We introduce

$$\begin{aligned} u_1^\varepsilon(x) &:= (2\mathrm{i}u_0k_d)\widetilde{S^{\varepsilon\mathbf{k}}_{+,p,0}}\left[\varepsilon\left(\psi_1^+ - M_1C^+_{D,\mathcal{R}}\psi_0^+\right) + g_s(\mu,\varepsilon)\left(C^+_{D,\mathcal{R}}\psi_0^+\right)\right](x) \\ &= (2\mathrm{i}u_0k_d)\mathrm{e}^{\mathrm{i}\varepsilon(k_dx_d-\bar{k}\cdot\bar{x})}\left(\varepsilon\alpha_{1,\infty} - g_s(\mu,\varepsilon)\alpha_{0,\infty}\right) \end{aligned}$$

and

$$\begin{aligned} u^\varepsilon_{\mathrm{BL}}(x) &:= (2\mathrm{i}u_0k_d)\widetilde{S^{\varepsilon\mathbf{k}}_{+,e,0}}\left[\varepsilon\left(\psi_1^+ - M_1C^+_{D,\mathcal{R}}\psi_0^+\right) + g_s(\mu,\varepsilon)\left(C^+_{D,\mathcal{R}}\psi_0^+\right)\right](x) \\ &= (2\mathrm{i}u_0k_d)\mathrm{e}^{-\mathrm{i}\varepsilon\bar{k}\cdot\bar{x}}\left[\varepsilon\left(\alpha_1(x) - \alpha_{1,\infty}\right) - g_s(\mu,\varepsilon)\left(\alpha_0(x) - \alpha_{0,\infty}\right)\right]. \end{aligned}$$

By (3.41) and Lemma 3.3.9, we deduce that there exists $C \geq 0$ such that,

$$\|u_s^\varepsilon - (u_1^\varepsilon + u^\varepsilon_{\mathrm{BL}})\|_{L^\infty(S_L)} + \frac{1}{\varepsilon}\|\nabla\left[u_s^\varepsilon - (u_1^\varepsilon + u^\varepsilon_{\mathrm{BL}})\right]\|_{L^\infty(S_L)} \leq C\left(\varepsilon^2 + \varepsilon|g_s(\mu,\varepsilon)|\right).$$

Going back to the macroscopic variable $X = \varepsilon x$ we can conclude the proof of Theorem 3.2.1.

## 3.4. Numerical illustrations

In this section, all the numerical results are obtained for the two-dimensional case $d = 2$. The bubbles are set along a lattice $a\mathbb{Z}$. We follow the approach taken in [8]. Recall that we are interested in the characteristic value $\widetilde{\omega_c^+} \in \mathbf{C}$ for which the operator $\mathcal{A}(\omega)$ becomes singular, where $\mathcal{A}(\omega)$ is the block operator matrix which has a similar expression to (3.30), yet depends on $\omega$ instead of $\varepsilon$ (and the physical parameters are fixed). We define

$$\lambda_{\min}(\omega) := \mathrm{argmin}\ \{|\lambda|, \quad \lambda \in \sigma(\mathcal{A}(\omega))\}, \tag{3.46}$$

where $\sigma(\mathcal{A})$ denotes the (complex) spectrum of $\mathcal{A}$, and

$$\omega_c^+ := \mathrm{argmin}\ \{|\lambda_{\min}(\omega)|, \quad \omega \in \mathbb{R}^+\}. \tag{3.47}$$

First, we compare how close the characteristic value $\omega_c^+$ is to the Minnaert frequency $\omega_M^+$ defined in (3.8), for realistic systems. We then study the dependence of $\omega_M^+$ with respect to the geometrical parameters.

### 3.4.1. Implementation details

**Implementation of the quasi-periodic Green's function** Determination of $\omega_c^+$ requires the calculation of the quasi-periodic Green's function for the Helmholtz equation (3.10). It is well known that this function suffers from extremely slow convergence. It can be written in the form

$$G_\sharp^{\mathbf{k}}(x,y) = -\frac{\mathrm{i}}{4}\sum_{n\in\mathbb{Z}} \mathrm{e}^{\mathrm{i}\bar{k}na} H_0^{(1)}(kP_n),$$

where $P_n := \sqrt{(\bar{x}-\bar{y}-na)^2 + (x_d-y_d)^2}$, and $H_0^{(1)}$ is the Hankel function of the first kind of order zero. The terms of the summation are of order $O(n^{-\frac{1}{2}})$ for large $n$, which makes the function computationally challenging.

In order to accelerate the convergence, we implement Ewald's method [44], tailored to two-dimensional problems featuring one-dimensional periodicity [35]. The quasi-periodic Green's function is split into two components: a spatial component $G_{\sharp,\mathrm{spat}}$ and a spectral component $G_{\sharp,\mathrm{spec}}$, *i.e.*,

$$G_\sharp^{\mathbf{k}} = G_{\sharp,\mathrm{spat}}^{\mathbf{k}} + G_{\sharp,\mathrm{spec}}^{\mathbf{k}},$$

where we set

$$G_{\sharp,\mathrm{spat}}^{\mathbf{k}}(x,y) := \frac{1}{4\pi}\sum_{n\in\mathbb{Z}} \mathrm{e}^{-\mathrm{i}\bar{k}na} \sum_{q=0}^{\infty} \left(\frac{k}{2\mathcal{E}}\right)^{2q} \frac{1}{q!} E_{q+1}(P_n^2\mathcal{E}^2), \tag{3.48}$$

and

$$\begin{aligned} G_{\sharp,\mathrm{spec}}^{\mathbf{k}}(x,y) := \frac{1}{4a}\sum_{p\in\mathbb{Z}} \frac{\mathrm{e}^{-\mathrm{i}k_{1p}(\bar{x}-\bar{y})}}{\mathrm{i}k_{2p}} \times \Bigg[ & \mathrm{e}^{\mathrm{i}k_{2p}|x_d-y_d|}\mathrm{erfc}\left(\frac{\mathrm{i}k_{2p}}{2\mathcal{E}} + |x_d-y_d|\mathcal{E}\right) \\ & + \mathrm{e}^{-\mathrm{i}k_{2p}|x_d-y_d|}\mathrm{erfc}\left(\frac{\mathrm{i}k_{2p}}{2\mathcal{E}} - |x_d-y_d|\mathcal{E}\right)\Bigg]. \end{aligned} \tag{3.49}$$

Here, we have denoted by

$$k_{1p} = \bar{k} + \frac{2\pi p}{a}, \quad \text{and} \quad k_{2p} = \sqrt{k^2 - k_{1p}^2},$$

the Floquet wavenumbers along the $\bar{x}$ and $x_d$ directions, respectively. The functions $E_q$ in (3.48) are the $q$-th order exponential integral (we refer to [35] for implementation details)

$$E_q(z) := \int_1^\infty \frac{\mathrm{e}^{-zt}}{t^q}\mathrm{d}t.$$

Finally, $\mathcal{E}$ is the splitting parameter, which we choose to be $\sqrt{\pi}/d$, an appropriate choice in a low frequency setting. The infinite sums in (3.48)-(3.49) converge exponentially fast, so in practice we approximate them with the finite sums $n \in [-5,5]$, $q \in [-15,15]$, and $p \in [-5,5]$.

**Numerical setup** In order to simulate a realistic system, we consider the case of air bubbles inside water, which can be modeled by setting

$$\rho = 1.0 \times 10^3 \text{ kg.m}^{-3}, \quad \rho_b = 1.2 \text{ kg.m}^{-3}, \quad \kappa = 2.2 \times 10^9 \text{ Pa}, \quad \text{and} \quad \kappa_b = 1.4 \times 10^5 \text{ Pa}.$$

This choice of parameters means that $\delta = 1.2 \times 10^{-3}$, which is much smaller than 1, and thus ensures that we are indeed in the appropriate regime described in Section 1.2.

Regarding the geometry of the problem, we consider (recall that $d = 2$) circular bubbles, each of radius $r$, whose centers are on a lattice of the form $(a\mathbb{Z}, \beta)$, where $\beta > r$ is the distance between the centers of the bubbles and the reflective plane (see Figure 3.2).

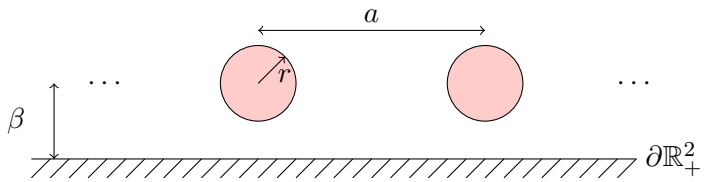


Figure 3.2.: Experimental setup for the numerical calculations

## 3.4.2. Validation of the Minnaert frequency formula

In this section, we compare $\omega_c^+$ with $\omega_M^+$, *i.e.*, the characteristic value defined in (3.47) obtained numerically, and analytical characteristic value given by the formula (3.8).

In Figure 3.3, we plot the function $\omega \mapsto |\lambda_{\min}(\omega)|$ for fixed period $a$ and offset $\beta$, and different values of $r$, where $\lambda_{\min}$ is defined in (3.46). We clearly observe the resonance phenomenon, whereby $\mathcal{A}(\cdot)$ becomes singular for a precise value of $\omega_c^+$ (the position of the minima in the figure).

In Table 3.1, we report the values of $\omega_M^+$ and $\omega_c^+$ for the same set of parameters as in Figure 3.3. It is clear that there is a very good agreement between our formula (3.8) for $\omega_M^+$, and the direct computation of $\omega_c^+$, even when the bubbles are very far apart. Note also that the wavelength is of order 10cm, while the periodicity of the structure is of order 1cm, and hence the resonance is indeed of a sub-wavelength nature.

| $r$ | $\omega_M^+$ | $\omega_c^+$ | $\lvert\lambda_{\min}\rvert$ | $(2\pi)/k$ |
|---|---|---|---|---|
| 1.0 | 13.692 | 13.674 | $-8.4 \times 10^{-7} + 1.14 \times 10^{-5}$i | 682 mm |
| 0.5 | 22.103 | 22.091 | $1.3 \times 10^{-7} + 1.7 \times 10^{-5}$i | 422 mm |
| 0.3 | 33.183 | 33.158 | $-9.9 \times 10^{-8} + 2.2 \times 10^{-5}$i | 281 mm |
| 0.1 | 84.356 | 84.324 | $1.9 \times 10^{-7} + 4.1 \times 10^{-5}$i | 111 mm |

Table 3.1.: The values $\omega_M^+$ and $\omega_c^+$ for $a = 10$mm, $\beta = 2$mm and $r = 0.1$mm, $r = 0.5$mm, $r = 0.3$mm and $r = 1$mm. We also report the values of $|\lambda_{\min}(\omega_c^+)|$ and the wavelengths $(2\pi)/k$.

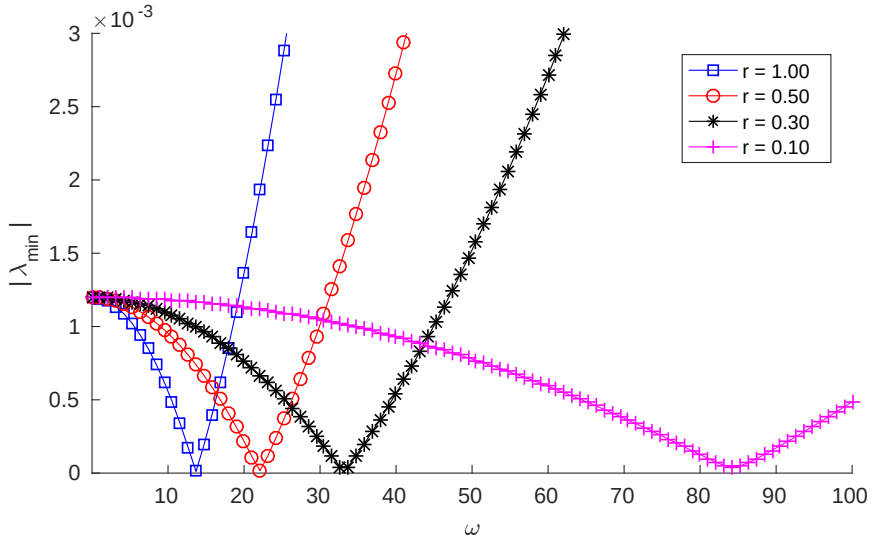


Figure 3.3.: The smallest eigenvalue (in norm) $\lambda_{\min}$ in the spectrum of $\mathcal{A}(\omega)$, for a period of $a = 10$mm, offset $\beta = 2$mm, and radii $r = 1$mm (square blue), $r = 0.5$mm (circle red), $r = 0.3$mm (star black), $r = 0.1$mm (plus cyan).

### 3.4.3. Dependence of the Minnaert resonance with respect to the geometry

We now study how $\omega_M^+$ depends on the geometrical parameters of the system. In Figure 3.4, we plot the Minnaert resonance as a function of the radius of the bubbles $r$, for different values of $\beta$. The periodicity $a$ is fixed at $a = 10$mm. We observe that when the size of the bubbles increase, the Minnaert frequency decreases (and hence the corresponding wavelength increases). Also, the farther away the bubbles are from the plane, the lower the Minnaert frequency.

Similarly, in Figure 3.5, we fix the radius of the bubbles at $r = 0.9$mm, and we plot the Minnaert resonance as a function of the periodicity $a$, for different values of $\beta$. We see that the Minnaert resonance increases as the bubbles are placed farther away from each other, but decreases as they get farther away from the reflective plane.

## 3.5. Concluding remarks

In this chapter we have analyzed an acoustic meta-screen constructed from bubbles and characterized its response to an incident acoustic wave in terms of an effective reflective coefficient. We have shown that due to the phenomenon of sub-wavelength resonance, the response of the meta-screen can range between an equivalent surface with Dirichlet boundary conditions to an equivalent surface with Neumann boundary

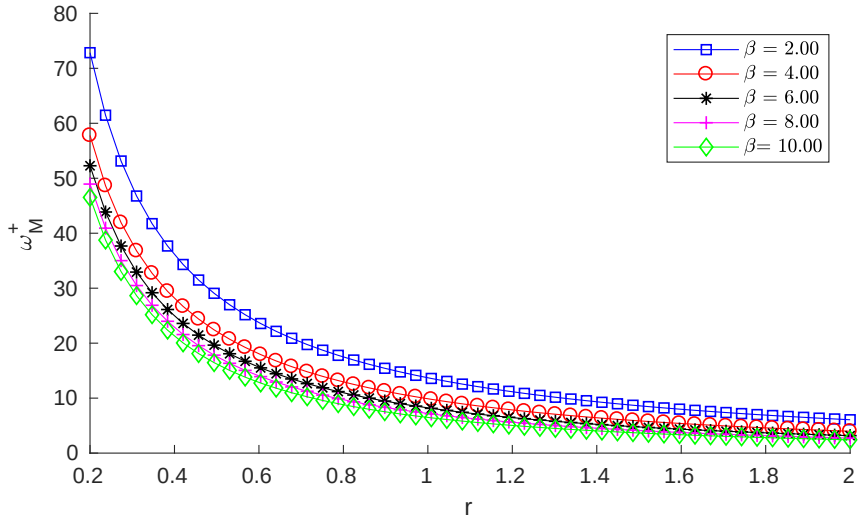


Figure 3.4.: The Minnaert resonance as a function of the radius of the bubbles (in mm). The periodicity is fixed at $a = 10$mm, and the offset is $\beta = 2$mm (square blue), $\beta = 4$mm (circle red), $\beta = 6$mm (star blue), $\beta = 82$mm (plus cyan), $\beta = 10$mm (losange green).

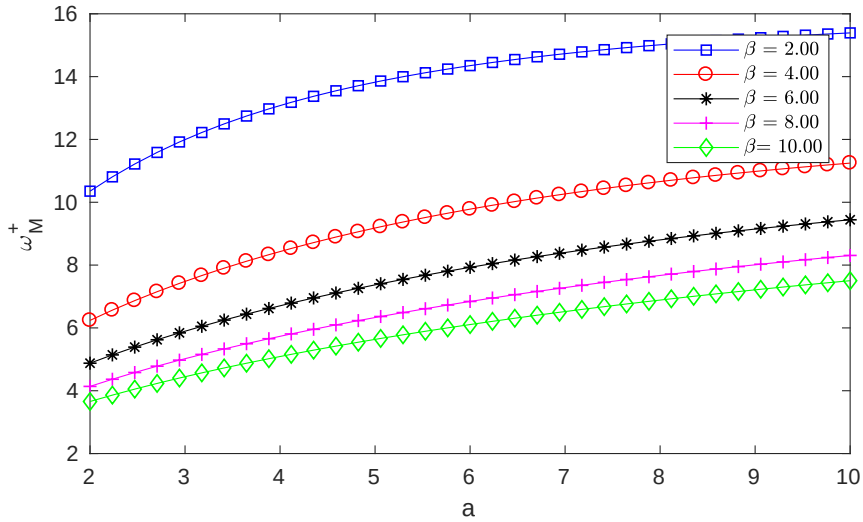


Figure 3.5.: The Minnaert resonance as a function of the periodicity $a$ (in mm). The radius of the bubbles is fixed at $r = 0.9$mm, and the offset is $\beta = 2$mm (square blue), $\beta = 4$mm (circle red), $\beta = 6$mm (star blue), $\beta = 82$mm (plus cyan), $\beta = 10$mm (losange green).

conditions. When the meta-screen is excited near the quasi-periodic Minnaert resonance, and damping effects are accounted for, the analysis in this chapter explains the super-

absorption observed experimentally in [72]. We have derived an analytical formula for the quasi-periodic Minnaert resonance and validated it in two dimensions using a numerical simulation. In addition we have numerically simulated the frequency response of the meta-screen to changes in bubble radius and lattice periodicity. The results in this chapter open a door to designing bubble meta-screens that can absorb practically all incoming energy in desired frequency ranges.

# 4. Sub-wavelength Phononic Bandgap Opening in Bubbly Media

The aim of this chapter is to show both analytically and numerically the existence of a sub-wavelength phononic bandgap in bubble phononic crystals. The key to this is an original formula for the quasi-periodic Minnaert resonance frequency of an arbitrarily shaped bubble. The main findings in this chapter are illustrated with a variety of numerical experiments.

## 4.1. Introduction

The past decade has witnessed growing interest in the fabrication of artificially engineered materials to effectively control mechanical waves such as sound waves. Phononic crystals which consist of periodic arrangements of components with controlled spatial size and elastic properties are typical examples. When excited by an acoustic or elastic wave, phononic crystals may exhibit bandgaps, or ranges of frequencies in which the wave cannot propagate through their bulk, instead decaying exponentially. The bandgaps in phononic crystals are due to destructive interference mechanisms from Bragg scattering of the waves, and can be quite wide. For bandgaps to occur, the period of the structure (or the lattice constant) must be of the order of the wavelength and the contrast in the material parameters must be large [17, 16, 13, 47, 54, 78]. This limits the use of phononic crystals in applications targeting low frequencies, because phononic crystals would require impractically large geometries [83, 96].

Based on the realization that composites with locally resonant microstructures can exhibit effective negative elastic parameters at certain frequency ranges, a class of phononic crystals that exhibits bandgaps with lattice constants two orders of magnitude smaller than the wavelength have been fabricated [81]. By varying the size and geometry of the microstructure, it was experimentally shown in [81] (and analytically verified using a simple model in [80]) that one can tune the frequency ranges over which the effective elastic parameters are negative. More recently, resonance has been shown both experimentally and numerically to be another way in which elastic waves can be prevented from propagating in the material [83].

In this chapter, to demonstrate the opening of a sub-wavelength phononic bandgap, we consider a periodic arrangement of bubbles and exploit their Minnaert resonance [86]. As shown in Chapter 2, the Minnaert resonant frequency depends on the bulk modulus of

the air, the density of the water and the shape of the bubble. In the dilute regime, it has been proven in [25] that around the Minnaert resonant frequency, an effective medium theory can be derived. Furthermore, above the Minnaert resonant frequency, the real part of the effective modulus is negative and consequently, the bubbly fluid behaves as a diffusive media for the acoustic waves. Meanwhile, below the Minnaert resonant frequency, with an appropriate bubble volume fraction, a high contrast effective medium can be obtained, making the super-focusing of waves achievable [24]. These findings show that the bubbly fluid functions like an acoustic metamaterial and indicate that a sub-wavelength bandgap opening occurs at the Minneaert resonant frequency [70]. We remark that such behavior is rather analogous to the coupling of electromagnetic waves with plasmonic nanoparticles, which results in effective negative or high contrast dielectric constants for frequencies near the plasmonic resonance frequencies [19, 22].

In this chapter, we provide a mathematical and numerical framework for analyzing bandgap opening in bubble phononic crystal at low frequencies. Through the application of layer potential techniques, Floquet theory, and Gohberg-Sigal theory we derive an original formula for the quasi-periodic Minnaert resonance frequencies of arbitrarily shaped bubbles, along with proving the existence of a sub-wavelength bandgap and estimate its width. Our results are complemented by several numerical examples which serve to validate them in two dimensions. Our results formally explain the experimental observations reported in [70]. They pave the mathematical foundation for the analysis of complex bubble-based phononic crystals that could have more than one structural period and contain bubbles of different sizes and shapes.

The chapter is organized as follows. In Section 4.2 we formulate the spectral problem for a bubble phononic crystal and introduce some basic results regarding the quasi-periodic Green's function. In Section 4.3 we derive an asymptotic formula in terms of the contrast between the mass densities of the air inside the bubbles and the fluid outside the bubbles. We prove the existence of a sub-wavelength bandgap and estimate its width. We also consider the dilute regime where the volume fraction of the bubbles is small. In Section 4.4 we perform numerical simulations in two dimensions to illustrate the main findings of this chapter. We make use of the multipole expansion method to compute the sub-wavelength bandgap. The chapter ends with some concluding remarks.

## 4.2. Problem formulation and preliminary results

We first describe the bubble phononic crystal under consideration. Assume that the bubbles are each of size order one and occupy $\cup_{n\in\mathbb{Z}^d}(D+n)$ for a bounded and simply connected domain $D$ with $\partial D \in C^{1,s}$ for $0 < s < 1$. To investigate its phononic gap we consider the following $\alpha$-periodic equation, subject to the regime specified in Section 1.2,

in the unit cell $Y = [0,1]^d$ for $d = 2, 3$:

$$\begin{cases} (\Delta + k^2)u = 0 & \text{in } Y\backslash\overline{D}, \\ (\Delta + k_b^2)u = 0 & \text{in } D, \\ u|_- = u|_+ & \text{on } \partial D, \\ \dfrac{1}{\rho_b}\dfrac{\partial u}{\partial \nu}\Big|_- = \dfrac{1}{\rho}\dfrac{\partial u}{\partial \nu}\Big|_+ & \text{on } \partial D, \\ e^{-i\alpha\cdot x}u & \text{is periodic.} \end{cases} \tag{4.1}$$

It is known that (4.1) has nontrivial solution for discrete values of $\omega$ such as (see [17])

$$0 \le \omega_1^\alpha \le \omega_2^\alpha \le \cdots$$

and we have the following band structure of propagating frequencies for the given periodic structure:

$$[0, \max_\alpha \omega_1^\alpha] \cup [\min_\alpha \omega_2^\alpha, \max_\alpha \omega_2^\alpha] \cup [\min_\alpha \omega_3^\alpha, \max_\alpha \omega_3^\alpha] \cup \cdots .$$

In this chapter we investigate whether there is a possibility of bandgap opening in this structure.

## 4.3. Sub-wavelength bandgaps

Let $\mathcal{S}_D^{\alpha,k}$ and $(\mathcal{K}_D^{-\alpha,k})^*$ be the quasi-periodic layer potentials defined in Section 1.4. We look for a solution $u$ of (4.1) of the form

$$u = \begin{cases} \mathcal{S}_D^{\alpha,k}[\psi] & \text{in } Y \setminus \overline{D}, \\ \mathcal{S}_D^{k_b}[\psi_b] & \text{in } D, \end{cases} \tag{4.2}$$

for some surface potentials $\psi, \psi_b \in L^2(\partial D)$ [14]. Using the jump relations for the single layer potentials, one can show that (4.1) is equivalent to the boundary integral equation

$$\mathcal{A}(\omega, \delta)[\Psi] = 0, \tag{4.3}$$

where

$$\mathcal{A}(\omega,\delta) = \begin{pmatrix} \mathcal{S}_D^{k_b} & -\mathcal{S}_D^{\alpha,k} \\ -\frac{1}{2}I + \mathcal{K}_D^{k_b,*} & -\delta(\frac{1}{2}I + (\mathcal{K}_D^{-\alpha,k})^*) \end{pmatrix}, \ \Psi = \begin{pmatrix} \psi_b \\ \psi \end{pmatrix}.$$

Throughout this chapter, we denote by $\mathcal{H} = L^2(\partial D) \times L^2(\partial D)$ and by $\mathcal{H}_1 = H^1(\partial D) \times L^2(\partial D)$. It is clear that $\mathcal{A}(\omega, \delta)$ is a bounded linear operator from $\mathcal{H}$ to $\mathcal{H}_1$, *i.e.*, $\mathcal{A}(\omega, \delta) \in \mathcal{L}(\mathcal{H}, \mathcal{H}_1)$. We can check that the characteristic values of $\mathcal{A}(\omega, \delta)$ can be written as

$$0 \le \omega_1^\alpha \le \omega_2^\alpha \le \cdots .$$

We first look at the limiting case when $\delta = 0$. The operator $\mathcal{A}(\omega, \delta)$ is a perturbation of

$$\mathcal{A}(\omega, 0) = \begin{pmatrix} \mathcal{S}_D^{k_b} & -\mathcal{S}_D^{\alpha,k} \\ -\frac{1}{2}I + \mathcal{K}_D^{k_b,*} & 0 \end{pmatrix}. \tag{4.4}$$

We see that $\omega_0$ is a characteristic value of $\mathcal{A}(\omega, 0)$ if only if $(\omega_0/v_b)^2$ is a Neumann eigenvalue of $D$ or $(\omega_0/v)^2$ is a Dirichlet eigenvalue of $Y\backslash D$ with $\alpha$-quasiperiodicity on $\partial Y$. Since zero is a Neumann eigenvalue of $D$, $\omega = 0$ is a characteristic value for the operator-valued analytic function $\mathcal{A}(\omega, 0)$. Besides, note that there is a positive lower bound for other Neumann eigenvalues of $D$ and all the Dirichlet eigenvalues of $Y\backslash D$ with $\alpha$-quasiperiodicity on $\partial Y$, we can conclude the following result by Gohberg-Sigal theory [17, 52].

**Lemma 4.3.1.** *For any $\delta$ sufficiently small, there exists one and only one characteristic value $\omega_0 = \omega_0(\delta)$ in a neighborhood of the origin in the complex plane to the operator-valued analytic function $\mathcal{A}(\omega, \delta)$. Moreover, $\omega_0(0) = 0$ and $\omega_0$ depends on $\delta$ continuously.*

### 4.3.1. The asymptotic behavior of $\omega_1^\alpha$

In this section we assume $\alpha \neq 0$. We define

$$\mathcal{A}_0 := \mathcal{A}(0, 0) = \begin{pmatrix} \mathcal{S}_D & -\mathcal{S}_D^{\alpha,0} \\ -\frac{1}{2}I + \mathcal{K}_D^* & 0 \end{pmatrix}, \tag{4.5}$$

We denote by $\mathcal{A}_0^* : \mathcal{H}_1 \to \mathcal{H}$ the adjoint of $\mathcal{A}_0$. We can easily check that $\mathrm{Ker}(\mathcal{A}_0)$ and $\mathrm{Ker}(\mathcal{A}_0^*)$ are spanned respectively by

$$\Psi_0 = \begin{pmatrix} \psi_0 \\ \tilde{\psi}_0 \end{pmatrix} \quad \text{and} \quad \Phi_0 = \begin{pmatrix} 0 \\ \mathbb{1}_{\partial D} \end{pmatrix},$$

where $\tilde{\psi}_0 = (\mathcal{S}_D^{\alpha,0})^{-1}\mathcal{S}_D[\psi_0]$.

We now perturb $\mathcal{A}_0$ by a rank-1 operator $\mathcal{P}_0$ from $\mathcal{H}$ to $\mathcal{H}_1$ given by $\mathcal{P}_0[\Psi] := (\Psi, \Psi_0)\Phi_0$, and denote it by $\tilde{\mathcal{A}}_0 = \mathcal{A}_0 + \mathcal{P}_0$.

**Lemma 4.3.2.** *The followings hold:*

*(i)* $\tilde{\mathcal{A}}_0[\Psi_0] = \|\Psi_0\|^2\Phi_0$, $\tilde{\mathcal{A}}_0{}^*[\Phi_0] = \|\Phi_0\|^2\Psi_0$.

*(ii) The operator $\tilde{\mathcal{A}}_0$ and its adjoint $\tilde{\mathcal{A}}_0{}^*$ are invertible in $\mathcal{L}(\mathcal{H}, \mathcal{H}_1)$ and $\mathcal{L}(\mathcal{H}_1, \mathcal{H})$, respectively.*

*Proof.* By construction, and the fact that $\mathcal{S}_D$ is bijective from $L^2(\partial D)$ to $H^1(\partial D)$ [15], we can show that $\tilde{\mathcal{A}}_0$ (hence $\tilde{\mathcal{A}}_0{}^*$) is bijective. The fact that $\tilde{\mathcal{A}}_0[\Psi_0] = \|\Psi_0\|^2\Phi_0$ is direct. Finally, by noticing that $\mathcal{P}_0^*[\theta] = \langle\theta, \Phi_0\rangle\Psi_0$, it follows that $\tilde{\mathcal{A}}_0{}^*[\Phi_0] = \mathcal{P}_0^*[\Phi_0] = \|\Phi_0\|^2\Psi_0$. □

**Theorem 4.3.3.** *For $\alpha \neq 0$ and sufficiently small $\delta$, we have*

$$\omega_1^\alpha = \omega_M \sqrt{c_2} + O(\delta^{3/2}), \tag{4.6}$$

*where $\omega_M = \sqrt{\frac{\delta v_b^2 \mathrm{Cap}_D}{|D|}}$ is the (free space) Minnaert resonant frequency and*

$$c_2 := \langle \tilde{\psi}_0, \left(\frac{1}{2} I + \mathcal{K}_D^{-\alpha,0}\right)[\mathbb{1}_{\partial D}]\rangle. \tag{4.7}$$

*Proof.* Using the results in Appendix A.1, we can expand $\mathcal{A}(\omega, \delta)$ as

$$\mathcal{A}(\omega,\delta) := \mathcal{A}_0 + \mathcal{B}(\omega,\delta) = \mathcal{A}_0 + \omega\mathcal{A}_{1,0} + \omega^2\mathcal{A}_{2,0} + \omega^3\mathcal{A}_{3,0} + \delta\mathcal{A}_{0,1} + \delta\omega^2\mathcal{A}_{2,1} + O(|\omega|^4 + |\delta\omega^3|) \tag{4.8}$$

where

$$\mathcal{A}_{1,0} = \begin{pmatrix} v_b^{-1}\mathcal{S}_{D,1} & 0 \\ 0 & 0 \end{pmatrix},\ \mathcal{A}_{2,0} = \begin{pmatrix} v_b^{-2}\mathcal{S}_{D,2} & -v^{-2}\mathcal{S}_{D,1}^\alpha \\ v_b^{-2}\mathcal{K}_{D,2}^* & 0 \end{pmatrix},\ \mathcal{A}_{3,0} = \begin{pmatrix} v_b^{-3}\mathcal{S}_{D,3} & 0 \\ v_b^{-3}\mathcal{K}_{D,3}^* & 0 \end{pmatrix},$$

$$\mathcal{A}_{0,1} = \begin{pmatrix} 0 & 0 \\ 0 & -(\frac{1}{2}I + (\mathcal{K}_D^{-\alpha,0})^*) \end{pmatrix},\ \mathcal{A}_{2,1} = \begin{pmatrix} 0 & 0 \\ 0 & -v^{-2}(\mathcal{K}_{D,1}^\alpha)^* \end{pmatrix}.$$

Since $\tilde{\mathcal{A}}_0 = \mathcal{A}_0 + \mathcal{P}_0$, the equation (4.3) is equivalent to

$$(\tilde{\mathcal{A}}_0 - \mathcal{P}_0 + \mathcal{B})[\Psi_0 + \Psi_1] = 0,$$

where

$$\langle \Psi_1, \Psi_0 \rangle = 0$$

Observe that the operator $\tilde{\mathcal{A}}_0 + \mathcal{B}$ is invertible for sufficiently small $\delta$ and $\omega$. Applying $(\tilde{\mathcal{A}}_0 + \mathcal{B})^{-1}$ to both sides of the above equation leads to

$$\Psi_1 = (\tilde{\mathcal{A}}_0 + \mathcal{B})^{-1}\mathcal{P}_0[\Psi_0] - \Psi_0 = \|\Psi_0\|^2 (\tilde{\mathcal{A}}_0 + \mathcal{B})^{-1}[\Phi_0] - \Psi_0. \tag{4.9}$$

Using the condition $\langle \Psi_1, \Psi_0 \rangle = 0$, we deduce that (4.3) has a nontrivial solution if and only if

$$\widetilde{A}(\omega,\delta) := \|\Psi_0\|^2 \left( \left\langle (\tilde{\mathcal{A}}_0 + \mathcal{B})^{-1}[\Phi_0], \Psi_0 \right\rangle - 1 \right) = 0. \tag{4.10}$$

Let us calculate $A(\omega,\delta) := \widetilde{A}(\omega,\delta)\|\Phi_0\|^2$. Using the Neumann series

$$(\tilde{\mathcal{A}}_0 + \mathcal{B})^{-1} = \left(1 + \tilde{\mathcal{A}_0}^{-1}\mathcal{B}\right)^{-1} \tilde{\mathcal{A}_0}^{-1} = \left(1 - \tilde{\mathcal{A}_0}^{-1}\mathcal{B} + \tilde{\mathcal{A}_0}^{-1}\mathcal{B}\tilde{\mathcal{A}_0}^{-1}\mathcal{B} - ...\right) \tilde{\mathcal{A}_0}^{-1},$$

and the fact that $\tilde{\mathcal{A}_0}^{-1}[\Phi_0] = \|\Psi_0\|^{-2}\Psi_0$ and $(\tilde{\mathcal{A}_0}^*)^{-1}[\Psi_0] = \|\Phi_0\|^{-2}\Phi_0$, we obtain that

$$A(\omega,\delta) = -\omega \langle \mathcal{A}_{1,0}[\Psi_0], \Phi_0\rangle - \omega^2 \langle \mathcal{A}_{2,0}[\Psi_0], \Phi_0\rangle - \omega^3 \langle \mathcal{A}_{3,0}[\Psi_0], \Phi_0\rangle - \delta \langle \mathcal{A}_{0,1}[\Psi_0], \Phi_0\rangle$$

$$
\begin{aligned}
&+\omega^2\left\langle \mathcal{A}_{1,0}\tilde{\mathcal{A}_0}^{-1}\mathcal{A}_{1,0}[\Psi_0],\Phi_0\right\rangle+\omega^3\left\langle \mathcal{A}_{1,0}\tilde{\mathcal{A}_0}^{-1}\mathcal{A}_{2,0}[\Psi_0],\Phi_0\right\rangle\\
&+\omega^3\left\langle \mathcal{A}_{2,0}\tilde{\mathcal{A}_0}^{-1}\mathcal{A}_{1,0}[\Psi_0],\Phi_0\right\rangle+\omega\delta\left\langle \mathcal{A}_{1,0}\tilde{\mathcal{A}_0}^{-1}\mathcal{A}_{0,1}[\Psi_0],\Phi_0\right\rangle\\
&+\omega\delta\left\langle \mathcal{A}_{0,1}\tilde{\mathcal{A}_0}^{-1}\mathcal{A}_{1,0}[\Psi_0],\Phi_0\right\rangle\\
&+\omega^3\left\langle \mathcal{A}_{1,0}\tilde{\mathcal{A}_0}^{-1}\mathcal{A}_{1,0}\tilde{\mathcal{A}_0}^{-1}\mathcal{A}_{1,0}[\Psi_0],\Phi_0\right\rangle+O(|\omega|^4+|\delta|\,|\omega|^2+|\delta|^2).
\end{aligned}
$$

It is clear that $\mathcal{A}^*_{1,0}[\Phi_0]=0$. Consequently, the expression simplifies into

$$
\begin{aligned}
A(\omega,\delta)=&-\omega^2\left\langle \mathcal{A}_{2,0}[\Psi_0],\Phi_0\right\rangle-\omega^3\left\langle \mathcal{A}_{3,0}[\Psi_0],\Phi_0\right\rangle+\omega^3\left\langle \mathcal{A}_{2,0}\tilde{\mathcal{A}_0}^{-1}\mathcal{A}_{1,0}[\Psi_0],\Phi_0\right\rangle\\
&-\delta\left\langle \mathcal{A}_{0,1}[\Psi_0],\Phi_0\right\rangle+\omega\delta\left\langle \mathcal{A}_{0,1}\tilde{\mathcal{A}_0}^{-1}\mathcal{A}_{1,0}[\Psi_0],\Phi_0\right\rangle+O(|\omega|^4+|\delta|\,|\omega|^2+|\delta|^2).
\end{aligned}
\tag{4.11}
$$

We now calculate the five remaining terms.

• **Calculation of** $\langle \mathcal{A}_{2,0}[\Psi_0],\Phi_0\rangle$. Using the first point of Lemma A.1.3, we get

$$
\begin{aligned}
\langle \mathcal{A}_{2,0}[\Psi_0],\Phi_0\rangle &= v_b^{-2}\left\langle \mathcal{K}^*_{D,2}[\psi_0],\mathbb{1}_{\partial D}\right\rangle = v_b^{-2}\left\langle \psi_0,\mathcal{K}_{D,2}[\mathbb{1}_{\partial D}]\right\rangle\\
&= -v_b^{-2}\int_{\partial D}\psi_0(x)\int_D G_0(x-y)\mathrm{d}y\mathrm{d}\sigma(x) = -v_b^{-2}\int_D \mathcal{S}_D[\psi_0](x)\mathrm{d}x = \frac{|D|}{v_b^2\mathrm{Cap}_D},
\end{aligned}
$$

where we used the fact that $\mathcal{S}_D[\psi_0](x)=-\mathrm{Cap}_D^{-1}$ for all $x\in D$.

• **Calculation of** $\langle \mathcal{A}_{3,0}[\Psi_0],\Phi_0\rangle$. Similarly, using the second point of Lemma A.1.3, we get

$$
\langle \mathcal{A}_{3,0}[\Psi_0],\Phi_0\rangle \;=\; v_b^{-3}\left\langle \psi_0,\mathcal{K}_{D,3}[\mathbb{1}_{\partial D}]\right\rangle = v_b^{-3}\left\langle \psi_0,\frac{\mathrm{i}|D|}{4\pi}\mathbb{1}_{\partial D}\right\rangle = \frac{\mathrm{i}|D|}{4\pi v_b^3}.
$$

• **Calculation of** $\langle \mathcal{A}_{0,1}[\Psi_0],\Phi_0\rangle$. We directly have

$$
\langle \mathcal{A}_{0,1}[\Psi_0],\Phi_0\rangle = -\langle\tilde{\psi}_0,\left(\frac{1}{2}I+\mathcal{K}_D^{-\alpha,0}\right)[\mathbb{1}_{\partial D}]\rangle.
$$

• **Calculation of** $\left\langle \mathcal{A}_{0,1}\tilde{\mathcal{A}_0}^{-1}\mathcal{A}_{1,0}[\Psi_0],\Phi_0\right\rangle$. We have

$$
\begin{aligned}
\mathcal{A}_{1,0}[\Psi_0] &= \frac{1}{v_b}\begin{pmatrix}\mathcal{S}_{D,1}[\psi_0]\\ 0\end{pmatrix} = \frac{1}{v_b}\frac{-\mathrm{i}}{4\pi}\begin{pmatrix}\mathbb{1}_{\partial D}\\ 0\end{pmatrix},\\
\mathcal{A}^*_{0,1}[\Phi_0] &= \begin{pmatrix}0\\ -\left(\frac{1}{2}I+\mathcal{K}_D^{-\alpha,0}\right)[\mathbb{1}_{\partial D}]\end{pmatrix}.
\end{aligned}
$$

Let us calculate $\tilde{\mathcal{A}}_0^{-1}\begin{pmatrix}\mathbb{1}_{\partial D}\\0\end{pmatrix}$. We look for $(a\psi_0, b\tilde{\psi}_0)\in\mathcal{H}$ so that

$$\begin{pmatrix}\mathbb{1}_{\partial D}\\0\end{pmatrix} = (\mathcal{A}_0+\mathcal{P}_0)\begin{pmatrix}a\psi_0\\b\tilde{\psi}_0\end{pmatrix} = \begin{pmatrix}(a-b)\mathcal{S}_D[\psi_0]\\0\end{pmatrix} + (a\|\psi_0\|^2+b\|\tilde{\psi}_0\|^2)\begin{pmatrix}0\\\mathbb{1}_{\partial D}\end{pmatrix}.$$

By solving the above equations directly, we obtain

$$\tilde{\mathcal{A}}_0^{-1}\begin{pmatrix}\mathbb{1}_{\partial D}\\0\end{pmatrix} = \frac{\mathrm{Cap}_D}{\|\psi_0\|^2+\|\tilde{\psi}_0\|^2}\begin{pmatrix}-\|\tilde{\psi}_0\|^2\psi_0\\\|\psi_0\|^2\tilde{\psi}_0\end{pmatrix}. \tag{4.12}$$

It follows that

$$\left\langle \mathcal{A}_{0,1}{\tilde{\mathcal{A}}_0}^{-1}\mathcal{A}_{1,0}[\Psi_0],\Phi_0\right\rangle = \frac{\mathrm{iCap}_D\|\psi_0\|^2\langle\tilde{\psi}_0,\left(\frac{1}{2}I+\mathcal{K}_D^{-\alpha,0}\right)[\mathbb{1}_{\partial D}]\rangle}{4\pi v_b(\|\psi_0\|^2+\|\tilde{\psi}_0\|^2)}.$$

• **Calculation of** $\left\langle \mathcal{A}_{2,0}{\tilde{\mathcal{A}}_0}^{-1}\mathcal{A}_{1,0}[\Psi_0],\Phi_0\right\rangle$. Using similar calculations, we obtain

$$\begin{aligned}\left\langle \mathcal{A}_{2,0}{\tilde{\mathcal{A}}_0}^{-1}\mathcal{A}_{1,0}[\Psi_0],\Phi_0\right\rangle &= \left\langle {\tilde{\mathcal{A}}_0}^{-1}\mathcal{A}_{1,0}[\Psi_0],\mathcal{A}_{2,0}^*[\Phi_0]\right\rangle\\ &= \frac{\mathrm{iCap}_D\|\tilde{\psi}_0\|^2}{4\pi v_b^3(\|\psi_0\|^2+\|\tilde{\psi}_0\|^2)}\left\langle\psi_0,\mathcal{K}_{D,2}[\mathbb{1}_{\partial D}]\right\rangle\\ &= \frac{\mathrm{i}|D|\|\tilde{\psi}_0\|^2}{4\pi v_b^3(\|\psi_0\|^2+\|\tilde{\psi}_0\|^2)}.\end{aligned}$$

• **Conclusion.** Considering the above the results, we can derive from (4.11) that

$$A(\omega,\delta) = -\omega^2\frac{|D|}{v_b^2\mathrm{Cap}_D} - \omega^3\frac{\mathrm{i}c_1|D|}{4\pi v_b^3} + c_2\delta + \omega\delta\frac{\mathrm{i}c_1c_2\mathrm{Cap}_D}{4\pi v_b} + O(|\omega|^4+|\delta|\,|\omega|^2+|\delta|^2), \tag{4.13}$$

where

$$c_1 := \frac{\|\psi_0\|^2}{\|\psi_0\|^2+\|\tilde{\psi}_0\|^2}, \tag{4.14}$$

and

$$c_2 := \langle\tilde{\psi}_0,\left(\frac{1}{2}I+\mathcal{K}_D^{-\alpha,0}\right)[\mathbb{1}_{\partial D}]\rangle. \tag{4.15}$$

We now solve $A(\omega,\delta)=0$. It is clear that $\delta=O(\omega^2)$ and thus $\omega_0(\delta)=O(\sqrt{\delta})$. We write $\omega_0(\delta)=a_1\delta^{\frac{1}{2}}+a_2\delta+O(\delta^{\frac{3}{2}})$, and get

$$-\frac{|D|}{v_b^2\mathrm{Cap}_D}\left(a_1\delta^{\frac{1}{2}}+a_2\delta+O(\delta^{\frac{3}{2}})\right)^2 - \frac{\mathrm{i}c_1|D|}{4\pi v_b^3}\left(a_1\delta^{\frac{1}{2}}+a_2\delta+O(\delta^{\frac{3}{2}})\right)^3$$

$$+ c_2\delta + \frac{\mathrm{i}c_1c_2\mathrm{Cap}_D}{4\pi v_b}\left(a_1\delta^{\frac{3}{2}} + a_2\delta^2 + O(\delta^{\frac{5}{2}})\right) + O(\delta^2) = 0.$$

From the coefficients of the $\delta$ and $\delta^{\frac{3}{2}}$ terms, we obtain

$$-a_1^2\frac{|D|}{v_b^2\mathrm{Cap}_D} + c_2 = 0 \quad \text{and} \quad 2a_1a_2\frac{-|D|}{v_b^2\mathrm{Cap}_D} - a_1^3\frac{\mathrm{i}c_1|D|}{4\pi v_b^3} + a_1\frac{\mathrm{i}c_1c_2\mathrm{Cap}_D}{4\pi v_b} = 0$$

which yields

$$a_1 = \pm\sqrt{\frac{v_b^2c_2\mathrm{Cap}_D}{|D|}} \quad \text{and} \quad a_2 = 0.$$

This completes the proof of the theorem. □

**Remark 4.3.4.** *See Appendix A.2 for a discussion on the two-dimensional quasi-periodic Minnaert resonance.*

We have

$$\begin{aligned} c_2 &= -\frac{1}{\mathrm{Cap}_D}\langle\left(\frac{1}{2}I + (\mathcal{K}_D^{-\alpha,0})^*\right)(\mathcal{S}_D^{\alpha,0})^{-1}[\mathbb{1}_{\partial D}], \mathbb{1}_{\partial D}\rangle \\ &= -\frac{1}{\mathrm{Cap}_D}\langle(\mathcal{S}_D^{\alpha,0})^{-1}[\mathbb{1}_{\partial D}], \mathbb{1}_{\partial D}\rangle = \frac{\mathrm{Cap}_{D,\alpha}}{\mathrm{Cap}_D}, \end{aligned}$$

and (4.6) is written as

$$\omega_1^\alpha = \omega_{M,\alpha} + O(\delta^{3/2})$$

with $\omega_{M,\alpha} = \sqrt{\frac{\delta v_b^2\mathrm{Cap}_{D,\alpha}}{|D|}}$. We can see that

$$\omega_{M,\alpha} \to 0$$

as $\alpha \to 0$ because $\left(1/2I + (\mathcal{K}_D^{-\alpha,0})^*\right)(\mathcal{S}_D^{\alpha,0})^{-1}[\mathbb{1}_{\partial D}] \to 0$ and so $\mathrm{Cap}_{D,\alpha} \to 0$ as $\alpha \to 0$.

We define $\omega_1^* := \max_\alpha \omega_{M,\alpha}$. Then we deduce the following regarding a bandgap opening.

**Theorem 4.3.5.** *For every $\epsilon > 0$, there exists $\delta_0 > 0$ and $\tilde{\omega} > \omega_1^* + \epsilon$ such that*

$$[\omega_1^* + \epsilon, \tilde{\omega}] \subset [\max_\alpha \omega_1^\alpha, \min_\alpha \omega_2^\alpha] \tag{4.16}$$

*for $\delta < \delta_0$.*

*Proof.* Using $\omega_1^0 = 0$ and the continuity of $\omega_1^\alpha$ in $\alpha$ and $\delta$, we get $\alpha_0$ and $\delta_1$ such that $\omega_1^\alpha < \omega_1^*$ for every $|\alpha| < \alpha_0$ and $\delta < \delta_1$. Following the derivation of (4.6), we can check that it is valid uniformly in $\alpha$ as far as $|\alpha| \geq \alpha_0$. Thus there exists $\delta_0 < \delta_1$ such $\omega_1^\alpha \leq \omega_1^* + \epsilon$ for $|\alpha| \geq \alpha_0$.

We have shown that $\max_\alpha \omega_1^\alpha \leq \omega_1^* + \epsilon$ for sufficiently small $\delta$. To have $\min_\alpha \omega_2^\alpha > \omega_1^* + \epsilon$ for small $\delta$, it is enough to check that $\mathcal{A}(\omega, \delta)$ has no small characteristic value other than $\omega_1^\alpha$. For $\alpha$ away from 0, we can see that it is true following the proof of Theorem 4.3.3. If $\alpha = 0$, we have

$$\mathcal{A}(\omega, \delta) = \mathcal{A}(\omega, 0) + O(\delta), \tag{4.17}$$

near $\omega_2^0$ with $\delta = 0$. Since $\omega_2^0 \neq 0$, we have $\omega_2^0(\delta) > \omega_1^* + \epsilon$ for sufficiently small $\delta$. Finally, using the continuity of $\omega_2^\alpha$ in $\alpha$, we obtain $\min_\alpha \omega_2^\alpha > \omega_1^* + \epsilon$ for small $\delta$. This completes the proof. □

### 4.3.2. Dilute case

We emphasize that our calculations in the previous part hold even for the dilute case as long as $\delta/\eta^2$ is small where $\eta$ is the diameter of $D$.

We state an asymptotic behavior of $\mathrm{Cap}_{D,\alpha}$ when $D = \eta B$ for a small $\eta$. Note that $\mathrm{Cap}_D = \mathrm{Cap}_{\eta B} = \eta \mathrm{Cap}_B$. Fix $c > 0$, the following holds.

**Lemma 4.3.6.** *For $|\alpha| > c > 0$, we have*

$$\mathrm{Cap}_{D,\alpha} = \mathrm{Cap}_D - R_\alpha(0)\mathrm{Cap}_D^2 + O(\eta^3), \tag{4.18}$$

*where $R_\alpha(x) := G^{\alpha,0}(x) - G^0(x)$.*

*Proof.* Since $R_\alpha(x)$ is smooth and $R_\alpha(x) = R_\alpha(0) + O(|x|)$ as $|x| \to 0$, we have

$$\begin{aligned}
\mathcal{S}_D^{\alpha,0}[\phi](\eta x) &= \eta \int_{\partial B} G^0(x-y)\tilde{\phi}(y) d\sigma(y) + \eta^2 R_\alpha(0) \int_{\partial B} \tilde{\phi}(y) d\sigma(y) + O\left(\eta^3 \|\tilde{\phi}\|\right) \\
&= \eta \left( \mathcal{S}_B[\tilde{\phi}] + \eta R_\alpha(0) \int_{\partial B} \tilde{\phi} + O\left(\eta^2 \|\tilde{\phi}\|\right) \right),
\end{aligned}$$

with $\tilde{\phi}(x) := \phi(\eta x)$. Then

$$(\mathcal{S}_D^{\alpha,0})^{-1}[\mathbb{1}_{\partial D}](\eta x) = \eta^{-1} \left( (\mathcal{S}_B)^{-1}[\mathbb{1}_{\partial B}] - \eta R_\alpha(0)(\mathcal{S}_B)^{-1} \left[ \int_{\partial B} (\mathcal{S}_B)^{-1}[\mathbb{1}_{\partial B}] \right] + O\left(\eta^2\right) \right), \tag{4.19}$$

and so

$$\begin{aligned}
\mathrm{Cap}_{D,\alpha} = -\eta^2 \int_{\partial B} (\mathcal{S}_D^{\alpha,0})^{-1}[\mathbb{1}_{\partial D}](\eta x)\, d\sigma(x) &= \eta \left( \mathrm{Cap}_B - \eta R_\alpha(0)\mathrm{Cap}_B^2 + O\left(\eta^2\right) \right) \\
&= \mathrm{Cap}_D - R_\alpha(0)\mathrm{Cap}_D^2 + O(\eta^3).
\end{aligned}$$

□

By this approximation we have $\omega_{M,\alpha} \approx \omega_M$ for $\alpha$ away from 0 and so $\omega_1^* \approx \omega_M$. Combined with Theorem 4.3.5 this means that there is a bandgap opening slightly above the Minneart resonance frequency for a single bubble. It is coherent with the results in [25] showing an effective medium theory for the bubbly fluid as the number of bubbles tends to infinity. It is shown there that near and above the Minnaert resonant frequency, the obtained effective media can have a negative bulk modulus.

## 4.4. Numerical illustrations

Recall the formula for the $\alpha$-quasi-periodic Minneart resonance:

$$\omega_1^\alpha = \omega_M \sqrt{\frac{\mathrm{Cap}_{D,\alpha}}{\mathrm{Cap}_D}} + O(\delta^{3/2}).$$

We want to compare $\omega_{approx}^\alpha := \omega_M \sqrt{\frac{\mathrm{Cap}_{D,\alpha}}{\mathrm{Cap}_D}}$ with the true $\alpha$-quasi-periodic resonance $\omega_{exact}^\alpha$, which can be obtained through direct calculation of the minimum characteristic value of the operator $\mathcal{A}(\omega, \delta)$ in (4.3) using Muller's method [8].

We set the density and the bulk modulus of the bubbles to be $\rho_b = 1$ and $\kappa_b = 1$, respectively. In order to confirm that the formula becomes accurate in the appropriate regime, which features similar wavenumbers inside and outside the bubbles along with, in particular, a high contrast in the bulk modulii, we take the density and the bulk modulus of the background material to be $\rho = \kappa = \delta^{-1} \in (10, 1000)$. We assume that the bubble represented by $D$ is a disk of radius $R = 0.0125$. In Figure 4.3 we plot $\omega_{approx}^\alpha$ and $\omega_{exact}^\alpha$ against the contrast $\delta^{-1}$ and it is clear that the formula provides a highly accurate approximation when the contrast is sufficiently large.

Next we present numerical examples to illustrate sub-wavelength bandgap openings. As $D$ is a disk of radius $R$, we apply the multipole expansion method for computing the band structure (for the details, we refer to Appendix 4.5). As described in [28], the quasi-periodic Green's function is unsuitable for bandgap calculations due to empty resonance phenomenon. Therefore, we make use of the multiple expansion method which is efficient in the case of disk-shaped bubbles.

We first consider the dilute case. We set $R = 0.05$, $\rho = \kappa = 5000$ and $\rho_b = \kappa_b = 1$. In this case, we have $\delta = 0.0002$. Figure 4.1 shows the computed band structure. The points $\Gamma, X$ and $M$ represent $\alpha = (0, 0)$, $\alpha = (\pi, 0)$ and $\alpha = (\pi, \pi)$, respectively. We plot the first two characteristic values $\mathcal{A}(\omega, \delta)$ along the boundary of the triangle $\Gamma X M$. It can be seen that a sub-wavelength bandgap in the spectrum of $\mathcal{A}(\omega, \delta)$ does exist. Moreover, the bandgap between the first two bands is quite large. It is also worth mentioning that, by zooming in on the sub-wavelength bandgap (on the right in Figure 4.1), one can see that $\omega_1^*$ is attained at the point $M$ (that is, $\alpha = (\pi, \pi)$). We used $N = 7$ for the

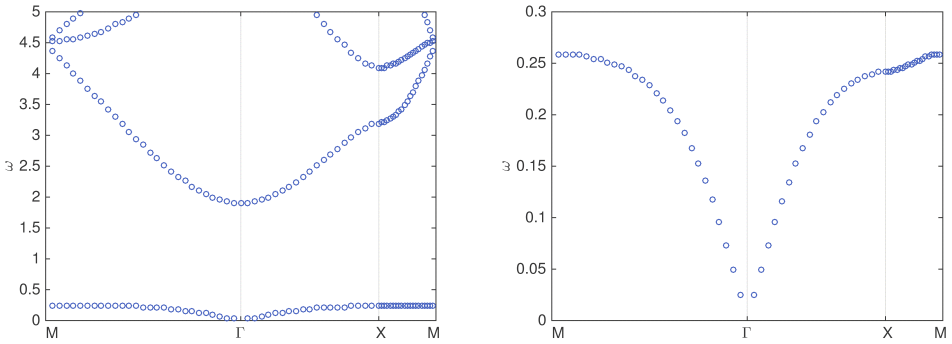


Figure 4.1.: (Dilute case) The band structure of a square array of circular bubbles with radius $R = 0.05$ and contrast $\delta^{-1} = 5000$.

truncation order of cylindrical waves. Further numerical experiments indicate that this phenomenon is independent of the bubble radius or position.

Next we consider a non-dilute regime. We set $R = 0.25$ and $\rho = \kappa = 1000$ and $\rho_b = \kappa_b = 1$. In this case we have $\delta = 0.001$. Figure 4.2 shows the computed band structure. Again, a sub-wavelength bandgap can be observed. We used $N = 3$ for the truncation order of cylindrical waves in the multipole expansion method.

Finally, in order to verify our conclusion from Lemma 4.3.6, namely that $\omega_1^* = \max_\alpha \omega_{M,\alpha} \approx \omega_M$ when $\alpha$ is non-zero, we fix the contrast to be $\delta^{-1} = 1000$ and observe $\omega_1^*$ and $\omega_M$ over a range of bubble sizes in Figure 4.4.

## 4.5. Multipole expansion method

When $D$ is a circular disk of radius $R$, the integral equation admits an explicit representation. In this case, the solution can be represented as a sum of cylindrical waves $J_n(kr)e^{in\theta}$ or $H_n^{(1)}(kr)e^{in\theta}$. Here we give a multipole expansion interpretation of the inte-

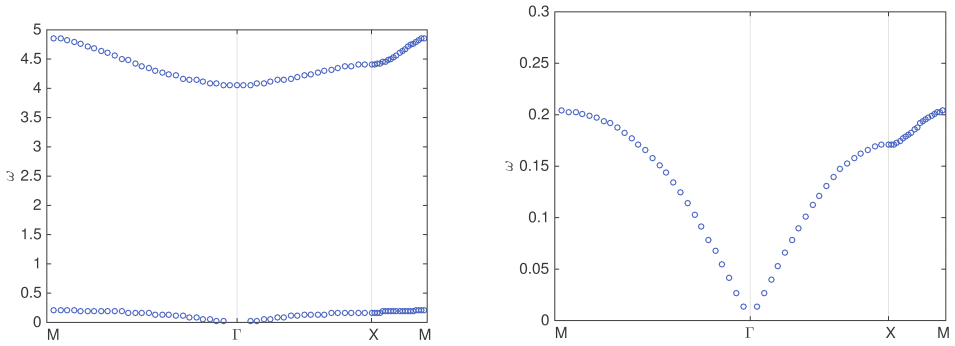


Figure 4.2.: (Non-dilute case) The band structure of a square array of circular bubbles with radius $R = 0.25$ and contrast $\delta^{-1} = 1000$.

gral operator $\mathcal{A}$, which leads to an efficient numerical scheme for computing its bandgap structure.

Recall that, for each fixed $k, \alpha$, we have to find a characteristic value of $\mathcal{A}(\omega, \delta)$ defined by

$$\mathcal{A}(\omega,\delta) = \begin{pmatrix} \mathcal{S}_D^{k_b} & -\mathcal{S}_D^{\alpha,k} \\ \dfrac{\partial \mathcal{S}_D^{k_b}}{\partial \nu}\Big|_- & -\delta \dfrac{\partial \mathcal{S}_D^{\alpha,k}}{\partial \nu}\Big|_+ \end{pmatrix}. \tag{4.20}$$

From the above expression, we see that $\mathcal{A}(\omega, \delta)$ is represented in terms of the single layer potential only. So it is enough to derive a multipole expansion version of the single layer potential.

Let us first consider the single layer potential $\mathcal{S}_D^k[\varphi]$ for a single disk $D$. We adopt the polar coordinates $(r, \theta)$. Then, since $D$ is a circular disk, the density function $\varphi = \varphi(\theta)$ is a $2\pi$-periodic function. It admits the following Fourier series expansion:

$$\varphi = \sum_{n\in\mathbb{Z}} a_n e^{\mathrm{i}n\theta},$$

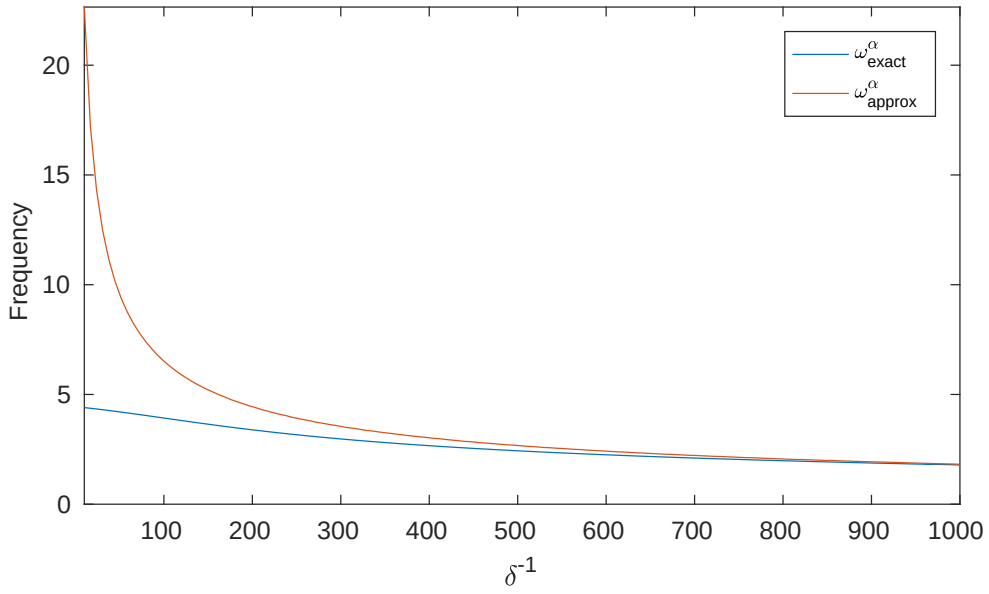


Figure 4.3.: When the contrast $\delta^{-1}$ is sufficiently large, the $\alpha$-quasi-periodic resonance $\omega_1^{\alpha}$ given by Theorem 7.2.2 provides a highly accurate approximation of the true resonance $\omega^{\alpha}_{\text{exact}}$.

for some coefficients $a_n$. Hence we only need to compute $u := \mathcal{S}_D^k[e^{in\theta}]$ which satisfies

$$\begin{cases} (\Delta + k^2)u = 0 & \text{in } \mathbb{R}^2 \setminus \overline{D}, \\ (\Delta + k^2)u = 0 & \text{in } D, \\ u|_+ = u|_- & \text{on } \partial D, \\ \left.\dfrac{\partial u}{\partial \nu}\right|_+ - \left.\dfrac{\partial u}{\partial \nu}\right|_+ = e^{in\theta} & \text{on } \partial D, \\ u & \text{satisfies the SRC.} \end{cases} \tag{4.21}$$

The above equation can be easily solved by the separation of variables technique in polar coordinates. It gives

$$\mathcal{S}_D^k[e^{in\theta}] = \begin{cases} cJ_n(kR)H_n^{(1)}(kr)e^{in\theta} & \text{for } |r| > R, \\ cH_n^{(1)}(kR)J_n(kr)e^{in\theta} & \text{for } |r| \le R, \end{cases} \tag{4.22}$$

where $c = \frac{-i\pi R}{2}$.

Now we compute the quasi-periodic single layer potential $\mathcal{S}_D^{\alpha,k}[e^{in\theta}]$. Since

$$G_\sharp^{\alpha,k}(x,y) = -\frac{i}{4}\sum_{m\in\mathbb{Z}^2} H_0^{(1)}(k|x-y-m|)e^{im\cdot\alpha},$$

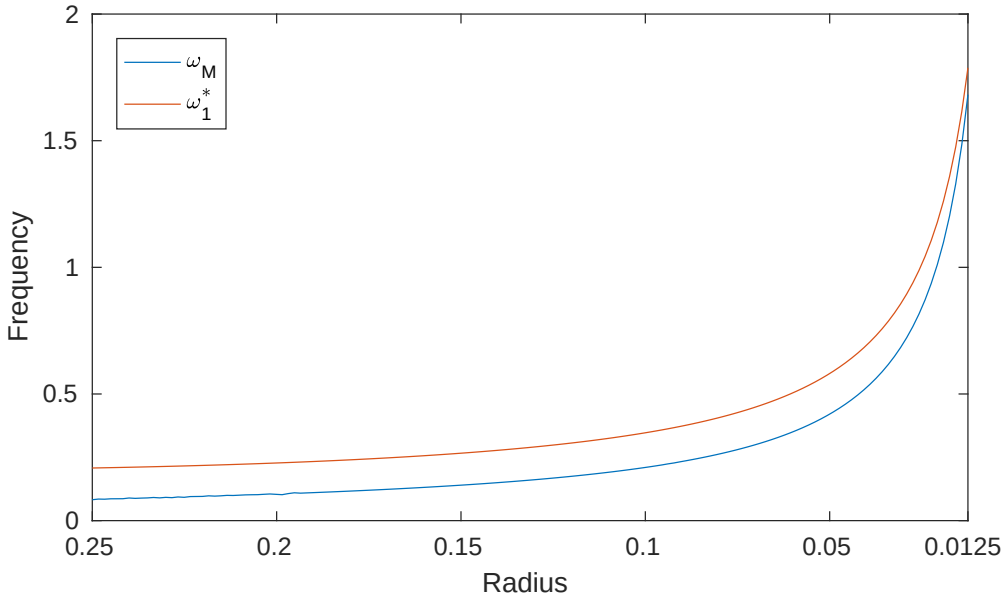


Figure 4.4.: As the bubbles becomes smaller, the maximum frequency in the first band of the spectrum of the operator $\mathcal{A}(\omega, \delta)$, $\omega_1^*$, approaches the Minnaert resonant frequency of a single bubble $\omega_M$.

we have

$$\begin{aligned}\mathcal{S}_D^{\alpha,k}[e^{in\theta}] &= \mathcal{S}_D^k[e^{in\theta}] + \sum_{m\in\mathbb{Z}^2, m\neq 0} \mathcal{S}_{D+m}^k[e^{in\theta}]e^{im\cdot\alpha} \\ &= \mathcal{S}_D^k[e^{in\theta}] + cJ_n(kR)\sum_{m\in\mathbb{Z}^2} H_n^{(1)}(kr_m)e^{in\theta_m}e^{im\cdot\alpha}.\end{aligned}$$

Here, $D+m$ means a translation of the disk $D$ by $m$ and $(r_m, \theta_m)$ is the polar coordinates with respect to the center of $D+m$. By applying the following addition theorem:

$$H_n^{(1)}(kr_m)e^{in\theta_m} = \sum_{l\in\mathbb{Z}}(-1)^{n-l}H_{n-l}^{(1)}(k|m|)e^{in\arg(m)}J_l(kr)e^{il\theta},$$

we obtain

$$\mathcal{S}_D^{\alpha,k}[e^{in\theta}] = \mathcal{S}_D^k[e^{in\theta}] + cJ_n(kR)\sum_{l\in\mathbb{Z}}(-1)^{n-l}Q_{n-l}J_l(kr)e^{il\theta}. \tag{4.23}$$

where $Q_n$ is so called the lattice sum defined by

$$Q_n := \sum_{m\in\mathbb{Z}^2, m\neq 0} H_n^{(1)}(k|m|)e^{in\arg(m)}e^{im\cdot\alpha}.$$

So, from (4.22) and (4.23), we finally obtain an explicit representation of $\mathcal{S}_D^{\alpha,k}$. For an efficient method for computing the lattice sum $Q_n$, see [76].

In the numerical computations, we should consider the truncated series

$$\sum_{n=-N}^{N} a_n \mathcal{S}_D^{\alpha,\omega}[e^{in\theta}]$$

instead of $\mathcal{S}_D^{\alpha,k}[\varphi] = \sum_{n\in\mathbb{Z}} a_n \mathcal{S}_D^{\alpha,k}[e^{in\theta}]$ for some large enough $N \in \mathbb{N}$. Then, using $e^{in\theta}$ as basis, we have the following matrix representation of the operator $\mathcal{S}^{\alpha,k}$:

$$\mathcal{S}_D^{\alpha,k}[\varphi]|_{\partial D} \approx \begin{pmatrix} S_{-N,-N} & S_{-N,-(N-1)} & \cdots & S_{-N,N} \\ S_{-(N-1),-N} & S_{-(N-1),-(N-1)} & \cdots & S_{-(N-1),N} \\ \vdots & & \ddots & \vdots \\ S_{N,-N} & \cdots & \cdots & S_{NN} \end{pmatrix} \begin{pmatrix} a_{-N} \\ a_{-(N-1)} \\ \vdots \\ a_N \end{pmatrix},$$

where $S_{m,n}$ is given by

$$S_{m,n} = cJ_n(kR)H_n^{(1)}(kR)\delta_{mn} + cJ_n(kR)(-1)^{n-m}Q_{n-m}J_m(kR).$$

Similarly, we also have the following matrix representation for $\frac{\partial \mathcal{S}_D^{\alpha,k}}{\partial \nu}|_{\partial D}^{\pm}$:

$$\frac{\partial \mathcal{S}_D^{\alpha,k}}{\partial \nu}[\varphi]\Big|_{\partial D}^{\pm} \approx \begin{pmatrix} S'^{\pm}_{-N,-N} & S'^{\pm}_{-N,-(N-1)} & \cdots & S'^{\pm}_{-N,N} \\ S'^{\pm}_{-(N-1),-N} & S'^{\pm}_{-(N-1),-(N-1)} & \cdots & S'^{\pm}_{-(N-1),N} \\ \vdots & & \ddots & \vdots \\ S'^{\pm}_{N,-N} & \cdots & \cdots & S'^{\pm}_{NN} \end{pmatrix} \begin{pmatrix} a_{-N} \\ a_{-(N-1)} \\ \vdots \\ a_N \end{pmatrix},$$

where $S'^{\pm}_{m,n}$ is given by

$$\begin{aligned} S'^{\pm}_{m,n} = \pm\frac{1}{2} + kc\Big(J_n \cdot (H_n^{(1)})' + J_n' \cdot H_n^{(1)}\Big)(kR)\delta_{mn} \\ + cJ_n(kR)(-1)^{n-m}Q_{n-m}kJ_m'(kR). \end{aligned}$$

The matrix representation of $\mathcal{A}(\omega, \delta)$ immediately follows.

## 4.6. Concluding remarks

In this chapter we have proved the existence of a sub-wavelength bandgap opening in bubble phononic crystals. We have illustrated our main findings with a variety of numerical experiments. We have also covered recently proved results on the effective medium theory in the dilute case [25]. It is worth mentioning that in [18], it is proven that the critical frequency $\omega_1^*$ is attained at the corner $M$ of the Brillouin zone. Moreover, above $\omega_1^*$, high frequency asymptotic analysis of the Bloch eigenfunctions is performed, leading to an explanation of the super-focusing of acoustic waves in bubbly crystals.

# 5. Sub-wavelength Focusing of Acoustic Waves in Bubbly Media

The purpose of this chapter is to investigate acoustic wave scattering by a large number of spherical bubbles in a liquid at frequencies near the Minnaert resonance frequency. This bubbly media has been exploited in practice to obtain super-focusing of acoustic waves. Using layer potential techniques we derive the scattering function for a single spherical bubble excited by an incident wave in the low frequency regime. We then propose a point scatterer approximation for $N$ bubbles, where $N$ is large, and describe several numerical simulations based on this approximation, that demonstrate the possibility of achieving super-focusing using bubbly media.

## 5.1. Introduction

In this chapter we are interested in acoustic wave propagation in a liquid containing a large number of bubbles. In particular, we are interested in the effect on the imaginary part of the Green's function of exciting bubbles at frequencies near the Minnaert resonance frequency. It is well known that the focal spot size which represents the resolution limit in imaging is dependent on the imaginary part of the Green's function due to the Helmholtz-Kirchoff Theorem [12]. Physical experiments have shown that it is possible to focus waves at the sub-wavelength scale by exploiting the strong scattering property of acoustic bubbles at their Minnaert resonance [65].

By generalizing the approach of Chapter 2 to the case of $N$ bubbles all having the same radius, we obtain an $N \times N$ block matrix in which the diagonal terms represent bubble self-interaction, while the off-diagonal terms represent the interaction between different bubbles. By letting the size of the bubbles go to zero we derive the point scatterer approximation which reduces the problem to an $N \times N$ linear system, which is recognizable as the classical Foldy-Lax formulation for a scattered field due to a collection of point scatterers [40].

We numerically simulate the system of point scatterers to analyze the super-focusing phenomenon observed in [65] and to demonstrate that it is possible to spatially localize a time reversed signal to a very high degree of accuracy in a bubbly media.

Due to the Helmholtz-Kirchhoff Theorem, the sharper the imaginary part of the Green's function, the smaller the focal size and the higher the resolution achieved [12, 23, 24].

To better understand the effect of the bubbly media on the imaginary part of the Greens function, we excite the point scatterers over a wide bandwidth. By averaging the imaginary part of the Green's function function over a range of frequencies, we demonstrate that sub-wavelength focusing is achievable in the region slightly below the Minnaert resonance frequency.

The chapter is organized as follows. In Section 5.2 we formulate the scattering problem for a single spherical bubble and derive the scattering function. This formula can be viewed as a particular case of the one derived in Chapter 2. In Section 5.3 we derive the point scatterer approximation for a system of $N$ bubbles. In Section 5.4 we demonstrate the super-focusing phenomenon by numerically showing that the imaginary part of the Green's function becomes sharper when the incident wave frequency is close to the Minnaert resonance frequency.

## 5.2. Single bubble

The purpose of this section is to justify the usual scattering function that one can find in the literature for spherical bubbles.

We consider a single bubble, which will be represented by a sphere $D$ of radius $R$, centered at the origin:

$$D := \left\{x \in \mathbb{R}^3,\ |x| \leq R\right\}.$$

Let $u^{in}$ be the incident wave defined in Section 1.6. The scattering problem, subject to the regime specified in Section 1.2, can be modeled by the following system of equations:

$$\begin{cases} (\Delta + k^2)u = 0 & \text{in } \mathbb{R}^3\backslash\overline{D}, \\ (\Delta + k_b^2)u = 0 & \text{in } D, \\ u|_- = u|_+ & \text{on } \partial D, \\ \dfrac{1}{\rho_b}\dfrac{\partial u}{\partial \nu}\Big|_- = \dfrac{1}{\rho}\dfrac{\partial u}{\partial \nu}\Big|_+ & \text{on } \partial D, \\ u^s := u - u^{in} & \text{satisfies the SRC.} \end{cases} \tag{5.1}$$

The solution $u$ of (5.1) can be written as

$$u = \begin{cases} u^{\text{in}} + \mathcal{S}_D^k[\psi] & \text{in } \mathbb{R}^3\backslash\overline{D}, \\ \mathcal{S}_D^{k_b}[\psi_b] & \text{in } D, \end{cases} \tag{5.2}$$

for some surface potentials $\psi, \psi_b \in L^2(\partial D)$ [14].

Using the jump relations (1.7) for the single layer potential, it is straightforward to derive that $\psi$ and $\psi_b$ satisfy the following system of boundary integral equations:

$$\mathcal{A}(\omega,\delta)[\Psi] = F, \tag{5.3}$$

where $\mathcal{A}(\omega,\delta) \in \mathcal{L}(\mathcal{H},\mathcal{H}_1)$ is given by

$$\mathcal{A}(\omega,\delta) = \begin{pmatrix} \mathcal{S}_D^{k_b} & -\mathcal{S}_D^{k} \\ -\delta^{-1}(\frac{1}{2}I + \mathcal{K}_D^{k_b,*}) & -(\frac{1}{2}I + \mathcal{K}_D^{k,*}) \end{pmatrix},$$

and

$$\Psi = \begin{pmatrix} \psi_b \\ \psi \end{pmatrix}, \quad F = \begin{pmatrix} u^{in} \\ \frac{\partial u^{in}}{\partial \nu} \end{pmatrix}.$$

### 5.2.1. The breathing approximation

Note that on the surface of the bubble, we have $u^{\text{in}}(x) = u^{\text{in}}(0) + O(kR)$, and $\frac{\partial u^{\text{in}}}{\partial \nu} = O(kR)$. If the wavelength is much larger than the size of the bubble, *i.e.*, $kR \ll 1$, then we may approximate $u^{\text{in}}$ by $u^{\text{in}}(0)$ and $\frac{\partial u^{\text{in}}}{\partial \nu}$ by zero on the surface of the bubble, respectively. In this case, we may look for solutions to (5.3) with the right-hand side given by $\begin{pmatrix} \mathbb{1}_{\partial D} \\ 0 \end{pmatrix}$.

Thanks to the spherical symmetry of $D$, the operator $\mathcal{A}$ can be diagonalised by spherical harmonic functions. We denote by $X = L^2(\partial D) \times L^2(\partial D)$, and we define the two-dimensional subspace $X_1$ of $X$ by

$$X_1 := \text{Vect}\left\{ \begin{pmatrix} \mathbb{1}_{\partial D} \\ 0 \end{pmatrix}, \begin{pmatrix} 0 \\ \mathbb{1}_{\partial D} \end{pmatrix} \right\}. \tag{5.4}$$

The breathing approximation [40] consists of projecting the equation (5.3) on $X_1$. More specifically, we write $\psi_{b/w} = C_{b/w}\mathbb{1}_{\partial D}$, and we solve the $2 \times 2$ equation

$$A \begin{pmatrix} C_b \\ C_w \end{pmatrix} = \begin{pmatrix} u^{\text{in}}(0) \\ 0 \end{pmatrix}, \tag{5.5}$$

where $A$ is the $2 \times 2$ matrix containing the coefficients of $\mathcal{A}$ in the basis (5.4). The values of the components of $A$ are deduced from the next lemma (see Appendix A.3 for the proof).

**Lemma 5.2.1.** *It holds that*

$$\forall x \in \mathbb{R}^3,\ |x| \geq R, \quad \mathcal{S}_D^k[\mathbb{1}_{\partial D}](x) = -\frac{\mathrm{e}^{\mathrm{i}k|x|}}{|x|}\frac{R\sin(kR)}{k},$$

*and*

$$\left(\mathcal{K}_D^k\right)^*[\mathbb{1}_{\partial D}] = \frac{\sin(kR)}{kR}\mathrm{e}^{\mathrm{i}Rk} - \frac{\mathrm{e}^{2\mathrm{i}kR}}{2}.$$

By introducing the dimensionless parameters $x_b = k_b R$ and $x_w = kR = \frac{v_b}{v} x_b$, we obtain that (5.5) is equivalent to solving

$$\widetilde{A}\begin{pmatrix} C_b \\ C_w \end{pmatrix} = \begin{pmatrix} \frac{u^{\text{in}}(0)}{R} \\ 0 \end{pmatrix} \quad \text{with} \quad \widetilde{A} := \begin{pmatrix} -\dfrac{\mathrm{e}^{\mathrm{i}x_b}}{x_b}\sin(x_b) & \dfrac{\mathrm{e}^{\mathrm{i}x_w}}{x_w}\sin(x_w) \\ \dfrac{\mathrm{e}^{\mathrm{i}x_b}}{\delta}\left(\dfrac{\sin(x_b)}{x_b} - \cos(x_b)\right) & -\mathrm{e}^{\mathrm{i}x_w}\left(\dfrac{\sin(x_w)}{x_w} - \mathrm{i}\sin(x_w)\right) \end{pmatrix}.$$

After some straightforward calculations, we obtain

$$C_w = \left[\frac{\mathrm{e}^{-\mathrm{i}x_w} x_w \left(1 - x_b \cot(x_b)\right)}{\sin(x_w)\left(1 - x_b \cot(x_b) - \delta\left(1 - \mathrm{i}x_w\right)\right)}\right] \frac{u^{\text{in}}(0)}{R}. \tag{5.6}$$

Note that in the breathing approximation, we assume that $x_b, x_w \ll 1$ (we will see in the sequel that $x_b, x_w \approx 0.1$ in the regime we are interested in), so that indeed $\sin(x_w) \neq 0$, and the expression (5.6) makes sense.

### Scattering function

The pressure scattered by the bubble is $u^{\text{s}} := \mathcal{S}_D^k[\psi]$. Since $\psi = C_w \mathbb{1}_{\partial D}$, we obtain $u^{\text{s}} = C_w \mathcal{S}_D^k[\mathbb{1}_{\partial D}]$, whose expression was given in Lemma 5.2.1. Together with (5.6), we obtain that the value of $u^{\text{s}}$ on the boundary $\partial D$ is

$$u^{\text{s}}(|x| = R) = -C_w R\left(\frac{\sin(x_w)}{x_w}\mathrm{e}^{\mathrm{i}x_w}\right) = \left(\frac{x_b \cot(x_b) - 1}{1 - \delta - x_b \cot(x_b) + \mathrm{i}\delta\dfrac{v_b}{v} x_b}\right) u^{\text{in}}(0).$$

The complex-valued dimensionless function

$$f_s(x_b) = \frac{\left(1 - x_b \cot(x_b)\right)}{x_b \cot(x_b) - 1 + \delta - \mathrm{i}\delta\dfrac{v_b}{v} x_b}, \tag{5.7}$$

is called the scattering function. It links the value of the incoming pressure on the boundary of the bubble to the value of the radiated pressure on the same boundary. Using the scattering function, we have the following monopole approximation for the scattered field

$$u_{\text{s}}(x) = f_s(x_b) u^{\text{in}}(0) R \frac{\mathrm{e}^{ik(|x|-R)}}{|x|}. \tag{5.8}$$

Let us study the function $f_s$. The Minnaert resonance corresponds to the point $x_b = x_M$ such that

$$1 - \delta - x_M \cot(x_M) = 0 \quad \text{or} \quad \tan(x_M) = \frac{x_M}{1 - \delta}.$$

To leading order in $\delta$, we find $x_M \approx \sqrt{3\delta} \approx 0.06$. At this particular frequency, it holds that

$$f_s(x_M) = \mathrm{i}\frac{v}{v_b x_M} \quad \text{with} \quad \frac{v}{v_b x_M} \approx 70.$$

Hence, at the Minnaert frequency, the pressure gains a phase of $\mathrm{e}^{\mathrm{i}\pi/2}$, and the amplitude is multiplied by a factor of 70 at the boundary.

In the physical literature (e.g. [70]), the scattering function is usually approximated by the simpler function

$$f_s(x_b) \approx \widetilde{f}_s(x_b) := \frac{1}{\left(\frac{x_M}{x_b}\right)^2 - 1 - \mathrm{i}\left(\frac{v_b}{v}\right) x_b}. \tag{5.9}$$

The functions $f_s(\omega)$ and $\tilde{f}_s(\omega)$ are shown in Figure 5.1. Numerically, we find that $\sup_{x\in[0,0.1]} \left|f_s - \widetilde{f}_s\right| \approx 0.47$, so that $\widetilde{f}_s$ is an accurate approximation of $f_s$.

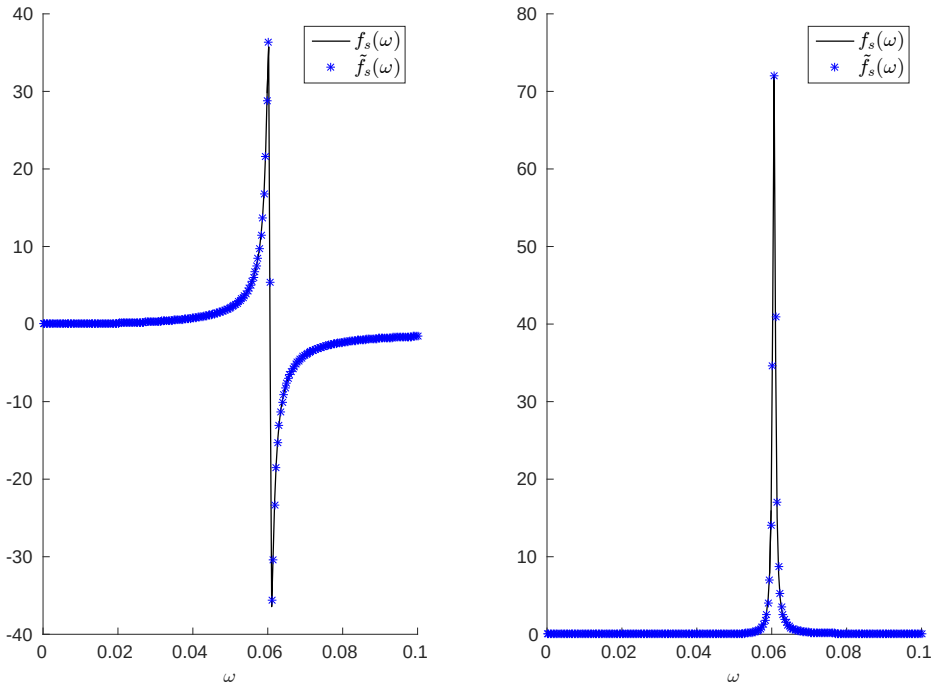


Figure 5.1.: The real part and the imaginary part of $f_s$ (solid black line) and $\widetilde{f}_s$ (blue crosses).

## 5.3. System of N bubbles

We now consider a set of $N$ disjoint bubbles. In order to keep the notation simple, we will assume that all the bubbles have the same radius $R$. This is not a very restrictive assumption, and this case contains effects we are interested in. The volume occupied by bubble number $j$ is

$$D_j := \left\{x \in \mathbb{R}^3,\ |x - x_j| \leq R\right\}, \quad 1 \leq j \leq N.$$

The distance between the centers of bubble $i$ and bubble $j$ is $d_{ij} = |x_i - x_j|$. The non-intersecting condition implies that $d_{ij} \geq 2R$ for all $i \neq j$. We finally denote by $D := \bigcup_{1\leq j\leq N} D_j$ the volume occupied by all the bubbles.

We want to solve the Helmholtz equation $(\Delta + k^2)u = 0$ subject to boundary conditions analogous to the ones in (1.4). We make the ansatz

$$u = \begin{cases} u^{\text{in}} + \left(\sum_{j=1}^N \mathcal{S}_{D_j}^k[\psi_j]\right) & \text{in } \mathbb{R}^3\backslash\overline{D}, \\ \mathcal{S}_{D_j}^{k_b}[\psi_{j,b}] & \text{in } D_j, \quad 1 \leq j \leq N. \end{cases} \tag{5.10}$$

where $\psi_j, \psi_{j,b} \in L^2(\partial D_j)$ are layer potentials associated to the $j$-th bubble. By introducing $X := \prod_{j=1}^N L^2(\partial D_j) \times L^2(\partial D_j)$ , this leads to a system of equations of the form

$$\mathcal{A}_{D_1,\dots D_N} \begin{pmatrix} \psi_{1,b} \\ \psi_1 \\ \vdots \\ \psi_{N,b} \\ \psi_N \end{pmatrix} = \begin{pmatrix} u^{\text{in}}\Big|_{\partial D_1} \\ \frac{\partial u^{\text{in}}}{\partial \nu_1}\Big|_{\partial D_1} \\ \vdots \\ u^{\text{in}}\Big|_{\partial D_N} \\ \frac{\partial u^{\text{in}}}{\partial \nu_N}\Big|_{\partial D_N} \end{pmatrix}, \tag{5.11}$$

The operator $\mathcal{A}_{D_1,\dots,D_N}$ has the block diagonal form

$$\mathcal{A}_{D_1,\dots,D_N} = \begin{pmatrix} \mathcal{M}_1 & \mathcal{L}_{1,2} & \mathcal{L}_{1,3} & \dots \\ \mathcal{L}_{2,1} & \mathcal{M}_2 & \mathcal{L}_{2,3} & \dots \\ \vdots & \vdots & \vdots & \vdots \\ \mathcal{L}_{N,1} & \mathcal{L}_{N,2} & \dots & \mathcal{M}_N \end{pmatrix},$$

where $\mathcal{M}_j$ is the self-interaction for the $j$-th bubble (see also (5.3)), defined by

$$\mathcal{M}_j := \begin{pmatrix} \mathcal{S}_{D_j}^{k_b} & -\mathcal{S}_{D_j}^{k} \\ \frac{1}{\delta}\left(-\frac{1}{2}I + \left(\mathcal{K}_{D_j}^{k_b}\right)^*\right) & -\left(\frac{1}{2}I + \left(\mathcal{K}_{D_j}^{k}\right)^*\right) \end{pmatrix},$$

and where, for $i \neq j$, $\mathcal{L}_{i,j}$ encodes the effect of the $j$-th bubble $j$ to the $i$-th bubble:

$$\mathcal{L}_{i,j} = \begin{pmatrix} 0 & -\mathcal{S}_{D_i,D_j}^k \\ 0 & -\mathcal{L}_{D_i,D_j}^k \end{pmatrix}.$$

Here, we introduced the operators $\mathcal{S}^k_{D_i,D_j} : L^2(\partial D_j) \to L^2(\partial D_i)$ and $\mathcal{L}^k_{D_i,D_j} : L^2(\partial D_j) \to L^2(\partial D_i)$, which are respectively defined by

$$\mathcal{S}^k_{D_i,D_j}[\psi] = \mathcal{S}^k_{D_j}[\psi]\Big|_{\partial D_i}, \quad \text{and} \quad \mathcal{L}^k_{D_i,D_j}[\psi] = \frac{\partial}{\partial \nu_i}\mathcal{S}^k_{D_j}[\psi]\Big|_{\partial D_i}, \qquad \psi \in L^2(\partial D_j).$$

Such a system is usually called a system of $N$ scatterers for the Helmholtz equation, and has been the starting point for a large number of articles (e.g. [65]).

### 5.3.1. The point scatterer approximation for N-bubbles

The point scatterer approximation for the $N$-bubble system comes directly from the breathing approximation on each bubble. More specifically, we assume that the pressure field applied to each bubble is constant on the boundary of this bubble. This is an accurate approximation when the bubbles are well-separated, *i.e.*, their distance is much greater than their size. Under this approximation, we can derive an approximate solution for the system parameters.

We denote by $u_i^{\text{in}}$ the total pressure field incident on the $i$-th bubble $D_i$, and by $u_i^{\text{s}}$ the pressure field scattered from $D_i$. It is clear that

$$u_i^{\text{in}} = u^{\text{in}} + \sum_{j \neq i} u_j^s. \tag{5.12}$$

Using (5.8), and the fact that $|x_i - x_j| \gg R$ (so that $\mathrm{e}^{\mathrm{i}k(|x_i - x_j| - R)} \approx \mathrm{e}^{\mathrm{i}k|x_i - x_j|}$, the scattered field $u_i^{\text{s}}(x)$ far from the $i$-th bubble can be approximated by

$$u_i^{\text{s}}(x) = -4\pi R f_s(x_b) G^k(x - x_i) u_i^{\text{in}}(x). \tag{5.13}$$

By taking $x = x_j$ in the above equation and using (5.12), we obtain the following system of linear equations for $u_i^{\text{in}}$:

$$u_i^{\text{in}} + \sum_{j \neq i} 4\pi R f_s(x_b) G^k(x_i - x_j) u_j^{\text{in}} = u^{\text{in}}(x_i), \quad \text{or, equivalently,} \quad M \begin{pmatrix} u_1^{\text{in}} \\ \vdots \\ u_N^{\text{in}} \end{pmatrix} = \begin{pmatrix} u^{\text{in}}(x_1) \\ \vdots \\ u^{\text{in}}(x_N) \end{pmatrix},$$

where $M$ is the $N \times N$ matrix defined by

$$M_{ij} = \begin{cases} 1, & i = j, \\ 4\pi R f_s(x_b) G^k(x_i - x_j), & i \neq j. \end{cases} \tag{5.14}$$

Finally, the total pressure field is the sum of the incoming wave and all the waves scattered by the different bubbles. Together with (5.13), we obtain

$$u(x) = u^{\text{in}}(x) + \sum_{1 \leq i \leq N} -4\pi R f_s(x_b) G^k(x - x_j) \sum_{1 \leq j \leq N} (M^{-1})_{ij} u^{\text{in}}(x_j), \tag{5.15}$$

This is called the point interaction approximation. See also [25] for a rigorous justification of this approximation.

## 5.4. Numerical illustrations

We now perform a numerical investigation of the results that have been observed in [65] to assist us in developing a mathematical theory that explains the super-focusing phenomenon. We first calculate the imaginary part of the Green's function for a bubbly medium over a range of frequencies to ascertain the optimal frequency range for super-focusing. We then simulate wave propagation through the bubbly medium to evaluate the actual focusing performance. We begin by defining the syste

### 5.4.1. System parameters

We take the density of water and air to be $\rho_w = 1.0 \times 10^3$ kg.m$^{-3}$, and $\rho_b = 1.2$ kg.m$^{-3}$, respectively. We take the bulk modulus of water and air to be $\kappa_b = 2.07 \times 10^9$ N.m$^{-2}$, and $\kappa_b = 127 \times 10^3$ N.m$^{-2}$, respectively. This results in a speed of sound in water of $v \approx 1440$ m.s$^{-1}$.

We set the common radius of the bubbles to be $R = 50 \times 10^{-6}$ m. In light of these parameters, the Minnaert resonant frequency is $\omega_M \approx 59 \times 2\pi$ kHz. We denote by $\lambda_w = 2\pi/k$ the wavelength in water. We denote by $\lambda_w^M$ the wavelength at the Minnaert resonance frequency, with $\lambda_w^M \approx 0.025$ m. The scattering function $f_s$ is taken to be

$$f_s(\omega) := \frac{1}{\left(\frac{\omega_M}{\omega}\right)^2 - 1 - \mathrm{i}\alpha},$$

where $\alpha = \alpha_{rad} + \alpha_{th} + \alpha_{vis}$ is the damping coefficient which represents dissipation due to acoustic radiation, thermal damping, and viscous damping [39, 66]. $\alpha_{th}$ depends on the ratio of the heat capacities of air, which we take to be $\gamma = 1.1$, and $\alpha_{vis}$ depends on the viscosity of water, which we take to be $\eta = 10^{-3}$ Pa.s.

Although viscous damping is the dominant form of dissipation for very small bubbles, thermal damping domaintes for the bubble size we are considering at frequencies close to the Minnaert resonance. We neglect the effect of surface tension for simplicity. If, however, we were to consider very small bubbles, *i.e.*, such that the radii were less than, say, $1 \times 10^{-5}$ m, then accounting for surface tension would become important [3, 84].

### 5.4.2. A priori evaluation of focusing performance via the imaginary part of the Green's function

In imaging, the imaginary part of the Green's function is the point spread function [12, 24]. Thus the sharper the effective $\Im(G)$ is for some inhomogeneous medium (compared to $\Im(G)$ for the homogeneous background medium), the better the focusing. In this section we investigate the properties of the imaginary part of the Green's function in the case of a bubbly medium. We remark that all simulations in this section are averaged over 25 bubble cloud configurations to make the results more apparent.

We consider a source at the origin surrounded by a cube of uniformly distributed bubbles, for a range of gas volume fractions, *i.e.*, $\Phi = \phi \times 10^{-4}$ where $\phi \in \{0, 0.5, 1, 2\}$. We denote by $G_{\mathrm{m}}(x, \omega)$ the Green's function in the presence of the bubbles at frequency $\omega$. Using the point interaction approximation, we have (see (5.15))

$$G_{\mathrm{m}}(x, \omega) := G_v^{\omega}(x) - \sum_i 4\pi R f_s(\omega) G_v^{\omega}(x - x_i) \sum_j (M^{-1})_{ij} G_v^{\omega}(x_j). \tag{5.16}$$

We set $\omega_{\min} = 15 \times 2\pi$ kHz and $\omega_{\max} = 155 \times 2\pi$ kHz. In Figure 5.2 we plot $|\Im(G_m(x, \omega))|$ when no bubbles are present, and in Figure 5.3 we plot $|\Im(G_{\mathrm{m}}(x, \omega))|$, for bubble clouds of increasing volume fraction.

When the volume fraction reaches $\Phi = 2 \times 10^{-4}$ we obtain a very sharp peak over the origin just below the Minnaert resonance frequency, which indicates that focusing performance should be greatly enhanced in this frequency regime.

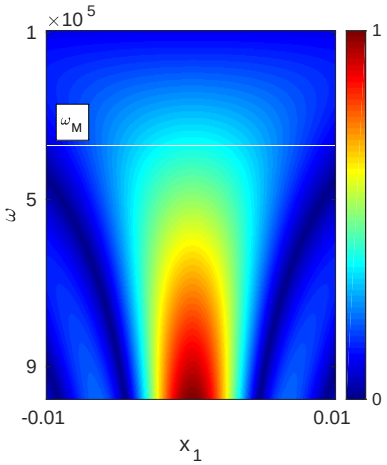


Figure 5.2.: The normalized imaginary part of the Green's function when no bubbles are present in the liquid. The white line indicates the Minnaert resonance frequency $\omega_M \approx 3.7 \times 10^5$ kHz.

To get a better picture of the enhanced focusing near the Minnaert resonance, we next consider the average of the imaginary part of the Green's function over different frequency intervals $[\omega_-, \omega_+]$ (and again, averaged over 25 bubble cloud configurations):

$$\langle \mathrm{Im}(G_{\mathrm{m}}(x)) \rangle := \frac{1}{\omega_+ - \omega_-} \int_{\omega_-}^{\omega_+} \mathrm{Im}(G_{\mathrm{m}}(x, \omega)) \mathrm{d}\omega. \tag{5.17}$$

In Figure 5.4 we examine the magnitude of this expression for various bubble cloud concentrations, for three separate cases. First, the averaging is performed over a range of frequencies just above the Minnaert resonance frequency, *i.e.*, $\omega_- = 1.1\ \omega_M$ and $\omega_+ = 2\ \omega_M$. In this case the presence of the bubbles can be seen to have a strong effect on wave propagation and $\langle \mathrm{Im}(G_{\mathrm{m}}(x)) \rangle$ vanishes almost completely, indicating a severe

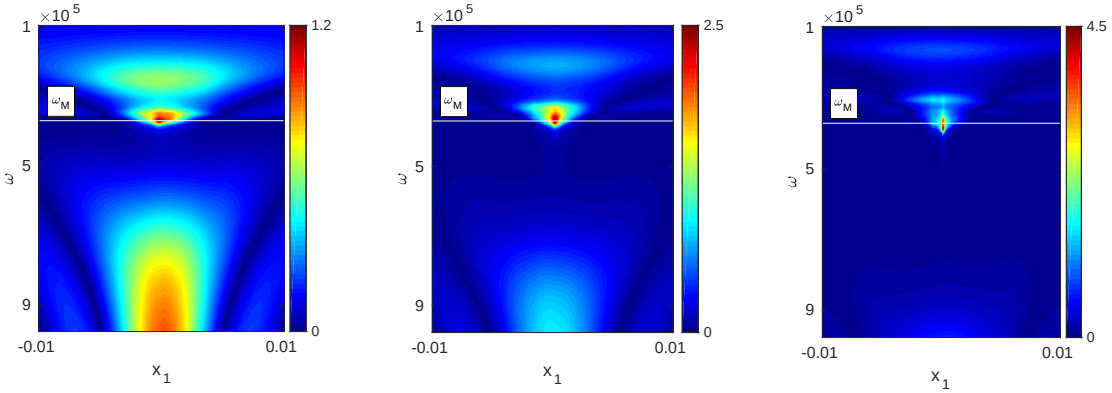


(a) $\Phi = 0.5 \times 10^{-4}$ (b) $\Phi = 1 \times 10^{-4}$ (c) $\Phi = 2 \times 10^{-4}$

Figure 5.3.: The imaginary part of the Green's function averaged over 25 bubble cloud configurations for increasing bubble concentrations $\Phi$. The results are normalized with respect to the background Green's function in Figure 5.2. The function peaks over the source at $x = (x_1, x_2, x_3)^\top = (0, 0, 0)^\top$ when the excitation frequency is very near the Minnaert resonance frequency, indicating the potential for enhanced focusing.

degradation in focusing. Next, we perform the averaging well away from and above the Minnaert resonance frequency, *i.e.*, $\omega_- = 2\,\omega_M$ and $\omega_+ = 4\,\omega_M$. It is clear that in this case the effect of the bubbles is greatly diminished and $\langle \mathrm{Im}(G_\mathrm{m}(x)) \rangle$ appears much the same as it would in a bubble free system.

Finally, we perform the averaging over a range of frequencies just below the Minnaert resonance frequency, *i.e.*, we set $\omega_- = 0.8\,\omega_M$ and $\omega_+ = 0.99\,\omega_M$. Here, we observe a very strong peak near the origin, which is indicative of the super-focusing phenomenon. The full width at half maximum (FWHM) of $\langle \mathrm{Im}(G_\mathrm{m}(x)) \rangle$ is approximately $\lambda_w^M/72$, a huge increase over the corresponding FWHM for the imaginary part of the background Green's function which is approximately $\lambda_w^M/2$. The results in this section can be explained by the strong resonant coupling which occurs near the Minnaert resonance frequency.

### 5.4.3. Simulating wave propagation in a bubbly medium

Our aim in this section is to simulate wave propagation through bubble clouds of increasing gas volume fractions in water, for two cases: (i) a realistic situation in which thermal and viscous damping are present; (ii) an idealized scenario in which the liquid is free from thermal and viscous damping.

In both cases, we emit a short impulse signal from the origin that propagates through the bubbly medium, and record it at a set of receivers (time-reversal mirrors) in the far-field. We then time-reverse the recorded signals and send them back towards the source. The initial impulse signal was emitted from a single point, the origin, so we are interested in how well the time-reversed signals focus back at this point. In particular,

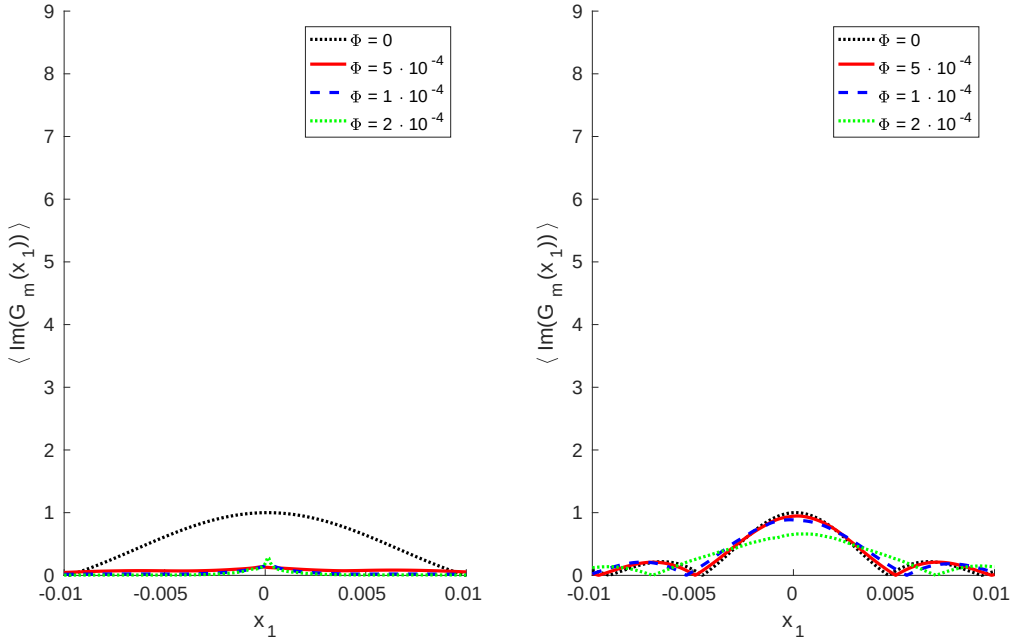


(a) Averaging over the interval $\omega_M \times [1.1, 2]$

(b) Averaging over the interval $\omega_M \times [2, 4]$

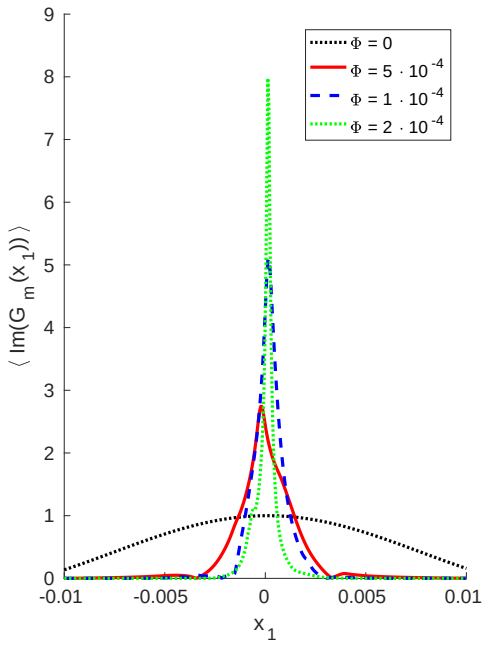


(c) Averaging over the interval $\omega_M \times [0.8, 0.99]$

Figure 5.4.: The imaginary part of the Green's function averaged over three different frequency regimes (and also averaged over 25 bubble cloud configurations) for increasing bubble concentrations $\Phi$.

we are interested in evaluating the quality of the focusing, which we judge by comparing the full width at half maximum (FWHM) of the focal spot with the diffraction limit of a numerical aperture of 1, *i.e.*, $\lambda_w/2$.

Our results from the previous section suggest that super-focusing is achievable if we excite the bubbles with a reference frequency $\omega_R$ which is slightly below the Minnaert resonance frequency. Hence, we choose $\omega_R = 57.5 \times 2\pi$ kHz.

We consider a source, located at the origin $\text{BS} = (0,0,0)^\top$, that is surrounded by a cube containing uniformly distributed bubbles. The length of the cube is $L = 0.01$ m, which is approximately half the wavelength at the Minnaert resonance. We consider several gas volume fractions, *i.e.*, $\Phi = \phi \times 10^{-4}$ where $\phi \in \{0, 0.5, 1, 2\}$. Note that $\Phi = 2 \times 10^{-4}$ corresponds to a collection of approximately 380 bubbles. We assume that the water outside this cube does not contain any bubbles. Finally, four receivers (time-reversal mirrors) are located at $\mathbf{r}_1 = (0.05, 0, 0)^\top$, $\mathbf{r}_2 = (-0.05, 0, 0)^\top$, $\mathbf{r}_3 = (0, 0.05, 0)^\top$ and $\mathbf{r}_4 = (0, -0.05, 0)^\top$.

### Propagating an impulse signal to the time-reversal mirrors

We begin the simulation by sending a short pulse from the origin. The signal $s(t)$ (shown in Figure 5.5a) is given by

$$s(t) := \sin(\omega_R t) \times \sin\left(\pi \frac{(t - t_0)}{\tau}\right) \times \mathbb{1}\left(0 < t - t_0 < \tau\right),$$

where

$$t_0 = 2 \times 10^{-3} \text{ s}, \qquad \tau = 0.2 \times 10^{-3} \text{s}. \tag{5.18}$$

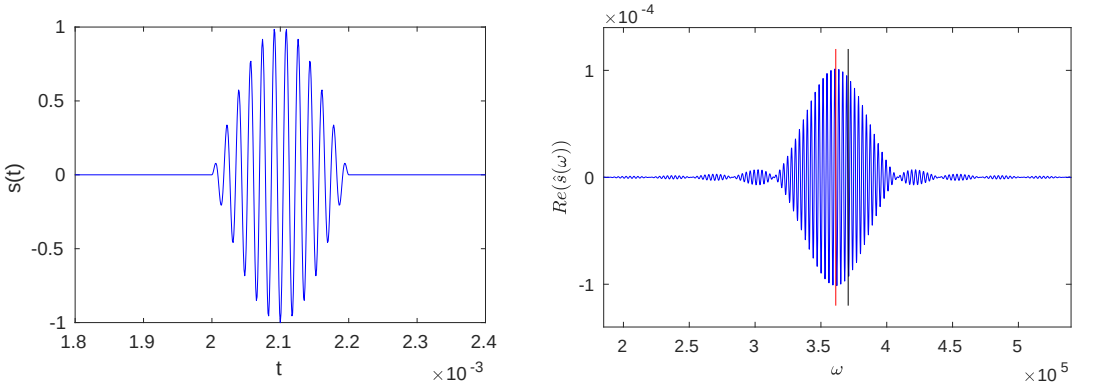


(a) The function $s(t)$ given in (5.4.3).

(b) The function $\Re(\hat{s}(\omega))$ given in (5.19). The red line indicates the reference frequency $\omega_R$, and the black line is the Minnaert frequency $\omega_M$.

Figure 5.5.

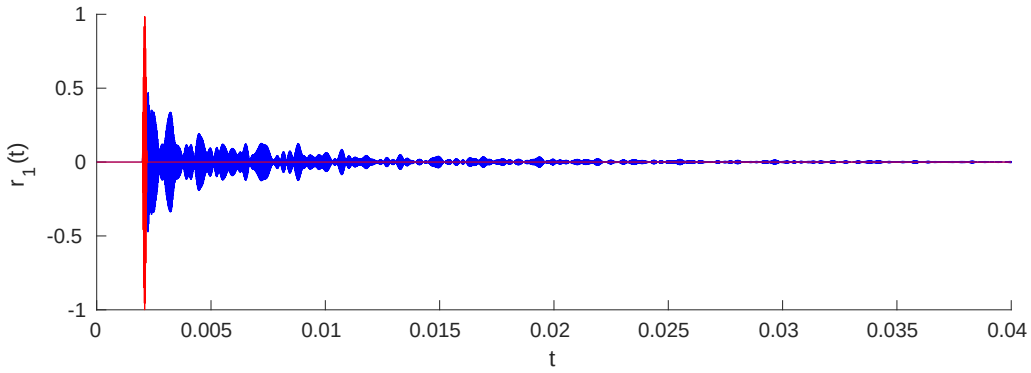


Figure 5.6.: The recording at the first receiver $r_1(t)$ (blue). The red plot is $s(t)$.

To compute the forward problem, the signal is time-Fourier transformed with

$$s(t) = \int_{\mathbb{R}} \hat{s}(\omega) \mathrm{e}^{-\mathrm{i}\omega t}. \tag{5.19}$$

The choice of an appropriate sampling rate and recording time is influenced by two factors. Firstly, the signal recorded at each receiver must naturally be longer than the initial impulse signal to capture the multiple scattering of waves among the bubbles. Secondly, for an inappropriate choice of sampling rate and recording interval, the signals recorded at each receiver may feature non-zero artifacts prior to $t_0$ which is non-causal.

Choosing a numerical signal resolution of $\Delta t = 0.5 \times 10^{-6}$ s, which corresponds to a sampling rate of 2 Mhz, and a recording interval of $[0, T]$ where $T = 1 \times 10^{-1}$ s, captures the multiple scattering and eliminates non-causal artifacts. We remark that this sampling rate is approximately 35 samples per cycle with respect to the Minnaert resonance frequency ($f_M \approx$ 59 kHz or $\omega_M \approx 59 \times 2\pi$ kHz).

We perform the Fourier Transform using MatLab's `fft` routine, which provides us with the Fourier transformed values for all frequencies $f \in [-f_{\max}/2, f_{\max}/2]$, with $f_{\max} = 2 \times 10^6$ Hz, and $\Delta f = 10$ Hz. In terms of angular frequency this corresponds to $\omega \in [-\omega_{\max}/2, \omega_{\max}/2]$, with $\omega_{\max} \approx 1.3 \times 10^7$ Hz, and $\Delta\omega \approx 63$ Hz. A plot of the non-trivial part of $\hat{s}(\omega)$ is given in Figure 5.5b.

Due to the fact that the signal is real-valued, and oscillates near $\omega_R$, only the frequencies near $\omega_R$ are considered. Upon truncating redundant sections of the spectrum for efficiency, we are left with approximately 11500 Helmholtz problems to solve. We use the point scatterer model described in the previous section to solve these problems, and obtain the frequency domain representations of the recorded signals $\hat{r}_j(\omega)$ for $1 \leq j \leq 4$. Through application of the inverse Fourier transform, we retrieve the recordings in the time domain $r_j(t)$ (see Figure 5.6). Note that while the initial signal is a short pulse, the recorded signal is much longer, which is due to the phenomenon of multiple echoing of waves among the bubbles.

### Focusing using time-reversed waves

We now simulate time-reversal. Each receiver now acts as a source, and emits the signal $r_j^\sharp(t) = r_j(T-t)$. Proceeding as in the forward problem, we time-Fourier transform the signal, and then solve the resulting Helmholtz problems.

The time-reversed signal $s^\sharp(t)$, which arrives at the origin at approximately 0.098 $s$, is recorded in the interval $[-0.03, 0.03]$ on the $x_1$-axis. In Figure 5.7, we show the result for the case of water subject to thermal and viscous damping, for various bubble volume fractions. It transpires that super-focusing is not achieved, even though we have excited the bubbles with a seemingly optimal frequency. The FWHM of the focal spot for a bubble volume fraction of $\Phi = 2 \times 10^{-4}$ is approximately $\lambda_w^M/2$, which is essentially the same as the FWHM in the background medium, *i.e.*, when there are no bubbles present. Furthermore, the amplitude of the focal spot is less than half the magnitude of the corresponding focal spot for a bubble free-medium.

The problem is that since scattering is greatly enhanced due to resonant coupling, a great deal of energy is lost via dissipation in the medium during transmission. This leads to a significant degradation in focusing performance. This phenomenon was also noticed in [65], in which the authors observed that although the Minnaert resonance frequency was the optimal excitation frequency for super-focusing in an idealized medium, when thermal and viscous damping were accounted for, the focusing enhancement was lost.

### Focusing in an idealized medium

We now repeat the simulation, this time for the case of an idealized liquid free from thermal or viscous damping, although still subject to radiative damping. The results are shown in Figure 5.8. As the volume fraction of the bubble cloud increases, a sub-wavelength focal spot develops at the origin. A FWHM of approximately $\lambda_w^M/10$ is achieved, indicating super-focusing. The FWHMs for a bubbly medium subject to thermal, viscous and radiative damping, and a bubbly medium subject only to radiative damping, are shown in Figure 5.9. The FWHM for a fully damped bubble-free medium is also plotted for reference.

We conclude that although the Minnaert resonance frequency provides the theoretically optimal frequency for focusing in the idealized case, in practical situations it is not ideal due to amplified dissipation at near resonant frequencies. Thus, examination of the imaginary part of the Green's function is not alone sufficient to predict focusing performance in this medium.

The numerical simulations in this section indicate that further analysis is required to build a deeper understanding of the interplay between resonant effects in the bubble cloud and thermal and viscous damping, with the aim being to balance the (theoretical) enhancement in focusing near the Minnaert resonance frequency with the amplified dissipation in that regime, and to derive the true optimal frequency regime for focusing

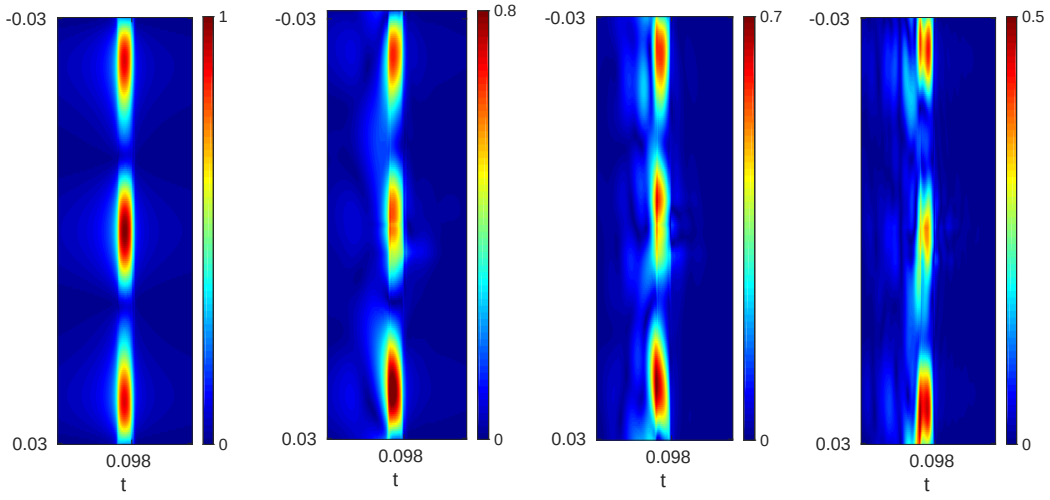


(a) $\Phi = 0$ (b) $\Phi = 0.5 \times 10^{-4}$ (c) $\Phi = 1 \times 10^{-4}$ (d) $\Phi = 2 \times 10^{-4}$

Figure 5.7.: Focusing in water: Time reversed pressure fields for bubble clouds of increasing volume fraction $\Phi$, when the exciting frequency is just below the Minnaert resonance frequency and acoustic, thermal, and viscous damping are considered. The results are normalized with respect to the field in the bubble-free case. The greatly enhanced enhanced dissipation at resonance prevents the occurrence of super-focusing.

in a dissipative bubbly medium. One interesting possibility is the use of bubble clouds in which the bubble radii are are non-constant. Bubble clouds featuring non-uniform radius distributions have been shown to match better with theory for wave propagation in bubbly media near resonant frequencies than monodisperse mixtures [37].

## 5.5. Concluding remarks

In this chapter we have investigated the phenomenon of super-focusing of acoustic waves in a liquid containing a large number of bubbles. We formulated a layer potential representation of the scattering problem and then derived a point scatterer approximation for $N$ bubbles, in the low frequency regime. Using this point scatterer approximation, we numerically analyzed the imaginary part of the Green's function for the bubbly medium and asserted that super-focusing may be achievable at frequencies just below the Minnaert resonance frequency.

Upon numerically simulating acoustic wave propagation, it transpires that this frequency regime is, in fact, not ideal for super-focusing in practise due to severe degradation of focusing performance via enhanced dissipation at near resonant frequencies. Further simulations confirm that the Minnaert resonance provides the optimal excitation frequency only in an idealized medium which is free from thermal and viscous damping. In this situation a sub-wavelength focal spot with a FWHM of approximately $\lambda_w^M/10$

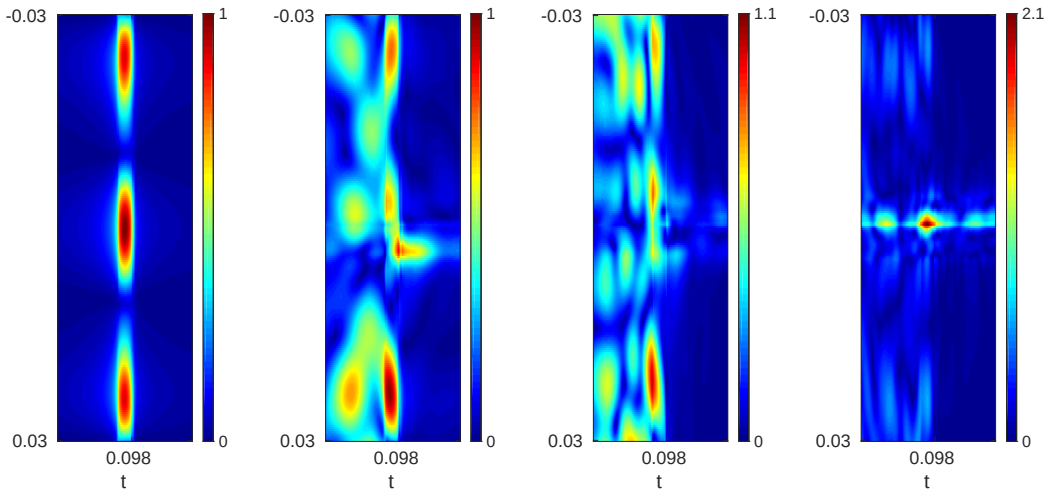


(a) $\Phi = 0$ (b) $\Phi = 0.5 \times 10^{-4}$ (c) $\Phi = 1 \times 10^{-4}$ (d) $\Phi = 2 \times 10^{-4}$

Figure 5.8.: Focusing in an idealized liquid (no thermal or viscous damping): Time reversed pressure fields for bubble clouds of increasing volume fraction $\Phi$, when the exciting frequency is just below the Minnaert resonance frequency and the only damping considered is acoustic radiation. The results are normalized with respect to the field in the bubble-free case. A sub-wavelength focal spot, with a peak over twice as large as that found when no bubbles are present, is obtained when the volume fraction reaches $\Phi = 2 \cdot 10^{-4}$.

is achieved. It would be very interesting to further investigate the connection between focusing performance and damping, and derive the correct optimal frequency regime for super-focusing in a realistic damped medium.

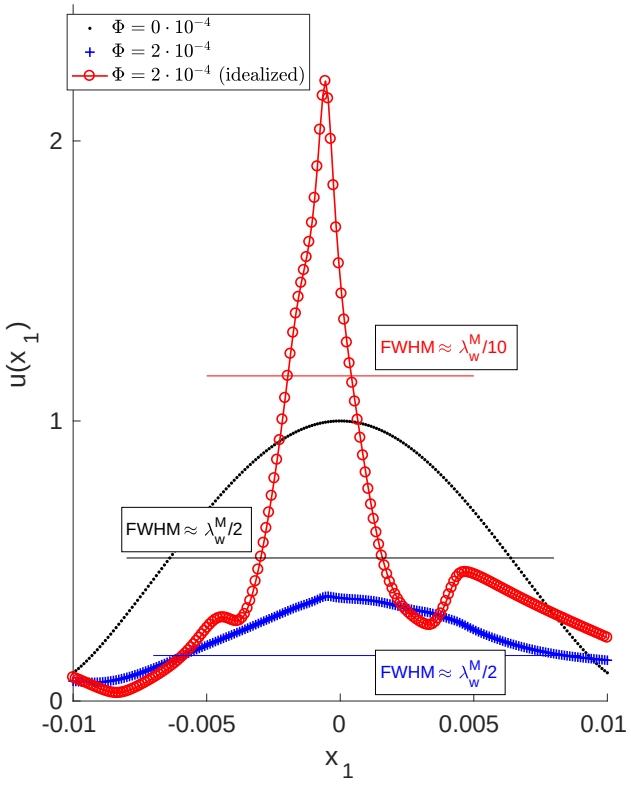


Figure 5.9.: The full width at half maximum (FWHM) of the focal spot in a bubbly medium subject to thermal and viscous damping (blue crossses) is approximately $\lambda_w^M/2$ for an excitation frequency just below the Minnaert resonance frequency. Thus there is essentially no improvement in focusing over the case of water without bubbles (black dots). On the other hand, the FWHM of the focal spot in an idealized bubbly liquid free from thermal and viscous damping (red circles) is one-tenth the diffraction limit at that same frequency. The results are normalized with respect to the FWHM in the bubble-free case.

# 6. Double-negative Acoustic Metamaterials

The aim of this chapter is to provide a mathematical theory for understanding the mechanism behind the double-negative refractive index phenomenon in bubbly fluids. The design of double-negative metamaterials generally requires the use of two different kinds of sub-wavelength resonators, which may limit the applicability of double-negative metamaterials. Herein we rely on media that consists of only a single type of resonant element, and show how to turn the acoustic metamaterial with a single negative effective property obtained in [H. Ammari and H. Zhang, Effective medium theory for acoustic waves in bubbly fluids near Minnaert resonant frequency. SIAM J. Math. Anal., 49 (2017), 3252–3276.] into a negative refractive index metamaterial, which refracts waves negatively, hence acting as a super-lens. Using bubble dimers made of two identical bubbles, it is proved that both the effective mass density and the bulk modulus of the bubbly fluid can be negative near the anti-resonance of the two hybridized Minnaert resonances for a single constituent bubble dimer. A rigorous justification of the Minnaert resonance hybridization, in the case of a bubble dimer in a homogeneous medium, is established. The acoustic properties of a single bubble dimer are analyzed. Asymptotic formulas for the two hybridized Minnaert resonances are derived. Moreover, it is proved that the bubble dimer can be approximated by a point scatterer with monopole and dipole modes. For an appropriate volume fraction of bubble dimers with certain conditions on their configuration, a double-negative effective medium when the frequency is near the anti-resonance of the hybridized Minnaert resonances can be obtained.

## 6.1. Introduction

Metamaterials are man-made composite media structured on a scale much smaller than a wavelength. They raise the possibility of an unprecedented level of control when it comes to engineering the propagation of waves. A particularly interesting capability is the prospect of focusing or imaging beyond the diffraction limit. Metamaterials can manipulate and control sound waves in ways that are not possible in conventional materials. Their study has also drawn increasing interest in recent times due to their potential application in cloaking [69, 57, 82].

Metamaterials can be assembled into structures (typically periodic but not necessarily so) that are similar to continuous materials, yet have unusual wave properties that differ substantially from those of conventional media. Sub-wavelength resonators are the building blocks of metamaterials. Because of the sub-wavelength scale of the resonators,

it is possible to describe the marcoscopic behavior of a metamaterial using homogenization theory, and this results in an effective medium having negative or high contrast parameters. Metamaterials with negative or high contrast refractive indices offer new possibilities for imaging and for the control of waves at deep sub-wavelength scales [38].

As shown in Chapter 2, due to the high contrast between the mass density inside and outside an air bubble in a fluid, a quasi-static acoustic resonance known as the Minnaert resonance occurs. At or near this resonant frequency, the size of a bubble can be up to three orders of magnitude smaller than the wavelength of the incident wave, and the bubble behaves as a strong monopole scatterer of sound. From Chapter 5 it follows that the Minnaert resonance phenomenon makes air bubbles good candidates for acoustic sub-wavelength resonators. They have the potential to serve as the basic building blocks for acoustic metamaterials, which include bubbly fluids [70, 65, 72].

As shown in [25], around the Minnaert resonant frequency, an effective medium theory can be derived in the dilute regime. Furthermore, above the Minnaert resonant frequency, the real part of the effective bulk modulus is negative, and consequently the bubbly fluid behaves as a diffusive medium for the acoustic waves. Meanwhile, as shown in Chapter 5, below the Minnaert resonant frequency, with an appropriate bubble volume fraction, a high contrast effective medium can be obtained, making the sub-wavelength focusing or super-focusing of waves achievable. These properties show that the bubbly fluid functions like an acoustic metamaterial, and indicate that a sub-wavelength bandgap opening occurs at the Minneaert resonant frequency. We remark that such behavior is rather analogous to the coupling of electromagnetic waves with plasmonic nanoparticles, which results in effective negative or high contrast dielectric constants for frequencies near the plasmonic resonance frequencies [5, 19, 22].

In Chapter 4, the opening of a sub-wavelength phononic bandgap is demonstrated by considering a periodic arrangement of bubbles and exploiting their Minnaert resonance. It is shown that there exists a sub-wavelength band gap in such a bubbly crystal. This sub-wavelength band gap is mainly due to the cell resonance of the bubbles in the quasi-static regime and is quite different from the usual band gaps in photonic/phononic crystals, where the gap opens at a wavelength which is comparable to the period of the structure [47, 16, 17]. In [18], the homogenization theory of the bubbly crystal near the frequency where the band gap opens is further investigated. It is shown that the band gap opens at the corner (edge in two dimensions) of the Brillouin zone. Moreover, explicit formulas for the Bloch eigenfunctions are derived. This makes both the homogenization theory and the justification of the superfocusing phenomenon in the non-dilute case possible.

In this chapter, we aim to understand the mechanism behind the double-negative refractive index phenomenon in bubbly fluids. The design of double-negative metamaterials generally requires the use of two different kinds of building blocks or specific sub-wavelength resonators presenting multiple overlapping resonances. Such a requirement limits the applicability of double-negative metamaterials. Herein we rely on media that consists of only a single type of resonant element, and show how to turn the acoustic

metamaterial with a single negative effective property obtained in [25] into a negative refractive index metamaterial, which refracts waves negatively, hence acting as a super-lens [91, 88, 85].

Our main result is to prove that, using bubble dimers, the effective mass density and bulk modulus of the bubbly fluid can both be negative over a non empty range of frequencies. A bubble dimer is a system consisting of two identical slightly separated spherical bubbles. It features two slightly different sub-wavelength resonances, called the hybridized Minnaert resonances. We establish a rigorous mathematical justification of the Minnaert resonance hybridization in the case of a bubble dimer in a homogeneous medium. We analyze the acoustic properties of the bubble dimer, derive asymptotic formulas for the two resonances, and prove that the bubble dimer can be approximated as a point scatterer with monopole and dipole modes. The hybridized Minnaert resonances are fundamentally different modes. The first mode is, as in the case of a single bubble, a monopole mode, while the second mode is a dipole mode. The resonance associated with the dipole mode is usually referred to as the anti-resonance. For an appropriate volume fraction, when the excitation frequency is close to the anti-resonance, we obtain a double-negative effective mass density and bulk modulus for bubbly media consisting of a large number of bubble dimers with certain conditions on their distribution. The dipole modes in the background medium contribute to the effective mass density while the monopole modes contribute to the effective bulk modulus.

The chapter is organized as follows. In Section 6.2 we introduce some preliminaries on layer potentials. In Section 6.3 we describe the hybridization phenomenon for a bubble dimer, prove that two sub-wavelength resonances occur, and compute their asymptotic expansions in terms of the mass density contrast. In Section 6.4 we prove that the bubble dimer can be approximated as the sum of a monopole source and a dipole source. In Section 6.5 we derive a double-negative effective medium theory for bubbly media. Finally, in Section 6.6 we compute effective mass density and bulk modulus dispersion curves near the hybridized Minnaert resonances to illustrate the double-negative property of bubbly media.

## 6.2. Preliminaries

Recall that in three dimensions $\mathcal{S}_D : L^2(\partial D) \to H^1(\partial D)$ is invertible and that its inverse is bounded [17].

Throughout the chapter we assume that $D$ has two connected components $D_1$ and $D_2$, and we use the following notation:

$$\int_{\partial D_1 - \partial D_2} f(y) d\sigma(y) = \int_{\partial D_1} f(y) d\sigma(y) - \int_{\partial D_2} f(y) d\sigma(y), \tag{6.1}$$

where $f$ is a function defined on $\partial D = \partial D_1 \cup \partial D_2$.

Finally, we present some useful formulas which are frequently used in the sequel.

**Lemma 6.2.1.** *The following identities hold for any $\phi \in L^2(\partial D)$: for $j = 1, 2$,*

*(i)* $\int_{\partial D_j} \left(\frac{1}{2}I - \mathcal{K}_D^*\right) \phi(y) d\sigma(y) = 0$;

*(ii)* $\int_{\partial D_j} \left(\frac{1}{2}I + \mathcal{K}_D^*\right) \phi(y) d\sigma(y) = \int_{\partial D_j} \phi(y) d\sigma(y)$;

*(iii)* $\int_{\partial D_j} \mathcal{K}_D^2[\phi] = -\int_{D_j} \mathcal{S}_D[\phi]$;

*(iv)* $\int_{\partial D_j} \mathcal{K}_D^3[\phi] = i|D_j|/(4\pi) \int_{\partial D} \phi$.

*Proof.* (i) follows from the jump relation $(-\frac{1}{2}I + \mathcal{K}_D^*)[\phi] = \partial \mathcal{S}_D[\phi]/\partial \nu|_{\partial D}^-$ and the fact that $\mathcal{S}_D[\phi]$ is harmonic in $D$. (ii) immediately follows from (i). For (iii), we have

$$\int_{\partial D_j} \mathcal{K}_D^2 \phi = \frac{1}{8\pi} \int_{\partial D_j} \frac{\partial}{\partial \nu_x} \int_{\partial D} |x - y| \phi(y) = \frac{1}{8\pi} \int_{D_j} \int_{\partial D} \frac{2}{|x - y|} \phi(y) = -\int_{D_j} \mathcal{S}_D[\phi].$$

Finally, it holds that

$$\int_{\partial D_j} \mathcal{K}_D^3[\phi] = \frac{i}{12\pi} \int_{\partial D_j} \int_{\partial D} \langle x - y, \nu_x \rangle \phi(y) = \frac{i|D_j|}{4\pi} \int_{\partial D} \phi,$$

which proves (iv). □

### 6.2.1. Capacitance coefficients

Let $\psi_1$, $\psi_2 \in L^2(\partial D)$ be given by

$$\mathcal{S}_D[\psi_1] = \begin{cases} 1 & \text{on } \partial D_1, \\ 0 & \text{on } \partial D_2, \end{cases} \qquad \mathcal{S}_D[\psi_2] = \begin{cases} 0 & \text{on } \partial D_1, \\ 1 & \text{on } \partial D_2. \end{cases} \tag{6.2}$$

Then, using the jump relations (1.7), it is easy to check that

$$\ker\left(-\frac{1}{2}I + \mathcal{K}_D^*\right) = \text{span } \{\psi_1, \psi_2\}. \tag{6.3}$$

We define the capacitance coefficients matrix $C = (C_{ij})$ by

$$C_{ij} := -\int_{\partial D_j} \psi_i, \quad i, j = 1, 2.$$

We remark that the matrix $C$ is positive definite and symmetric.

Suppose $D_1$ and $D_2$ are identical balls of radius $r_0$ separated by a distance $d_0$ such that the distance between the centers of the balls is $d_0 + 2r_0$. Then $C_{11} = C_{22}$, $C_{12} =$

$C_{21},\ C_{11} > 0$, and $C_{12} < 0$. Explicit formulas for the capacitance coefficients for two balls can be obtained using bispherical coordinates [67]. We have the following result:

$$\begin{aligned} C_{11} &= 8\pi\alpha \sum_{n=0}^{\infty} \frac{e^{(2n+1)T}}{e^{2(2n+1)T}-1}, \\ C_{12} &= -8\pi\alpha \sum_{n=0}^{\infty} \frac{1}{e^{2(2n+1)T}-1}, \\ C_{21} &= C_{12}, \quad C_{22} = C_{11}, \end{aligned}$$

where

$$\alpha = \sqrt{d_0(r_0 + d_0/4)}, \quad T = \sinh^{-1}(r_0/a).$$

**Lemma 6.2.2.** *Suppose that $D_1$ and $D_2$ are two identical balls. Then the following identities hold for any $\phi \in L^2(\partial D)$:*

*(i)* $\int_{\partial D_j} \mathcal{K}_D^3[\psi_1 - \psi_2]d\sigma = 0, \quad j = 1, 2;$

*(ii)* $\int_{\partial D_1 - \partial D_2} (\mathcal{S}_D)^{-1}\mathcal{S}_D^1[\phi]d\sigma = 0;$

*(iii)* $\int_{\partial D_1 - \partial D_2} (\mathcal{S}_D)^{-1}[y_i]d\sigma(y) = \int_{\partial D} y_i(\psi_1 - \psi_2)d\sigma(y).$

*Proof.* (i) and (ii) follow from Lemma 6.2.1 (iv), the definition of $\mathcal{S}_D^1$ and the symmetry of $D_1 \cup D_2$. For (iii), by letting $\phi_i(x) := (\mathcal{S}_D)^{-1}[y_i](x)$ and using the jump relations (1.7) and the fact that $\mathcal{S}_D[\phi]$ is harmonic in $D$, we can check that

$$\begin{aligned} \int_{\partial D_1 - \partial D_2} (\mathcal{S}_D)^{-1}[y_i]d\sigma(y) &= \int_{\partial D_1 - \partial D_2} 1 \cdot \left( \frac{\partial \mathcal{S}_D[\phi_i]}{\partial \nu}\Big|_+ - \frac{\partial \mathcal{S}_D[\phi_i]}{\partial \nu}\Big|_- \right) \\ &= \int_{\partial D_1 - \partial D_2} 1 \cdot \frac{\partial \mathcal{S}_D[\phi_i]}{\partial \nu}\Big|_+ = \int_{\partial D} \mathcal{S}_D[\psi_1 - \psi_2] \cdot \frac{\partial \mathcal{S}_D[\phi_i]}{\partial \nu}\Big|_+ . \end{aligned}$$

Then, since and $\mathcal{S}_D[\phi_i]|_{\partial D} = y_i$, Green's identity yields (iii). □

## 6.3. Resonance for a dimer consisting of two identical bubbles

In this section, we consider the quasi-static resonances of a bubble dimer. Throughout, we denote by $D$ the normalized bubble dimer which consists of two identical balls $D_1$ and $D_2$, both with volume one. We assume that the two balls $D_1$ and $D_2$ are symmetric with respect to the origin. Moreover, $D_1$ and $D_2$ are aligned with respect to the $x_1$-axis. For a general dimer featuring two identical balls, we call the unit direction vector along which the two balls are aligned the orientation of the dimer.

Let $u^{in}$ be the incident wave defined in Section 1.6. The scattering problem, subject to the regime specified in Section 1.2, can be modeled by the following system of equations:

$$\begin{cases} (\Delta + k^2)u = 0 & \text{in } \mathbb{R}^3\backslash\overline{D}, \\ (\Delta + k_b^2)u = 0 & \text{in } D, \\ u|_- = u|_+ & \text{on } \partial D, \\ \dfrac{1}{\rho_b}\dfrac{\partial u}{\partial \nu}\Big|_- = \dfrac{1}{\rho}\dfrac{\partial u}{\partial \nu}\Big|_+ & \text{on } \partial D, \\ u^s := u - u^{in} & \text{satisfies the SRC.} \end{cases} \tag{6.4}$$

The solution to (6.4) can be represented using the single layer potentials $\mathcal{S}_D^{k_b}$ and $\mathcal{S}_D^k$ as follows [14]:

$$u = \begin{cases} u^{in} + \mathcal{S}_D^k[\psi] & \text{in } \mathbb{R}^3\backslash\overline{D}, \\ \mathcal{S}_D^{k_b}[\phi] & \text{in } D, \end{cases} \tag{6.5}$$

where the pair $(\phi, \psi) \in L^2(\partial D) \times L^2(\partial D)$ is a solution to

$$\begin{cases} \mathcal{S}_D^{k_b}[\phi] - \mathcal{S}_D^k[\psi] = u^{in} \\ \dfrac{1}{\rho_b}\left(-\dfrac{1}{2}I + \mathcal{K}_D^{k_b,*}\right)[\phi] - \dfrac{1}{\rho}\left(\dfrac{1}{2}I + \mathcal{K}_D^{k,*}\right)[\psi] = \dfrac{1}{\rho}\dfrac{\partial u^{in}}{\partial \nu} \end{cases} \quad \text{on } \partial D. \tag{6.6}$$

We denote by

$$\mathcal{A}_\delta^\omega := \begin{pmatrix} \mathcal{S}_D^{k_b} & -\mathcal{S}_D^k \\ \left(-\frac{1}{2}I + \mathcal{K}_D^{k_b,*}\right) & -\delta\left(\frac{1}{2}I + \mathcal{K}_D^{k,*}\right) \end{pmatrix}. \tag{6.7}$$

Then (6.6) can be written as

$$\mathcal{A}_\delta^\omega \begin{pmatrix} \phi \\ \psi \end{pmatrix} = \begin{pmatrix} u^{in} \\ \delta\frac{\partial u^{in}}{\partial \nu} \end{pmatrix}.$$

It is well-known that the above integral equation has a unique solution for all real frequencies $\omega$.

The resonance of the bubble dimer $D$ in the scattering problem (6.4) can be defined as all the complex numbers $\omega$ with negative imaginary part such that there exists a nontrivial solution to the following equation:

$$\mathcal{A}_\delta^\omega \begin{pmatrix} \phi \\ \psi \end{pmatrix} = 0. \tag{6.8}$$

These can be viewed as the characteristic values of the operator-valued analytic function $\mathcal{A}_\delta^\omega$ (with respect to $\omega$); see [17].

It can be shown that $\omega = 0$ is a characteristic value of $\mathcal{A}_0^\omega$ when $\delta = 0$. Then Gohberg-Sigal theory tells us that there exists a characteristic value $\omega_0 = \omega_0(\delta)$ such that $\omega_0(0) = 0$ and $\omega_0$ depends on $\delta$ continuously. We call this characteristic value the quasi-static resonance (or Minnaert resonance). We now present the main result on the quasi-static resonances of the bubble dimer $D$.

**Theorem 6.3.1.** *There are exist two quasi-static resonances with positive real part for the bubble dimer $D$. Moreover, they have the following asymptotic expansions as $\delta$, defined by (1.2), goes to zero:*

$$\omega_1 = \sqrt{\delta v_b^2(C_{11} + C_{12})} - i\tau_1\delta + O(\delta^{3/2}), \tag{6.9}$$

$$\omega_2 = \sqrt{\delta v_b^2(C_{11} - C_{12})} + \delta^{3/2}\hat{\eta}_1 + i\delta^2\hat{\eta}_2 + O(\delta^{5/2}), \tag{6.10}$$

*where*

$$\tau_1 = \frac{v_b^2}{4\pi v}(C_{11} + C_{12})^2,$$

*and $\hat{\eta}_1$ and $\hat{\eta}_2$ are real numbers which are determined by $D$, $v$, and $v_b$. The two resonances $\omega_1$ and $\omega_2$ are called the hybridized resonances of the bubble dimmer $D$. The resonance $\omega_2$ is referred to as the anti-resonance.*

*Proof.*
**Step 1.** Suppose that $(\phi,\ \psi)$ is a nontrivial solution to (6.8) for some small $\omega = \omega(\delta)$.

Using the asymptotic expansions (A.1.1) of the single layer potential and the Neumann-Poincaré operator, together with the fact that $k = O(\omega)$, we have

$$\begin{cases} \mathcal{S}_D[\phi - \psi] + k_b\mathcal{S}_D^1[\phi] - k\mathcal{S}_D^1[\psi] = O(\omega^2), \\ \left(-\frac{1}{2}I + \mathcal{K}_D^* + k_b^2\mathcal{K}_D^2 + k_b^3\mathcal{K}_D^3\right)[\phi] - \delta\left(\frac{1}{2}I + \mathcal{K}_D^*\right)[\psi] = O(\omega^4 + \delta\omega^2). \end{cases} \tag{6.11}$$

From the first equation of (6.11) and the definition of $\mathcal{S}_D^1$, it holds that

$$\psi = \phi - \frac{1}{4\pi i}(\mathcal{S}_D)^{-1}\left(k_b\int_{\partial D}\phi - k\int_{\partial D}\psi\right) + O(\omega^2).$$

Then, from the fact that $\phi - \psi = O(\omega)$ and the definition of $\psi_j$, we obtain

$$\psi = \phi + \frac{(k_b - k)}{4\pi i}(\psi_1 + \psi_2)\int_{\partial D}\phi + O(\omega^2). \tag{6.12}$$

Plugging (6.12) into the second equation of (6.11), we get

$$\left(-\frac{1}{2}I + \mathcal{K}_D^*\right)[\phi] + \left(k_b^2\mathcal{K}_D^2 + k_b^3\mathcal{K}_D^3 - \delta\left(\frac{1}{2}I + \mathcal{K}_D^*\right)\right)[\phi]$$

$$-\frac{\delta(k_b-k)}{4\pi i}(\psi_1+\psi_2)\int_{\partial D}\phi = O(\omega^4+\delta\omega^2), \tag{6.13}$$

where we have used the identity

$$\begin{aligned}\psi_j &= \frac{\partial \mathcal{S}_D}{\partial\nu}\Big|_{\partial D}^{+}[\psi_j] - \frac{\partial \mathcal{S}_D}{\partial\nu}\Big|_{\partial D}^{-}[\psi_j]\\ &= \frac{\partial \mathcal{S}_D}{\partial\nu}\Big|_{\partial D}^{+}[\psi_j] - 0 = \left(\frac{1}{2}I + \mathcal{K}_D^*\right)[\psi_j].\end{aligned}$$

In view of (6.3), a nontrivial solution $\phi$ to (6.13) can be written as

$$\phi = a\psi_1 + b\psi_2 + O(\omega^2+\delta), \tag{6.14}$$

for some nontrivial constants $a,\ b$ with $|a|+|b| = O(1)$.

**Step 2.** Recall that $|D_1| = |D_2| = 1$, $C_{11} = C_{22}$, and $C_{12} = C_{21} < 0$. By integrating (6.13) over $\partial D_j,\ j = 1, 2$, and then using Lemma 6.2.1, we have, up to an error of order $O(\omega^4+\delta\omega^2)$,

$$\begin{cases} -\dfrac{\omega^2}{v_b^2}a - \dfrac{i\omega^3}{4\pi v_b^3}C(a,b) + \delta(aC_{11}+bC_{12}) + \dfrac{i(v_b^{-1}-v^{-1})\delta\omega}{4\pi}(C_{11}+C_{12})C(a,b) = 0,\\ -\dfrac{\omega^2}{v_b^2}b - \dfrac{i\omega^3}{4\pi v_b^3}C(a,b) + \delta(aC_{12}+bC_{11}) + \dfrac{i(v_b^{-1}-v^{-1})\delta\omega}{4\pi}(C_{12}+C_{11})C(a,b) = 0, \end{cases} \tag{6.15}$$

where

$$C(a,b) := a(C_{11}+C_{12}) + b(C_{21}+C_{22}).$$

Then it follows that for $\delta \ll 1$, the characteristic values of $\mathcal{A}_\delta^\omega$ are given by

$$\omega_* = \omega_0 + O(\delta^{3/2}), \tag{6.16}$$

for some $\omega_0 = O(\sqrt{\delta})$. Solving (6.15) for $\omega$, we find two characteristic values with positive real parts:

$$\omega_1 = \sqrt{\delta v_b^2(C_{11}+C_{12})} + O(\delta), \quad \omega_2 = \sqrt{\delta v_b^2(C_{11}-C_{12})} + O(\delta),$$

where the corresponding $(a,b)$'s are given by

$$(a,b) = (1,1),\ (1,-1), \tag{6.17}$$

up to an error of order $O(\delta)$. Plugging these values for $a$, $b$ and $\omega_j$ into (6.15) and solving for the $O(\delta)$ term in $\omega_j$, we obtain

$$\omega_1 = \sqrt{\delta v_b^2(C_{11}+C_{12})} - i\tau_1\delta + O(\delta^{3/2}), \quad \omega_2 = \sqrt{\delta v_b^2(C_{11}-C_{12})} + 0\cdot\delta + O(\delta^{3/2}).$$

The proof of the estimate (6.9) for $\omega_1$ is concluded. We refine the estimate for $\omega_2$ in the next step.

**Step 3.** Note that $\Im\omega_2$ is of order $\delta^{3/2}$. We perform a further calculation to find an explicit formula for $\Im\omega_2$. Since $(a,b) = (1,-1) + O(\delta)$, we write

$$\phi = \psi_1 - \psi_2 + \delta\phi_1 + \delta^{3/2}\phi_2 + \delta^2\phi_3 + \delta^{5/2}\phi_4 + O(\delta^3),$$

and

$$\omega_2 = \delta^{1/2}\eta_0 + \delta^{3/2}\eta_1 + \delta^2\eta_2 + O(\delta^{5/2}),$$

where $\eta_0 := \sqrt{v_b^2(C_{11} - C_{12})}$. From the symmetry of $D$, we can normalize $\phi$ so that

$$\phi_j \perp \text{span}\,\{\psi_1, \psi_2\} = \ker\left(-\frac{1}{2}I + \mathcal{K}_D^*\right), \quad \text{for } j = 1,2,3,4, \quad \text{in } L^2(\partial D).$$

**Step 4.** By using the expansions in Appendix (A.1.1), we have

$$\mathcal{S}_D[\phi - \psi] + k_b\mathcal{S}_D^1[\phi] - k\mathcal{S}_D^1[\psi] + k_b^2\mathcal{S}_D^2[\phi] - k^2\mathcal{S}_D^2[\psi] + k_b^3\mathcal{S}_D^3[\phi] - k^3\mathcal{S}_D^3[\psi] = O(\delta^2),$$

and

$$\begin{aligned}&\left(-\frac{1}{2}I + \mathcal{K}_D^* + k_b^2\mathcal{K}_D^2 + k_b^3\mathcal{K}_D^3 + k_b^4\mathcal{K}_D^4 + k_b^5\mathcal{K}_D^5\right)[\phi]\\ &-\delta\left(\tfrac{1}{2}I + \mathcal{K}_D^* + k^2\mathcal{K}_D^2 + k^3\mathcal{K}_D^3\right)[\psi] = O(\delta^3).\end{aligned} \tag{6.18}$$

Hence, we get

$$\begin{aligned}\psi &= (\mathcal{S}_D + k\mathcal{S}_D^1 + k^2\mathcal{S}_D^2 + k^3\mathcal{S}_D^3)^{-1}(\mathcal{S}_D + k_b\mathcal{S}_D^1 + k_b^2\mathcal{S}_D^2 + k_b^3\mathcal{S}_D^3)[\phi] + O(\delta^2)\\
&= \phi + (\mathcal{S}_D + k\mathcal{S}_D^1 + k^2\mathcal{S}_D^2)^{-1}((k_b - k)\mathcal{S}_D^1 + (k_b^2 - k^2)\mathcal{S}_D^2 + (k_b^3 - k^3)\mathcal{S}_D^3)[\phi] + O(\delta^2)\\
&= \phi + (\mathcal{S}_D + k\mathcal{S}_D^1)^{-1}((k_b^2 - k^2)\mathcal{S}_D^2 + (k_b^3 - k^3)\mathcal{S}_D^3)[\psi_1 - \psi_2] + \delta(k_b - k)(\mathcal{S}_D)^{-1}\mathcal{S}_D^1[\phi_1] + O(\delta^2)\\
&= \phi + (k_b^2 - k^2)(\mathcal{S}_D)^{-1}\mathcal{S}_D^2[\psi_1 - \psi_2] + (k_b^3 - k^3)(\mathcal{S}_D)^{-1}\mathcal{S}_D^3[\psi_1 - \psi_2]\\
&\quad - k(k_b^2 - k^2)(\mathcal{S}_D)^{-1}\mathcal{S}_D^1(\mathcal{S}_D)^{-1}\mathcal{S}_D^2[\psi_1 - \psi_2] + \delta(k_b - k)(\mathcal{S}_D)^{-1}\mathcal{S}_D^1[\phi_1] + O(\delta^2).\end{aligned}$$

Plugging this into (6.18) and equating terms of the same order of $\delta$, $\delta^{3/2}$, $\delta^2$, $\delta^{5/2}$, we arrive at

- $O(\delta)$-terms:

$$\left(-\frac{1}{2}I + \mathcal{K}_D^*\right)[\phi_1] + \eta_0^2 v_b^{-2}\mathcal{K}_D^2[\psi_1 - \psi_2] - (\psi_1 - \psi_2) = 0, \tag{6.19}$$

  whence $\phi_1$ is uniquely determined.

- $O(\delta^{3/2})$-terms:

$$\left(-\frac{1}{2}I + \mathcal{K}_D^*\right)[\phi_2] + \eta_0^3 v_b^{-3}\mathcal{K}_D^3[\psi_1 - \psi_2] = 0, \tag{6.20}$$

  whence $\phi_2$ is uniquely determined.

- $O(\delta^2)$-terms:

$$\left(-\frac{1}{2}I+\mathcal{K}_D^*\right)[\phi_3]+2\eta_0\eta_1 v_b^{-2}\mathcal{K}_D^2[\psi_1-\psi_2]+\eta_0^2 v_b^{-2}\mathcal{K}_D^2[\phi_1]+\eta_0^4 v_b^{-4}\mathcal{K}_D^4[\psi_1-\psi_2]$$
$$-\left(\frac{1}{2}I+\mathcal{K}_D^*\right)[\eta_0^2(v_b^{-2}-v^{-2})(\mathcal{S}_D)^{-1}\mathcal{S}_D^2[\psi_1-\psi_2]+\phi_1]-v^{-2}\eta_0^2\mathcal{K}_D^2[\psi_1-\psi_2]=0.$$

- $O(\delta^{5/2})$-terms:

$$\left(-\frac{1}{2}I+\mathcal{K}_D^*\right)[\phi_4]+2\eta_0\eta_2 v_b^{-2}\mathcal{K}_D^2[\psi_1-\psi_2]+\eta_0^2 v_b^{-2}\mathcal{K}_D^2[\phi_2]+\eta_0^3 v_b^{-3}\mathcal{K}_D^3[\phi_1]$$
$$+3\eta_0^2\eta_1 v_b^{-3}\mathcal{K}_D^3[\psi_1-\psi_2]+\eta_0^5 v_b^{-5}\mathcal{K}_D^5[\psi_1-\psi_2]$$
$$-\eta_0^3\left(\frac{1}{2}I+\mathcal{K}_D^*\right)\Big[(v_b^{-3}-v^{-3})(\mathcal{S}_D)^{-1}\mathcal{S}_D^3[\psi_1-\psi_2]$$
$$-v^{-1}(v_b^{-2}-v^{-2})(\mathcal{S}_D)^{-1}\mathcal{S}_D^1(\mathcal{S}_D)^{-1}\mathcal{S}_D^2[\psi_1-\psi_2]\Big]$$
$$-\eta_0^3\left(\frac{1}{2}I+\mathcal{K}_D^*\right)\left[(v_b^{-1}-v^{-1})(\mathcal{S}_D)^{-1}\mathcal{S}_D^1[\phi_1]\right]$$
$$-\left(\frac{1}{2}I+\mathcal{K}_D^*\right)[\phi_2]-\eta_0^3 v^{-3}\mathcal{K}_D^3[\psi_1-\psi_2]=0.$$

**Step 5.** We consider the terms of order $O(\delta^2)$. Integrating over $\partial D_1-\partial D_2$ and using Lemma 6.2.2, we get

$$-2\eta_0\eta_1 v_b^{-2}+\int_{\partial D_1-\partial D_2}\left(\eta_0^2 v_b^{-2}\mathcal{K}_D^2[\phi_1]-\phi_1\right)+\eta_0^4 v_b^{-4}\int_{\partial D_1-\partial D_2}\mathcal{K}_D^4[\psi_1-\psi_2]$$
$$-\eta_0^2(v_b^{-2}-v^{-2})\int_{\partial D_1-\partial D_2}(\mathcal{S}_D)^{-1}\mathcal{S}_D^2[\psi_1-\psi_2]+\eta_0^2 v^{-2}=0. \tag{6.21}$$

It follows that $\eta_1$ is uniquely determined from the above equation. Moreover, we can check that $\eta_1$ is a real number.

**Step 6.** Finally, we consider the $\delta^{5/2}$ terms. Integrating over $\partial D_1-\partial D_2$ and using Lemma 6.2.2 again, we get

$$-4\eta_0\eta_2 v_b^{-2}+\int_{\partial D_1-\partial D_2}\eta_0^2 v_b^{-2}\mathcal{K}_D^2[\phi_2]-\phi_2+\eta_0^3 v_b^{-3}\mathcal{K}_D^3[\phi_1]$$
$$+\int_{\partial D_1-\partial D_2}\eta_0^5 v_b^{-5}\mathcal{K}_D^5[\psi_1-\psi_2]-\eta_0^3(v_b^{-3}-v^{-3})(\mathcal{S}_D)^{-1}\mathcal{S}_D^3[\psi_1-\psi_2]=0. \tag{6.22}$$

Therefore, $\eta_2$ is uniquely determined. We also note that $\eta_2$ is a purely imaginary number. Indeed, from (6.19), (6.20), we see that $\Im\phi_1=0, \Re\phi_2=0$. This combined with the integral representation of $\mathcal{K}_D^2, \mathcal{K}_D^3, \mathcal{K}_D^5$ yields the desired result.

Thus we conclude that the resonance frequency $\omega_2$ has the following asymptotic expansion:

$$\omega_2 = \sqrt{\delta v_b^2 (C_{11} - C_{12})} + \delta^{3/2}\hat{\eta}_1 + i\delta^2\hat{\eta}_2 + O(\delta^{5/2}), \tag{6.23}$$

where $\hat{\eta}_1 := \eta_1$ and $\hat{\eta}_2 := -i\eta_2$ are real numbers given by (6.21) and (6.22), respectively. □

**Remark 6.3.2.** *The above approach is applicable to a general bubble dimer which may consist of two non-identical spherical bubbles.*

## 6.4. The point scatterer approximation of bubbles

In this section we prove an approximate formula for the solution $u$ to the scattering problem for the bubble dimer $D = D_1 \cup D_2$.

We need the following lemma which can be proved using a simple symmetry argument.

**Lemma 6.4.1.** *We have*

$$\int_{\partial D} y_2(\psi_1 - \psi_2)d\sigma(y) = \int_{\partial D} y_3(\psi_1 - \psi_2)d\sigma(y) = 0,$$

*while*

$$\int_{\partial D} y_1(\psi_1 - \psi_2)d\sigma(y) = P,$$

*for some nonzero real number $P$.*

In the next theorem, we prove that the bubble dimer can be approximated as a point scatterer with monopole and dipole modes.

**Theorem 6.4.2.** *For $\omega = O(\delta^{1/2})$ and a given plane wave $u^{in}$, the solution $u$ to* (6.4) *can be approximated as $\delta \to 0$ by*

$$u(x) - u^{in}(x) = g^0(\omega)u^{in}(0)G^k(x) + \nabla u^{in}(0) \cdot g^1(\omega)\nabla G(x,k) + O(\delta|x|^{-1}), \tag{6.24}$$

*when $|x|$ is sufficiently large, where*

$$g^0(\omega) := \frac{C(1,1)}{1 - \omega_1^2/\omega^2}(1 + O(\delta^{1/2})), \tag{6.25}$$

$$g^1(\omega) = (g^1_{ij}(\omega)),\ g^1_{ij}(\omega) := \int_{\partial D} (\mathcal{S}_D)^{-1}[x_i](y)y_j + \frac{\delta v_b^2}{|D|(\omega_2^2 - \omega^2)}P^2\delta_{i,1}\delta_{j,1}. \tag{6.26}$$

*Proof.*
**Step 1.** Let $(\phi,\ \psi)$ be the solution to (6.6). Using the asymptotic expansions (A.1.1), we have

$$\begin{cases} \mathcal{S}_D[\phi-\psi]+k_b\mathcal{S}_D^1[\phi]-k\mathcal{S}_D^1[\psi]=u^{in}+O(\delta), \\ \left(-\frac{1}{2}I+\mathcal{K}_D^*+k_b^2\mathcal{K}_D^2+k_b^3\mathcal{K}_D^3\right)[\phi]-\delta\left(\frac{1}{2}I+\mathcal{K}_D^*\right)[\psi]=\delta\frac{\partial u^{in}}{\partial\nu}+O(\delta^2), \end{cases} \tag{6.27}$$

where the remainders $O(\delta)$ and $O(\delta^2)$ are in the operator norm.

From the first equation of (6.27), and following the same approach used to derive (6.12), we obtain

$$\psi=\phi+\frac{(k_b-k)}{4\pi i}(\psi_1+\psi_2)\int_{\partial D}\phi-(\mathcal{S}_D)^{-1}[u^{in}]+O(\delta). \tag{6.28}$$

Plugging (6.28) into the second equation of (6.27), we get

$$\mathcal{C}_\delta^\omega[\phi]=-\delta\left(\frac{1}{2}I+\mathcal{K}_D^*\right)(\mathcal{S}_D)^{-1}[u^{in}]+\delta\frac{\partial u^{in}}{\partial\nu}+O(\delta^2), \tag{6.29}$$

where $\mathcal{C}_\delta^\omega$ is defined by

$$\begin{aligned}\mathcal{C}_\delta^\omega[\phi]:=&\left(-\frac{1}{2}I+\mathcal{K}_D^*[\phi]\right)+\left(k_b^2\mathcal{K}_D^2+k_b^3\mathcal{K}_D^3-\delta\left(\frac{1}{2}I+\mathcal{K}_D^*\right)\right)[\phi]\\&-\frac{\delta(k_b-k)}{4\pi i}(\psi_1+\psi_2)\int_{\partial D}\phi.\end{aligned}$$

Note that $\mathcal{C}_\delta^\omega[\phi]$ is equal to the left-hand side of (6.13).

**Step 2.** Using the Taylor expansion of $u^{in}$ at the origin, and the fact that $\nabla u^{in}=O(\omega)=O(\delta^{1/2})$ and $\nabla^2u^{in}=O(\omega^2)=O(\delta)$, the right-hand side of (6.29) can be approximated by

$$\begin{aligned}&-\delta\left(\frac{1}{2}I+\mathcal{K}_D^*\right)(\mathcal{S}_D)^{-1}[u^{in}](x)+\delta\frac{\partial u^{in}}{\partial\nu}(x)\\&=-\delta\left(\frac{1}{2}I+\mathcal{K}_D^*\right)(\mathcal{S}_D)^{-1}[u^{in}(0)+\nabla u^{in}(0)\cdot y](x)+\delta\nabla(u^{in}(0))\cdot\nu(x)+O(\delta^{3/2})\\&=-\delta u^{in}(0)(\psi_1+\psi_2)-\delta(\mathcal{S}_D)^{-1}[\nabla u^{in}(0)\cdot y]+0+O(\delta^{3/2}).\end{aligned}$$

Therefore, (6.29) becomes

$$\mathcal{C}_\delta^\omega[\phi]=-\delta u^{in}(0)(\psi_1+\psi_2)-\delta(\mathcal{S}_D)^{-1}[\nabla u^{in}(0)\cdot y]+O(\delta^{3/2}). \tag{6.30}$$

**Step 3.** In the statement and proof of Theorem 6.3.1, we have verified that the characteristic values of $\mathcal{C}_\delta^\omega$ are given by (6.9) and (6.10), and that their corresponding singular functions are $\phi_1$, $\phi_2$, *i.e.*,

$$\mathcal{C}_\delta^{\omega_1}[\phi_1]=\mathcal{C}_\delta^{\omega_2}[\phi_2]=0.$$

Recall from (6.14) and (6.17) that

$$\phi_1 = \psi_1 + \psi_2 + O(\delta),\ \phi_2 = \psi_1 - \psi_2 + O(\delta).$$

We decompose the solution $\phi \in L^2(\partial D)$ to (6.30) as

$$\phi = a\phi_1 + b\phi_2 + \phi_3 \tag{6.31}$$

with $\langle \phi_1,\, \phi_3 \rangle = 0$ and $\langle \phi_2,\, \phi_3 \rangle = 0$.

We have

$$\begin{aligned} a(\mathcal{C}_\delta^\omega - \mathcal{C}_\delta^{\omega_1})[\phi_1] + b(\mathcal{C}_\delta^\omega - \mathcal{C}_\delta^{\omega_2})[\phi_2] + \mathcal{C}_\delta^\omega[\phi_3] \\ = -\delta u^{in}(0)(\psi_1 + \psi_2) - \delta(\mathcal{S}_D)^{-1}[\nabla u^{in}(0) \cdot y]. \end{aligned} \tag{6.32}$$

Since

$$(\mathcal{C}_\delta^\omega - \mathcal{C}_\delta^{\omega_j})[\phi_j] = \frac{\omega^2 - \omega_j^2}{v_b^2}\mathcal{K}_D^2[\phi_j] + O(\delta^{3/2}), \quad j = 1, 2,$$

we have $\|(\mathcal{C}_\delta^\omega - \mathcal{C}_\delta^{\omega_j})[\phi_j]\| = O(\delta)$, and hence we conclude from (6.32) that

$$\|\phi_3\| = O((|a| + |b| + 1)\delta). \tag{6.33}$$

Integrating (6.32) over $\partial D$ and then using Lemma 6.2.1, we obtain

$$-a\left(\frac{\omega^2 - \omega_1^2}{v_b^2}|D| + O(\delta^{3/2})\right) + bO(\delta^2) + \|\phi_3\|O(\delta) = 2\delta u^{in}(0)(C_{11} + C_{12}). \tag{6.34}$$

Similarly, by integrating (6.32) over $\partial D_1 - \partial D_2$, we have

$$aO(\delta^2) - b\left(\frac{\omega^2 - \omega_2^2}{v_b^2}|D| + O(\delta^{3/2})\right) + \|\phi_3\|O(\delta) = -\delta \int_{\partial D_1 - \partial D_2} (\mathcal{S}_D)^{-1}[\nabla u^{in}(0) \cdot y]. \tag{6.35}$$

We observe that

$$a = O(1), \quad b = O(\delta^{1/2}), \quad \|\phi_3\| = O(\delta). \tag{6.36}$$

By solving (6.34) and (6.35) for $a$ and $b$, and then using (6.9), we get

$$a = -\frac{2\delta v_b^2(C_{11} + C_{12})}{|D|(\omega^2 - \omega_1^2)}(u^{in}(0) + O(\delta)) = -\frac{\omega_1^2 + O(\delta^{3/2})}{\omega^2 - \omega_1^2}(u^{in}(0) + O(\delta)), \tag{6.37}$$

$$b = \frac{\delta v_b^2}{|D|(\omega^2 - \omega_2^2)}\left(\int_{\partial D_1 - \partial D_2} (\mathcal{S}_D)^{-1}[\nabla u^{in}(0) \cdot y] + O(\delta)\right). \tag{6.38}$$

Now we can calculate $\psi$. By using (6.28), (6.36), (6.37) and (6.38), we obtain

$$\psi = a(1 + O(\delta^{1/2}))\phi_1 + b\phi_2 + \phi_3 - (\mathcal{S}_D)^{-1}[u^{in}(0) + \nabla u^{in}(0) \cdot y] + O(\delta)$$

$$
\begin{aligned}
&= -\frac{\omega_1^2 + O(\delta^{3/2})}{\omega^2 - \omega_1^2}(u^{in}(0) + O(\delta))(1 + O(\delta^{1/2}))\phi_1 - u^{in}(0)\phi_1 \\
&\quad + b\phi_2 + (\mathcal{S}_D)^{-1}[\nabla u^{in}(0) \cdot y] + O(\delta) \\
&= \frac{\omega^2 + O(\delta^{3/2})}{\omega_1^2 - \omega^2}(u^{in}(0) + O(\delta))(1 + O(\delta^{1/2}))\phi_1 + b\phi_2 - \nabla u^{in}(0) \cdot (\mathcal{S}_D)^{-1}[y] + O(\delta).
\end{aligned}
$$

**Step 4.** Finally, we consider the scattered field $u^s(x) := u(x) - u^{in}(x) = \mathcal{S}_D^k[\psi](x)$. It is enough to consider $\mathcal{S}_D^k[\phi_1]$ and $\mathcal{S}_D^k[\phi_2]$.

Note that

$$
G^k(x - y) = G^k(x) - \nabla G^k(x) \cdot y + O(\delta |x|^{-1}).
$$

Note also that, due to the symmetry of $D_1$ and $D_2$, we have

$$
\int_{\partial D} y(\psi_1 + \psi_2)(y) d\sigma(y) = 0, \quad \int_{\partial D} \psi_1 - \psi_2 = 0.
$$

Therefore, for sufficiently large $|x|$, we have

$$
\begin{aligned}
\mathcal{S}_D^k[\phi_1](x) &= \mathcal{S}_D^k[\psi_1 + \psi_2](x) + O(\delta |x|^{-1}) \\
&= \int_{\partial D} G^k(x - y)(\psi_1 + \psi_2)(y) d\sigma(y) + O(\delta |x|^{-1}) \\
&= \int_{\partial D} G^k(x)(\psi_1 + \psi_2)(y) d\sigma(y) \\
&\quad - \nabla G^k(x) \cdot \int_{\partial D} y(\psi_1 + \psi_2)(y) d\sigma(y) + O(\delta |x|^{-1}), \\
&= -2(C_{11} + C_{12}) G^k(x) + 0 + O(\delta |x|^{-1}).
\end{aligned}
$$

Similarly, we have

$$
\begin{aligned}
\mathcal{S}_D^k[\phi_2](x) &= \mathcal{S}_D^k[\psi_1 - \psi_2](x) + O(\delta |x|^{-1}) \\
&= \int_{\partial D} G^k(x - y)(\psi_1 - \psi_2)(y) d\sigma(y) + O(\delta |x|^{-1}) \\
&= -\left( \int_{\partial D} (\psi_1 - \psi_2) y \right) \cdot \nabla G^k(x) + O(\delta |x|^{-1}).
\end{aligned}
$$

The proof is then complete. □

**Corollary 6.4.3.** *For the rescaled bubble dimer $sR_dD$ with size $s$ and orientation $d$, where $R_d$ represents a rotation transform which aligns the bubble dimer $D$ in the direction $d$, we have*

$$
\omega_1(\delta, sR_dD) = \frac{1}{s}\omega_1(\delta, D), \tag{6.39}
$$

$$
\omega_2(\delta, sR_dD) = \frac{1}{s}\omega_2(\delta, D), \tag{6.40}
$$

$$g^0(\omega,\delta,sR_dD)=\frac{2(C_{11}+C_{12})s}{1-\omega_1(\delta,sR_dD)^2/\omega^2}(1+O(\delta^{1/2})) \tag{6.41}$$

$$g^1(\omega,\delta,sR_dD)=s^3\int_{\partial D}(\mathcal{S}_D)^{-1}[(R_dx)_i](y)(R_dy)_j+\frac{\delta v_b^2 s}{|D|(\omega_2(\delta,sR_dD)^2-\omega^2)}P^2d_id_j. \tag{6.42}$$

*Proof.* By a scaling argument, one can show that

$$C_{ij}(sD)=sC_{ij}(D),\quad P(sD)=s^2P(D),$$

and

$$\int_{\partial(sR_dD)}(\mathcal{S}_{sR_dD})^{-1}[x_i](y)y_j=s^3\int_{\partial D}(\mathcal{S}_D)^{-1}[(R_dx)_i](y)(R_dy)_j.$$

The proof is then complete. □

**Remark 6.4.4.** *The coefficients $C_{11}, C_{12}$ and $P$ can be explicitly computed using bispherical coordinates. Explicit formulas for $C_{11}$ and $C_{12}$ are given in subsection 6.2.1. Using the same approach as in the derivation of $C_{ij}$ [67], we can also obtain an explicit formula for $P$. It holds that*

$$P=-4\pi r_0(r_0+d_0/2)-8\pi\alpha^2\sum_{n=0}^{\infty}(2n+1)e^{-(2n+1)T}\coth((n+1/2)T).$$

## 6.5. Homogenization theory

We consider the scattering of an incident acoustic plane wave $u^{in}$ by $N$ identical bubble dimers with different orientations distributed in a homogeneous fluid in $\mathbb{R}^3$. The $N$ identical bubble dimers are generated by scaling the normalized bubble dimer $D$ by a factor $s$, and then rotating the orientation and translating the center. More precisely, the bubble dimers occupy the domain

$$D^N:=\cup_{1\le j\le N}D_j^N,$$

where $D_j^N=z_j^N+sR_{d_j^N}D$ for $1\le j\le N$, with $z_j^N$ being the center of the dimer $D_j^N$, $s$ being the characteristic size, and $R_{d_j^N}$ being the rotation in $\mathbb{R}^3$ which aligns the dimer $D_j^N$ in the direction $d_j^N$. Here, $d_j^N$ is a vector of unit length in $\mathbb{R}^3$.

We assume that $0<s\ll 1$, $N\gg 1$ and that $\{z_j^N : 1\le j\le N\}\subset\Omega$ where $\Omega$ is a bounded domain. Let $u^{in}$ be the incident wave defined in Section 1.6. The scattering of acoustic waves by the bubble dimers, subject to the regime specified in Section 1.2, can be modeled by the following system of equations:

$$\begin{cases} (\Delta + k^2)u^N = 0 & \text{in } \mathbb{R}^3\backslash\overline{D}^N, \\ (\Delta + k_b^2)u^N = 0 & \text{in } D^N, \\ u^N|_- = u^N|_+ & \text{on } \partial D^N, \\ \dfrac{1}{\rho_b}\dfrac{\partial u^N}{\partial \nu}\Big|_- = \dfrac{1}{\rho}\dfrac{\partial u^N}{\partial \nu}\Big|_+ & \text{on } \partial D^N, \\ u^N - u^{in} & \text{satisfies the SRC}, \end{cases} \tag{6.43}$$

where $u^N$ is the total field and $\omega$ is the frequency. Then the solution $u^N$ can be written as

$$u^N = \begin{cases} u^{in} + \mathcal{S}_{D^N}^k[\psi^N] & \text{in } \mathbb{R}^3\backslash\overline{D^N}, \\ \mathcal{S}_D^{k_b}[\psi_b^N] & \text{in } D^N, \end{cases} \tag{6.44}$$

for some surface potentials $\psi^N, \psi_b^N \in L^2(\partial D^N)$. Here, we have used the notations

$$\begin{aligned} L^2(\partial D^N) &= L^2(\partial D_1^N) \times L^2(\partial D_2^N) \times \cdots \times L^2(\partial D_N^N), \\ \mathcal{S}_{D^N}^k[\psi^N] &= \sum_{1\le j\le N} \mathcal{S}_{D_j^N}^k[\psi_j^N], \\ \mathcal{S}_D^{k_b}[\psi_b^N] &= \sum_{1\le j\le N} \mathcal{S}_{D_j^N}^k[\psi_{bj}^N]. \end{aligned}$$

Using the jump relations for the single layer potentials, it is easy to derive that $\psi$ and $\psi_b$ satisfy the following system of boundary integral equations:

$$\mathcal{A}^N(\omega, \delta)[\Psi^N] = F^N, \tag{6.45}$$

where

$$\mathcal{A}^N(\omega,\delta) = \begin{pmatrix} \mathcal{S}_{D^N}^{k_b} & -\mathcal{S}_{D^N}^k \\ -\frac{1}{2}I + \mathcal{K}_{D^N}^{k_b,*} & -\delta(\frac{1}{2}I + \mathcal{K}_{D^N}^{k,*}) \end{pmatrix}, \ \Psi^N = \begin{pmatrix} \psi_b^N \\ \psi^N \end{pmatrix}, \ F^N = \begin{pmatrix} u^{in} \\ \delta\frac{\partial u^{in}}{\partial \nu} \end{pmatrix}\Big|_{\partial D^N}.$$

One can show that the scattering problem (6.43) is equivalent to the system of boundary integral equations (6.45) [17, 15]. Furthermore, it is well-known that there exists a unique solution to the scattering problem (6.43), or equivalently to the system (6.45).

We are concerned with the case when there is a large number of small identical bubble dimers distributed in a bounded domain and the frequency of the incident wave is close to the hybridized Minnaert resonances for a single bubble dimer.

We recall that for a bubble dimer $z + sR_dD$, there exist two quasi-static resonances which are given by

$$\omega_1(\delta, z + sR_dD) = \frac{1}{s}\omega_1(\delta, D),$$

$$\omega_2(\delta, z + sR_d D) = \frac{1}{s}\omega_2(\delta, D).$$

We are interested in the limit when the size $s$ tends to zero while the frequency is of order one. In order to fix the order of the resonant frequency, we make the following assumption.

**Assumption 6.5.1.** *$\delta = \mu^2 s^2$ for some positive number $\mu > 0$.*

As a result, the two hybridized resonances have the following asymptotic expansions:

$$\omega_1(\delta, D_j^N) = \omega_{M,1} - i\tau_1\mu^2 s + O(s^2),$$
$$\omega_2(\delta, D_j^N) = \omega_{M,2} + \mu^3\hat{\eta}_1 s^2 - i\mu^4\hat{\eta}_2 s^3 + O(s^4),$$

where

$$\omega_{M,1} = v_b\mu\sqrt{(C_{11} + C_{12})}, \quad \omega_{M,2} = v_b\mu\sqrt{(C_{11} - C_{12})}.$$

Moreover, the monopole and dipole coefficients are given by

$$g^0(\omega, \delta, D_k^N) := \frac{2s(C_{11} + C_{12})}{1 - \omega_1(\delta, D_k^N)^2/\omega^2}(1 + O(\delta^{1/2})), \tag{6.46}$$
$$g^1(\omega, \delta, D_k^N) = (g_{ij}^1(\omega, \delta, D_k^N)), \tag{6.47}$$

where

$$g_{ij}^1(\omega, \delta, D_k^N) := s^3 \int_{\partial D} (\mathcal{S}_D)^{-1}[(R_{d_k^N} x)_i](y)(R_{d_k^N} y)_j + \frac{\mu^2 v_b^2 s^3}{2(\omega_2(\delta, D_k^N)^2 - \omega^2)} P^2 (d_k^N)_i (d_k^N)_j.$$

**Assumption 6.5.2.** *$\omega = \omega_{M,2} + as^2$ for some real number $a \neq \mu^3\hat{\eta}_1$.*

Then

$$g^0(\omega, \delta, D_k^N) := \frac{2s(C_{11} + C_{12})}{1 - \omega_{M,1}^2/\omega_{M,2}^2}(1 + O(s)), \tag{6.48}$$
$$g_{ij}^1(\omega, \delta, D_k^N) := \frac{\mu^2 v_b^2 s}{2|D|\omega_{M,2}\left((\mu^3\hat{\eta}_1 - a) - i\mu^4\hat{\eta}_2 s\right)} P^2 (d_k^N)_i (d_k^N)_j + O(s^3). \tag{6.49}$$

We introduce the two constants

$$\tilde{g}^0 = \frac{2(C_{11} + C_{12})}{1 - \omega_{M,1}^2/\omega_{M,2}^2}, \quad \tilde{g}^1 = \frac{\mu^2 v_b^2}{2|D|\omega_{M,2}(\mu^3\hat{\eta}_1 - a)} P^2.$$

We now impose conditions on the distribution of the bubble dimers.

**Assumption 6.5.3.** *$sN = \Lambda$ for some positive number $\Lambda > 0$.*

Note that the volume fraction of the bubble dimers is of the order of $s^3N$. The above assumption implies that the bubble dimers are very dilute with the average distance between neighboring dimers being of the order of $\frac{1}{N^{1/3}}$.

**Assumption 6.5.4.** *The bubble dimers are regularly distributed in the sense that*

$$\min_{i\neq j}|z_i^N - z_j^N| \geq \eta N^{-\frac{1}{3}},$$

*for some constant $\eta$ independent of $N$. Here, $\eta N^{-\frac{1}{3}}$ can be viewed as the minimum separation distance between neighbouring bubble dimers.*

In addition, we also make the following assumptions on the regularity of the distribution $\{z_j^N : 1 \leq j \leq N\}$ and the orientation $\{d_j^N : 1 \leq j \leq N\}$.

**Assumption 6.5.5.** *There exists a function $\tilde{V} \in C^1(\bar{\Omega})$ such that for any $f \in C^{0,\alpha}(\Omega)$ with $0 < \alpha \leq 1$,*

$$\max_{1\leq j\leq N}|\frac{1}{N}\sum_{i\neq j} G^k(z_j^N - z_i^N)f(z_i^N) - \int_\Omega G^k(z_j^N - y)\tilde{V}(y)f(y)dy| \leq C\frac{1}{N^{\frac{\alpha}{3}}}\|f\|_{C^{0,\alpha}(\Omega)} \quad (6.50)$$

*for some constant $C$ independent of $N$.*

**Assumption 6.5.6.** *There exists a matrix valued function $\tilde{B} \in C^1(\bar{\Omega})$ such that for $f \in (C^{0,\alpha}(\Omega))^3$ with $0 < \alpha \leq 1$,*

$$\max_{1\leq j\leq N}|\frac{1}{N}\sum_{i\neq j}(f(z_i^N)\cdot d_i^N)(d_i^N\cdot\nabla G^k(z_i^N - z_j^N)) - \int_\Omega f(y)\tilde{B}\nabla_y G^k(y - z_j^N)dy| \leq C\frac{1}{N^{\frac{\alpha}{3}}}\|f\|_{C^{0,\alpha}(\Omega)} \quad (6.51)$$

*for some constant $C$ independent of $N$.*

**Remark 6.5.7.** *If we let $\{z_j^N : 1 \leq j \leq N\}$ be uniformly distributed, then $\tilde{V}$ is a positive constant in $\Omega$. We can also let the orientation be uniformly distributed in the unit sphere in the sense that the average of the matrix $d_j^N(d_j^N)^T$ in any neighborhood of any point in $\Omega$ tends to a multiple of the identity matrix as $N$ tends to infinity. In that case, $\tilde{B}$ is a positive constant multiple of the identity matrix at each point.*

### 6.5.1. The homogenized equations

In the same spirit as the point interaction approximation [20, 25, 46, 89, 90], we now formally derive the homogenized equation.

For $1 \leq j \leq N$, denote by

$$u_j^{i,N} = u^{in} + \sum_{i\neq j}\mathcal{S}_{D_i^N}^k[\psi_i^N], \quad (6.52)$$

$$u_j^{s,N} = \mathcal{S}^k_{D_j^N}[\psi_j^N]. \tag{6.53}$$

It is clear that $u_j^{i,N}$ is the total incident field which impinges on the bubble $D_j^N$, and $u_j^{s,N}$ is the corresponding scattered field. Denote by

$$\Omega_N = \Omega \backslash \cup_{1\le j\le N} B(z_j^N, \sqrt{s}).$$

Note that the volume fraction of the set $\cup_{1\le j\le N} B(z_j^N, \sqrt{s})$ is of the order

$$O(N \cdot s^{\frac{3}{2}}) = O(N \cdot s) \cdot s^{\frac{1}{2}},$$

which tends to zero as $N \to \infty$ under Assumption 6.5.3. We have

$$u^N(x) = u^{in} + \sum_{1\le k\le N} u_k^{s,N}(x) = u_j^{i,N}(x) + u_j^{s,N}(x), \text{ for each } 1 \le j \le N \text{ and } x \in \Omega_N.$$

**Proposition 6.5.8.** *Under Assumptions 6.5.1, 6.5.2, 6.5.3, we have that, for $x \in \Omega_N$,*

$$u_j^{s,N}(x) \approx g^0(\omega, \delta, D_j^N) u_j^{i,N}(z_j^N) G^k(x - z_j^N) + \nabla u_j^{i,N}(z_j^N) \cdot g^1(\omega, \delta, D_j^N) \nabla G^k(x - z_j^N).$$

We further assume that

**Assumption 6.5.9.** *There exists some macroscopic field $u \in C^{1,\alpha}(\Omega)$ such that*

$$u^N(x) \to u(x) \text{ for } x \in \Omega_N.$$

*Here the convergence is understood in the sense that for any $\epsilon > 0$, there exists $N_0$ such that for all $N \ge N_0$, we have*

$$\|u^N(x) - u(x)\|_{C^{1,\alpha}(\Omega_N)} \le \epsilon.$$

The above assumption implies in particular that $u_j^{i,N}(z_j^N) \to u(z_j^N)$. Therefore

$$g^0(\omega, \delta, D_j^N) u_j^{i,N}(z_j^N) G^k(x - z_j^N) \to \frac{1}{N} \Lambda u(z_j^N) \tilde{g}^0 G^k(x - z_j^N),$$
$$\nabla u_j^{i,N}(z_j^N) \cdot g^1(\omega, \delta, D_j^N, z_j^N) \nabla G^k(x - z_j^N) \to \frac{1}{N} \Lambda \tilde{g}^1 (\nabla u(z_j^N) \cdot d_j^N)(d_j^N \cdot \nabla G^k(x - z_j^N)).$$

On the other hand, we have

$$u^N(x) \approx u^{in} + \sum_{1\le j\le N} g^0(\omega, \delta, D_j^N) u_j^{i,N}(z_j^N) G^k(x - z_j^N) + \sum_{1\le j\le N} \nabla u_j^{i,N}(z_j^N) \cdot g^1(\omega, \delta, D_j^N) \nabla G^k(x - z_j^N).$$

By letting $N \to \infty$, we obtain

$$u(x) = u^{in} + \int_\Omega \Lambda \tilde{g}^0 u(y) \tilde{V}(y) G^k(x - y) dy + \int_\Omega \Lambda \tilde{g}^1 \nabla u(y) \tilde{B} \nabla G^k(x - y) dy. \tag{6.54}$$

By applying the operator $\triangle + k^2$ to both side of the above equation, we get

$$(\triangle + k^2)u(x) = \Lambda\tilde{g}^0\tilde{V}u(x) + \nabla \cdot \left(\Lambda\tilde{g}^1\tilde{B}\nabla u\right)(x), \quad \text{in } \Omega.$$

Or equivalently,

$$\nabla \cdot \left(I - \Lambda\tilde{g}^1\tilde{B}\right)\nabla u(x) + (k^2 - \Lambda\tilde{g}^0\tilde{V})u(x) = 0, \quad \text{in } \Omega. \tag{6.55}$$

Therefore, we have shown that the microscopic field $u^N$ tends to a macroscopic field $u$ which satisfies the following effective equation

$$\nabla \cdot M_1(x)\nabla u(x) + M_2(x)u(x) = 0, \quad \text{in } \mathbb{R}^3, \tag{6.56}$$

where

$$M_1 = \begin{cases} I, & \text{in } \mathbb{R}^3 \setminus \Omega, \\ I - \Lambda\tilde{g}^1\tilde{B}, & \text{in } \Omega, \end{cases}$$

and

$$M_2 = \begin{cases} k^2, & \text{in } \mathbb{R}^3 \setminus \Omega, \\ k^2 - \Lambda\tilde{g}^0\tilde{V}, & \text{in } \Omega. \end{cases}$$

**Remark 6.5.10.** *We have derived the effective media theory in a formal way under the crucial Assumption 6.5.9. We leave a rigorous justification as an open problem for future investigation. We refer to [25] for a similar but easier problem where a rigorous justification is possible.*

### 6.5.2. Double-negative refractive index media

If the bubble dimers are distributed such that $\tilde{B}$ is a positive matrix with $\tilde{B}(x) \geq C > 0$ for some constant C for all $x \in \Omega$, then we see that for $\omega$ in the form $\omega = \omega_{M,2} + as^2$ with $a < \mu^3\hat{\eta}_1$, and sufficiently large $\Lambda$, both the matrix $I - \Lambda\tilde{g}^1\tilde{B}$ and the scalar function $k^2 - \Lambda\tilde{g}^0\tilde{V}$ are negative. Therefore, we obtain an effective double-negative media with both negative mass density and negative bulk modulus. On the other hand, for $\omega$ in between $\omega_{M,1}$ and $\omega_{M,2}$ but away from the anti-resonance $\omega_{M,2}$, $\tilde{g}^1$ may be small enough such that the matrix $I - \Lambda\tilde{g}^1\tilde{B}$ is positive, while the matrix $k^2 - \Lambda\tilde{g}^0\tilde{V}$ remains negative. Then the obtained effective media has negative mass density and positive bulk modulus.

## 6.6. Numerical illustrations

In this section, we illustrate the double-negative refractive index phenomenon in bubbly media by numerical examples.

We consider a cubic array of identical spherical bubble dimers. Suppose $\Omega$ is a cube with a side length of $L = 20$, *i.e.*, $\Omega = [0, 20]^3$. Let $a = 0.2$ and define a small cube $\Omega_a = [0, a]^3$. Then $\Omega$ can be considered as a union of small cubes as follows:

$$\Omega = \bigcup_{n_1,n_2,n_3=0,1,\ldots,99} \Omega_a + a(n_1, n_2, n_3).$$

We assume that a bubble dimer is centered in each of the small cubes. Then the total number of dimers is $N = 10^6$ and the periodicity of the dimer array is $a = 0.2$.

Recall that a bubble dimer is described by $z + sR_dD$, where $z$ is the center of the dimer, $s$ is its characteristic size, and $R_d$ is a rotation in $\mathbb{R}^3$ which aligns the dimer in the direction $d$, where $d$ is a unit vector. We set the characteristic size of the dimers to be $s = 0.1$. Since $D$ has unit volume, the radius $r_0$ of the bubbles comprising the dimers is $r_0 = s(3/4\pi)^{1/3} \approx 0.005$.

We set $\tilde{\rho} = \tilde{\kappa} = 1$ and $\rho = \kappa = 5 \times 10^3$. Then $v = \tilde{v} = 1$, $k = \tilde{k} = \omega$, and $\delta = 2 \times 10^{-4}$. We assume that the two bubbles comprising each dimer are separated by a distance of $l = 5r_0 \approx 0.0248$. Moreover, each dimer is randomly oriented so that the unit vector $d$ is uniformly distributed on the unit sphere. Under these assumptions, we can easily check that $\Lambda = 8 \times 10^3$, $\tilde{V} \approx |\Omega|^{-1} = 1.25 \times 10^{-4}$, and $\tilde{B} \approx (2|\Omega|)^{-1} I = 6.25 \times 10^{-5} I$.

Now we consider the effective properties of the homogenized media. Recall that the effective coefficients of the homogenized equation (6.55) are $k^2 - \Lambda\tilde{g}^0\tilde{V}$ and $I - \Lambda\tilde{g}^1\tilde{B}$. Using the above parameters, we have

$$\begin{aligned} &k^2 - \Lambda\tilde{g}^0\tilde{V} \approx \omega^2 - \tilde{g}^0 = \omega^2(1 - \tilde{g}^0/\omega^2), \\ &I - \Lambda\tilde{g}^1\tilde{B} \approx (1 - \tilde{g}^1/2)I. \end{aligned} \tag{6.57}$$

Note that the coefficient $I - \Lambda\tilde{g}^1\tilde{B}$ can be roughly considered as a scalar quantity. The scattering functions $\tilde{g}_0$ and $\tilde{g}_1$ can be computed as follows. Since $\tilde{g}_0 \approx sg_0$ and $\tilde{g}_1 \approx sg_1$, we have from (6.41) and (6.42) that

$$\begin{aligned} \tilde{g}^0(\omega, \delta, sR_dD) &\approx \frac{2(C_{11} + C_{12})}{1 - \omega_1^2/\omega^2}, \\ \tilde{g}^1(\omega, \delta, sR_dD) &\approx \frac{\delta\tilde{v}^2}{2(\omega_2^2 - \omega^2)} P^2 d_i d_j. \end{aligned}$$

The resonance frequencies $\omega_1$ and $\omega_2$ can be easily calculated using a standard multipole expansion together with a root finding method such as Muller's method [17]. We find that $\omega_1 \approx 4.6171 - 0.0926i$ and $\omega_2 \approx 5.3253 - 0.0005i$. Then it is simple to compute $\tilde{g}^0$ and $\tilde{g}^1$.

In the left of Figure 6.1, we plot the two effective coefficients as functions of frequency. Clearly, there is a narrow region contained in the interval $[5.2, 5.4]$ in which both of the coefficients are negative. So we expect that the negative refraction occurs in this frequency region.

We next consider the refractive index. In view of (6.55) and (6.57), the effective mass density $\rho_{eff}$ and the effective bulk modulus $\kappa_{eff}$ can be computed approximately by

$$\rho_{eff} \approx 1 - \tilde{g}^1/2, \quad \kappa_{eff} \approx (1 - \tilde{g}^0/\omega^2)^{-1}.$$

As usual, we define the refractive index $n_{eff}$ by

$$n_{eff} = \sqrt{\rho}_{eff}\sqrt{\kappa_{eff}^{-1}}.$$

In the right figure of Figure 6.1, we plot the refractive index as a function of frequency. It is clear that the refractive index becomes negative in a narrow region contained in the interval $[5.2, 5.4]$, as expected.

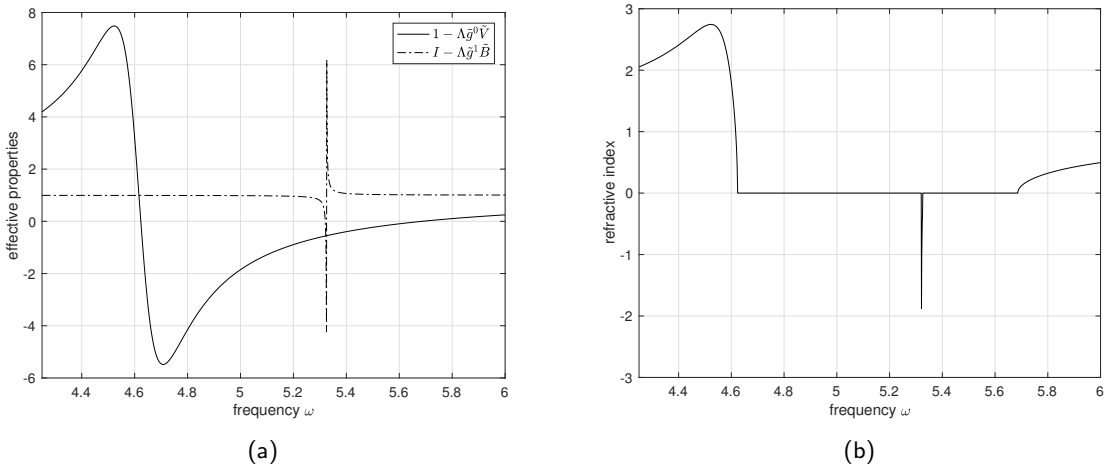


Figure 6.1.: The effective properties of the homogenized media (a), and the refractive index (b).

## 6.7. Concluding remarks

In this chapter we derived explicit formulas for the hybridized Minnaert resonances of a bubble dimer. We have shown that the dimer can be approximated as a point scatterer with monopole and dipole modes. We have proved that for an acoustic metamaterial consisting of a large number of bubble dimers, both the effective mass density and the effective bulk modulus of the bubbly fluid can be negative simultaneously near the anti-resonance of the two hybridized Minnaert resonances for a single constituent bubble dimer. The results in this chapter demonstrate that by taking advantage of the hybridized Minnaert resonances, it is not necessary to use two different types of sub-wavelength resonators in order to obtain a negative effective refractive index in an acoustic metamaterial.

# 7. Sub-wavelength Localized Modes for Acoustic Waves in Bubbly Crystals With a Defect

In Chapter 4, it was proved that a sub-wavelength bandgap opening occurs in bubble phononic crystals. To demonstrate the opening of a sub-wavelength phononic bandgap, a periodic arrangement of bubbles was considered and their sub-wavelength Minnaert resonance was exploited. In this chapter, this sub-wavelength bandgap is used to demonstrate cavities, very similar to those obtained in photonic and phononic crystals, albeit of deeply sub-wavelength dimensions. The key idea is to increase the size of a single bubble inside the crystal, thus creating a defect. The goal is then to analytically and numerically show that this crystal has a localized eigenmode close to the defect bubble.

## 7.1. Introduction

It is well-known in solid state physics that the periodicity of atoms comprising crystals is responsible for the existence of both conducting bands and bandgaps for electrons. This property is a consequence of the Floquet-Bloch theory applied to the wavefunction of electrons. Similarly, electromagnetic and elastic waves propagating in periodic media are subject to the same formalism giving rise to the existence of ranges of frequencies for which no propagation is allowed, so-called bandgaps. Such materials are known as photonic and phononic crystals. At an interface with free space, these types of crystals act as mirrors for incoming waves, termed Bragg mirrors. Similarly, a point defect can be created by locally modifying the properties of a crystal. This results in a cavity if the mode supported by the defect is resonant within the bandgap. Physically, the underlying mechanism is Bragg interference. In these periodic media, the Bragg condition typically occurs when the period of the medium scales with the wavelength [16, 17, 13, 47, 63, 54, 78, 79]. As a consequence, photonic and phononic crystals are typically structured with a period corresponding to half the operating wavelength. This constrains the range of applications, specifically in low-frequency regimes where the wavelength is large [83, 68].

Based on the phenomenon of sub-wavelength resonance, a class of phononic crystals that exhibit bandgaps with deep sub-wavelength spatial scales have been fabricated [81]. In Chapter 4, the opening of a sub-wavelength phononic bandgap in bubbly crystals has

been proved. This sub-wavelength bandgap is mainly due to the cell resonance of the bubbles in the quasi-static regime and is quite different from the usual bandgaps in photonic/phononic crystals where the gap opens at wavelengths which, as mentioned previously, are comparable to the period of the structure. In [18], it has been further proved that the first Bloch eigenvalue achieves its maximum at the corner of the Brillouin zone. Moreover, by computing the asymptotics of the Bloch eigenfunctions in the periodic structure near that critical frequency, it has been demonstrated that these eigenfunctions can be decomposed into two parts: one which is slowly varying and satisfies a homogenized equation, while the other is periodic across each elementary crystal cell and is varying more rapidly. The asymptotic analysis of wave fields near the critical frequency where a sub-wavelength bandgap opens rather than the zero frequency has been performed. This rigorously justifies the observed super-focusing of acoustic waves in bubbly crystals near and below the maximum of the first Bloch eigenvalue and confirms the bandgap opening near and above this critical frequency.

In phononic crystals, a point defect can be created by locally removing a scatterer. This results in a small cavity because a resonant mode is created by the defect within the bandgap [42, 41, 48, 61, 55, 62, 73, 74]. Following this concept, many components have been demonstrated based on periodic media such as waveguides using line defects [94, 75]. However, because of their wavelength scale period, phononic crystals result in relatively large devices. This seriously constrains the range of applications, especially in the low frequency regime where the wavelength is large.

If we remove one bubble inside the bubbly crystal, we cannot create a defect mode. The defect created in this fashion is actually too small to support a resonant mode, while in a phononic crystal removing one scatterer allows for the existence of a stationary defect mode since the typical scale of such a defect is the wavelength. This illustrates a strong difference between Bragg bandgaps and sub-wavelength bandgaps in bubbly crystals.

In order to tackle this issue, we have to physically introduce a resonant defect inside the crystal of sub-wavelength resonators, and this is achieved by simply detuning one resonator with respect to the rest of the medium. In the case of the bubbly medium, we prove in this chapter that by increasing the radius of one bubble, a detuned resonator is created with a resonance frequency that is upward shifted, thus falling within the sub-wavelength bandgap.

The aim of this chapter is to prove the existence of this defect mode. Through the application of layer potential techniques, Floquet-Bloch theory, and Gohberg-Sigal theory we derive an original formula for the defect mode frequency, along with proving the existence of a sub-wavelength localized mode. Our results are complemented by several numerical examples which serve to validate them in two dimensions. They formally explain the experimental observations reported in [68, 69] in the case of Helmholtz resonators. This paves the mathematical foundation for the analysis of wave propagation control at deeply sub-wavelength scales. Sub-wavelength cavities have a high quality factor and a low mode volume. These two effects are typically associated with the enhancement of the emission rate of an emitter, the so-called Purcell factor [92].

The chapter is organized as follows. In Section 7.2, for the readers convenience, we briefly review the main results of Chapter 4. In Section 7.3 we use the fictitious source superposition method introduced in [98] for modeling the defect and characterize the fictitious sources as the solution of some system of integral equations. In section 7.4, we prove existence of a localized defect mode and derive an asymptotic formula for the resonant frequency created inside the sub-wavelength bandgap by increasing the size of a single bubble in terms of the ratio between its radius and the radius of the original bubbles. In Section 7.5 we perform numerical simulations to illustrate the main findings of this chapter. We make use of the multipole expansion method to compute the defect mode inside the sub-wavelength bandgap. The chapter ends with some concluding remarks.

## 7.2. Preliminaries

Here we briefly review the sub-wavelength bandgap opening of a bubbly crystal from Chapter 4.

Let $Y$ be the unit cell $[0,1)^2$ in $\mathbb{R}^2$. For $\alpha \in [0,2\pi)^2$, the function $G^{\alpha,k}$ is defined to satisfy

$$(\triangle_x + k^2)G^{\alpha,k}(x,y) = \sum_{n\in\mathbb{R}^2} \delta(x-y-n)e^{in\cdot\alpha},$$

where $\delta$ is the Dirac delta function and $G^{\alpha,k}$ is $\alpha$-quasi-periodic, i.e., $e^{-i\alpha\cdot x}G^{\alpha,k}(x,y)$ is periodic in $x$ with respect to $Y$.

We recall the quasi-periodic single layer potential $\mathcal{S}_D^{\alpha,k}$ from Section 1.4 defined by

$$\mathcal{S}_D^{\alpha,k}[\psi](x) = \int_{\partial D} G^{\alpha,k}(x,y)\psi(y)d\sigma(y), \quad x \in \mathbb{R}^2.$$

It satisfies the following jump formulas:

$$\mathcal{S}_D^{\alpha,k}[\psi]\big|_+ = \mathcal{S}_D^{\alpha,k}[\psi]\big|_-,$$

and

$$\frac{\partial}{\partial\nu}\Big|_\pm \mathcal{S}_D^{\alpha,k}[\psi] = \left(\pm\frac{1}{2}I + (\mathcal{K}_D^{-\alpha,k})^*\right)[\psi] \quad \text{on } \partial D,$$

where $(\mathcal{K}_D^{-\alpha,k})^*$ is the operator given by

$$(\mathcal{K}_D^{-\alpha,k})^*[\psi](x) = \text{p.v.} \int_{\partial D} \frac{\partial}{\partial\nu(x)} G^{\alpha,k}(x,y)\psi(y)d\sigma(y).$$

We remark that it is known that $\mathcal{S}_D^{\alpha,0} : L^2(\partial D) \to H^1(\partial D)$ is invertible for $\alpha \neq 0$ [17].

Assume that a single bubble occupies $D$, which is a disk of radius $R < 1/2$ centered at the origin. Let $\mathcal{C} = \cup_{n\in\mathbb{Z}^2}(D+n)$ be the periodic bubbly crystal. In this chapter, for

the sake of simplicity of presentation, we shall assume that the wave speeds inside and outside the bubbles are $v = v_b = 1$. Consider the following quasi-periodic scattering problem:

$$\begin{cases} (\Delta + k^2)p = 0 & \text{in } Y\backslash\overline{D}, \\ (\Delta + k_b^2)p = 0 & \text{in } D, \\ v|_- = v|_+ & \text{on } \partial D, \\ \dfrac{1}{\rho_b}\dfrac{\partial p}{\partial \nu}\Big|_- = \dfrac{1}{\rho}\dfrac{\partial p}{\partial \nu}\Big|_+ & \text{on } \partial D, \\ e^{-i\alpha\cdot x}p & \text{is periodic.} \end{cases} \tag{7.1}$$

It is known that (7.1) has nontrivial solutions for discrete values of $\omega$ such as

$$0 \le \omega_1^\alpha \le \omega_2^\alpha \le \cdots$$

and thus we have the following band structure of propagating frequencies for the periodic bubbly crystal $\mathcal{C}$:

$$[0, \max_\alpha \omega_1^\alpha] \cup [\min_\alpha \omega_2^\alpha, \max_\alpha \omega_2^\alpha] \cup \cdots .$$

In Chapter 4, it was proved that there exists a sub-wavelength spectral gap opening in the band structure. Let us briefly review this result. We look for a solution of (7.1) which has the following form:

$$v = \begin{cases} \mathcal{S}_D^{\alpha,k}[\varphi^\alpha] & \text{in } Y \setminus \overline{D}, \\ \mathcal{S}_D^{k_b}[\psi^\alpha] & \text{in } D, \end{cases} \tag{7.2}$$

for some densities $\varphi^\alpha, \psi^\alpha \in L^2(\partial D)$. Using the jump relations for the single layer potentials, one can show that (7.1) is equivalent to the boundary integral equation

$$\mathcal{A}^\alpha(\omega, \delta)[\Phi^\alpha] = 0, \tag{7.3}$$

where

$$\mathcal{A}^\alpha(\omega,\delta) = \begin{pmatrix} \mathcal{S}_D^{k_b} & -\mathcal{S}_D^{\alpha,k} \\ -\frac{1}{2} + \mathcal{K}_D^{k_b,*} & -\delta(\frac{1}{2} + (\mathcal{K}_D^{-\alpha,k})^*) \end{pmatrix}, \ \Phi^\alpha = \begin{pmatrix} \varphi^\alpha \\ \psi^\alpha \end{pmatrix}.$$

Since it can be shown that $\omega = 0$ is a characteristic value for the operator-valued analytic function $\mathcal{A}(\omega, 0)$, we can conclude the following result by the Gohberg-Sigal theory [17, 52].

**Lemma 7.2.1.** *For any $\delta$ sufficiently small, there exists a characteristic value $\omega_1^\alpha = \omega_1^\alpha(\delta)$ to the operator-valued analytic function $\mathcal{A}^\alpha(\omega, \delta)$ such that $\omega_1^\alpha(0) = 0$ and $\omega_1^\alpha$ depends on $\delta$ continuously.*

The next theorem gives the asymptotic expansion of $\omega_1^\alpha$ as $\delta \to 0$.

**Theorem 7.2.2.** *For $\alpha \neq 0$ and sufficiently small $\delta$, we have*

$$\omega_1^\alpha = \omega_M \sqrt{\frac{\mathrm{Cap}_{D,\alpha}}{\mathrm{Cap}_D}} + O(\delta^{3/2}), \tag{7.4}$$

*where the constants $\mathrm{Cap}_{D,\alpha}$ and $\mathrm{Cap}_D$ are given by*

$$\mathrm{Cap}_{D,\alpha} := -\langle (\mathcal{S}_D^{\alpha,0})^{-1}[\mathbb{1}_{\partial D}], \mathbb{1}_{\partial D}\rangle, \quad \mathrm{Cap}_D = -\frac{2\pi}{\ln R},$$

*and $\omega_M$ is the (free space) Minnaert resonant frequency satisfying $(\omega_M)^2 \ln \omega_M = O(\delta)$ as $\delta \to 0$.*

Let $\omega_1^* = \max_\alpha \omega_1^\alpha$. The following theorem specifies the sub-wavelength bandgap opening.

**Theorem 7.2.3.** *For every $\epsilon > 0$, there exists $\delta_0 > 0$ and $\tilde{\omega} > \omega_1^*$ such that*

$$[\omega_1^* + \epsilon, \tilde{\omega}] \subset [\max_\alpha \omega_1^\alpha, \min_\alpha \omega_2^\alpha] \tag{7.5}$$

*for $\delta < \delta_0$.*

## 7.3. Integral representation for bubbly crystals with a defect

### 7.3.1. Bubbly crystals with a defect: problem formulation

Consider now a perturbed crystal, where the central disk $D$ is replaced by a defect disk $D_d$ of radius $R_d$ with $R < R_d < 1/2$. Let $\mathcal{C}_d = D_d \cup \left(\cup_{n\in\mathbb{Z}^2\setminus\{0,0\}} D + n\right)$ be the perturbed crystal and let $\epsilon = R_d - R > 0$ be the perturbation of the radius. We consider the following problem:

$$\begin{cases} (\Delta + k^2)u = 0 & \text{in } \mathbb{R}^2\setminus\overline{\mathcal{C}_d}, \\ (\Delta + k_b^2)u = 0 & \text{in } \mathcal{C}_d, \\ u|_- = u|_+ & \text{on } \partial\mathcal{C}_d, \\ \dfrac{1}{\rho_b}\dfrac{\partial u}{\partial \nu}\Big|_- = \dfrac{1}{\rho}\dfrac{\partial u}{\partial \nu}\Big|_+ & \text{on } \partial\mathcal{C}_d. \end{cases} \tag{7.6}$$

As discussed in Subsection 7.2, the unperturbed problem (with $\mathcal{C}$ instead of $\mathcal{C}_d$ in (7.6)), has the following essential spectrum for the propagating frequencies:

$$[0, \max_\alpha \omega_1^\alpha] \cup [\min_\alpha \omega_2^\alpha, \max_\alpha \omega_2^\alpha] \cup \cdots .$$

In fact, it can be easily shown that the perturbed crystal problem (7.6) has the same essential spectrum. This is because the essential spectrum is stable under compact perturbations [49].

In this chapter, we want to show that by modifying the central bubble $D$, there exists a frequency $\omega^\epsilon$, slightly above $\max_\alpha \omega_1^\alpha$, which results in a non-trivial solution to the problem (7.6). The solution $u$ associated with the frequency $\omega^\epsilon$ should be localized since $\omega^\epsilon$ lies in the bandgap. Moreover, it is of a sub-wavelength nature.

### 7.3.2. Effective sources for the defect

It is difficult to obtain the boundary integral formulation of the problem (7.6) directly. Here we consider the effective source solution which models the defect $D_d$ by placing non-trivial sources onto the boundary of the central bubble $D$ of the unperturbed crystal $\mathcal{C}$. Since the geometry of the unperturbed crystal is periodic, we can use the Floquet-Bloch theory. This is motivated by the fictitious source superposition method introduced in [98].

Let us consider the following problem:

$$\begin{cases} (\Delta + k^2)\tilde{u} = 0 & \text{in } \mathbb{R}^2 \setminus \overline{\mathcal{C}}, \\ (\Delta + k_b^2)\tilde{u} = 0 & \text{in } \mathcal{C}, \\ \tilde{u}|_+ - \tilde{u}|_- = f\delta_{m,(0,0)} & \text{on } \partial D + m,\ m \in \mathbb{Z}^2, \\ \dfrac{1}{\rho}\dfrac{\partial \tilde{u}}{\partial \nu}\Big|_+ - \dfrac{1}{\rho_b}\dfrac{\partial \tilde{u}}{\partial \nu}\Big|_- = g\delta_{m,(0,0)} & \text{on } \partial D + m,\ m \in \mathbb{Z}^2, \end{cases} \tag{7.7}$$

where $f, g$ are the source terms and $\delta_{m,n}$ is the Kronecker delta function. Note that the non-zero sources are present only on the boundary of the central bubble $D$.

If the source terms $f$ and $g$ satisfy some appropriate conditions, then we will have

$$u \equiv \tilde{u} \quad \text{in } (\mathbb{R}^2 \setminus D_d) \cup D.$$

Once this is achieved, the original solution $u$ can be recovered by extending the solution $\widetilde{u}$ to the whole region including $D_d \setminus D$ with boundary conditions on $\partial D$ and $\partial D_d$. The conditions for the effective sources $f$ and $g$, which are necessary in order to correctly model the defect, will be characterized in the next subsection.

### 7.3.3. Characterization of the effective sources

Here we clarify the relation between the effective source pair $(f, g)$ and the density pair $(\varphi, \psi)$.

First we consider the integral equation for the solution $\widetilde{u}$ inside the central unit cell $Y$. Inside $Y$, the solution $\tilde{u}$ can be represented as

$$\tilde{u} = \begin{cases} H + \mathcal{S}_D^k[\psi] & \text{in } Y \setminus \overline{D}, \\ \mathcal{S}_D^{k_b}[\varphi] & \text{in } D. \end{cases} \tag{7.8}$$

Here, the pair $(\varphi, \psi) \in L^2(\partial D)^2$ satisfies

$$\mathcal{A}_D \begin{pmatrix} \varphi \\ \psi \end{pmatrix} := \begin{pmatrix} \mathcal{S}_D^{k_b} & -\mathcal{S}_D^k \\ \partial_\nu \mathcal{S}_D^{k_b}|_- & -\delta \partial_\nu \mathcal{S}_D^k|_+ \end{pmatrix} \begin{pmatrix} \varphi \\ \psi \end{pmatrix} = \begin{pmatrix} H|_{\partial D} - f \\ \partial_\nu H|_{\partial D} - g \end{pmatrix}. \tag{7.9}$$

Next, let us consider the central cell $Y$ in the original problem (7.6). The central cell $Y$ contains a defect bubble $D_d$ and no sources. Inside $Y$, the solution $u$ is represented as

$$u = \begin{cases} H + \mathcal{S}_{D_d}^k[\psi_d] & \text{in } Y \setminus \overline{D_d}, \\ \mathcal{S}_{D_d}^{k_b}[\varphi_d] & \text{in } D_d, \end{cases}$$

where

$$\mathcal{A}_{D_d} \begin{pmatrix} \varphi_d \\ \psi_d \end{pmatrix} := \begin{pmatrix} \mathcal{S}_{D_d}^{k_b} & -\mathcal{S}_{D_d}^k \\ \partial_\nu \mathcal{S}_{D_d}^{k_b}|_- & -\delta \partial_\nu \mathcal{S}_{D_d}^k|_+ \end{pmatrix} \begin{pmatrix} \varphi_d \\ \psi_d \end{pmatrix} = \begin{pmatrix} H|_{\partial D_d} \\ \partial_\nu H|_{\partial D_d} \end{pmatrix}. \tag{7.10}$$

In order for the effective sources $f$ and $g$ to model the defect $D_d$ correctly, we should impose $u \equiv \widetilde{u}$ in $(Y \setminus D_d) \cup D$. In other words, the following conditions should be satisfied:

$$\mathcal{S}_{D_d}^{k_b}[\varphi_d] \equiv \mathcal{S}_D^{k_b}[\varphi] \quad \text{in } D_d, \tag{7.11}$$

and

$$\mathcal{S}_{D_d}^k[\psi_d] \equiv \mathcal{S}_D^k[\psi] \quad \text{in } Y \setminus \overline{D}. \tag{7.12}$$

Since $D$ and $D_d$ are circular disks, we can use a Fourier basis for functions on $\partial D$ or $\partial D_d$ in polar coordinates $(r, \theta)$ to make (7.10)-(7.12) more explicit. Let us write $\varphi$ and $\psi$ in the form of Fourier series:

$$\varphi(\theta) = \sum_{n \in \mathbb{Z}} \varphi_n e^{in\theta}, \quad \psi(\theta) = \sum_{n \in \mathbb{Z}} \psi_n e^{in\theta}.$$

Similarly, we also write $\varphi_d$ and $\psi_d$ as

$$\varphi_d(\theta) = \sum_{n \in \mathbb{Z}} \varphi_{d,n} e^{in\theta}, \quad \psi_d(\theta) = \sum_{n \in \mathbb{Z}} \psi_{d,n} e^{in\theta}.$$

We define the subspace $V_{mn}$ of $L^2(\partial D)^2$ as

$$V_{mn} := \operatorname{span}\{e^{im\theta}\} \times \operatorname{span}\{e^{in\theta}\}, \quad m, n \in \mathbb{Z}.$$

Similarly, let $V_{mn}^d$ be the subspace of $L^2(\partial D_d)^2$ with the same Fourier basis.

It is known that (see, for instance, [11])

$$\mathcal{S}_D^k[e^{in\theta}] = \frac{(-1)i\pi R}{2} \times \begin{cases} J_n(kR)H_n^{(1)}(kr)e^{in\theta}, & r \geq R, \\ H_n^{(1)}(kR)J_n(kr)e^{in\theta}, & 0 \leq r < R. \end{cases} \tag{7.13}$$

Therefore, the operator $\mathcal{A}_D$ in (7.9) has the following matrix representation as an operator from $V_{mn}$ to $V_{m'n'}$:

$$(\mathcal{A}_D)_{V_{mn}\to V_{m'n'}} = \delta_{mn}\delta_{m'n'}\frac{(-i)\pi R}{2}\begin{pmatrix} J_n(k_bR)H_n^{(1)}(k_bR) & -J_n(kR)H_n^{(1)}(kR) \\ k_bJ_n'(k_bR)H_n^{(1)}(k_bR) & -\delta k J_n(kR)\big(H_n^{(1)}\big)'(kR) \end{pmatrix}. \tag{7.14}$$

Similarly, the operator $\mathcal{A}_{D_d}$ in (7.10), as a mapping from $V_{mn}^d$ to $V_{m'n'}^d$, is represented as follows:

$$(\mathcal{A}_{D_d})_{V_{mn}^d\to V_{m'n'}^d} = \delta_{mn}\delta_{m'n'}\frac{(-i)\pi R_d}{2}\begin{pmatrix} J_n(k_bR_d)H_n^{(1)}(k_bR_d) & -J_n(kR_d)H_n^{(1)}(kR_d) \\ k_bJ_n'(k_bR_d)H_n^{(1)}(k_bR_d) & -\delta k J_n(kR_d)\big(H_n^{(1)}\big)'(kR_d) \end{pmatrix}. \tag{7.15}$$

Now, we consider (7.11) and (7.12). We have from (7.13) that, inside $D_d$,

$$\begin{aligned} \mathcal{S}_D^{k_b}[\varphi_d] &= \sum_{n\in\mathbb{Z}} \varphi_n \mathcal{S}_D^{k_b}[e^{in\theta}] = \frac{(-i)\pi R}{2}\sum_{n\in\mathbb{Z}} \varphi_n H_n^{(1)}(k_bR)J_n(k_br)e^{in\theta} \\ &= \frac{(-i)\pi R}{2}\sum_{n\in\mathbb{Z}} \varphi_n \frac{H_n^{(1)}(k_bR)}{H_n^{(1)}(k_bR_d)}H_n^{(1)}(k_bR)J_n(k_br)e^{in\theta} \\ &= \mathcal{S}_{D_d}^{k_b}\Big[\sum_{n\in\mathbb{Z}} \varphi_n \frac{H_n^{(1)}(k_bR)}{H_n^{(1)}(k_bR_d)}e^{in\theta}\Big]. \end{aligned}$$

Similarly, outside $D$,

$$\mathcal{S}_D^k[\psi] = \mathcal{S}_{D_d}^k\Big[\sum_{n\in\mathbb{Z}} \psi_n \frac{J_n(kR)}{J_n(kR_d)}e^{in\theta}\Big].$$

So, from (7.11) and (7.12), we see that

$$\begin{pmatrix} \varphi_d \\ \psi_d \end{pmatrix} = \mathcal{P}_1 \begin{pmatrix} \varphi \\ \psi \end{pmatrix},$$

where the operator $\mathcal{P}_1 : L^2(\partial D)^2 \to L^2(\partial D_d)^2$ is given by

$$(\mathcal{P}_1)_{V_{mn}\to V_{m'n'}^d} = \delta_{mn}\delta_{m'n'}\begin{pmatrix} \dfrac{H_n^{(1)}(k_bR)}{H_n^{(1)}(k_bR_d)} & 0 \\ 0 & \dfrac{J_n(kR)}{J_n(kR_d)} \end{pmatrix}.$$

In the same way, we can obtain that

$$\begin{pmatrix} H|_{\partial D_d} \\ \partial_\nu H|_{\partial D_d} \end{pmatrix} = \mathcal{P}_2^\epsilon \begin{pmatrix} H|_{\partial D} \\ \partial_\nu H|_{\partial D} \end{pmatrix},$$

where the operator $\mathcal{P}_2 : L^2(\partial D)^2 \to L^2(\partial D_d)^2$ is given by

$$(\mathcal{P}_2)_{V_n \to V_m^d} = \delta_{mn} \begin{pmatrix} \dfrac{J_n(kR_d)}{J_n(kR)} & 0 \\ 0 & \dfrac{J_n'(kR_d)}{J_n'(kR)} \end{pmatrix}.$$

Therefore, using (7.10), we arrive at

$$\mathcal{A}_D^\epsilon \begin{pmatrix} \varphi \\ \psi \end{pmatrix} := (\mathcal{P}_2)^{-1} \mathcal{A}_{D_d} \mathcal{P}_1 \begin{pmatrix} \varphi \\ \psi \end{pmatrix} = \begin{pmatrix} H|_{\partial D} \\ \partial_\nu H|_{\partial D} \end{pmatrix}. \tag{7.16}$$

Thus, (7.9) yields

$$(\mathcal{A}_D^\epsilon - \mathcal{A}_D) \begin{pmatrix} \varphi \\ \psi \end{pmatrix} = \begin{pmatrix} f \\ g \end{pmatrix}. \tag{7.17}$$

We have obtained an explicit relation between the pair $(\varphi, \psi)$ and the effective sources $(f, g)$. If the effective sources $f$ and $g$ satisfy (7.17), then the pair $(f, g)$ will result in the generation of the same scattered field as the one induced by the defect bubble $D_d$. In other words, $\widetilde{u} \equiv u$ outside $D_d \setminus \overline{D}$. In what follows, for convenience of notation, we identify the solution $\widetilde{u}$ with the original one $u$.

### 7.3.4. Floquet transform of the solution

Here we derive an integral equation for the effective source problem (7.7). We apply the Floquet transform to the solution $u$ with the quasi-periodic parameter $\alpha$ as follows

$$u^\alpha = \sum_{m \in \mathbb{Z}^2} u(x - m) e^{i\alpha \cdot m}.$$

The transformed solution $u^\alpha$ satisfies

$$\begin{cases} (\Delta + k^2) u^\alpha = 0 & \text{in } Y \backslash \overline{D}, \\ (\Delta + k_b^2) u^\alpha = 0 & \text{in } D, \\ u^\alpha|_+ - u^\alpha|_- = f & \text{on } \partial D, \\ \dfrac{1}{\rho} \dfrac{\partial u^\alpha}{\partial \nu}\Big|_+ - \dfrac{1}{\rho_b} \dfrac{\partial u^\alpha}{\partial \nu}\Big|_- = g & \text{on } \partial D, \\ e^{-i\alpha \cdot x} u^\alpha & \text{is periodic.} \end{cases} \tag{7.18}$$

The solution $u^\alpha$ can be represented using quasi-periodic layer potentials as

$$u^\alpha = \begin{cases} \mathcal{S}_D^{\alpha,k}[\psi_\alpha], & \text{in } Y \setminus \overline{D}, \\ \mathcal{S}_D^{k_b}[\varphi_\alpha], & \text{in } D, \end{cases}$$

where the pair $(\varphi^\alpha, \psi^\alpha) \in L^2(\partial D)^2$ is the solution to

$$\mathcal{A}^\alpha(\omega, \delta) \begin{pmatrix} \varphi^\alpha \\ \psi^\alpha \end{pmatrix} := \begin{pmatrix} \mathcal{S}_D^{k_b} & -\mathcal{S}_D^{\alpha,k} \\ \partial_\nu \mathcal{S}_D^{k_b}|_- & -\delta \partial_\nu \mathcal{S}_D^{\alpha,k}|_+ \end{pmatrix} \begin{pmatrix} \varphi^\alpha \\ \psi^\alpha \end{pmatrix} = \begin{pmatrix} -f \\ -g \end{pmatrix}. \tag{7.19}$$

Since the operator $\mathcal{A}_\alpha$ is invertible for small enough $\omega$ and $\delta$ [11], we have

$$\begin{pmatrix} \varphi^\alpha \\ \psi^\alpha \end{pmatrix} = \mathcal{A}^\alpha(\omega, \delta)^{-1} \begin{pmatrix} -f \\ -g \end{pmatrix}.$$

The original solution $u$ can be recovered by the inversion formula as follows

$$u(x) = \frac{1}{(2\pi)^2} \int_{BZ} u^\alpha(x) d\alpha. \tag{7.20}$$

Then, inside the region $D$, the solution $u$ satisfies

$$u = \mathcal{S}_D^{k_b}\big[\frac{1}{(2\pi)^2} \int_{BZ} \varphi^\alpha d\alpha\big].$$

Similarly, inside the region $Y \setminus \overline{D}$, we have

$$u = \frac{1}{(2\pi)^2} \int_{BZ} \mathcal{S}_D^{\alpha,k}[\psi^\alpha] d\alpha = \mathcal{S}_D^k\big[\frac{1}{(2\pi)^2} \int_{BZ} \psi^\alpha d\alpha\big] + \frac{1}{(2\pi)^2} \int_{BZ} \sum_{m \in \mathbb{Z}^2, m \neq 0} \mathcal{S}_D^k[\psi^\alpha](\cdot - m) e^{im\cdot\alpha} d\alpha.$$

Note that the second term in the right-hand side satisfies the homogeneous Helmholtz equation $(\Delta + k^2)u = 0$ in $Y \setminus \overline{D}$. So, in view of (7.8), we can identify $\varphi, \psi$ and $H$ as follows:

$$\varphi = \frac{1}{(2\pi)^2} \int_{BZ} \varphi^\alpha d\alpha, \quad \psi = \frac{1}{(2\pi)^2} \int_{BZ} \psi^\alpha d\alpha,$$

and

$$H = \frac{1}{(2\pi)^2} \int_{BZ} \sum_{m \in \mathbb{Z}^2, m \neq 0} \mathcal{S}_D^k[\psi^\alpha](\cdot - m) e^{im\cdot\alpha} d\alpha.$$

Therefore, from (7.19), we get the following result.

**Proposition 7.3.1.** *The density pair $(\varphi, \psi)$ and the effective source pair $(f, g)$ satisfy*

$$\begin{pmatrix} \varphi \\ \psi \end{pmatrix} = \left( \frac{1}{(2\pi)^2} \int_{BZ} \mathcal{A}^\alpha(\omega, \delta)^{-1} d\alpha \right) \begin{pmatrix} -f \\ -g \end{pmatrix} \tag{7.21}$$

*for small enough $\omega$ and $\delta$.*

### 7.3.5. The integral equation for the effective sources

Here we derive the integral equation for the effective source pair $(f, g)$. We have the following result.

**Proposition 7.3.2.** *The effective source pair $(f, g) \in L^2(\partial D)^2$ satisfies the following integral equation:*

$$\mathcal{M}^\epsilon(\omega)\begin{pmatrix} f \\ g \end{pmatrix} := \left( I + (\mathcal{A}_D^\epsilon(\omega,\delta) - \mathcal{A}_D(\omega,\delta))\frac{1}{(2\pi)^2}\int_{BZ} \mathcal{A}^\alpha(\omega,\delta)^{-1} d\alpha \right)\begin{pmatrix} f \\ g \end{pmatrix} = \begin{pmatrix} 0 \\ 0 \end{pmatrix}. \tag{7.22}$$

*Proof.* Applying $\mathcal{A}_{D_d}^{-1}$ to (7.9), we get

$$\mathcal{A}_{D_d}^{-1}\mathcal{A}_D\begin{pmatrix} \varphi \\ \psi \end{pmatrix} + A_{D_d}^{-1}\begin{pmatrix} f \\ g \end{pmatrix} = \mathcal{A}_{D_d}^{-1}\begin{pmatrix} H|_{\partial D} \\ \partial_\nu H|_{\partial D} \end{pmatrix}.$$

Then, by (7.16), we have

$$\mathcal{A}_{D_d}^{-1}\mathcal{A}_D\begin{pmatrix} \varphi \\ \psi \end{pmatrix} + A_{D_d}^{-1}\begin{pmatrix} f \\ g \end{pmatrix} = \begin{pmatrix} \varphi \\ \psi \end{pmatrix}.$$

So, from (7.21), we obtain

$$\left( \big( - \mathcal{A}_{D_d}^{-1}\mathcal{A}_D + I\big)\Big(\frac{1}{(2\pi)^2}\int_{BZ} (\mathcal{A}^\alpha)^{-1} d\alpha\Big) + \mathcal{A}_{D_d}^{-1} \right)\begin{pmatrix} f \\ g \end{pmatrix} = \begin{pmatrix} 0 \\ 0 \end{pmatrix}.$$

Finally, applying $\mathcal{A}_{D_d}$ to the above, we get the desired result. □

Thus, if we find a value of $\omega$ in the bandgap such that there exists a non-trivial solution pair $(f, g)$ to (7.22), then we have found a resonant frequency for the localized mode.

## 7.4. Sub-wavelength localized modes

### 7.4.1. The resonant frequency of the localized mode

Here we prove that a frequency for the localized mode can exist slightly above $\max_\alpha \omega_1^\alpha$. In what follows, we omit the subscript in $\omega_1^\alpha$ for ease of notation. We also do not make explicit the dependence on $\delta$.

We need to study the characteristic value of the operator $\mathcal{M}^\epsilon$ appearing in (7.22). Let us first analyze the operator $\int_{BZ}(\mathcal{A}^\alpha)^{-1}d\alpha$. Since $\omega^\alpha$ is a simple pole of the mapping $\omega \mapsto \mathcal{A}^\alpha(\omega)^{-1}$ in a neighborhood of $\omega^\alpha$, according to [17], we can write

$$\mathcal{A}^\alpha(\omega)^{-1} = \frac{\mathcal{L}^\alpha}{\omega - \omega^\alpha} + \mathcal{R}^\alpha(\omega), \tag{7.23}$$

where the operator-valued function $\mathcal{R}^\alpha(\omega)$ is holomorphic in a neighborhood of $\omega^\alpha$, and the operator $\mathcal{L}^\alpha$ maps $L^2(\partial D)^2$ onto $\ker \mathcal{A}^\alpha(\omega^\alpha, \delta)$. Let us write

$$\ker \mathcal{A}^\alpha(\omega^\alpha) = \mathrm{span}\{\Phi^\alpha\}.$$

Then, again from [17], it can be shown that

$$\mathcal{L}^\alpha = \frac{\langle \Phi^\alpha, \ \cdot \ \rangle \Phi^\alpha}{\langle \Phi^\alpha, \frac{d}{d\omega}\mathcal{A}^\alpha\big|_{\omega=\omega^\alpha}\Phi^\alpha\rangle}.$$

Hence the operator $\mathcal{M}^\epsilon$ can be decomposed as

$$\mathcal{M}^\epsilon = I + (\mathcal{A}_D^\epsilon - \mathcal{A}_D)\frac{1}{(2\pi)^2}\int_{BZ}\frac{\mathcal{L}^\alpha}{\omega-\omega_\alpha}d\alpha + (\mathcal{A}_D^\epsilon - \mathcal{A}_D)\frac{1}{(2\pi)^2}\int_{BZ}\mathcal{R}_\alpha d\alpha.$$

Note that the third term in the right-hand side is holomorphic with respect to $\omega$.

Denote by $\alpha^* = (\pi, \pi)$ and $\omega^* = \omega^{(\pi,\pi)}$. In [18], it was proved that, using the symmetry of the square array of bubbles, $\omega^\alpha$ attains its maximum at $\alpha = \alpha^*$. Since we are assuming that each bubble is a circular disk, we can derive a slightly more refined result as shown in the following lemma.

**Lemma 7.4.1.** *The characteristic value $\omega_\alpha$ attains its maximum at $\alpha = \alpha^*$. Moreover, for $\alpha$ near $\alpha_*$, we have*

$$\omega^\alpha = \omega^* - \frac{1}{2}c_\delta|\alpha - \alpha_*|^2 + o(|\alpha-\alpha_*|^2).$$

*Here, $c_\delta$ is a positive constant depending on $\delta$.*

In view of the above lemma, we can expect that the operator $\int_{BZ}\frac{\mathcal{L}^\alpha}{\omega-\omega^\alpha}$ becomes singular when $\omega \to \omega^*(= \max_\alpha \omega^\alpha)$. Let us extract its singular part explicitly. Before doing this, we introduce some notations. Denote by $\mathcal{A}^* = \mathcal{A}^{(\pi,\pi)}, \Phi^* = \Phi^{(\pi,\pi)}$, and $\mathcal{L}^* = \mathcal{L}^{(\pi,\pi)}$. We also define a small neighborhood $V$ of $\omega^*$ which excludes the real interval $(-\infty, \omega^*]$, namely,

$$V = \{|\omega - \omega^*| < r_*\} \setminus (-\infty, \omega^*],$$

for some small enough $r_* > 0$. By Lemma 7.4.1, we have

$$\begin{aligned}\frac{1}{(2\pi)^2}\int_{BZ}\frac{\mathcal{L}^\alpha}{\omega-\omega^\alpha}d\alpha &= \mathcal{L}^*\frac{1}{(2\pi)^2}\int_{BZ}\frac{1}{\omega-\omega^*+\frac{1}{2}c_\delta|\alpha-\alpha^*|^2}d\alpha + b_1(\omega)\\ &= \mathcal{L}^*\frac{1}{(2\pi)^2}\int_{|\alpha-\alpha^*|<1}\frac{}{\omega-\omega^*+\frac{1}{2}c_\delta|\alpha-\alpha^*|^2}d\alpha + b_2(\omega).\end{aligned}$$

Hereafter, $b_j$ means a bounded function with respect to $\omega$ in $V$. Then, using the polar coordinates $\alpha - \alpha_* = (r', \theta')$, we get

$$\frac{1}{(2\pi)^2}\int_{BZ}\frac{\mathcal{L}^\alpha}{\omega-\omega^\alpha}d\alpha = \frac{1}{(2\pi)^2}\int_0^1\frac{2\pi r'}{\omega-\omega_*+\frac{1}{2}c_\delta r'^2}dr' + b_2(\omega)$$

$$= \frac{1}{2\pi c_\delta} \ln(\omega - \omega_*) + b_3(\omega).$$

Here, the usual principal branch is taken for the logarithm and so the operator $\int_{BZ} \frac{\mathcal{L}^\alpha}{\omega - \omega^\alpha} d\alpha$ has a branch cut on $(-\infty, \omega^*]$. We also observe that, for $\omega \in V$,

$$\ln(\omega - \omega^*)(\mathcal{A}_D^\epsilon(\omega) - \mathcal{A}_D(\omega)) = \ln(\omega - \omega^*)(\mathcal{A}_D^\epsilon(\omega^*) - \mathcal{A}_D(\omega)^*) + b_4(\omega).$$

Therefore, the integral equation (7.22) can be rewritten as

$$\mathcal{M}^\epsilon(\omega) \begin{pmatrix} f \\ g \end{pmatrix} = \Big( I + \frac{\ln(\omega - \omega^*)}{2\pi c_\delta} (\mathcal{A}_D^\epsilon(\omega^*) - \mathcal{A}_D(\omega^*)) \mathcal{L}^* + \mathcal{R}^\epsilon(\omega) \Big) \begin{pmatrix} f \\ g \end{pmatrix} = \begin{pmatrix} 0 \\ 0 \end{pmatrix},$$

where $\mathcal{R}^\epsilon$ is analytic and bounded with respect to $\omega$ in $V$ and satisfies $\mathcal{R}^\epsilon = O(\epsilon)$. We first consider the principal part $\mathcal{N}^\epsilon(\omega)$, namely,

$$\mathcal{N}^\epsilon : \omega \mapsto \mathcal{N}^\epsilon(\omega) = I + \frac{1}{2\pi c_\delta} \log(\omega - \omega^*)(\mathcal{A}_D^\epsilon(\omega^*) - \mathcal{A}_D(\omega^*)) \mathcal{L}^*.$$

Let us find its characteristic value $\widehat{\omega}$, *i.e.*, $\widehat{\omega} \in V$ such that there exists a nontrivial function $\widehat{\Phi}$ satisfying $\mathcal{N}^\epsilon(\widehat{\omega})\widehat{\Phi} = 0$. Equivalently, we have

$$\widehat{\Phi} + \frac{1}{2\pi c_\delta} \log(\widehat{\omega} - \omega^*) \frac{(\mathcal{A}_D^\epsilon - \mathcal{A}_D)(\omega^*)\Phi^*}{\langle \Phi^*, \frac{d}{d\omega} \mathcal{A}^* \big|_{\omega = \omega^*} \Phi^* \rangle} \langle \Phi^*, \widehat{\Phi} \rangle = 0.$$

Then, by multiplying by $\Phi^*$,

$$\langle \Phi^*, \widehat{\Phi} \rangle \left( 1 + \frac{1}{2\pi c_\delta} \log(\widehat{\omega} - \omega^*) \frac{\langle \Phi^*, (\mathcal{A}_D^\epsilon - \mathcal{A}_D)(\omega^*)\Phi^* \rangle}{\langle \Phi^*, \frac{d}{d\omega} \mathcal{A}^* \big|_{\omega = \omega^*} \Phi^* \rangle} \right) = 0.$$

Since $\langle \Phi^*, \widehat{\Phi} \rangle = 0$ would imply $\widehat{\Phi} = 0$, we get

$$1 + \frac{1}{2\pi c_\delta} \log(\widehat{\omega} - \omega^*) \frac{\langle \Phi^*, (\mathcal{A}_D^\epsilon - \mathcal{A}_D)(\omega^*)\Phi^* \rangle}{\langle \Phi^*, \frac{d}{d\omega} \mathcal{A}^* \big|_{\omega = \omega^*} \Phi^* \rangle} = 0. \tag{7.24}$$

Before solving the above equation for $\omega$, we need the following lemmas whose proof will be given in Subsection 7.4.2.

**Lemma 7.4.2.** *The following results hold:*

*(i) For small enough $\delta$, we have*

$$\Big\langle \Phi^*, \frac{d}{d\omega} \mathcal{A}^*(\omega^*, \delta) \Phi^* \Big\rangle \approx -\omega^* \ln \omega^* \frac{R^2}{2} > 0.$$

*(ii) For small enough $\delta$ and $\epsilon$, we have*

$$\Big\langle \Phi^*, \big( \mathcal{A}_D^\epsilon(\omega^*, \delta) - \mathcal{A}_D(\omega^*, \delta) \big) \Phi^* \Big\rangle \approx 4\pi\epsilon \Big( -\frac{R^2}{2} (\omega^*)^2 \ln \omega^* + \delta \Big) > 0.$$

In view of Lemma 7.4.2, we see from (7.24) that

$$\widehat{\omega} - \omega_* = \exp\big( - 2\pi c_\delta \big\langle \Phi^*, \frac{d}{d\omega}\mathcal{A}^*(\omega^*)\Phi^* \big\rangle \big\langle \Phi^*, \big(\mathcal{A}_D^\epsilon(\omega^*) - \mathcal{A}_D(\omega^*)\big)\Phi^* \big\rangle^{-1}\big).$$

We can also see that the right-hand side is positive and goes to zero as $\epsilon$ tends to zero. In other words, $\widehat{\omega} \to \omega^*$ as $\epsilon \to 0$. Now we turn to the full operator $\mathcal{M}^\epsilon$. Recall that $\mathcal{M}^\epsilon = \mathcal{N}^\epsilon + \mathcal{R}^\epsilon$and $\mathcal{R}^\epsilon$ is holomorphic, bounded and satisfies $\mathcal{R}^\epsilon = O(\epsilon)$ in $V$. So by Gohberg-Sigal theory [17], we can conclude that there exists a characteristic value $\omega^\epsilon$ of the operator-valued function $\mathcal{M}^\epsilon$ near $\omega^*$. Let us denote its associated root function by $\Phi^\epsilon$. We choose $\Phi^\epsilon$ so that $\langle \Phi^*, \Phi^\epsilon \rangle = 1$. Then, as in the derivations of (7.24), we can obtain

$$1 + \frac{1}{2\pi c_\delta}\log(\widehat{\omega} - \omega^*)\frac{\langle \Phi^*, (\mathcal{A}_D^\epsilon - \mathcal{A}_D)(\omega^*)\Phi^* \rangle}{\langle \Phi^*, \frac{d}{d\omega}\mathcal{A}^*\big|_{\omega=\omega^*}\Phi^* \rangle} + \langle \Phi^*, \mathcal{R}^\epsilon(\omega)\Phi^\epsilon \rangle = 0.$$

Note that $\langle \Phi^*, \mathcal{R}^\epsilon(\omega)\Phi^\epsilon \rangle = O(\epsilon)$.

Therefore, we have proved the following theorem which is the main result of this chapter.

**Theorem 7.4.3.** *For small enough $\epsilon$ and $\delta$, there exists one frequency value $\omega^\epsilon$ such that the problem* (7.6) *has a nontrivial solution and $\omega^\epsilon$ is slightly above $\omega^*$. Moreover, we have*

$$\omega^\epsilon - \omega_* = \exp\big( - \frac{c_\delta}{2\epsilon}\frac{\frac{R^2}{2}\omega^*(-\ln\omega^*)}{(\frac{R^2}{2}(\omega^*)^2(-\ln\omega^*) + \delta)}\big) + o(1),$$

*as $\epsilon \to 0$.*

**Remark 7.4.4.** *Since $\omega^\epsilon$ is slightly above $\omega^* = \max_\alpha \omega^\alpha$, we have that $\omega^\epsilon$ is located in the bandgap region. This means that the corresponding function $u^\epsilon$, the solution to* (7.6)*, should be localized around the defect.*

## 7.4.2. Proof of Lemma 7.4.2

**Proof of (i)**. Recall that $(\omega^*)^2 \ln\omega^* = O(\delta)$ as $\delta \to 0$ [11]. Hence we need the low frequency asymptotics of the operator $\mathcal{A}^*(\omega^*, \delta)$. We use the following asymptotic expansions of the Hankel function for small argument:

$$\big(H_0^{(1)}\big)'(z) = \frac{2i}{\pi}\frac{1}{z} - \frac{i}{\pi}z\ln z + O(z),$$
$$\big(H_0^{(1)}\big)''(z) = -\frac{2i}{\pi}\frac{1}{z^2} - \frac{i}{\pi}\ln z + O(1).$$

Straightforward computations show that, for small $k$,

$$\frac{d}{dk}\mathcal{S}_D^k[\phi] = \frac{1}{2\pi k}\int_{\partial D}\phi(y)d\sigma(y) - \frac{k\ln k}{4\pi}\int_{\partial D}|x-y|^2\phi(y)d\sigma(y) + O(k),$$

and

$$\frac{d}{dk}(\mathcal{K}_D^k)^*[\phi] = -\frac{k\ln k}{4\pi}\int_{\partial D}\langle x-y,\nu(x)\rangle\phi(y)d\sigma(y) + O(k).$$

Also, by the symmetry argument for $\alpha^* = (\pi,\pi)$, one can see that

$$\mathcal{S}_D^{k,\alpha^*}[\phi] = \mathbf{S}_D[\phi] + O(k\ln k), \tag{7.25}$$

and

$$\frac{d}{dk}\mathcal{S}_D^{k,\alpha^*}[\phi] = \frac{1}{2\pi k}\int_{\partial D}\phi(y)d\sigma(y) - \frac{k\ln k}{4\pi}\int_{\partial D}|x-y|^2\phi(y)d\sigma(y) + O(k).$$

Recall that $\ker\mathcal{A}^*(\omega^*,\delta)$ is spanned by $\Phi^*$. Let us write

$$\Phi^* = \begin{pmatrix}\varphi^*\\ \psi^*\end{pmatrix},$$

and assume that $\Phi^*$ is chosen so that $\int_{\partial D}\varphi^* = 2\pi R$. Next we consider the kernel of the limiting operator of $\ker\mathcal{A}^*(\omega,\delta)$ when $\omega = 0$, $\delta = 0$, *i.e.*,

$$\mathcal{A}^*(0,0) = \begin{pmatrix}\mathcal{S}_D & -\mathcal{S}_D^{\alpha^*,0}\\ -\frac{1}{2}I + \mathcal{K}_D^* & 0\end{pmatrix}.$$

It is known that $\ker(-\frac{1}{2}I + \mathcal{K}_D^*)$ is one dimensional (see, for instance, [15]). We choose an element $\varphi_0^* \in L^2(\partial D)$ such that

$$\Big(-\frac{1}{2}I + \mathcal{K}_D^*\Big)[\varphi_0^*] = 0, \quad \int_{\partial D}\varphi_0^* = 2\pi R,$$

Then we define $\psi_0^* = (\mathcal{S}_D^{0,\alpha^*})^{-1}[\mathcal{S}_D[\varphi_0]]$ and denote

$$\Phi^{0,*} = \begin{pmatrix}\varphi_0^*\\ \psi_0^*\end{pmatrix}.$$

It can be shown that $\Phi^* \to \Phi^{0,*}$ as $\delta \to 0$.

Since $D$ is a disk, $\varphi_0^* = a\mathbb{1}_{\partial D}$ for some positive constant $a > 0$. Since $\int_{\partial D}\varphi_0^* = 2\pi R$ implies $a = 1$, by (7.25), we get $\psi_0^* = \mathbb{1}_{\partial D} + o(1)$ as $\delta \to 0$. Therefore, for small $\delta$, we have

$$\begin{aligned}\Big\langle\Phi^*, \frac{d}{d\omega}\mathcal{A}^*(\omega^*,\delta)\Phi^*\Big\rangle &\approx \Big\langle\Phi^{0,*}, \frac{d}{d\omega}\mathcal{A}^*(\omega^*,\delta)\Phi^{0,*}\Big\rangle\\ &\approx \langle\mathbb{1}_{\partial D}, \frac{d}{d\omega}\mathcal{S}_D^{k_b}[\mathbb{1}_{\partial D}]\rangle - \langle\mathbb{1}_{\partial D}, \frac{d}{d\omega}\mathcal{S}_D^{k_b,\alpha^*}[\mathbb{1}_{\partial D}]\rangle + \langle\mathbb{1}_{\partial D}, \frac{d}{d\omega}(\mathcal{K}_D^{k_b})^*[\mathbb{1}_{\partial D}]\rangle\\ &\approx -\frac{\omega^*\ln\omega^*}{4\pi}\int_{\partial D}\langle x-y,\nu(x)\rangle d\sigma(y) = -\omega^*\ln\omega^*\frac{R^2}{2}.\end{aligned}$$

Since $\omega^* \ln \omega^* < 0$, the conclusion follows. □

**Proof of (ii)**. Using asymptotic expansions of the Bessel function $J_n(z)$ and the Hankel function $H_n^{(1)}(z)$, for small $z$, straightforward computations yield

$$(\mathcal{A}_{D_d})_{V_{00}^d \to V_{00}^d} \approx \begin{pmatrix} R_d \ln R_d & -R_d \ln R_d \\ -\frac{R_d^2}{2}(\omega^*)^2 \ln \omega^* & -\delta \end{pmatrix},$$

and

$$(\mathcal{P}_1)_{V_{00} \to V_{00}^d} \approx \begin{pmatrix} \dfrac{\ln R}{\ln R_d} & 0 \\ 0 & 1 \end{pmatrix}, \quad (\mathcal{P}_2)_{V_{00}^d} \to V_{00} \approx \begin{pmatrix} 1 & 0 \\ 0 & \dfrac{R_d}{R} \end{pmatrix}.$$

Therefore,

$$\begin{aligned} (\mathcal{A}_D^\epsilon)_{V_{00} \to V_{00}} &= (\mathcal{P}_2^{-1} \mathcal{A}_{D_d} \mathcal{P}_1)_{V_{00} \to V_{00}} \\ &\approx \begin{pmatrix} R_d \ln R & -R_d \ln R \\ -\frac{1}{2} R R_d (\omega^*)^2 \ln \omega^* & -\delta \frac{R}{R_d} \end{pmatrix} \\ &\approx \begin{pmatrix} R \ln R & -R \ln R \\ -\frac{1}{2} R^2 (\omega^*)^2 \ln \omega^* & -\delta \end{pmatrix} + \epsilon \begin{pmatrix} \ln R & -\ln R \\ -\frac{R}{2}(\omega^*)^2 \ln \omega^* & \delta/R \end{pmatrix}. \end{aligned}$$

Finally, we obtain

$$\begin{aligned} \left\langle \Phi^*, \left(\mathcal{A}_D^\epsilon(\omega^*, \delta) - \mathcal{A}_D(\omega^*, \delta)\right) \Phi^* \right\rangle &\approx \left\langle \begin{pmatrix} 1 \\ 1 \end{pmatrix}, \begin{pmatrix} \ln R & -\ln R \\ -\frac{1}{2} R (\omega^*)^2 \ln \omega^* & \delta/R \end{pmatrix} \begin{pmatrix} 1 \\ 1 \end{pmatrix} \right\rangle \\ &\approx 4\pi \Big( -\frac{R^2}{2} (\omega^*)^2 \ln \omega^* + \delta \Big). \end{aligned}$$

The proof is then completed. □

## 7.5. Numerical illustrations

Here we provide numerical examples showing the existence of the sub-wavelength localized modes.

**Implementation.** For numerical computations, we discretize the operator $\mathcal{M}^\epsilon$ appearing in (7.22). Recall that it is given by

$$\mathcal{M}^\epsilon(\omega) = \left( I + (\mathcal{A}_D^\epsilon(\omega, \delta) - \mathcal{A}_D(\omega, \delta)) \frac{1}{(2\pi)^2} \int_{BZ} \mathcal{A}^\alpha(\omega, \delta)^{-1} d\alpha \right).$$

We use the Fourier basis for the discretization as in [11]. Specifically, we use $e^{in\theta}, n = -N, \ldots, N$ as a basis where $N$ is the truncation order.

The operators $\mathcal{A}_D$ and $\mathcal{A}_D^\epsilon$ are already represented in the Fourier basis in (7.14) and (7.16), respectively. We next consider the operator $\mathcal{A}^\alpha$. In [11], it was shown that, the operators $\mathcal{S}^{\alpha,k}$ and $\partial\mathcal{S}_D^{\alpha,k}/\partial\nu|_{\partial D}^{\pm}$ have the following matrix representations in the Fourier basis:

$$\mathcal{S}_D^{\alpha,k}|_{\partial D} \approx (S_{m,n}^\alpha)_{m,n=-N}^N, \quad \frac{\partial\mathcal{S}_D^{\alpha,k}}{\partial\nu}|_{\partial D}^{\pm} \approx (\widetilde{S}_{m,n}^{\alpha,\pm})_{m,n=-N}^N,$$

where the matrix elements $S_{m,n}^\alpha$ and $\widetilde{S}_{m,n}^\alpha$ are given by

$$\begin{aligned} S_{m,n}^\alpha &= -\frac{i\pi R}{2}J_n(kR)H_n^{(1)}(kR)\delta_{mn} - \frac{i\pi R}{2}J_n(kR)(-1)^{n-m}Q_{n-m}J_m(kR), \\ \widetilde{S}_{m,n}^{\alpha,\pm} &= \pm\frac{1}{2} - k\frac{i\pi R}{2}\Big(J_n\cdot(H_n^{(1)})' + J_n'\cdot H_n^{(1)}\Big)(kR)\delta_{mn} \\ &\quad -\frac{i\pi R}{2}J_n(kR)(-1)^{n-m}Q_{n-m}kJ_m'(kR). \end{aligned} \tag{7.26}$$

Here, $Q_n$ is the so-called lattice sum defined by

$$Q_n := \sum_{m\in\mathbb{Z}^2, m\neq 0} H_n^{(1)}(k|m|)e^{in\arg(m)}e^{im\cdot\alpha}.$$

For an efficient method for computing the lattice sum $Q_n$, we refer the reader to [76]. From (7.26), the matrix representation of $\mathcal{A}^\alpha$ immediately follows.

It remains to consider the integral $\int_{BZ}(\mathcal{A}^\alpha)^{-1}d\alpha$. We compute the two-dimensional integration with respect to $\alpha$ using Gauss quadrature. The discretization $(M_{m,n}^\epsilon)$ of the operator $\mathcal{M}^\epsilon(\omega)$ follows. To find the resonant frequency for the localized mode, we apply Muller's method [17] to the determinant of the matrix $(M_{m,n}^\epsilon)$. The maximum frequency $\omega^*$ of the first band can be used as a good initial guess.

**Example 1.** We first consider a dilute case where the radius of the bubble is small compared to the periodicity. We set the radius to be $R = 0.05$. For the material parameters, we use $\rho = \kappa = 5000$ and $\rho_b = \kappa_b = 1$. In this case, we have $\delta = 0.0002$. In Figure 7.1, we show the computed band structure for this dilute case and the frequency $\omega^\epsilon$ for the localized mode. Specifically, the frequency $\omega^\epsilon$ is the characteristic value of $\mathcal{M}^\epsilon$ near $\omega^*$. The black circles represent the band structure of the unperturbed crystal $\mathcal{C}$. The horizontal red line corresponds to the frequency $\omega^\epsilon$ for the localized mode. The band strucutre is computed in the exactly same way as in 4. The points $G, X$ and $M$ represent $\alpha = (0,0)$, $\alpha = (\pi,0)$, and $\alpha = (\pi,\pi)$, respectively. We used $N = 7$ for the truncation order of the Fourier basis.

To better illustrate the results, we also plot the magnified sub-wavelength band by changing the range of $\omega$ to a low frequency region $\{\omega : \omega \in (0, 0.39)\}$ (the right figure of Figure 7.1). In the first band, the maximum of $\omega$ is attained at the point $M$ (or $\alpha = \alpha^* = (\pi,\pi)$). The maximum frequency $\omega^*$ of the first band is $\omega^* \approx 0.2591$. The computed frequency for the localized mode is $\omega^\epsilon \approx 0.2846$. So the shift of the frequency

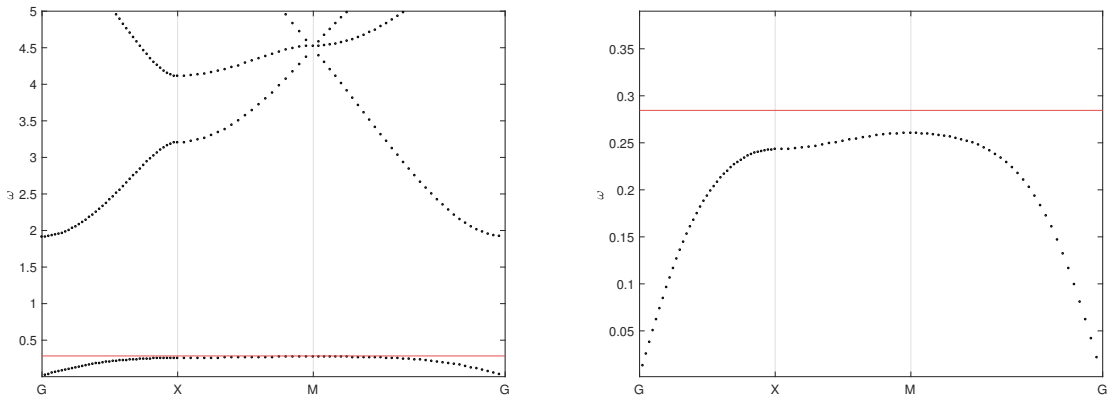


(a) (b)

Figure 7.1.: (Dilute case) The black circles represent a band structure of the unperturbed crystal with radius $R = 0.05$, $\delta = 1/5000$. The horizontal red line represents the frequency of localized mode for the perturbed crystal $\mathcal{C}_d$ with $\epsilon = 0.03 \times R = 0.0015$.

is $\omega^\epsilon - \omega^* \approx 0.0254 > 0$. Clearly, the frequency $\omega^\epsilon$ is located slightly above the sub-wavelength band. As desired, the frequency $\omega^\epsilon$ lies in the bandgap region. Note that $\omega^\epsilon$ is also in the sub-wavelength regime. Therefore it indicates the existence of a sub-wavelength localized mode.

**Example 2.** Next we turn to the non-dilute case. We set the radius to be $R = 0.25$. For the material parameters, we use $\rho = \kappa = 1000$ and $\rho_b = \kappa_b = 1$. This means $\delta = 0.001$. In Figure 7.2, we show the computed band structure for this non-dilute case. The maximum frequency $\omega^*$ of the first band is $\omega^* \approx 0.2039$. The computed frequency $\omega^\epsilon$ for the localized mode is $\omega^\epsilon \approx 0.2398$. So the shift of the frequency is $\omega^\epsilon - \omega^* \approx 0.0359 > 0$. Again, the frequency $\omega^\epsilon$ is located above the sub-wavelength band. We used $N = 3$ for the truncation order.

## 7.6. Concluding remarks

In this chapter, we have proved for the first time the possibility of localizing waves at a deep sub-wavelength scale. We have considered a bubbly crystal and produced a localized mode by increasing the size of one bubble. We have illustrated our findings with numerical experiments. Our results in this chapter shed light on the mechanism behind the control and guiding of waves at deep sub-wavelength scales. It would be very interesting to investigate the robustness of such sub-wavelength defect modes with respect to spatial disorder. A further challenge is the possibility of guiding waves at deep sub-wavelength scales using line defects. Another interesting problem we plan to

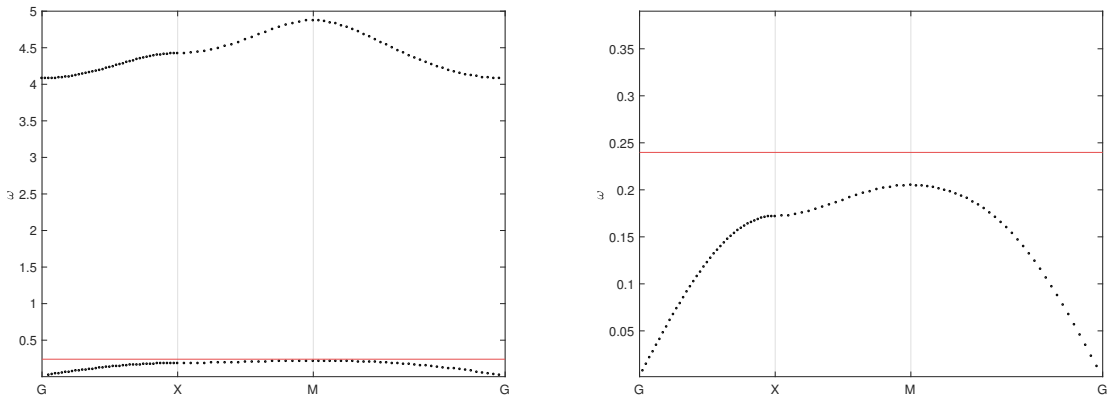


(a) (b)

Figure 7.2.: (Non-dilute case) The black circles represent a band structure of the unperturbed crystal with radius $R = 0.25$, $\delta = 1/1000$. The horizontal red line represents the frequency of localized mode for the perturbed crystal $\mathcal{C}_d$ with $\epsilon = 0.03 \times R = 0.0075$.

tackle is to prove or disprove the existence of fundamental limits on the Purcell factor in sub-wavelength bandgap materials.

# Appendices

# A. Appendix

## A.1. Asymptotic expansions

We recall some basic asymptotic expansion for the layer potentials in three and two dimensions from [17]; see also the appendix in [19].

### A.1.1. Asymptotic expansions in three dimensions

We expand the Green's function $G_k$ with

$$G^k(x) = -\frac{\mathrm{e}^{\mathrm{i}k|x|}}{4\pi|x|} = G_0(x) + \sum_{n=1}^{\infty} k^n G_n(x), \quad \text{with} \quad G_n(x) := -\frac{\mathrm{i}^n}{4\pi n!}|x|^{n-1}. \tag{A.1}$$

In particular, $G_1(x) = -\frac{\mathrm{i}}{4\pi}$. Developing in powers of $k$ the equation $(\Delta + k^2)G^k = \delta_0$ leads to

$$\forall n \geq 1, \quad \Delta G_{n+2} = -G_n. \tag{A.2}$$

We first consider the single layer potential:

$$\mathcal{S}_D^k[\psi](x) = \int_{\partial D} G^k(x,y)\psi(y)d\sigma(y), \quad x \in \partial D.$$

We have the following asymptotic expansion:

$$\mathcal{S}_D^k = \mathcal{S}_D + \sum_{n=1}^{\infty} k^n \mathcal{S}_{D,n}, \tag{A.3}$$

where

$$\begin{aligned} \mathcal{S}_{D,n}[\psi](x) &= \int_{\partial D} G_n(x-y)\psi(y)\mathrm{d}y \\ &= -\frac{i}{4\pi}\int_{\partial D} \frac{(i|x-y|)^{n-1}}{n!}\psi(y)d\sigma(y). \end{aligned}$$

In particular, we have

$$\mathcal{S}_D[\psi](x) = -\int_{\partial D} \frac{1}{4\pi|x-y|}\psi(y)d\sigma(y), \tag{A.4}$$

$$\mathcal{S}_{D,1}[\psi](x) = -\frac{i}{4\pi}\int_{\partial D}\psi(y)d\sigma(y), \tag{A.5}$$

$$\mathcal{S}_{D,2}[\psi](x) = -\frac{1}{8\pi}\int_{\partial D}|x-y|\psi(y)d\sigma(y). \tag{A.6}$$

**Lemma A.1.1.** *The norm $\|\mathcal{S}_{D,j}\|_{\mathcal{L}(L^2(\partial D),H^1(\partial D))}$ is uniformly bounded with respect to $j$. Moreover, the series in (A.3) is convergent in $\mathcal{L}(L^2(\partial D), H^1(\partial D))$.*

We now consider the boundary integral operator $\mathcal{K}_D^{k,*}$ defined by

$$\mathcal{K}_D^{k,*}[\psi](x) = \int_{\partial D}\frac{\partial G^k(x,y)}{\partial\nu(x)}\psi(y)d\sigma(y), \quad x\in\partial D.$$

We have

$$\mathcal{K}_D^{k,*} = \mathcal{K}_D^* + k\mathcal{K}_{D,1}^* + k^2\mathcal{K}_{D,2}^* + \dots, \tag{A.7}$$

where

$$\begin{aligned}\mathcal{K}_{D,n}^*[\psi](x) &= -\frac{i}{4\pi}\int_{\partial D}\frac{\partial G_n(x-y)}{\partial\nu(x)}\psi(y)d\sigma(y)\\ &= -\frac{i}{4\pi}\int_{\partial D}\frac{\partial(i|x-y|)^{n-1}}{n!\partial\nu(x)}\psi(y)d\sigma(y)\\ &= -\frac{i^n(n-1)}{4\pi n!}\int_{\partial D}|x-y|^{n-3}(x-y)\cdot\nu(x)\psi(y)d\sigma(y).\end{aligned}$$

In particular, we have

$$\begin{aligned}\mathcal{K}_{D,1}^* &= 0,\\ \mathcal{K}_{D,2}^*[\psi](x) &= \frac{1}{8\pi}\int_{\partial D}\frac{(x-y)\cdot\nu(x)}{|x-y|}\psi(y)d\sigma(y),\\ \mathcal{K}_{D,3}^*[\psi](x) &= \frac{i}{12\pi}\int_{\partial D}(x-y)\cdot\nu(x)\psi(y)d\sigma(y).\end{aligned}$$

**Lemma A.1.2.** *The norm $\|\mathcal{K}_{D,j}\|_{\mathcal{L}(L^2(\partial D))}$ is uniformly bounded for $j\geq 1$. Moreover, the series in (A.7) is convergent in $\mathcal{L}(L^2(\partial D))$.*

Using (A.2), we deduce the following useful identities.

**Lemma A.1.3.** *It holds:*

$$(i)\quad \mathcal{K}_{D,2}[\mathbb{1}_{\partial D}](x) = \int_{\partial D}\frac{\partial G_2(x-y)}{\partial\nu(y)}\mathrm{d}\sigma(y) = \int_D\Delta_y G_2(x-y)\mathrm{d}y = -\int_D G_0(x-y)\mathrm{d}y,$$

$$(ii)\quad \mathcal{K}_{D,3}[\mathbb{1}_{\partial D}](x) = \int_{\partial D}\frac{\partial G_3(x-y)}{\partial\nu(y)}\mathrm{d}\sigma(y) = \int_D\Delta_y G_3(x-y)\mathrm{d}y = -\int_D G_1(x-y)\mathrm{d}y = \frac{\mathrm{i}|D|}{4\pi}.$$

### A.1.2. Asymptotic expansions in two dimensions

In two dimensions, the single-layer potential for the Helmholtz equation is defined by

$$\mathcal{S}_D^k[\psi](x) = \int_{\partial D} G^k(x,y)\psi(y)d\sigma(y), \quad x \in \partial D,$$

where $G^k(x,y) = -\frac{i}{4}H_0^{(1)}(k|x-y|)$ and $H_0^{(1)}$ is the Hankel function of first kind and order 0. We have

$$-\frac{i}{4}H_0^{(1)}(k|x-y|) = \frac{1}{2\pi}\ln|x-y| + \eta_k + \sum_{j=1}^{\infty}(b_j \ln k|x-y| + c_j)(k|x-y|)^{2j},$$

where

$$\eta_k = \frac{1}{2\pi}(\ln k + \gamma - \ln 2) - \frac{i}{4}, \quad b_j = \frac{(-1)^j}{2\pi}\frac{1}{2^{2j}(j!)^2}, \quad c_j = b_j\left(\gamma - \ln 2 - \frac{i\pi}{2} - \sum_{n=1}^{j}\frac{1}{n}\right),$$

and $\gamma$ is the Euler constant. Especially,

$$b_1 = -\frac{1}{8\pi},\ c_1 = -\frac{1}{8\pi}(\gamma - \ln 2 - 1 - \frac{i\pi}{2}).$$

Thus,

$$\mathcal{S}_D^k = \hat{\mathcal{S}}_D^k + \sum_{j=1}^{\infty}\left(k^{2j}\ln k\right)\mathcal{S}_{D,j}^{(1)} + \sum_{j=1}^{\infty}k^{2j}\mathcal{S}_{D,j}^{(2)}, \tag{A.8}$$

where

$$\hat{\mathcal{S}}_D^k[\psi](x) = \mathcal{S}_D[\psi](x) + \eta_k\int_{\partial D}\psi\, d\sigma, \tag{A.9}$$

and

$$\begin{aligned}\mathcal{S}_{D,j}^{(1)}[\psi](x) &= \int_{\partial D} b_j|x-y|^{2j}\psi(y)d\sigma(y),\\ \mathcal{S}_{D,j}^{(2)}[\psi](x) &= \int_{\partial D}|x-y|^{2j}(b_j\ln|x-y| + c_j)\psi(y)d\sigma(y).\end{aligned}$$

We next consider the boundary integral operator $\mathcal{K}_D^{k,*}$ defined by

$$\mathcal{K}_D^{k,*}[\psi](x) = \int_{\partial D}\frac{\partial G^k(x,y)}{\partial\nu(x)}\psi(y)d\sigma(y), \quad x \in \partial D.$$

We have

$$\mathcal{K}_D^{k,*} = \mathcal{K}_D^{*} + \sum_{j=1}^{\infty}\left(k^{2j}\ln k\right)\mathcal{K}_{D,j}^{(1),*} + \sum_{j=1}^{\infty}k^{2j}\mathcal{K}_{D,j}^{(2,*)}, \tag{A.10}$$

where

$$\begin{aligned}\mathcal{K}_{D,j}^{(1),*}[\psi](x) &= \int_{\partial D} b_j \frac{\partial |x-y|^{2j}}{\partial \nu(x)} \psi(y) d\sigma(y),\\ \mathcal{K}_{D,j}^{(2),*}[\psi](x) &= \int_{\partial D} \frac{\partial \left(|x-y|^{2j}(b_j \ln|x-y| + c_j)\right)}{\nu(x)} \psi(y) d\sigma(y).\end{aligned}$$

**Lemma A.1.4.** *The following estimates hold in $\mathcal{L}(L^2(\partial D), H^1(\partial D))$ and $\mathcal{L}(L^2(\partial D), L^2(\partial D))$, respectively:*

$$\begin{aligned}\mathcal{S}_D^k &= \hat{\mathcal{S}}_D^k + k^2 \ln k \mathcal{S}_{D,1}^{(1)} + k^2 \mathcal{S}_{D,1}^{(2)} + O(k^4 \ln k);\\ \mathcal{K}_D^{k,*} &= \mathcal{K}_D + k^2 \ln k \mathcal{K}_{D,1}^{(1),*} + k^2 \mathcal{K}_{D,1}^{(2),*} + O(k^4 \ln k).\end{aligned}$$

**Lemma A.1.5.** *The following identities hold:*

*(i)*

$$\mathcal{K}_{D,1}^{(1)}[1](x) = 4\bar{b}_1 |D|;$$

*(ii)*

$$\mathcal{K}_{D,1}^{(2)}[1](x) = (2\bar{b}_1 + 4\bar{c}_1)|D| + 4\bar{b}_1 \int_D \ln|x-y| dy,$$

*where $\bar{b}_1$ and $\bar{c}_1$ are the complex conjugates of $b_1$ and $c_1$.*

*Proof.* First, we have

$$\begin{aligned}\mathcal{K}_{D,1}^{(1)}[1](x) &= \bar{b}_1 \int_{\partial D} 2\langle y-x, \nu(y)\rangle d\sigma(y)\\ &= \bar{b}_1 \int_{\partial D} \frac{\partial |y-x|^2}{\partial \nu(y)} d\sigma(y)\\ &= \bar{b}_1 \int_D \Delta_y |y-x|^2 dy\\ &= 4\bar{b}_1 |D|.\end{aligned}$$

We now prove the second identity. We have

$$\begin{aligned}\mathcal{K}_{D,1}^{(2)}[1](x) &= \int_{\partial D} \frac{\partial \left[|y-x|^2(\bar{b}_1 \ln|x-y| + \bar{c}_1)\right]}{\partial \nu(y)} d\sigma(y)\\ &= \int_D \Delta_y [|y-x|^2(\bar{b}_1 \ln|x-y| + \bar{c}_1)] dy\\ &= 4\bar{c}_1 |D| + \bar{b}_1 \int_D \Delta_y [|y-x|^2 \ln|x-y|] dy\\ &= 4\bar{c}_1 |D| + \bar{b}_1 \int_D 4\ln|x-y|] dy + \bar{b}_1 \int_D 2dy + \bar{b}_1 \int_D |y-x|^2 \Delta \ln|y-x| dy\end{aligned}$$

$$= \quad (2\bar{b}_1 + 4\bar{c}_1)|D| + 4\bar{b}_1 \int_D \ln|x-y|dy,$$

where we have used the fact that

$$\int_D |y-x|^2 \Delta \ln|y-x| dy = 0, \text{ for } x \in \partial D \ .$$

This completes the proof of the Lemma. □

### A.1.3. Asymptotic expansions in three dimensions for quasi-periodic operators

For the $\alpha$-quasi-periodic Green's function $G^{\alpha,k}$, we have

$$G^{\alpha,k}(x,y) = G^{\alpha,0} + \sum_{\ell=1}^{\infty} k^{2\ell} G_\ell^{\alpha,\#} := G^{\alpha,0}(x,y) - \sum_{\ell=1}^{\infty} k^{2\ell} \sum_{n\in\mathbb{Z}^d} \frac{e^{\mathrm{i}(2\pi n+\alpha)\cdot(x-y)}}{|2\pi n+\alpha|^{2(\ell+1)}}, \quad \text{(A.11)}$$

when $\alpha \neq 0$, and $k \to 0$.

From (A.11), we decompose the single layer potential as

$$\mathcal{S}_D^{\alpha,k} = \mathcal{S}_D^{\alpha,0} + \sum_{\ell=1}^{\infty} k^{2\ell} \mathcal{S}_{D,\ell}^{\alpha} \quad \text{with} \quad \mathcal{S}_{D,\ell}^{\alpha}[\psi] := \int_{\partial D} G_\ell^{\alpha,\#}(x-y)\psi(y)\mathrm{d}y, \quad \text{(A.12)}$$

where the convergence holds in $\mathcal{L}(L^2(\partial D), H^1(\partial D))$. Similarly, the asymptotic expansion for the operator $\left(\mathcal{K}_D^{-\alpha,k}\right)^*$ is

$$(\mathcal{K}_D^{-\alpha,k})^* = (\mathcal{K}_D^{-\alpha,0})^* + \sum_{\ell=1}^{\infty} k^{2\ell} (\mathcal{K}_{D,\ell}^{\alpha})^* \quad \text{with} \quad (\mathcal{K}_{D,\ell}^{\alpha})^*[\psi](x) := \int_{\partial D} \frac{\partial G_\ell^{\alpha,\#}(x-y)}{\partial \nu(x)} \psi(y)\mathrm{d}y, \quad \text{(A.13)}$$

where the convergence holds in $\mathcal{L}(L^2(\partial D), L^2(\partial D))$.

## A.2. Subwavelength bandgap opening in two dimensions

The aim of this appendix is to check that formula (4.6) holds in the two-dimensional case, where $\omega_M$ is the (free space) Minnaert resonant frequency and $c_2$ is defined by (4.7). Note that for $\alpha \neq 0$, the quasi-periodic single layer operator $\mathcal{S}_D^{\alpha,0} : L^2(\partial D) \to H^1(\partial D)$ is invertible. Moreover, the definitions in Section 1.7 of both the capacity and the $\alpha$-quasi-periodic capacity remain valid.

In the two-dimensional case, using the asymptotic expansions in A.1.2 as $k \to 0$, the asymptotic expansion (4.8) should be replaced with

$$\mathcal{A}(\omega,\delta) := \mathcal{A}_0 + \mathcal{B}(\omega,\delta) = \mathcal{A}_0 + \omega^2 \ln\omega \mathcal{A}_{1,1,0} + \omega^2 \mathcal{A}_{1,2,0} + \delta \mathcal{A}_{0,1} + O(\delta\omega^2 \ln\omega) + O(\omega^4 \ln\omega),$$

where $\mathcal{A}_0$ is defined by (4.5), and

$$\mathcal{A}_{1,1,0} = \begin{pmatrix} v_b^{-2}\mathcal{S}_{D,1}^{(1)} & 0 \\ v_b^{-2}\mathcal{K}_{D,1}^{(1),*} & 0 \end{pmatrix},$$
$$\mathcal{A}_{1,2,0} = \begin{pmatrix} v_b^{-2}\left(\ln v_b^{-1}\mathcal{S}_{D,1}^{(1)} + \mathcal{S}_{D,1}^{(2)}\right) & -v^{-2}\mathcal{S}_{D,1}^{\alpha} \\ v_b^{-2}\left(\ln v_b^{-1}\mathcal{K}_{D,1}^{(1),*} + \mathcal{K}_{D,1}^{(2),*}\right) & 0 \end{pmatrix},$$
$$\mathcal{A}_{0,1} = \begin{pmatrix} 0 & 0 \\ 0 & -(\frac{1}{2}I + (\mathcal{K}_D^{-\alpha,0})^*) \end{pmatrix}.$$

Using the definition of the free space Minnaert resonance in dimension two in 2, it is not difficult to see that (4.6) holds.

## A.3. Proof of Lemma 5.2.1

This is a classical result, which is a special case of a more general result. It is usually proven using the properties of spherical Bessel functions (see for instance [87]). We include here a simple proof for completeness.

**Step 1**: Proof for $\mathcal{S}_D^k$ with $x \in \partial D$.
Let us first prove the result for $\mathcal{S}_D^k$. We have that for $x \in \partial D$,

$$\mathcal{S}_D^k[\mathbb{1}_{\partial D}](x) = -\frac{1}{4\pi}\int_{\partial D}\frac{\mathrm{e}^{\mathrm{i}k|x-y|}}{|x-y|}\mathrm{d}\sigma(y).$$

Since the problem is invariant under rotation, it is sufficient to compute the integral for $x = (0, 0, R)$. We use the spherical coordinates

$$\partial D \ni y = (y_1, y_2, y_3)^\top = (R\sin\phi\cos\theta, R\sin\phi\sin\theta, R\cos\phi)^\top$$

with $0 \le \theta \le 2\pi$ and $0 \le \phi \le \pi$. Then, for $y \in \partial D$, it holds that

$$|x-y| = R\sqrt{\sin^2\phi + (1-\cos\phi)^2} = 2R\sin\left(\frac{\phi}{2}\right),$$

so that

$$\mathcal{S}_D^k[\mathbb{1}_{\partial D}](x) = -\frac{2\pi R^2}{4\pi}\int_0^\pi \frac{\mathrm{e}^{2\mathrm{i}kR\sin\left(\frac{\phi}{2}\right)}}{2R\sin\left(\frac{\phi}{2}\right)}\sin(\phi)\,\mathrm{d}\phi.$$

Together with the equality $\sin(\phi) = 2\sin(\phi/2)\cos(\phi/2)$ and the change of variable $u = \sin(\phi/2)$, we end up with

$$\mathcal{S}_D^k[\mathbb{1}_{\partial D}](x) = -R\int_0^1 \mathrm{e}^{\mathrm{i}k2Ru}\mathrm{d}u = -R\left(\frac{\mathrm{e}^{\mathrm{i}k2R}-1}{2\mathrm{i}kR}\right) = -\frac{\mathrm{e}^{\mathrm{i}kR}}{k}\sin(kR). \tag{A.14}$$

**Step 2**: Exact expression of $\mathcal{S}_D^k[\mathbb{1}_{\partial D}]$ with $x \in \partial D$.
From the previous step, we can easily deduce an expression of $\mathcal{S}_D^k[\mathbb{1}_{\partial D}]$ on $\mathbb{R}^3 \setminus D$. Indeed, the function $\mathcal{S}_D^k[\mathbb{1}_{\partial D}]$ outside $D$ is the (unique) solution to the Dirichlet equation

$$\begin{cases} (\Delta + k^2)u = 0, \\ u\Big|_{\partial D} = \mathcal{S}_D^k[\mathbb{1}_{\partial D}] = -\dfrac{\mathrm{e}^{\mathrm{i}kR}}{k}\sin(kR), \end{cases}$$

together with the Sommerfeld radiation condition. The solution is therefore

$$\mathcal{S}_D^k[\mathbb{1}_{\partial D}](x) = -\frac{R\sin(kR)}{k}\frac{\mathrm{e}^{\mathrm{i}k|x|}}{|x|}. \tag{A.15}$$

**Step 3**: Proof for $\left(\mathcal{K}_D^k\right)^*$.
For all $x \in \partial D$, jump formula for the layer potentials lead to

$$\left(\mathcal{K}_D^k\right)^*[\mathbb{1}_{\partial D}](x) = \frac{\partial}{\partial \nu(x)}\mathcal{S}_D^k[\mathbb{1}_{\partial D}]\Big|_+(x) - \frac{1}{2}.$$

Together with (A.15), we obtain

$$\left(\mathcal{K}_D^k\right)^*[\mathbb{1}_{\partial D}](x) = -\frac{R\sin(kR)}{k}\mathrm{e}^{\mathrm{i}kR}\left(-\frac{1}{R^2} + \frac{\mathrm{i}k}{R}\right) - \frac{1}{2} = \frac{\sin(kR)}{kR}\mathrm{e}^{\mathrm{i}kR} - \frac{\mathrm{e}^{2\mathrm{i}kR}}{2}.$$

# References


[1] Toufic Abboud and Habib Ammari. Diffraction at a curved grating: Tm and te cases, homogenization. *Journal of mathematical analysis and applications*, 202(3):995–1026, 1996.

[2] Yves Achdou, O Pironneau, and F Valentin. Effective boundary conditions for laminar flows over periodic rough boundaries. *Journal of Computational Physics*, 147(1):187–218, 1998.

[3] Michael A Ainslie and Timothy G Leighton. Review of scattering and extinction cross-sections, damping factors, and resonance frequencies of a spherical gas bubble. *The Journal of the Acoustical Society of America*, 130(5):3184–3208, 2011.

[4] Grégoire Allaire and Micol Amar. Boundary layer tails in periodic homogenization. *ESAIM: Control, Optimisation and Calculus of Variations*, 4:209–243, 1999.

[5] Habib Ammari, Youjun Deng, and Pierre Millien. Surface plasmon resonance of nanoparticles and applications in imaging. *Archive for Rational Mechanics and Analysis*, 220(1):109–153, 2016.

[6] Habib Ammari, Brian Fitzpatrick, David Gontier, Hyundae Lee, and Hai Zhang. A mathematical and numerical framework for bubble meta-screens. *SIAM Journal on Applied Mathematics*, 77(5):1827–1850, 2017.

[7] Habib Ammari, Brian Fitzpatrick, David Gontier, Hyundae Lee, and Hai Zhang. Sub-wavelength focusing of acoustic waves in bubbly media. *Proc. R. Soc. A*, 473(2208):20170469, 2017.

[8] Habib Ammari, Brian Fitzpatrick, David Gontier, Hyundae Lee, and Hai Zhang. Minnaert resonances for acoustic waves in bubbly media. *Annales de l'Institut Henri Poincaré: Analyse Nonlinéaire, to appear (doi.org10.1016j.anihpc.2018.03.007)*, 2018.

[9] Habib Ammari, Brian Fitzpatrick, Erik Orvehed Hiltunen, and Sanghyeon Yu. Sub-wavelength localized modes for acoustic waves in bubbly crystals with a defect. *arXiv preprint arXiv:1804.00756*, 2018.

[10] Habib Ammari, Brian Fitzpatrick, Hyundae Lee, Sanghyeon Yu, and Hai Zhang. Double-negative acoustic metamaterials. *arXiv preprint arXiv:1709.08177*, 2017.

[11] Habib Ammari, Brian Fitzpatrick, Hyundae Lee, Sanghyeon Yu, and Hai Zhang. Subwavelength phononic bandgap opening in bubbly media. *Journal of Differential Equations*, 263(9):5610–5629, 2017.

[12] Habib Ammari, Josselin Garnier, Wenjia Jing, Hyeonbae Kang, Mikyoung Lim, Knut Sølna, and Han Wang. *Mathematical and statistical methods for multistatic imaging*, volume 2098. Springer, 2013.

[13] Habib Ammari, Hyeoenbae Kang, Sofiane Soussi, and Habib Zribi. Layer potential techniques in spectral analysis. part ii: Sensitivity analysis of spectral properties of high contrast band-gap materials. *Multiscale Modeling & Simulation*, 5(2):646–663, 2006.

[14] Habib Ammari and Hyeonbae Kang. Boundary layer techniques for solving the helmholtz equation in the presence of small inhomogeneities. *Journal of mathematical analysis and applications*, 296(1):190–208, 2004.

[15] Habib Ammari and Hyeonbae Kang. *Polarization and moment tensors: with applications to inverse problems and effective medium theory*, volume 162. Springer Science & Business Media, 2007.

[16] Habib Ammari, Hyeonbae Kang, and Hyundae Lee. Asymptotic analysis of high-contrast phononic crystals and a criterion for the band-gap opening. *Archive for rational mechanics and analysis*, 193(3):679, 2009.

[17] Habib Ammari, Hyeonbae Kang, and Hyundae Lee. *Layer potential techniques in spectral analysis*. Number 153. American Mathematical Soc., 2009.

[18] Habib Ammari, Hyundae Lee, and Hai Zhang. High frequency homogenization of bubbly crystals. *arXiv preprint arXiv:1708.07955*, 2017.

[19] Habib Ammari, Pierre Millien, Matias Ruiz, and Hai Zhang. Mathematical analysis of plasmonic nanoparticles: the scalar case. *Archive for Rational Mechanics and Analysis*, 224(2):597–658, 2017.

[20] Habib Ammari, Jean-Claude Nédélec, and Kamel Hamdache. Chirality in the maxwell equations by the dipole approximation. *SIAM Journal on Applied Mathematics*, 59(6):2045–2059, 1999.

[21] Habib Ammari, Matias Ruiz, Wei Wu, Sanghyeon Yu, and Hai Zhang. Mathematical and numerical framework for metasurfaces using thin layers of periodically distributed plasmonic nanoparticles. *Proc. R. Soc. A*, 472(2193):20160445, 2016.

[22] Habib Ammari, Matias Ruiz, Sanghyeon Yu, and Hai Zhang. Mathematical analysis of plasmonic resonances for nanoparticles: the full maxwell equations. *Journal of Differential Equations*, 261(6):3615–3669, 2016.

[23] Habib Ammari and Hai Zhang. A mathematical theory of super-resolution by using a system of sub-wavelength helmholtz resonators. *Communications in Mathematical Physics*, 337(1):379–428, 2015.

[24] Habib Ammari and Hai Zhang. Super-resolution in high-contrast media. *Proc. R. Soc. A*, 471(2178):20140946, 2015.

[25] Habib Ammari and Hai Zhang. Effective medium theory for acoustic waves in bubbly fluids near minnaert resonant frequency. *SIAM Journal on Mathematical Analysis*, 49(4):3252–3276, 2017.

[26] Kazunori Ando and Hyeonbae Kang. Analysis of plasmon resonance on smooth domains using spectral properties of the neumann–poincaré operator. *Journal of Mathematical Analysis and Applications*, 435(1):162–178, 2016.

[27] Kazunori Ando, Hyeonbae Kang, and Hongyu Liu. Plasmon resonance with finite frequencies: a validation of the quasi-static approximation for diametrically small inclusions. *SIAM Journal on Applied Mathematics*, 76(2):731–749, 2016.

[28] Alex Barnett and Leslie Greengard. A new integral representation for quasi-periodic fields and its application to two-dimensional band structure calculations. *Journal of Computational Physics*, 229(19):6898–6914, 2010.

[29] Guy Bouchitté and Didier Felbacq. Homogenization near resonances and artificial magnetism from dielectrics. *Comptes Rendus Mathematique*, 339(5):377–382, 2004.

[30] Marc Briane and Laurent Pater. Homogenization of high-contrast two-phase conductivities perturbed by a magnetic field. comparison between dimension two and dimension three. *Journal of Mathematical Analysis and applications*, 393(2):563–589, 2012.

[31] Russel E Caflisch, Michael J Miksis, George C Papanicolaou, and Lu Ting. Effective equations for wave propagation in bubbly liquids. *Journal of Fluid Mechanics*, 153:259–273, 1985.

[32] Russel E Caflisch, Michael J Miksis, George C Papanicolaou, and Lu Ting. Wave propagation in bubbly liquids at finite volume fraction. *Journal of Fluid Mechanics*, 160:1–14, 1985.

[33] David C Calvo, Abel L Thangawng, and Christopher N Layman. Low-frequency resonance of an oblate spheroidal cavity in a soft elastic medium. *The Journal of the Acoustical Society of America*, 132(1):EL1–EL7, 2012.

[34] Mohamed Camar-Eddine and Laurent Pater. Homogenization of high-contrast and non symmetric conductivities for non periodic columnar structures. *arXiv preprint arXiv:1302.7222*, 2013.

[35] Filippo Capolino, Donald R Wilton, and William A Johnson. Efficient computation of the 2-d green's function for 1-d periodic structures using the ewald method. *IEEE Transactions on Antennas and Propagation*, 53(9):2977–2984, 2005.

[36] H Cheng, WY Crutchfield, M Doery, and L Greengard. Fast, accurate integral equation methods for the analysis of photonic crystal fibers i: Theory. *Optics Express*, 12(16):3791–3805, 2004.

[37] Kerry W Commander and Andrea Prosperetti. Linear pressure waves in bubbly liquids: Comparison between theory and experiments. *The Journal of the Acoustical Society of America*, 85(2):732–746, 1989.

[38] Steven A Cummer, Johan Christensen, and Andrea Alù. Controlling sound with acoustic metamaterials. *Nature Reviews Materials*, 1:16001, 2016.

[39] Nico de Jong, Lars Hoff, Tore Skotland, and Nicolaas Bom. Absorption and scatter of encapsulated gas filled microspheres: theoretical considerations and some measurements. *Ultrasonics*, 30(2):95–103, 1992.

[40] Martin Devaud, Thierry Hocquet, Jean-Claude Bacri, and Valentin Leroy. The minnaert bubble: an acoustic approach. *European Journal of Physics*, 29(6):1263, 2008.

[41] Vincent Duchêne, Iva Vukićević, and Michael I Weinstein. Homogenized description of defect modes in periodic structures with localized defects. *arXiv preprint arXiv:1301.0837*, 2013.

[42] Vincent Duchêne, Iva Vukicevic, and Michael I Weinstein. Oscillatory and localized perturbations of periodic structures and the bifurcation of defect modes. *SIAM Journal on Mathematical Analysis*, 47(5):3832–3883, 2015.

[43] Claudia Errico, Juliette Pierre, Sophie Pezet, Yann Desailly, Zsolt Lenkei, Olivier Couture, and Mickael Tanter. Ultrafast ultrasound localization microscopy for deep super-resolution vascular imaging. *Nature*, 527(7579):499, 2015.

[44] Paul Peter Ewald. Die berechnung optischer und elektrostatischer gitterpotentiale. *Annalen der Physik*, 369(3):253–287, 1921.

[45] D Felbacq and Guy Bouchitté. Homogenization of a set of parallel fibres. *Waves in random media*, 7(2):245–256, 1997.

[46] R Figari, G Papanicolaou, and J Rubinstein. Remarks on the point interaction approximation. In *Hydrodynamic behavior and interacting particle systems*, pages 45–55. Springer, 1987.

[47] Alex Figotin and Peter Kuchment. Spectral properties of classical waves in high-contrast periodic media. *SIAM Journal on Applied Mathematics*, 58(2):683–702, 1998.

[48] Alexander Figotin and Vladimir Goren. Resolvent method for computations of localized defect modes of h-polarization in two-dimensional photonic crystals. *Physical Review E*, 64(5):056623, 2001.

[49] Alexander Figotin and Abel Klein. Localized classical waves created by defects. *Journal of statistical physics*, 86(1-2):165–177, 1997.

[50] Leslie L Foldy. The multiple scattering of waves. i. general theory of isotropic scattering by randomly distributed scatterers. *Physical Review*, 67(3-4):107, 1945.

[51] Vahe Galstyan, On Shun Pak, and Howard A Stone. A note on the breathing mode of an elastic sphere in newtonian and complex fluids. *Physics of Fluids*, 27(3):032001, 2015.

[52] IC Gohberg and EI Sigal. An operator generalization of the logarithmic residue theorem and the theorem of rouché. *Sbornik: Mathematics*, 13(4):603–625, 1971.

[53] Daniel Grieser. The plasmonic eigenvalue problem. *Reviews in Mathematical Physics*, 26(03):1450005, 2014.

[54] Rainer Hempel and Karsten Lienau. Spectral properties of periodic media in the large coupling limit: Properties of periodic media. *Communications in Partial Differential Equations*, 25(7-8):1445–1470, 2000.

[55] Mark A Hoefer and Michael I Weinstein. Defect modes and homogenization of periodic schrödinger operators. *SIAM Journal on Mathematical Analysis*, 43(2):971–996, 2011.

[56] Paul A Hwang and William J Teague. Low-frequency resonant scattering of bubble clouds. *Journal of Atmospheric and Oceanic Technology*, 17(6):847–853, 2000.

[57] Nadège Kaina, Fabrice Lemoult, Mathias Fink, and Geoffroy Lerosey. Negative refractive index and acoustic superlens from multiple scattering in single negative metamaterials. *Nature*, 525(7567):77, 2015.

[58] Hyeonbae Kang, Kyoungsun Kim, Hyundae Lee, Jaemin Shin, and Sanghyeon Yu. Spectral properties of the neumann–poincaré operator and uniformity of estimates for the conductivity equation with complex coefficients. *Journal of the London Mathematical Society*, 93(2):519–545, 2016.

[59] Steven G Kargl. Effective medium approach to linear acoustics in bubbly liquids. *The Journal of the Acoustical Society of America*, 111(1):168–173, 2002.

[60] Damir B Khismatullin. Resonance frequency of microbubbles: Effect of viscosity. *The Journal of the Acoustical Society of America*, 116(3):1463–1473, 2004.

[61] Abel Klein and Alexander Figotin. Midgap defect modes in dielectric and acoustic media. *SIAM Journal on Applied Mathematics*, 58(6):1748–1773, 1998.

[62] Abel Klein and Andrew Koines. A general framework for localization of classical waves: I. inhomogeneous media and defect eigenmodes. *Mathematical Physics, Analysis and Geometry*, 4(2):97–130, 2001.

[63] Peter Kuchment. An overview of periodic elliptic operators. *Bulletin of the American Mathematical Society*, 53(3):343–414, 2016.

[64] Peter A Kuchment. *Floquet theory for partial differential equations*, volume 60. Birkhäuser, 2012.

[65] Maxime Lanoy, Romain Pierrat, Fabrice Lemoult, Mathias Fink, Valentin Leroy, and Arnaud Tourin. Subwavelength focusing in bubbly media using broadband time reversal. *Physical Review B*, 91(22):224202, 2015.

[66] Timothy Leighton. *The acoustic bubble*. Academic press, 2012.

[67] John Lekner. Capacitance coefficients of two spheres. *Journal of Electrostatics*, 69(1):11–14, 2011.

[68] Fabrice Lemoult, Nadège Kaina, Mathias Fink, and Geoffroy Lerosey. Wave propagation control at the deep subwavelength scale in metamaterials. *Nature Physics*, 9(1):55, 2013.

[69] Fabrice Lemoult, Nadège Kaina, Mathias Fink, and Geoffroy Lerosey. Soda cans metamaterial: a subwavelength-scaled phononic crystal. *Crystals*, 6(7):82, 2016.

[70] Valentin Leroy, Alice Bretagne, Mathias Fink, Herve Willaime, Patrick Tabeling, and Arnaud Tourin. Design and characterization of bubble phononic crystals. *Applied Physics Letters*, 95(17):171904, 2009.

[71] Valentin Leroy, A Strybulevych, MG Scanlon, and JH Page. Transmission of ultrasound through a single layer of bubbles. *The European Physical Journal E*, 29(1):123–130, 2009.

[72] Valentin Leroy, Anatoliy Strybulevych, Maxime Lanoy, Fabrice Lemoult, Arnaud Tourin, and John H Page. Superabsorption of acoustic waves with bubble metascreens. *Physical Review B*, 91(2):020301, 2015.

[73] J Lin. A perturbation approach for near bound-state resonances of photonic crystal with defect. *European Journal of Applied Mathematics*, 27(1):66–86, 2016.

[74] Junshan Lin and Fadil Santosa. Resonances of a finite one-dimensional photonic crystal with a defect. *SIAM Journal on Applied Mathematics*, 73(2):1002–1019, 2013.

[75] Shawn-Yu Lin, Edmund Chow, Vince Hietala, Pierre R Villeneuve, and JD Joannopoulos. Experimental demonstration of guiding and bending of electromagnetic waves in a photonic crystal. *Science*, 282(5387):274–276, 1998.

[76] Chris M Linton. Lattice sums for the helmholtz equation. *SIAM review*, 52(4):630–674, 2010.

[77] JL Lions and E Magenes. Non-homogeneous boundary value problems, vol. 1, 1972.

[78] Robert Lipton and Robert Viator Jr. Creating band gaps in periodic media. *Multiscale Modeling & Simulation*, 15(4):1612–1650, 2017.

[79] Robert Lipton and Robert Viator. Bloch waves in crystals and periodic high contrast media. *ESAIM: Mathematical Modelling and Numerical Analysis*, 51(3):889–918, 2017.

[80] Zhengyou Liu, Che Ting Chan, and Ping Sheng. Analytic model of phononic crystals with local resonances. *Physical Review B*, 71(1):014103, 2005.

[81] Zhengyou Liu, Xixiang Zhang, Yiwei Mao, YY Zhu, Zhiyu Yang, Che Ting Chan, and Ping Sheng. Locally resonant sonic materials. *Science*, 289(5485):1734–1736, 2000.

[82] Guancong Ma and Ping Sheng. Acoustic metamaterials: From local resonances to broad horizons. *Science advances*, 2(2):e1501595, 2016.

[83] Kathryn H Matlack, Anton Bauhofer, Sebastian Krödel, Antonio Palermo, and Chiara Daraio. Composite 3d-printed metastructures for low-frequency and broadband vibration absorption. *Proceedings of the National Academy of Sciences*, 113(30):8386–8390, 2016.

[84] H Medwin. Counting bubbles acoustically: a review. *Ultrasonics*, 15(1):7–13, 1977.

[85] Graeme W Milton, Nicolae-Alexandru P Nicorovici, and Ross C McPhedran. Opaque perfect lenses. *Physica B: Condensed Matter*, 394(2):171–175, 2007.

[86] Marcel Minnaert. Xvi. on musical air-bubbles and the sounds of running water. *The London, Edinburgh, and Dublin Philosophical Magazine and Journal of Science*, 16(104):235–248, 1933.

[87] Jean-Claude Nédélec. *Acoustic and electromagnetic equations: integral representations for harmonic problems*, volume 144. Springer Science & Business Media, 2001.

[88] NA Nicorovici, RC McPhedran, and GW Milton. Optical and dielectric properties of partially resonant composites. *Physical Review B*, 49(12):8479, 1994.

[89] Shin Ozawa. Point interaction potential approximation for $(-\delta + u)^{-1}$ and eigenvalues of the laplacian on wildly perturbed domain. *Osaka Journal of Mathematics*, 20(4):923–937, 1983.

[90] George C Papanicolaou. Diffusion in random media. In *Surveys in applied mathematics*, pages 205–253. Springer, 1995.

[91] John Brian Pendry. Negative refraction makes a perfect lens. *Physical review letters*, 85(18):3966, 2000.

[92] Edward Mills Purcell. Spontaneous emission probabilities at radio frequencies. In *Confined Electrons and Photons*, pages 839–839. Springer, 1995.

[93] Michael Reed and Barry Simon. *IV: Analysis of Operators*, volume 4. Elsevier, 1978.

[94] Fadil Santosa and Habib Ammari. Guided waves in a photonic bandgap structure with a line defect. *SIAM Journal on Applied Mathematics*, 64(6):2018–2033, 2004.

[95] B Schweizer. The low-frequency spectrum of small helmholtz resonators. *Proc. R. Soc. A*, 471(2174):20140339, 2015.

[96] Edwin L Thomas. Applied physics: Bubbly but quiet. *Nature*, 462(7276):990, 2009.

[97] Gregory Verchota. Layer potentials and regularity for the dirichlet problem for laplace's equation in lipschitz domains. *Journal of Functional Analysis*, 59(3):572–611, 1984.

[98] S Wilcox, LC Botten, RC McPhedran, CG Poulton, and C Martijn de Sterke. Modeling of defect modes in photonic crystals using the fictitious source superposition method. *Physical Review E*, 71(5):056606, 2005.

# Curriculum Vitae

## Personal details

| | |
|---|---|
| Name | Brian Fitzpatrick |
| Date of birth | April 16, 1980 |
| Place of birth | Dublin, Ireland |
| Citizenship | Irish |

## Education

| | |
|---|---|
| 2015–2018 | PhD. Applied Mathematics<br>ETH Zürich<br>Zürich, Switzerland |
| 2014–2015 | MSc. Mathematical Modelling<br>University of Limerick<br>Limerick, Ireland |
| 2010–2014 | BSc. Computer Science<br>National University of Ireland Galway<br>Galway, Ireland |

## Publications

H. Ammari, B. Fitzpatrick, H. Kang, M. Ruiz, S. Yu, and H. Zhang, Mathematical and Computational Methods in Photonics and Phononics

- Mathematical Surveys and Monographs, American Mathematical Society, Providence, (2018), to appear
- Draft version

H. Ammari, B. Fitzpatrick, D. Gontier, H. Lee and H. Zhang, Minnaert resonances for acoustic waves in bubbly media

- Annales de l'Institut Henri Poincaré: Analyse Nonlinéaire, (2018), to appear
- https://www.sciencedirect.com/science/article/pii/S0294144918300362

H. Ammari, B. Fitzpatrick, D. Gontier, H. Lee and H. Zhang, A mathematical and numerical framework for bubble meta-screens

- SIAM Journal on Applied Mathematics, 77.5 (2017), 1827-1850
- http://epubs.siam.org/doi/pdf/10.1137/16M1090235

H. Ammari, B. Fitzpatrick, H. Lee, S. Yu and H. Zhang, Sub-wavelength phononic bandgap opening in bubbly media

- Journal of Differential Equations, 263 (2017), 5610-5629
- http://www.sciencedirect.com/science/article/pii/S0022039617303327

H. Ammari, B. Fitzpatrick, D. Gontier, H. Lee and H. Zhang, Sub-wavelength focusing of acoustic waves in bubbly media

- Proceedings of the Royal Society A, (2017), 473.2208 (2017), 20170469
- http://rspa.royalsocietypublishing.org/content/473/2208/20170469

H. Ammari, B. Fitzpatrick, H. Lee, S. Yu and H. Zhang, Double-negative acoustic metamaterials

- http://arxiv.org/pdf/1709.08177, (2018), Preprint

H. Ammari, B. Fitzpatrick, E. Hiltunen, and S. Yu, Sub-wavelength localized modes for acoustic waves in bubbly crystals with a defect

- https://arxiv.org/abs/1804.00756, (2018), Preprint

**Talks**

European Workshop on Acoustic and Mechanical Metamaterials

- Imperial College London, London, United Kingdom, July 10, 2018

Imperial College London Plasmonics and Metamaterials group

- Centre for Plasmonics and Metamaterials, Imperial College London, London, UK, March 7, 2018

The Neumann-Poincaré Operator, Plasmonics, and Field Concentration

- Ramda Jeju Hamdeok Hotel, Jeju Island, South Korea, February 9, 2018

IAS Program on Inverse Problems, Imaging and Partial Differential Equations

- HKUST Jockey Club Institute for Advanced Study, Hong Kong University of Science and Technology, Hong Kong, China, February 6, 2018

SIAM Conference on Analysis of Partial Differential Equations

- The Baltimore Convention Center, Baltimore, USA, December 10, 2017

Neumann-Poincaré Operator and Plasmonic Resonances Workshop

- Université Grenoble Alpes, Grenoble, France, November 29, 2017

WAVES 2017, 13th International Conference on Mathematical and Numerical Aspects of Wave Propagation

- University of Minnesota, Twin Cities, Minneapolis, USA, May 17, 2017

14th International Conference on Integral Methods in Science and Engineering

- University of Padova, Padova, Italy, July 26, 2016